Effects of Nonlinear Soil-Structure Interaction on Lateral Behavior of Pile Foundations

Mahmoud Nasser Hussien Ahmed

Abstract

Pile foundation subjected to static or dynamic lateral loading is one of a class of problems that involve soil-structure interaction (SSI). The behavior of these foundations has a long history of research and these researches have formed the basis for the current design practice of pile foundations under lateral loads. However, several aspects of SSI and its effects on pile performance under lateral loads have not been explicitly studied in research and consequently not fully considered in design practice. There are strong needs to pursue the studies on SSI and to evaluate its effects on the performance of piles.

Piles expected to behave nonlinearly under extreme loading conditions. Additionally, the soil is known to exhibit nonlinear behavior even at relatively low strain levels. Consequently, ignoring nonlinear SSI effects could lead to serious errors on evaluating pile performance under lateral loads. The present research is concerned with identifying the effects of three aspects of nonlinear SSI on the performance of piles and pile groups under static and dynamic lateral load. Brief descriptions of these three aspects of SSI are given in the following words.

One aspect of SSI that is still not fully understood and poses a challenge to geotechnical engineers is soil-pile gap formation at soil-pile interface. In this situation, two primary variables of SSI have to be carefully evaluated. One is the deformation of soil due to pile displacement. This variable has to be evaluated even when the soil-pile separation occurs. The other is the soil-pile gap formation, especially the threshold level of displacement or the triggering level of the gap formation.

Another aspect of SSI that is not considered in the current design practice is the interaction between axial and lateral structural loads transmitted to the soil through the piles. According to the current practice, piles are independently analyzed first for the axial load to determine their bearing capacity and settlement and then for the lateral load to determine the stresses and deflections, ignoring the interaction between vertical and lateral loads.

When the seismic load is considered, the superstructure forms an integral part of the pile-foundation system, and the SSI in this case become more challenge. The analysis of a superstructure-foundation system for earthquake loads is a very complex process involving inertial interaction between structure and pile foundation, kinematic interaction between piles and soils, and the nonlinear response of the coupled soil-pile-structure system to strong earthquake motions. In this situation, which are very complex but of the utmost importance in practical design, a proper understanding of SSI effects on the performance of the soil-pile-structure system is needed.

This study aims at advancing the knowledge and understanding on the above mentioned three aspects of nonlinear SSI and their effects on the pile performance. To this end, nonlinear finite elements models (FEM) are constructed and applied in a practical way to deal with these three issues. These models cover a large range of soil strain levels under variety of loading conditions. Some modeling strategies are introduced and validated in order to reduce the computational cost. Therefore, an equivalent two dimensional (2D) model, implemented in FLIP is adopted and used throughout the current study.

The soil in front of a pile actually moves around the pile in a three dimensional (3D) manner whereas in this study this phenomenon is idealized through 2D type using soil-pile interaction springs. The soil-pile interaction spring is formed by analyzing the soil behavior in horizontal plane around a pile. With a unit thickness in vertical direction, the horizontal deformation of soil mass around the pile is analyzed by applying the forced displacement at the pile. Using several thousand FE meshes of nonlinear soil model of multiple shear mechanism, nonlinear load-displacement relationships are computed, where the displacement is defined by the displacement of the pile relative to that of the soil at the boundary (coincided with the mid-position between the piles in group piles aligned perpendicular to the displacement direction). The study shows that the nonlinear load-displacement relationships computed through the FE analysis in horizontal plane coincided with the nonlinear stress-strain relationships of a single soil element in shape. Thus, the soil-pile interaction spring can be idealized by substituting a single soil element with empirical scaling factors for conversion from stress-strain to load-displacement variables. This spring element makes it possible to approximate the 3D behavior of soil-pile interaction through 2D analyses. In addition, the gap formed between the soil and the pile is idealized through a joint element that incorporates the separation-contact and sliding mechanisms.

The effect of soil-pile gap is studied with respect to the performance of laterally loaded single and group piles. Full-scale tests consisting of a combination of a single and 3 by 5 group pile under static and dynamic lateral loads presents a unique opportunity for this end and allows rigorous study without arbitrary parameter back-fitting. In these tests, piles were installed in the deposit formed with alternating layers of saturated clay (with shear strength ranging from 20-40 kPa) and sand. The single pile is made of steel pipe pile 11.6 m long with pile diameter 0.324 m and 9.5 mm thick and the group pile is formed in 3 by 5 layout with a spacing of 3.92 times the pile diameter. The static load was applied by hydraulic jack and the dynamic load was applied using statnamic test device. In the analysis, coupled soil-pile system is idealized through the 2D FEM mentioned earlier. For a statically loaded single pile, ignoring soil-pile separation leads to 43% overestimation of the lateral loading-carrying capacity of the pile. For a statically loaded pile group, the effect of soil-pile separation is most prominent at the trailing pile. Ignoring soil-pile separation leads to 73% overestimation of the load-carrying capacity of the trailing pile. Similar results have been obtained for dynamically loaded piles,

indicating that the appropriate evaluation of the effect of soil-pile gap formation is essential for accurate estimation of the lateral response of piles under static and dynamic lateral loads.

The effect of vertical loads on the lateral resistance of piles is evaluated using the pile dimensions and configuration used for the full-scale model tests. In these analyses, the vertical load is applied by enforcing a vertical displacement equivalent to 10% of pile diameter (i.e. vertical load = 75 % of the ultimate vertical capacity of the pile (P_u)) at the pile-head and then the lateral resistance of the pile is analyzed. The increase in the lateral resistance due to the vertical load is 8% for the single pile and 9% for the group piles. The vertical load leads to a 10% decrease in the lateral resistance of the leading pile (pile 1) and 9, 14, 17, 35% increase in the lateral resistance of piles 2 through 5, respectively. The increase in the confining pressures in the sand deposit is the major driving factor to contribute the change in the lateral resistance of piles, depending on the position of the pile in the group. When a footing is added above the pile-head, and the same vertical load is applied through this footing, the rate of increase in the confining pressures in the sand deposit is more pronounced, contributing to the more pronounced effect of the vertical load on the lateral response of the piles.

The effect of the frequency content of input motion on the SSI is evaluated through centrifuge model tests and numerical analyses. Dry sand deposit is used in this study, thereby aiming at the fundamental knowledge on the soil-pile-structure interactions under seismic loading. In this series of the study, the most fundamental case of linear elastic analysis of a single pile is analyzed first. The results of these fundamental analyses are compared with the previously published results of linear SSI available in the literature, and the applicability of the simplified FEM adopted in this study is confirmed. The study moves to include nonlinear SSI using centrifuge model tests of a superstructure (Double-Degree Of Freedom (DDOF)) supported by a single pile foundation and shaken at the centrifugal acceleration of 40 g. Applicability of the nonlinear FEM adopted in this study is confirmed in frequencies ranging from 0.1 to 1.0 Hz. Based on the confirmed applicability of the numerical model adopted in this study, the effect of the frequency content of input motion on the dynamic SSI is studied as follows:

(1) A series of systematic centrifuge tests is conducted in order to study the seismic response of end bearing single and 3 by 3 group piles embedded in dry sand layer and supporting SDOF and DDOF structures. Resonant frequencies are 7 Hz for ground, 5 Hz for SDOF superstructure on rigid ground, and 2 Hz (for the fundamental mode) and 11 Hz (for the second mode) for DDOF superstructure on rigid ground. All tests are conducted with the centrifugal acceleration of 40 g. A total of 7 tests including free-field, single and group pile cases were performed. Each model was subjected to 12 sinusoidal waves as input base accelerations. These waves have constant amplitude of about 1.5 m/s^2 and varying frequencies ranging from 1 to 12 Hz. The centrifuge test results indicate that the pile-head motion is found to be dominated by two discrete frequencies: a lower frequency (the

effective natural frequency (f_{SSI})) where the pile-head motion is amplified and a higher one (the pseudo-natural frequency (f_{pSSI}) of the system) where the response is suddenly de-amplified with respect to the free-field motion. These results confirm the numerical results found in the literature and generalize their findings to include group piles supporting higher DOF structures. Moreover, as the frequency content of base excitation approaches the fundamental frequency of the ground (7 Hz), the bending moment of all piles (in a free-head pile group) increase as well as the difference between piles bending moments indicating strong effect of pile-soil-pile interaction. In this case, the center pile in the group has the minimum value of bending moment followed by the side pile followed by the corner pile. For group piles supporting structures, as the frequency content of base excitation approaches f_{SSI} of the coupled soil-pile-structure system, the bending moment of all piles also increase as well as the difference between piles bending moments indicating strong effect of pile-soil-pile interaction. Unlike the free-head case, the center pile in the group has the maximum value of bending moment followed by the side pile followed by the corner pile.

(2) A series of linear and nonlinear parameter studies of soil-pile superstructure systems conducted using the simplified FEM shows that the reduction rate in the resonant frequency of the superstructure by changing the rigid foundation ground to soil-pile foundation (to be called frequency ratio) can be expressed as a function of wave parameter (represented by normalized resonant frequency of superstructure on the rigid foundation ground with a height of the structure and the shear wave velocity of ground) and foundation flexibility (pile length over diameter ratio normalized by the quadruple of Young's modulus ratio of pile and ground). The results also indicate that SSI effects were observed for coupled systems that comprise of stiff superstructures founded on flexible and/or long piles; leading to significant reductions in f_{SSI} of the system (i.e. the frequency ratio becomes smaller for larger wave parameter and larger foundation flexibility). The nonlinearity of the ground induces larger reduction in frequency ratio indicating the strong need to revisit the current interaction methodologies based on linear elastic SSI.

Keywords: *lateral, vertical, static, dynamic, bending moment, pile group, nonlinear, soil-pile spring, soil-pile separation, pile-soil-pile interaction, soil-pile interaction, coupled soil-pile-structure interaction, finite elements, centrifuge, kinematic, inertial, effective natural frequency, pseudo-natural frequency*

I would like to dedicate this thesis to my loving parents, my lovely wife, my lovely daughters (Dai and Maryam) & my lovely country Egypt.....

Acknowledgments

My first and last gratitude to the Almighty "Allah", the God of all mankind, for giving me the health, strength, patient, and faith to undertake this work. In my human endeavors, I humbly implore him to grant that my labor my serve all the living.

The research reported in this thesis was started while I was a doctoral student in the Graduate School of Engineering at Kyoto University. Many people have contributed to this project and supported me in various ways. It is impossible to name all the people involved; however, the author would like to express his thanks by specifying some of the most important persons.

I would like to express my deeply-felt thanks to my thesis advisor, Professor Susumu Iai at the Disaster Prevention Research Institute (DPRI), Kyoto University, for welcoming me in his laboratory to work on this challenging research topic, and for his warm encouragement and thoughtful guidance. Professor Iai provided a wealth of ideas and encouragement, and was always available to discuss this work. I greatly appreciate the opportunities he has given me to become involved with other aspects of his work. I would like also to thank Dr. Tetsuo Tobita for his hands on assistance with all aspects of the testing program as well as the successive analysis of the obtained data. Dr. Tobita's mentorship and inquisitiveness will always be valued.

I am deeply thankful to Professor Kyle M. Rollins, Brigham Young University, USA for providing me with huge amount of full-scale pile loading test data that helped me visualize and understand the topic as well as to validate the finite element numerical model adopted in this study.

I also wish to thank Professor Fusao Oka and Professor Takeshi Koike for their critical review of the manuscript and constructive suggestions and active discussions as committee members of my doctoral degree. I want to thank the members of Iai Lab. for their support and friendship; Mamoru Mimura, Associate Professor, Hiroki Shimizu and Kazuhide Tomisaka, Technicians, Wake Yuyama, Secretary, ByungGon Jeon, Doctoral student, Youhei Inoue, Master student and all other students. I received a lot of help and advice from them. Many students, who graduated from Professor Iai's Laboratory, helped me in performing centrifuge experiments as well as numerical analyses described in this thesis. I would like to thank Kyohei Ueda, Gi-Chun Kang, Ryo Moritani, and Kazuma Nishida among other.

I also gratefully acknowledge the financial support received from the Egyptian Government and the Egyptian Culture, Education and Science Bureau in Tokyo. A word of appreciation is due to the Head and staff of Civil Engineering Department, Assiut University for their invaluable teaching of the fundamentals of soil mechanics, foundation engineering

and other civil engineering subjects. Sincere thanks and indebtedness are due to my respected teachers in Civil Engineering Department, Assiut University.

I would like to express my acknowledgments to many friends in Japan, Mohamed Fathi, Mohamed Saber, Sameh Kantoush, Amr Mohamed, Mahmoud Baker, Sadat Kattab, Alhossien Hamada, Maged Serag, Sayed Abd Elfatah, Ahmed Kamal, Mohamed Omer, and Mohmed El kashef

Words are not enough to thank my family for the support they have given me during this long and sometimes difficult journey. My wife Mona has kept me going through it all, with her patience, encouragement, and love, and helping me to keep life in balance. Without her, I would not be able to achieve or enjoy these successes. Though they may not quite realize it yet, Dai and Maryam are sources of great joy that sustain me and help keep life in perspective. Finally, I want to thank my parents and my brothers and sisters for their love and support, and for instilling in me the value of learning and providing me outstanding opportunities to do so throughout my life. Without them, my PhD endeavor would not have been possible.

Table of contents

CHAPTER 1

Introduction

Contents

1.1 Introduction

Pile foundations are relatively long and slender structural members which have the function of transferring load from the superstructure through weak compressible strata or through water to more compact and less compressible soil or onto rock. In addition to axial loads that must be sustained by the piles, substantial lateral loads may be present and must be accounted for in design. These lateral loads can come from variety of sources such as wind forces and earth pressures. More powerful lateral loads occur as a result of unpredicted events such as earthquakes, slope failure, and lateral spread induced by liquefaction.

The problem of lateral loading piles is not as simple as that of vertical loading one in that the resistance of a pile to a lateral load and the deflection of the pile as the load builds up to its ultimate value are very complex matters involving the interaction between a semi-rigid structural element and the soil (SSI), which deforms partially elastically and partially plastically. In addition, the soil adjacent to a laterally loaded pile at ground surface yields at the very smallest lateral load. As the load increases, yielding progresses down the pile further. The surface of the pile opposite to the loading direction may separates from the soil and, to some depth, leaves a gap. Some soil such as cohesionless sand inevitably moves falls into the gap, so that when the load is removed the plastic deformations and the presence of the soil filling behind the pile prevent it from returning to its pristine position. If the pile-soil system were to be modeled elastically, the model parameter would depend on the load or displacement level specified (Scott 1981).

The available procedures of analyzing the lateral performance of piles in this complex SSI situation have included those based on simplified interactions models as well as those based on more rigorous FE and boundary element models (BEM). Simplified procedures are an essential feature of pile design, and they are the tools for code regulated designs. In these models, piles are typically analyzed by idealizing the ground through linear elastic or nonlinear springs attached at different depths to the pile that is modeled as a beam. The former is called Chang's method (1937) and used in Japan in design practice whereas the latter is called *p-y* curve, where *y* represents the lateral displacement and *p* represents the soil resistance per unit length of the pile, and this method is used in North America and Europe in design practice since 1970s. Seismic soil-pile interaction analysis has been also made by using these springs by Penzien and others since 1960s. Lateral behavior of single pile is converted to that of group pile

by using *p*-multiplier as suggested by Brown et al (1988). With this approach, the soil resistance, *p*, is scaled down by a constant factor. The appropriate *p*-multiplier is likely dependent on a number of factors such as pile spacing, row position in the group, deflection level and soil type.

A superstructure forms an integral part of the pile-foundation system when seismic load is considered. Thus the design of a superstructure-foundation system for earthquake loads must take into account the effects of the foundation on earthquake ground motion as well as the inertial loads imposed by the structure on the foundation. The former effect would cause the motion of the base of the structure to deviate from the free-field motion (*kinematic interaction*) whereas the latter would induce deformation on the supporting soil (*inertial interaction*). In the past, free-field accelerations or velocities or displacements were considered as input motion for the seismic design of structures without considering the effects of kinematic interaction. However, depending on the soil profile, pile properties and dimension, and the excitation frequency, pile response may be greater than or less than the free-field response. Thus proper design of structures and their foundation must account for both of these effects.

In a seismic soil-pile-structure interaction analysis, kinematic and inertial interactions can be examined directly or indirectly. The direct or coupled method analyzes the entire soil-pile-structure system and is often performed using FEM which is very complicated and requires an enormous amount of time and resources. The indirect (multi-step) method decomposes the kinematic and inertial interaction as two separate stages which can later be coupled together to obtain the actual response. Although the decoupling of the system's response provides insight as to the distinct role of inertial and kinematic interaction, the implementation of the coupled system gives a direct and often more convenient estimation of the response, since inertial and kinematic effects are simultaneously modeled (Rovithis et al. 2009).

Several aspects of SSI and its effects on pile performance under lateral loads have not been explicitly studied in previous research briefly described above. Three of these aspects are given in the following:

(1) Level of loadings assumed for the previous study and existing design practice is often for the condition of moderate strain level induced in the ground. Lateral behavior of piles at extensive nonlinearity induced in the ground, such as for liquefaction or soil-pile gap formation, as encountered in recent strong earthquakes, is not fully studied.

(2) In the conventional studies, the lateral behavior of piles has been studied independently from

their vertical responses. The interaction between axial and lateral structural loads transmitted to the soil through the piles is not considered; the justification being that the magnitude of applied axial load has a little influence on the laterally loaded soil-pile system. However, when the magnitude of the axial load of the pile approaches its ultimate vertical capacity, a careful evaluation of the effect of vertical loads on the lateral resistance of piles and pile groups is required.

(3) In the seismic loading condition, the fundamental frequencies that dominate pile-head motion as well as dynamic pile bending in the coupled soil-pile-structure system as affected by the combined effect of kinematic and inertial interaction have not been explicitly studied.

1.2 Objectives and Scope

This study aims at advancing the knowledge and understanding on the above mentioned three aspects of nonlinear SSI. The most recent results for lateral behavior of piles through numerical analyses and centrifuge model tests as well as full-scale tests are presented in this study. The study is systematically performed from the most fundamental single pile to group piles, and from the most fundamental loading condition for applying the static and dynamic load at pile-heads to dynamic response of soil-pile-structure system. Table 1.1 lists the loading conditions of single and grouped piles investigated in the current study through numerical analyses and centrifuge model tests.

Table 1.1 Loading conditions of single and grouped piles investigated through numerical analyses and centrifuge model tests

Loading conditions	Numerical analysis		Centrifuge model test	
	Single pile	Group pile	Single pile	Group pile
Static load	●	●		
Dynamic load applied at pile head	●	●		
Seismic load	●		●	●

1.3 Methodology

1.3.1 Numerical analysis

Nonlinear FEM are constructed and applied in a practical way to deal with the above mentioned three issues of SSI. These models cover a large range of soil strain levels under variety of loading conditions. Some modeling strategies are introduced and validated in order to reduce the computational cost. Therefore, an equivalent 2D model, implemented in FLIP (**F**inite Element Analysis Program for **LI**quefaction **P**rocess) is adopted and used throughout the current study. A brief description of the simplified 2D model is given as follows:

The interaction between a pile and the surrounding soil in 3D was idealized using 2D analyses. Nonlinear spring elements were used to represent the soil-pile interaction. Parameters of these spring elements were determined by parametric studies on the soil-pile interaction in a 2D horizontal plane. With a unit thickness in vertical direction, the horizontal deformation of soil mass around the pile is analyzed by applying the forced displacement at the pile. Using several thousand FE meshes of nonlinear soil model of multiple shear mechanism, nonlinear load-displacement relationships are computed, where the displacement is defined by the displacement of the pile relative to that of the soil at the boundary (coincided with the mid-position between piles in a single row of equally spaced group piles aligned perpendicular to the displacement direction). The study shows that the nonlinear load-displacement relationships computed through the FE analysis in horizontal plane coincided with the nonlinear stress-strain relationships of a single soil element in shape. Thus, the soil-pile interaction spring can be idealized by substituting a single soil element with empirical scaling factors for conversion from stress-strain to load-displacement variables. This spring element makes it possible to approximate the 3D behavior of soil-pile interaction through 2D analyses. In addition, the gap formed between the soil and the pile is idealized through a joint element that incorporates the separation-contact and sliding mechanisms.

The most fundamental loading condition is to apply the load at the pile-head, either statically or dynamically. Single and group pile behavior is analyzed with a focus on the effects of pile-soil gap formation. The model tests referred to in this study is the full-scale model tests of piles installed in the deposit formed with alternating layers of clay (with shear strength ranging from 20-40 kPa) and sand. The single pile is made of steel pipe pile 11.6 m long with pile diameter 0.324 m and 9.5 mm thick and the group pile is formed in a 3 by 5 layout with a spacing of 3.92 times the pile diameter. The static load was applied by hydraulic jack and the dynamic load was applied using statnamic test device. The effect of vertical loads on the lateral

resistance of the pile is evaluated using the pile dimensions used for the full-scale model tests. In these analyses, the vertical load is applied by enforcing the vertical displacement equivalent to 10% of pile diameter at the pile-head and then the lateral resistance of piles is analyzed.

The effect of the frequency content of input motion on the SSI is evaluated through numerical analyses. Dry sand deposit is used in this study, thereby aiming at the fundamental knowledge on the soil-pile interaction under seismic loading. In this series of the study, the most fundamental case of linear elastic response of a single pile is analyzed first. The results of these fundamental analyses are compared with the previously published results of linear SSI available in the literature, and the applicability of the numerical model adopted in this study is confirmed. Applicability of the numerical model adopted in this study is confirmed also by comparing the numerical results with centrifuge tests results in the frequency ranging from 0.1 to 1.0 Hz. Based on the confirmed applicability of the numerical model adopted in this study, the effect of frequency of input motion on the dynamic soil-pile-structure interaction is parametrically studied. A series of linear and nonlinear parameter studies of soil-pile superstructure systems shows that the reduction rate in the resonant frequency of the superstructure by changing the rigid foundation ground to soil-pile foundation can be expressed as a function of wave parameter and foundation flexibility.

1.3.2 Centrifuge model tests

The study moves on to the centrifuge model tests. The effect of the frequency content of input motion on the pile-soil interaction is evaluated through centrifuge model tests. All tests are conducted at the centrifugal acceleration of 40 g. The centrifuge model tests are performed for single and group piles (3 by 3) embedded in dry sand with and without superstructures. A total of seven cases of model tests are performed with the input frequency ranging from 1 to 12 Hz in prototype. Resonant frequencies are 7 Hz for ground, 5 and 9 Hz for SDOF superstructures on rigid ground, and 2 and 6 Hz (for the fundamental modes) and 11 Hz (for the second modes) for DDOF superstructures on rigid ground. The obtained results provide a clear insight about the seismic coupled soil-pile-structure interaction as well as the seismic pile-soil-pile interaction.

The originality of this study is confirmed for the academic development on static and dynamic lateral behavior of piles as well as for the usefulness in practice for designing piles and pile groups against strong earthquake motions.

1.4 Organization of the Dissertation

This dissertation consists of ten chapters:

Chapter 1: *Introduction*—includes background, objectives, scope, methodology of the research, and organization of the dissertation.

Chapter 2: *Previous Studies on Laterally Loaded Piles*—presents a critical review of the current numerical models and centrifuge model tests as well as full-scale tests used to study the SSI and its effects on the behavior of laterally loaded piles and pile groups.

Chapter 3: *Modeling of Soil-pile Interaction in Horizontal Plane*—presents a simplified approach for idealizing the soil-pile interaction in horizontal plane in terms of a nonlinear soil-pile interaction spring.

Chapter 4: *Effect of Soil-Pile Separation on Performance of Pile Group*—in this chapter, the effect of soil-pile separation is studied with respect to the performance of laterally loaded pile group based on full-scale tests consisting of a combination of a single and 3 by 5 group piles under static and dynamic lateral loads.

Chapter 5: *Effect of Vertical Loads on Lateral Resistance of Pile Group*—presents a numerical study of the effect of vertical loads on the lateral resistance of piles using the pile properties and dimension used for the full-scale model tests described in Chapter 4.

Chapter 6: *Analyses of Coupled Soil-Pile-Structure System under Sinusoidal Excitations with Various Frequencies*—the most fundamental case of linear elastic seismic response of a single pile is analyzed in this chapter. The results of these fundamental analyses are compared with the previously published results of linear SSI available in the literature, and the applicability of the numerical model adopted in this study is confirmed.

Chapter 7: *Centrifuge Model Tests and Analyses of Nonlinear Seismic Response of Soil-Pile-Structure System*—this chapter presents a comparison between nonlinear seismic analyses using the 2D FEM and the results of shaking table centrifuge model tests of pile-supported structures in a dense sand profile. The overall comparisons indicated that these FE models could be used to parametrically evaluate the influence of other key factors, such as varying structural periods, pile slenderness, soil-pile relative stiffness, and input motions.

Chapter 8: *Effect of Soil-Pile-Structure Interaction on Performance of Pile Group: Centrifuge Model Tests*–in this chapter, a series of systematic centrifuge tests is conducted in order to study the seismic response of end bearing single and 3×3 group piles embedded in dry sand layer and supporting SDOF and DDOF structures. The obtained results provide a clear insight about the seismic coupled soil-pile-structure interaction as well as the seismic pile-soil-pile interaction.

Chapter 9: *Seismic Performance of Coupled Soil-Pile-Structure System: Parametric Study*–in this chapter, linear and nonlinear seismic response of SDOF structures supported on single piles embedded in dry sand is parametrically studied, emphasizing on the vibrational characteristics of the soil-structure system. These series of parameter study are the base to develop simple charts for predicting linear and nonlinear seismic response of SDOF structures supported on piles.

Chapter 10: *Conclusions*–includes a summary of the dissertation and its findings.

References

1. Brown, D., Morrison, C., and Reese, L. 1988. Lateral load behavior of a pile group in sand, *J. Geotechnical Engineering, ASCE,* 114(11), 1261-1276.
2. Chang, Y.L. 1937. Lateral pile loading tests. *Transactions of the American Society of Civil Engineers*, 102, 273–276.
3. Penzien, J., Scheffy, C., and Parmelee, R. 1964. Seismic analysis of bridges on long piles, *J. Engineering Mechanics Division, ASCE*, 90(3), 223-254.
4. Rovithis, E.N., Pitilakis, K.D., and Mylonakis, G.E. 2009. Seismic analysis of coupled soil-pile-structure systems leading to the definition of a *pseudo*-natural SSI frequency, *Soil Dynamics and Earthquake Engineering*, 29(6), 1005-1015.
5. Scott, R.F. 1981. Foundation analysis. Prentice Hall.

CHAPTER 2

Previous Studies on Laterally Loaded Piles

Contents

2.1 Introduction

The majority of pile foundations are subjected to at least some degree of lateral loading. In some cases, the magnitude of the horizontal loads relative to the applied vertical loads will be small, and no additional design calculations would be necessary. In other cases where piles are used, for example, to support offshore platforms or bridges or overhead structures sustaining a variety of facilities, lateral loading may prove critical in the design. The ability of pile foundations to withstand these lateral loads has been a subject of great concern for many years.

2.2 Description of the Problem

In practice, the problem of lateral loaded piles is immensely complex SSI problem, not only because of the soil behavior but also because of the interdependency of the pile deflection and the soil lateral resistance. To visualize this distinct behavior of soil-pile interaction under lateral load, it is helpful to consider the following case history, shown in Fig. 2.1, reported by Kishida et al. (1985). Figures 2.1(a) and (b) show soil deformation surrounding the pile due to cyclic loading applied at pile-head level for both sand and clay soil layer, respectively.

The relationships between load and displacement at the pile-head are shown in Figs. 2.2(a) and (b). The test results in the sand (Fig. 2.2 (a)) indicates that the hysteresis curves under cyclic loadings show about the same shape and that the area enclosed by the curve increases with increment of load. The test result in the clay (Fig. 2.2(b)), however, indicates different shape of the hysteresis curves compared with those of sand. The areas enclosed by the curves are smaller than the ones in the sand. The load-displacement curve shows a "pinched" character. Movements of the sand and the pile in Fig. 2.1(a) show that the sand in front of the pile is compacted due to movements of the pile and that the sand in back of the pile moves down to the pile shaft increasing its density near the shaft and decreasing it away from the shaft. No gap between the sand and the pile was observed. Figure 2.1(b) shows the gap between the clay and the pile at the back of the pile. The clay in front of the pile is remolded and may decrease its strength significantly (Prakash 1992).

According to the above discussed case history, two primary variables of the soil-pile system have to be carefully evaluated when analyzing laterally loaded pile problem. One is the deformation of soil due to pile displacement. This variable has to be evaluated even when the

soil-pile separation occurs. The other is the soil-pile gap formation, especially the threshold level of displacement or the triggering level of the gap formation. These two variables might be relatively easy to analyze if only single pile is considered. The analysis becomes more challenging when the analysis is extended to include pile-soil-pile interaction or when a dynamically loaded pile group associated with dynamic soil response is involved.

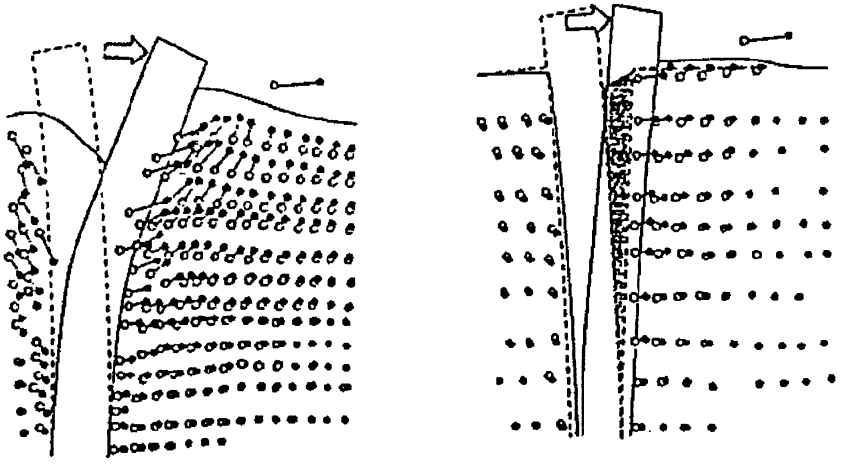

(a) (b)

Fig. 2.1 Movements of soil surrounding the pile: (a) sand, (b) clay (After Kishida et al. 1985)

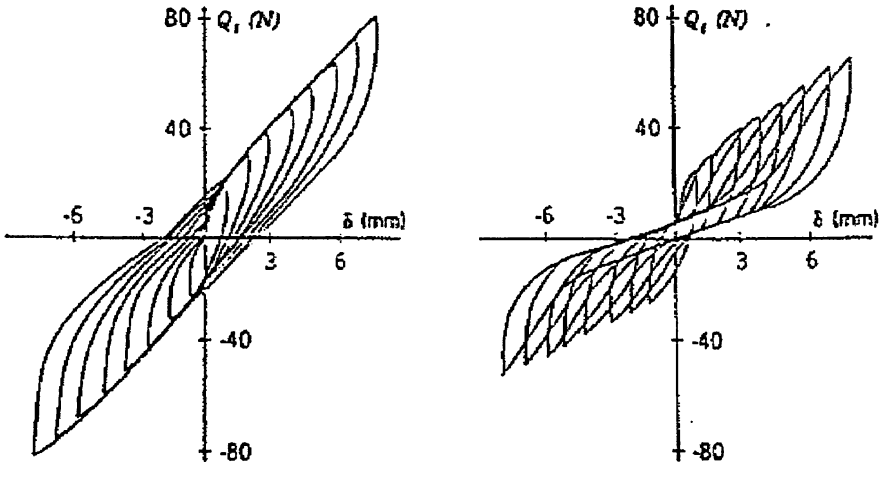

(a) (b)

Fig. 2.2 Load-displacement relationships: (a) sand, (b) clay (After Kishida et al. 1985)

From another point of view, a pile may function as an active element, when the loads originate in forces acting on the superstructure and reach the foundation via stresses in the cross-section of the structure-foundation connection, with the soil resisting the load, or a passive element, when movement of the soil subjects the pile to bending stresses. Monotonic, cyclic, and dynamic loading at pile-head level are examples of the former category, while seismic loading is an example of the latter category. The superstructure forms an integral part of the pile-foundation system when the seismic load is considered. Although the problem become more challenge, an analysis of the soil-pile-structure system and its proper understanding is necessary.

The design of a superstructure-foundation system for earthquake loads is a very complex SSI process involving inertial interaction between structure and pile foundation, kinematic interaction between piles and soils, seismically induced pore-water pressures (PWP) and the nonlinear response of soils to strong earthquake motions (Finn 2005). Kinematic interaction is the seismic response of the soil profile transmitted to the pile foundation. Seismic soil deformation forces the pile to move under the action of vibrating soil, the different levels of stiffness between soil, pile, and foundation generates a seismic modified motion of the foundation which is different from the free-field motion. The inertial interaction consists of structural inertial forces being transferred to the pile foundation. These forces impose lateral loads which are concentrated near the pile-head, and axial loads, if a rocking mode of the structure is present. In the past, free-field accelerations or velocities or displacements were considered as input motion for the seismic design of structures without considering the effects of kinematic interaction. However, depending on the soil profile, pile properties and dimension, and the excitation frequency, pile response may be greater than or less than the free-field response.

It is in the light of these complex SSI situations that "rational" methods of analysis have been developed to enable a foundation designer to assess the likely response of a soil-pile system to static, dynamic, and seismic lateral loads. In addition, a wide range of field and laboratory experiments has been performed by researchers attempting to provide parameters for and to validate soil-pile analytical methods. This chapter aimed at presenting some of the more important findings from the comprehensive study of SSI and its effects on the performance of laterally loaded single and grouped piles. Techniques for the analysis of single piles and pile groups under static, dynamic, and seismic dynamic loading have also been described. It is hoped

that the overview may provide a better understanding of soil-pile, pile-soil-pile, and soil-pile-structure interactions.

2.3 Analytical Methods

Pile-supported structures in the past were frequently subjected to lateral loading, but the piles were designed using judgment or by referring to building codes, which usually allowed a modest load on each pile if the soil met certain conditions (Reese et al. 2006). Design becomes more critical especially when piles are used to support critical facilities such as offshore platforms or nuclear power plants, or where the magnitude of the lateral load is large. The most powerful lateral loads occur as a result of unpredicted events such as earthquakes, vessel impacts, slope failure, and lateral spread induced by soil liquefaction. In these situations, more reliable and efficient solution is needed. Therefore, substantial research efforts have been carried on this topic to revamp the design codes and construction regulations. The available procedures of analyzing this kind of SSI problem have included those based on simplified interactions models such as Winkler Foundation approach, as well as those based on more rigorous FEM or BEM. The following sections present a brief overview of soil-pile, pile-soil-pile, and soil-pile-structure interactions analyses; these generally fall into the discrete and continuum classes of models.

2.3.1 Evolution of simplified interaction model

2.3.1.1 Beam-on-elastic foundation

The origins of simplified methods that are in wide use today can be traced back to a discussion by Chang (1937) of a paper by Feagin (1937) on lateral pile loading tests. The tests were conducted to provide design data for the design of the pile foundations for Lock and Dam 26 on the Mississippi River at Altona, Illinois, USA. These tests were the earliest reported full-scale tests on laterally-loaded piles and generated great interest and discussion. The tests were conducted on concrete and timber single piles and pile groups of 4, 12, and 20 piles and driven to an average penetration of 9.0 m. The heads of the piles were fixed by embedding them 0.6 m into the concrete. The piles were installed by a combination of jetting and driving. All pile groups were arranged in a 2×N configuration and spaced about 3 pile-diameters. Chang (1937) presented a method for the analysis of Feagin's test data in which the interactions between soil and pile were presented by elastic springs as those shown in Fig. 2.3, and the spring constant was

assumed to be constant with depth. Chang (1937) developed solutions for deflections, moments and shears in the piles. He appears to have been the first to introduce the concept of critical pile length. He recognized that the upper layers of soil contributed most to resistance against lateral loads and suggested that the constant soil modulus, E_s, should be taken as the value at one third of the modulus at the critical depth, in effect recommending a characteristic modulus. Using a modulus backfigured from the test data, which inherently included nonlinear effects of the loading, he showed that his model of soil-pile interaction could simulate the results of Feagin's tests satisfactorily (Finn 2005).

Chang's method is still widely used today and appears in the latest Japanese codes with a yield cut-off. The soil modulus is given in Japanese codes as a function of the standard penetration resistance, N. Computer programs readily allow a variable E_s corresponding to the distribution of N values.

In another attempt, Hetenyi (1946) in his book analyzed the response of a single pile to lateral loads using the equation of an elastic beam supported on an elastic foundation, which is represented by the 4th order differential beam bending equation:

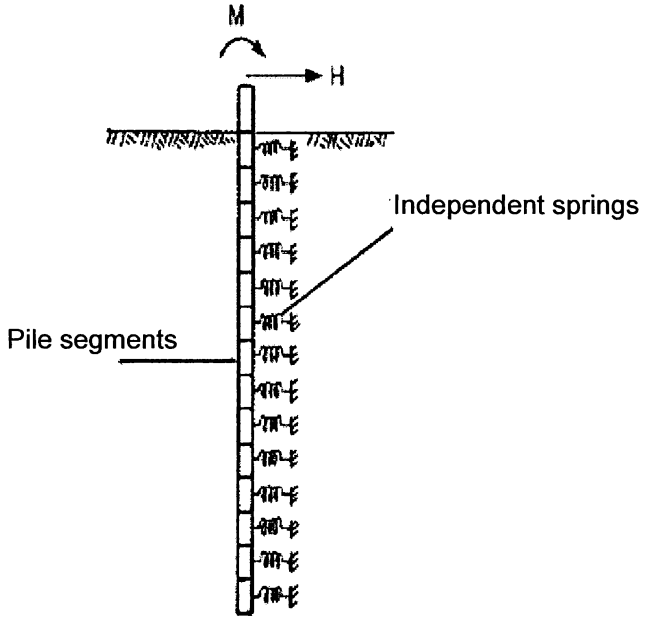

Fig. 2.3 Subgrade reaction (elastic springs) model of soil

$$E_p I_p \left(\frac{d^4 y}{dz^4} \right) + k(z) y = 0 \tag{2.1}$$

where E_p is the modulus of elasticity of the pile material, I_p is the moment of inertia of the pile section, k is the modulus of subgrade reaction, z is the depth from the ground surface down the pile and y is the horizontal displacement of the pile shaft. Solutions to Equation 2.1 have been obtained by making simplifying assumptions regarding the variation of k (or E_s) with depth. The most common assumption is that E_s is constant with depth for clays and E_s varies linearly with depth for sands. Using the same parameters, Lee and Harrison (1970) determined the characteristics of a beam on a homogenous Winkler subgrade loaded at its tip using closed form solutions such as those developed by Hetenyi (1946). Reese et al. (2006) provided tables and charts that can be used to determine pile deflections, slopes, and moments as a function of depth and non-dimensional coefficients. Further research has extended the elastic springs by accounting for the following characteristics that are detailed in the following subsections:

- Using nonlinear springs to represent soil nonlinearity
- Gapping effects adjacent to the pile
- Effects of dynamic loading
- Pile-soil-pile interaction

2.3.1.2 Beam-on-nonlinear Winkler foundation

The next major development was to replace the elastic springs by nonlinear supports described by a family of specified curves called *p-y* curves that gives soil reaction (p) as a function of the lateral deflection of the pile (y). McClelland and Focht (1958) were the first to describe the *p-y* method for the analysis of laterally loaded piles. They proposed a procedure for correlating triaxial stress-strain data to a pile-deflection curve at discrete depths, and estimating the modulus of subgrade reaction at each layer.

The nature of *p-y* curves may be understood by referring to Fig. 2.4, where a slice of soil is examined (Reese et al. 2006). Figure 2.4(a) shows a section through a pile at depth below the ground surface. The behavior of a thin stratum of soil at a depth z_1 below the ground surface will be discussed. Figure 2.4(b) shows a possible earth pressure distribution around the pile after it has been installed and before the pile has been loaded laterally. If the pile is assumed to be

moved laterally through a distance y_1, the distribution of stresses after the deflection is symmetrical but no longer uniform as shown in Fig. 2.4(c). The stresses on the side in the direction of movement (front side) have increased, and those on the back side have decreased. The soil resistance p_1 is the force per unit length from the soil against the pile which develops as a result of the pile deflection.

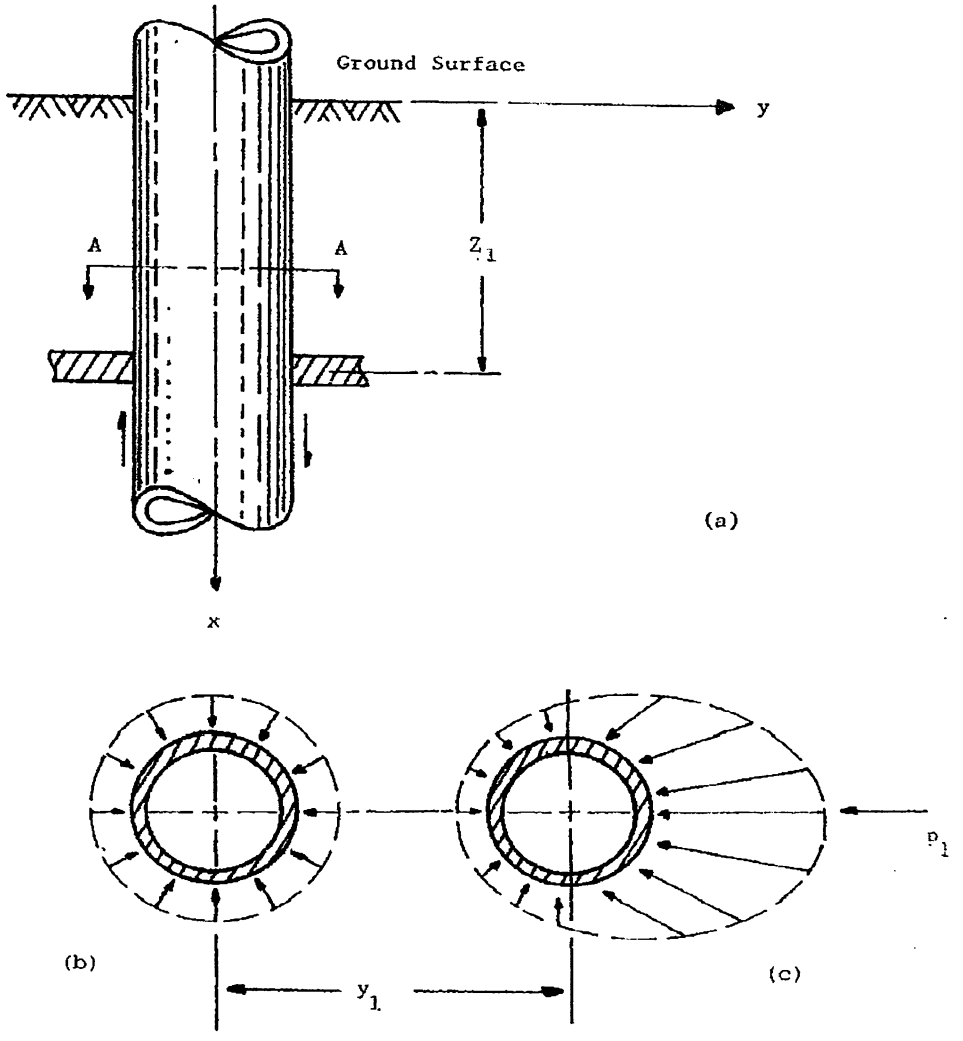

Fig. 2.4 Distribution of unit stresses against a pile before and after lateral deflection: (a) elevation view of section of pile, (b) earth pressure prior to lateral loading, (c) earth pressure after lateral loading (After Reese et al. 2006)

For a particular value of z below the ground surface, the value of p will vary with the deflection y of the pile and with the type of soil into which the pile is installed. A pile subjected to a lateral load is shown in Fig. 2.5(a). A possible shape of the deflected pile is shown in Fig. 2.5(b), along with a set of nonlinear mechanisms that serve to resist the deflection. A set of p-y curves is shown in Fig. 2.5(c), representing the response of the soil as simulated by the mechanisms (Reese et al. 2006).

The design procedures require the construction of p-y curves at different depths along the pile; these are then employed in computer calculations of the pile response under lateral load. The p-y curves for a given soil can be determined by back-figuring data from lateral load tests, as well as general procedures that were developed for constructing these relationships for a variety of soil conditions. Recommendations for the prediction of p-y curves will be presented here on clays and sands under both static and cyclic loading conditions. These recommendations are currently used in many designs.

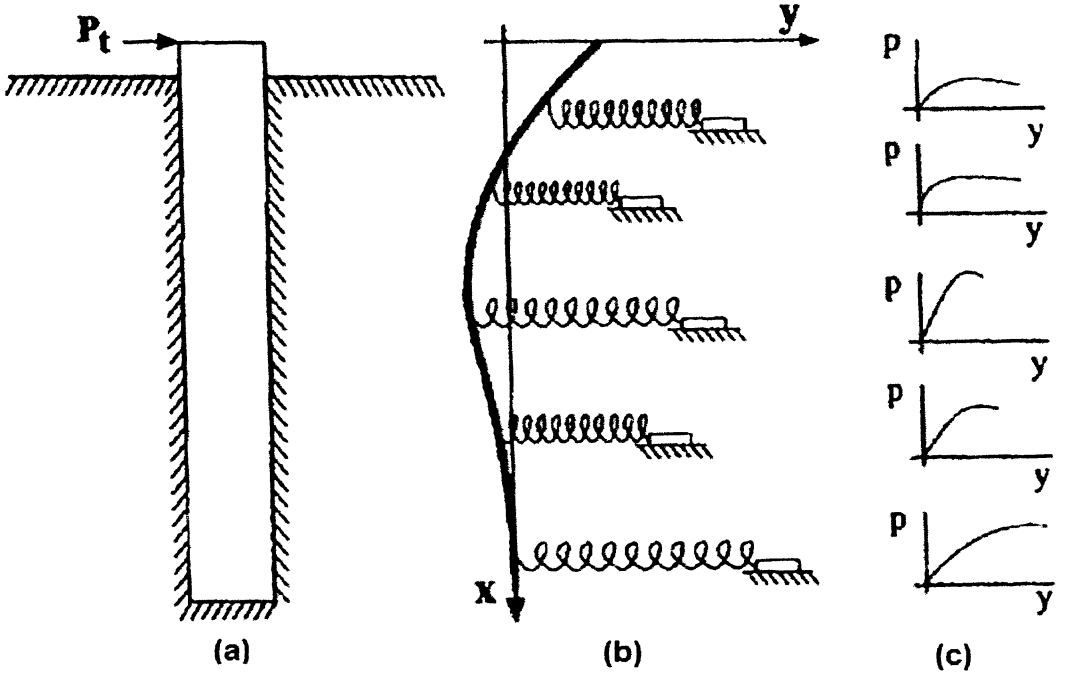

Fig. 2.5 Model of a pile subjected to lateral loading with a set of p-y curves: (a) pile under lateral loading, (b) soil-spring model, (c) p-y curves (After Reese 2006)

Soft clay p-y curves

The basic reference on this topic is a paper by Matlock (1970) which summarizes a great deal of an integrated field and laboratory work on which the semi-empirical analysis procedure is based. Matlock's study included static and cyclic lateral head loading on 0.3 m diameter instrumented steel pipe piles at two different soft clay sites at Lake Austin and Sabine, Texas, USA. *P-y* curves shown in Figs. 2.6(a) and (b) were back calculated from the test results for static and cyclic loading, respectively. The main difference between static and cyclic loading is that the soil resistance for cyclic loading at large strain levels is decreased.

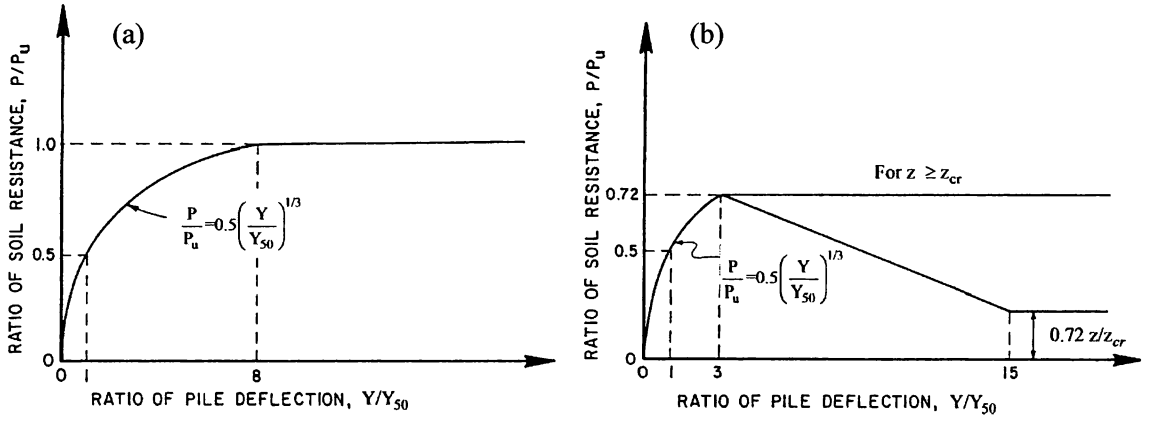

Fig. 2.6 Characteristic *p-y* curves for soft clay: (a) static loading, (b) cyclic loading (Matlock 1970)

The characteristic shape of the *p-y* curves for the static loading case can be represented by using a parabolic equation as:

$$\frac{p}{p_u} = 0.5\left(\frac{y}{y_{50}}\right)^{1/3} \tag{2.2}$$

where p is the lateral soil resistance, p_u is the ultimate soil resistance, y_{50} is the critical pile deflection (y_{50} =2.5 ε_{50} D), ε_{50} is the strain at one-half maximum deviator stress in a UU triaxial compression test, and z_{cr} is the critical depth where soil wedge failure transforms to flow failure.

Matlock (1970) recognized that the *p-y* curves are independent on pile-head fixedly and highly nonlinear and inelastic, with characteristic pile bending moment patterns as shown in Fig.

(2.7). Matlock (1970) concluded that static and cyclic nonlinear soil-pile response is most severe at shallow depths, and approaches linear response at greater depths. After a large number of cycles of loading and degradation of resistance, the soil-pile system tends to stabilize (a condition known as "shakedown").

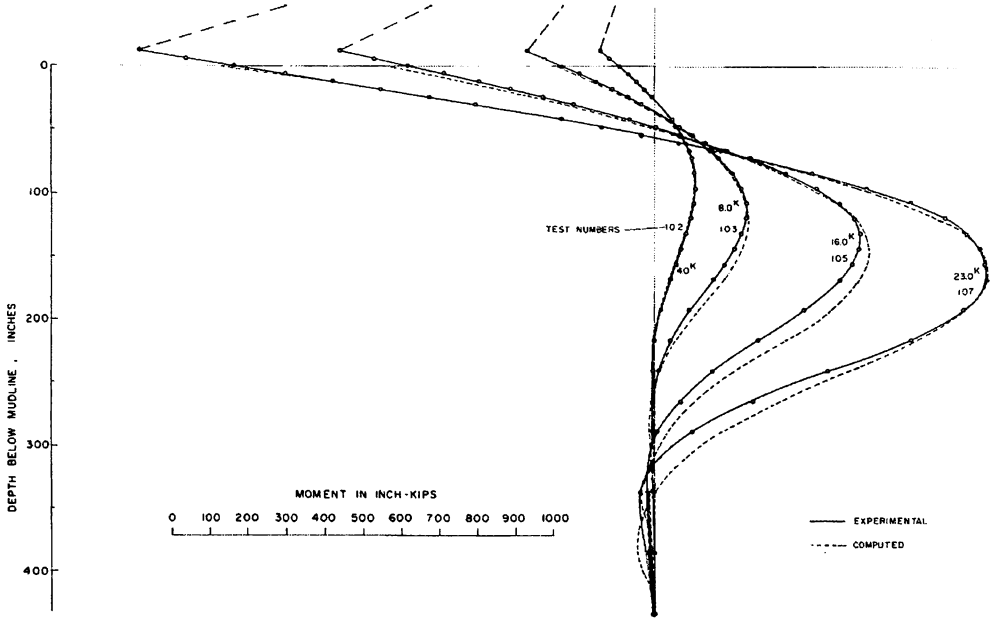

Fig. 2.7 Characteristic fixed head laterally loaded pile bending moment pattern (after Matlock 1970)

This method is codified in the API (American Petroleum Institute) Recommended Practice (API, 1993) and is the established criterion for laterally loaded pile analysis in soft clays in the nearly ubiquitous computer program COM624P (Reese 1984).

Stiff clay p-y curves below the water table

Figures 2.8(a) and (b) show the characteristic shape of *p-y* curves for both static and cyclic loading, respectively obtained from a lateral load tests performed by Reese et al. (1975) with steel pipe piles that were 0.641 m in diameter and 15.2 m long. The piles were driven into stiff clay at a site near Manor, Texas, USA. The same parameters used in the soft clay *p-y* curves are used to describe the characteristic shape of the stiff clay *p-y* curves. This comprises the currently recommended API design curve for stiff clay. Guidelines for computing the ultimate soil

resistance P_u, the static and cyclic stiffness parameters k_s and k_c, and the empirical A and B factors were given.

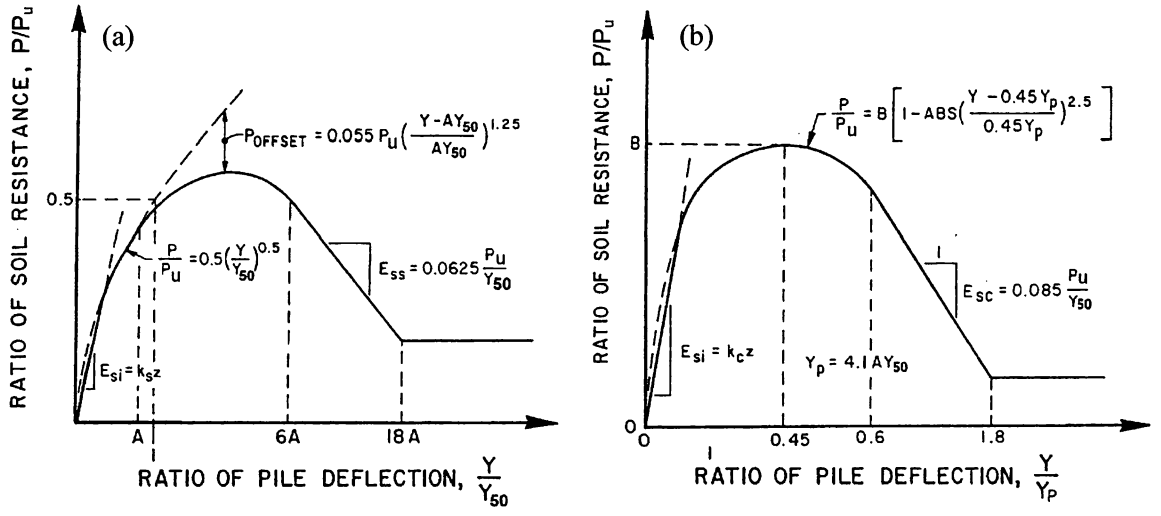

Fig. 2.8 Characteristic p-y curves for stiff clay below the water table: (a) static loading, (b) cyclic loading (after Reese et al. 1975)

Stiff clay p-y curves above the water table

Figures 2.9(a) and (b) show the characteristic shape of *p-y* curves for both static and cyclic loading, respectively based on lateral load tests on a 0.76 m diameter bored pile in stiff clay above the water table at a site in Houdton Texas, USA (Welch and Reese 1972). In Fig. 2.9(b), N is the number of cycles of load application, C is the parameter describing the effect of repeated loading on deformation, y_c is the deflection under N cycles of the load, and y_s is the deflection under static load.

Sand p-y curves

Cox et al. (1974) carried out an experiment on two 0.6 m diameter, flexible driven piles embedded in a deposit of submerged, dense, fine sand. Reese et al. (1974) used the results of the above experiment to develop a procedure for obtaining *p-y* curves for sands. The characteristic shape of the *p-y* curve is composed of 3 straight lines and a parabolic curve (Fig. 2.10). In this approach, the initial modulus of subgrade reaction and ultimate soil resistance are needed to develop *p-y* curves. Reese et al. (1974) suggested suitable values for the initial modulus of

subgrade reaction for different relative density of sands. *P-y* curve developed by Reese et al. (1974) is the currently recommended API design curve in sand.

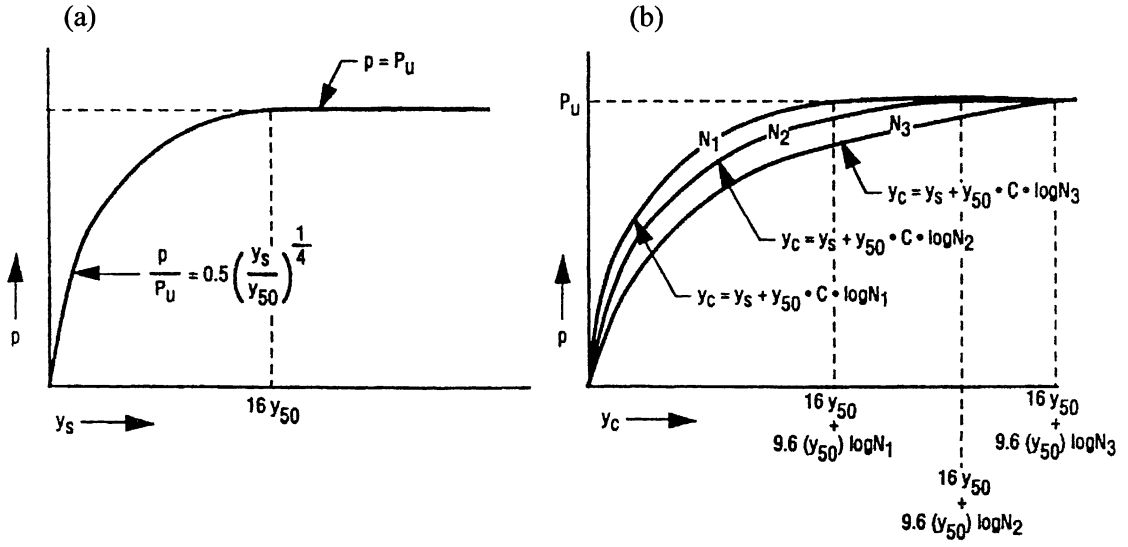

Fig. 2.9 Characteristic *p-y* curves for stiff clay above water table: (a) static loading, (b) cyclic loading (after Welch and Reese 1972)

Reliability of the p-y curves

O'Neill and Murchison (1983) carried out a systematic evaluation of the reliability of *p-y* relationships in sands and compared the predictive accuracy of three methods against a set of pile load test data. The methods tested included the segmented curve of Reese et al. (1974), a modification suggested by Bogard and Matlock (1980), and a continuous hyperbolic tangent curve described by Parker and Reese (1970). Their study included 24 full-scale tests on piles in cohesionless soils; 14 static tests and 10 slow cyclic tests. The site conditions varied from very loose clayey sands to very dense sands. The hyperbolic curve proved to be the best of the set for both static and cyclic loading. The form of the *p-y* curve is given by:

$$p = Ap_u \tanh\left(\frac{kzy}{Ap_u}\right) \tag{2.3}$$

where A is a constant depending on the loading being static or cyclic loading, k is the modulus of subgrade reaction, z is depth, and p_u is the ultimate lateral resistance.

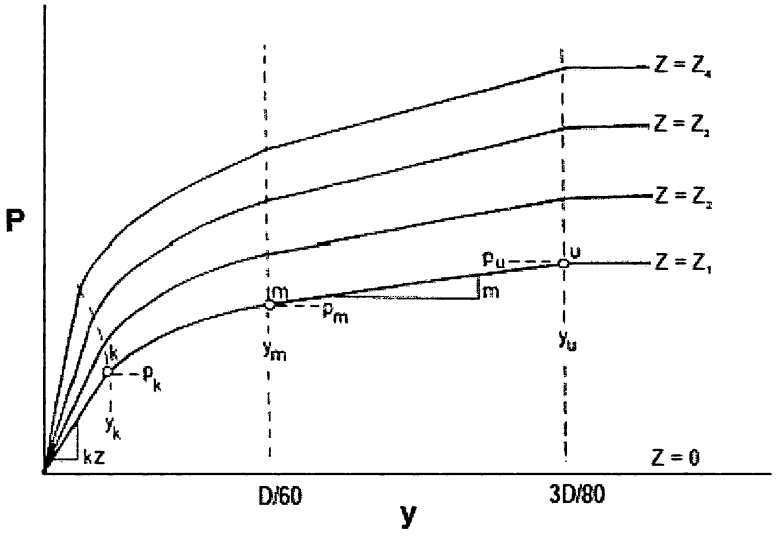

Fig. 2.10 Characteristic *p-y* curves for sand (After Reese 1974)

Although the hyperbolic curve is the best of the set, gave poor predictions with large errors. As a result of their study, O'Neill and Murchison (1983) concluded that the API curves were not adequate for the analysis of static or slow cyclic loading tests. They stated that "*It is likely that other factors, not included in the p–y formulation are operative and this observation suggests that further study into the fundamental mechanisms of lateral pile–soil interaction in cohesionless soils is warranted.*" One obviously missing fundamental mechanism is shear transfer between the springs.

Gazioglu and O'Neill (1984) carried out a similar evaluation of the *p–y* relationships proposed for use in cohesive soils with similar results. After studying 30 full-scale tests in clayey soils; 21 static and 9 slow cyclic tests, they concluded that "– *the confidence in predicting deflections and moments – is unfortunately rather poor*".

2.3.1.3 Gapping effects adjacent to the pile

Matlock (1970) reported from the full-scale tests of lateral loaded piles at soft clay sites that a principle effect of cyclic loading appears to be the permanent physical displacement of the soil away from the pile in the direction of loading. Anagnostopoulos (1983) and Prater (1979) describe a range of methods for generating *p-y* curves for soft to stiff clays and some sands based on previous investigations. Cyclic and monotonic *p-y* curves are investigated with the inclusion

of a gap formation in some clay. Soil degradation or "shakedown" is incorporated into some *p-y* models which are dependent on the number of cycles of loading and strain amplitude of the soil elements. Matlock et al. (1978) and Swane and Poulos (1984) used the Winkler model to represent the gapping phenomenon, modeling the foundation system as two series of detachable Winkler springs on either side of the pile. The soil adjacent to the pile was modeled with zero tensile strength, therefore when the force in a spring element reduced to zero, the spring detached from the foundation element. The element reattached when the forces in the soil were no longer tensile. Once detached, the spring no longer had any influence in the system, as would be the case when gapping occurs. Swane and Poulos identified that during cyclic loading a stable gap length may be generated where there is no further reduction in pile stiffness or growth in gap length. Pender and Pranjoto (1996) updated a nonlinear soil-pile interaction model originally proposed by Carter (1984) to include the effects of gapping. Compression-only springs were attached to both sides of the pile, preloaded to reflect the effects of pile installation, and provided with the ability to detach and form a gap when the spring force reached zero. A hyperbolic form of the nonlinear spring stiffness was adopted, defined by initial stiffness and ultimate resistance parameters. This model neglected the effect of soil damping on the behavior of the foundation system. Soil-pile gap was considered by other researchers in their analyses using the beam in Winkler foundation approach (e.g., Mostafa and El Naggar 2002; Allotey and El Naggar 2008).

2.3.1.4 Beam-on-dynamic Winkler foundation

Analysis of piles under dynamic loading requires definition of the stiffness and damping characteristics of the soil-pile system. Several methods have been developed to determine these characteristics which are functions of the loading frequency (Gazetas and Dobry 1984; Novak et al. 1978; Randolph 1977). Material damping dissipates energy due to hysteretic action in the soil and radiation damping dissipates energy by radiating it away from the soil. Damping effects have been included in the Winkler models using dashpot elements attached to the pile using methods similar to the spring elements (Wotherspoon 2009).

Penzien et al. (1964) were some of the first researchers to present a method for seismic pile response analysis, and focused their efforts on the problem of bridge structures supported on long piles driven through soft clays. They constructed a multi-degree of freedom discrete parameter system for modeling the soil medium response initiated by seismic base excitation.

This response then served as the input for the response analysis of the discrete parameter structural system. Bilinear springs afforded nonlinear hysteretic soil response, with parallel and series dashpots provided for soil damping and creep, respectively, and lumped masses to contribute soil inertial effects. The conclusions of their study regarding site response, pile curvature demands, and superstructure ductility, all remain valid to this day (Meymand 1998).

Nogami and Konagai (1988) and Nogami et al. (1988) have developed a time domain analysis method for flexural response of single piles based on the frequency domain solution developed by Novak et al. (1978) as shown schematically in Fig. 2.11. Nogami et al. (1991) accounted for the soil nonlinearity by introducing a multi-linear element for the inner field, and a gap element with a pre-estimated factor to account for plastic deformations and gap opening at the soil-pile interface. Nogami et al. (1992) developed a rational dynamic soil-pile interaction model adopting Winkler's hypothesis with the consideration of nonlinearity in the vicinity of single piles. The model uses frequency independent mass, springs, and dashpots and uses direct time-domain analysis to predict lateral response due to pile-head loading or prescribed displacement at the pile-head. Either the static behavior of the soil-pile system or static *p-y* curves is used as initial soil-pile properties. With the consideration of a gap formation at the soil-pile interface, the model can successfully predicts the pile response observed in dynamic load tests in the field. The study is limited to a single pile case. El-Naggar and Novak (1995) developed a computationally efficient time domain model as shown in Fig. 2.12 for the lateral response analysis of piles. In their model, the piles are assumed to be elastic, vertical, and embedded in a nonlinear horizontally layered soil. Based on the Winkler hypothesis, the soil is divided into a number of layers. In each layer the soil model consists of two regions; the first region is an inner field to which nonlinearity is confined, and the second region is a linear viscoelastic far field which accounts for wave propagation away from the pile. In the lateral response model, the soil reactions at both sides of the pile are modeled separately to account for the state of stress and discontinuity conditions (i.e. allowing for gap forming or closure automatically) at both sides as the load direction changes.

2.3.1.5 Pile group effects

Piles are very rarely isolated but are usually put into pile-groups. If piles are arrayed in groups with large pile-to-pile spacing (greater than 6-8 pile diameters), pile group interaction effects are

normally ignored for static loading as shown in Fig. 2.13. But this may be an inaccurate approach for dynamically loaded piles, as much of the pile group interaction effects arise from wave energy reflected between neighboring piles, which does not attenuate as rapidly as static loading pile group interaction. Pile group dynamic response is also a function of load level; many of the group analysis methods that will be described address small strain elastic response, and few researchers have investigated nonlinear pile group interaction. There is evidence however to suggest that pile group effects lessen with increasing soil-pile nonlinearity, which inhibits wave energy transmission between piles (Meymand 1998).

The springs, which were developed to model single soil-pile interaction, are not applicable directly to pile groups because the over-lapping displacements fields of piles in the group affect the individual pile stiffness. A solution for this difficulty was developed by Poulos (1971). He used interaction factors to quantify the incremental deformation of one pile due to the presence of a similarly loaded neighboring pile. He described interaction factor as:

$$\alpha = \frac{\text{additional displaceme nt (rotation)due to adjacent pile}}{\text{displacement (rotation)of pile due to its own loading}} \tag{2.4}$$

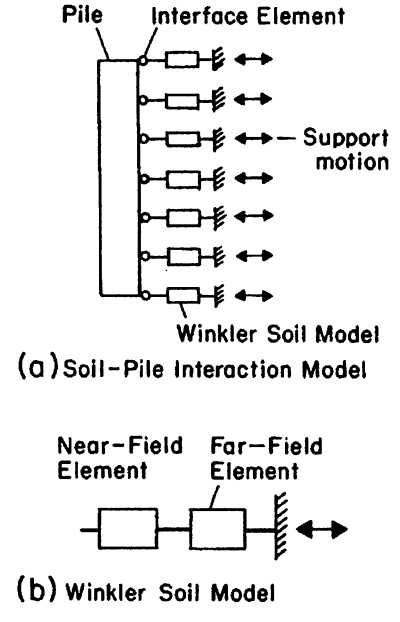

Fig. 2.11 Nogamai's beam-on-Winkler foundation soil-pile interaction model (after Nogamai et al., 1988)

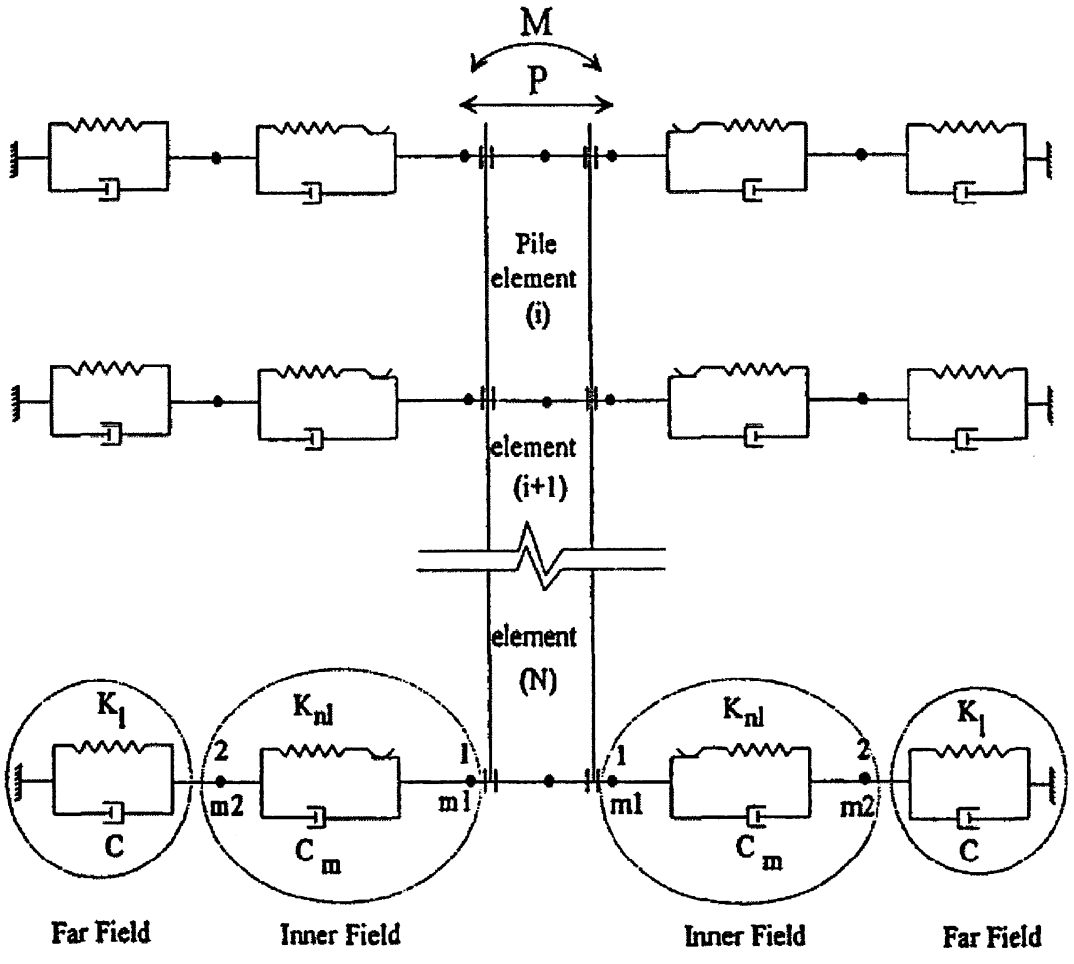

Fig. 2.12 Elements of the proposed model for nonlinear dynamic analysis of lateral response of single piles. (after El-Naggar and Novak 1995)

He presented charts of α factor for both fixed and free-head piles subject to lateral and moment loadings as functions of pile flexibility, pile spacing, pile diameter, pile length, and departure angle (angle between piles and direction of loading). Analysis of groups was accomplished by superposition, calculating each pile's interaction with all other piles in the group, and ignoring the presence of intervening piles.

Randolph (1981) greatly simplified the use of interaction factors by developing simple equations for the interaction between fixed-head piles, which is generally the most relevant interaction factor in engineering practice. For a while, the state of best practice was to use

nonlinear *p-y* curves for the individual piles in the group and describe the interaction between the piles by elastic interaction factors.

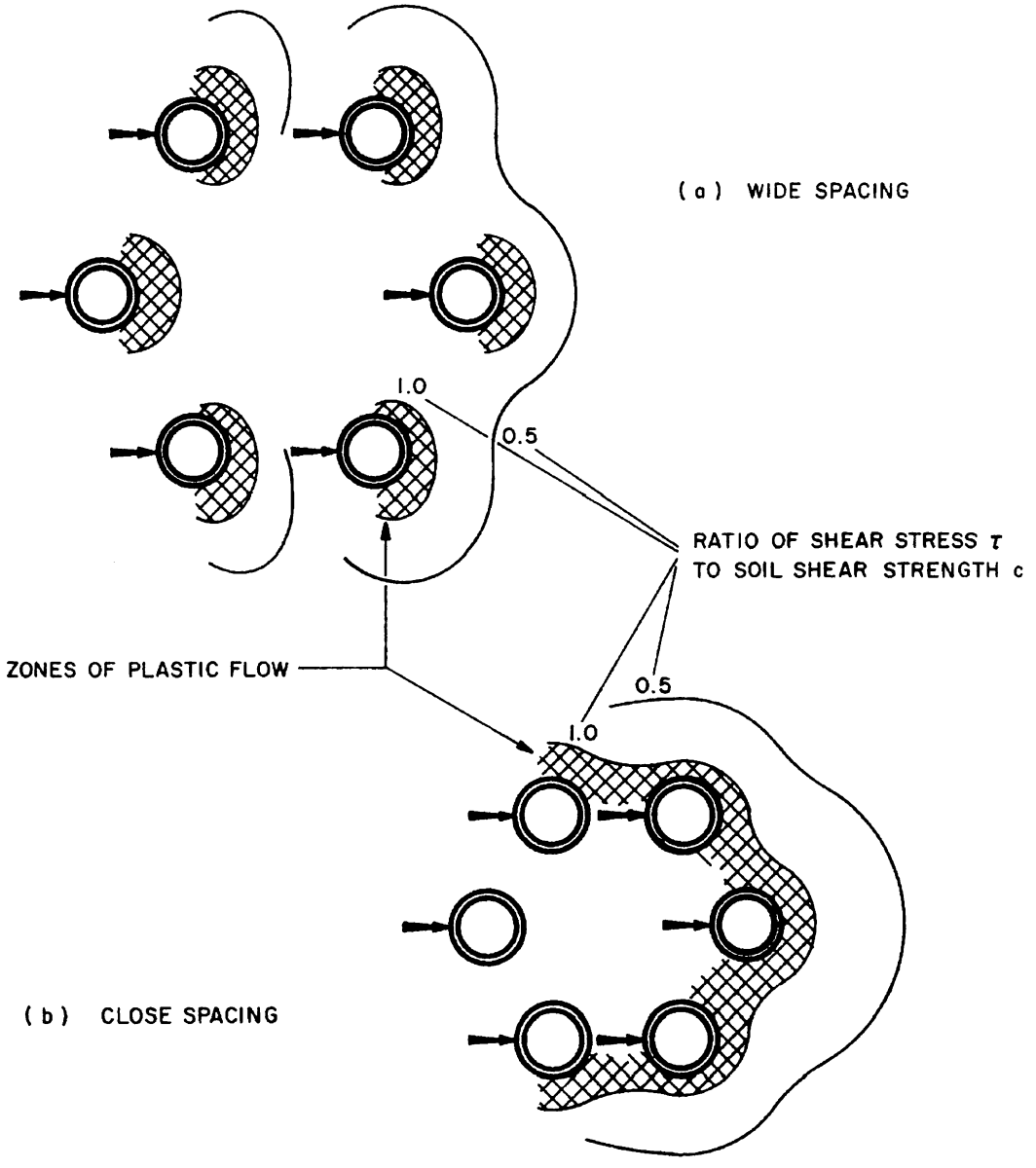

Fig. 2.13 Pile Group Interaction as Function of Pile Spacing (after Bogard and Matlock, 1983)

The second approach to the analysis of group response uses *p*-multipliers (Brown et al. 1987 and 1988). The *p*-multiplier is a reduction factor that is applied to the *p*-term in the *p-y* curve for a single pile to simulate the behavior of piles in the group. These reduction factors are a function of pile spacing and orientation to loading, and are implemented in the pile group analysis program GROUP (Reese et al., 1996). For the 3×3 group, Pinto et al. (1997) found the multipliers to be 0.8, 0.45 and 0.3 for the leading, middle and trailing rows respectively of piles in sand with a relative density of 55%. Brown and Bollman (1996) recommend the factors in Table 1.1 for design. The factors are representative of significant pile-head displacements of the order of 10% of the pile diameter.

Rollins et al. (1998) backfigured *p*-multipliers from their full-scale test in clay to be 0.6, 0.38 and 0.43. These multipliers are at the low end of the *p*-multipliers obtained from other available full-scale tests and the third row shows a higher multiplier than the second row. Clearly *p*-multipliers and group efficiencies are quite dependent on site conditions, soil types and the details of stratification. A very significant finding from the Rollins test is that the bending moments in piles in the group were 50–100% higher than in the single pile and that the location of maximum moment was deeper.

Table 1.1 *p*-multipliers for pile group design (after Brown and Bollman, 1996)

Row spacing	Front row	2nd row	3rd and more rows
3 pile diameter	0.8	0.45	0.35
4 pile diameter	0.9	0.65	0.55
5 pile diameter	1.0	0.85	0.75

The studies on the dynamic impedance of groups have shown that the dynamic characteristics of groups are very complex and they are strongly dependent on frequency, and different from the values obtained for single piles due to pile-soil-pile interaction. For high and middle frequency values Novak (1991) and Gazetas et al (1993) suggest ignoring the interaction pile-soil-pile and to consider the static interaction factor.

Kaynia and Kausel (1982) derived dynamic interaction factors for floating pile group interaction analysis by combining a numerical integration for the evaluation of the influence coefficients with an analytical solution for the pile stiffness and flexibility matrices. This BEM

computed Green's functions from imposed barrel and disk loads in a homogeneous soil medium, and used a consistent stiffness matrix to account for the far field. Their interaction factors were presented as complex-valued frequency dependent ratios of the dynamic displacement of pile i to the static displacement of pile j, due to a unit harmonic load on pile j. Vertical and horizontal interaction factors are shown in Fig. 2.14, demonstrating positive and negative group efficiencies. Normalized dynamic stiffness and damping of a 4x4 pile group for different spacing is shown in Fig. 2.15, indicating the strong frequency dependence of dynamic group response. They also derived expressions for the distribution of forces over the pile group (see Fig. 2.16), which was shown to vary from static loading force distributions. Other important conclusions from this study were that the superposition technique is valid for dynamic pile group solutions (in homogeneous soil), pile groups are less influenced by near-surface ground conditions than isolated piles, group interaction effects are stronger for softer soil, and radiation damping increases with foundation size. Dobry and Gazetas (1988) presented a simplified method for calculating dynamic pile interaction factors in homogeneous soil by assuming that cylindrical wave propagation governs vibration of source piles and displacement of neighboring piles. Fan and Gazetas (1991) studied pile group kinematic interaction effects, and as shown in Fig. 2.17, the generalized pile-head to free-field transfer function illustrates the pile group effect in filtering out high frequency components of motion. They found that pile group configuration and spacing have little influence on kinematic response, as pile-head fixity and relative soil-pile stiffness play a stronger role. Gazetas and Makris (1991) and Makris and Gazetas (1992) developed simplified methods of analysis for pile group axial and lateral dynamic response, respectively (see Fig. 2.18). Using a dynamic Winkler model, they found pile group effects to be more pronounced for inertial than kinematic loading. The substructuring approach unifying the kinematic and inertial analyses is described in Gazetas et al. (1992), and is shown schematically in Fig. 2.19. Mylonakis et al. (1997) applied this substructuring approach in an equivalent linear method to analyze pile supported bridge piers (Meymand 1998).

2.3.2 Continuum approach

2.3.2.1 Elastic continuum

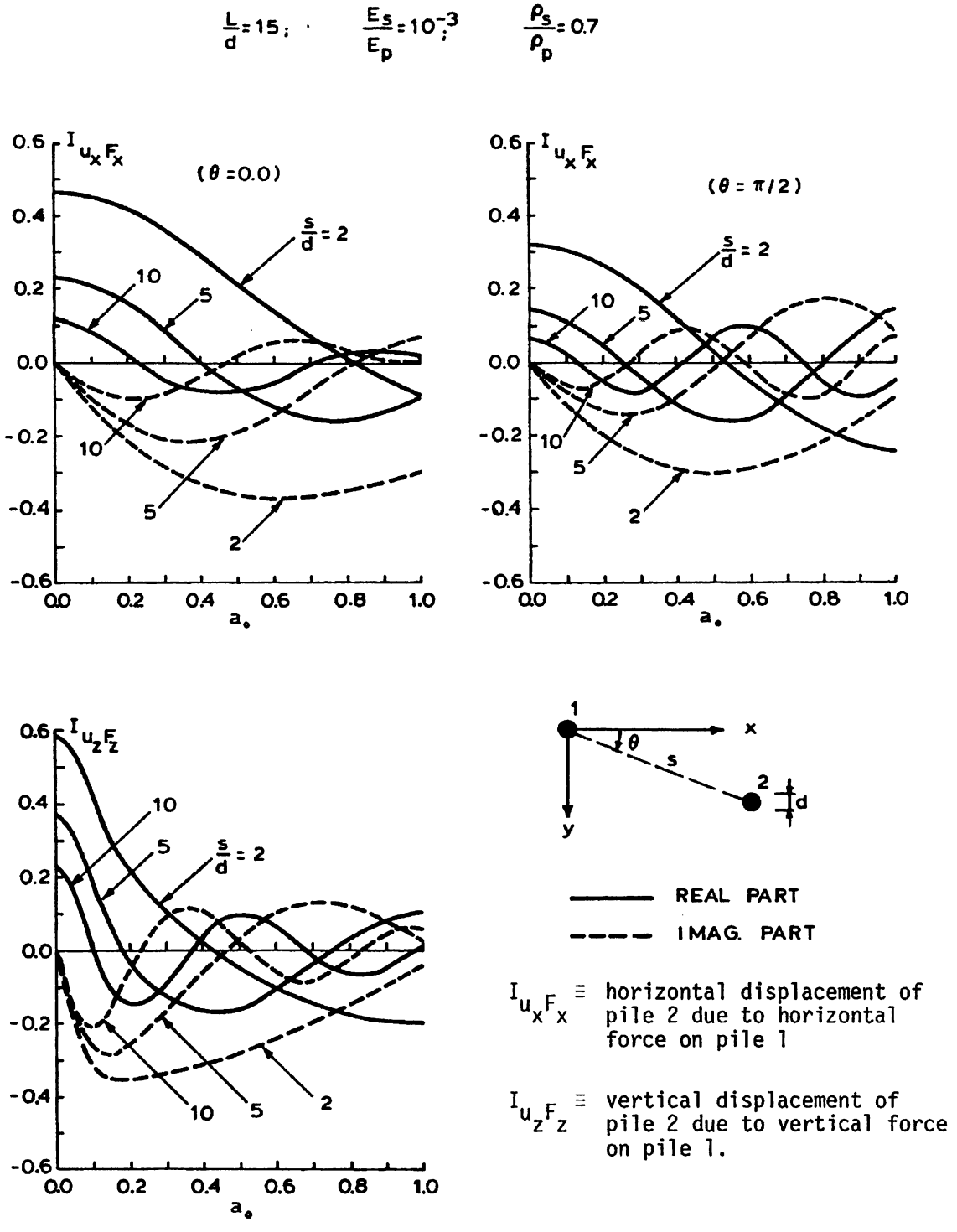

Fig. 2.14 Vertical and horizontal dynamic pile interaction factors (after Kaynia and Kausel, 1982)

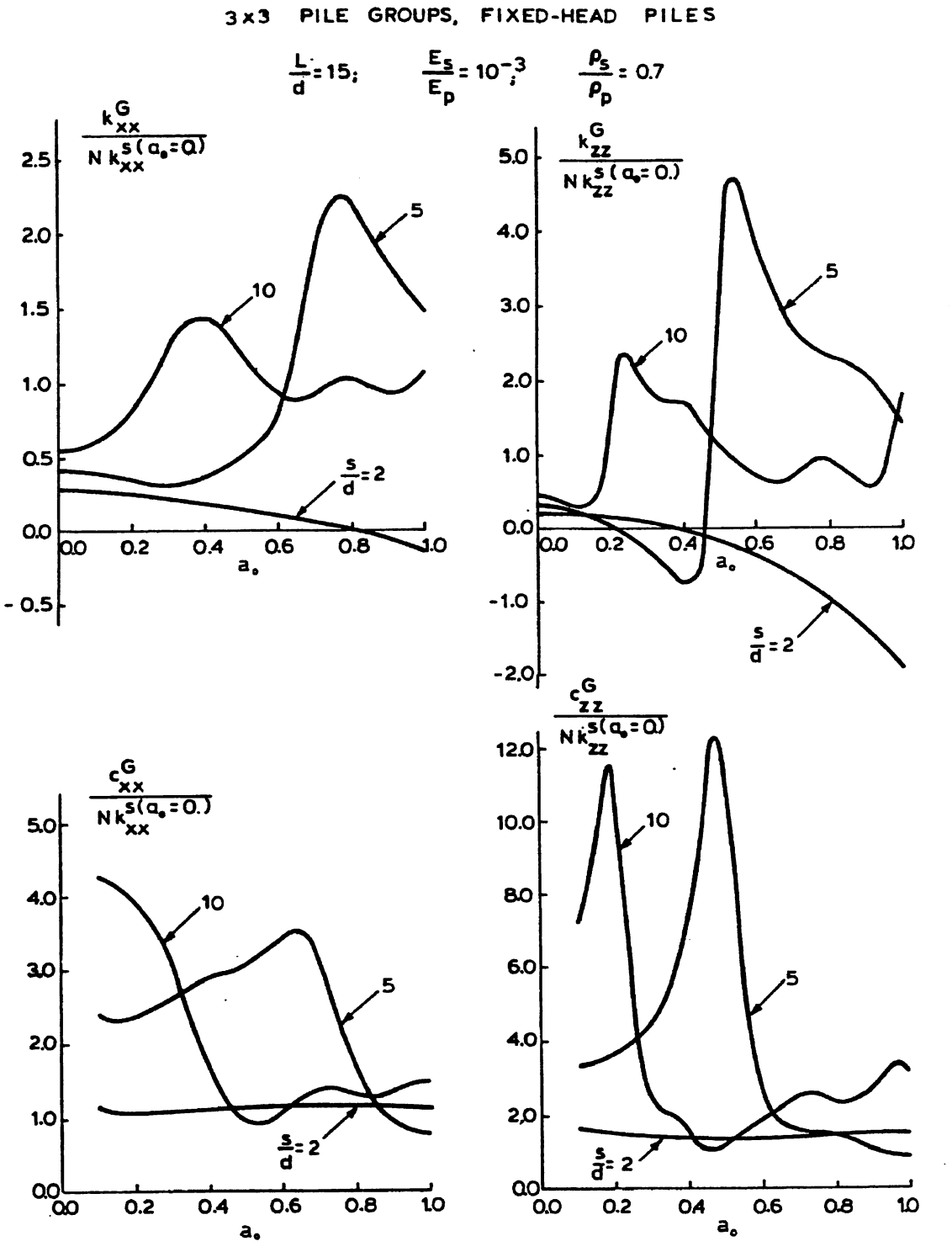

Fig. 2.15 Normalized horizontal and vertical dynamic stiffness and damping of 3x3 pile group in soft soil (after Kaynia and Kausel, 1982)

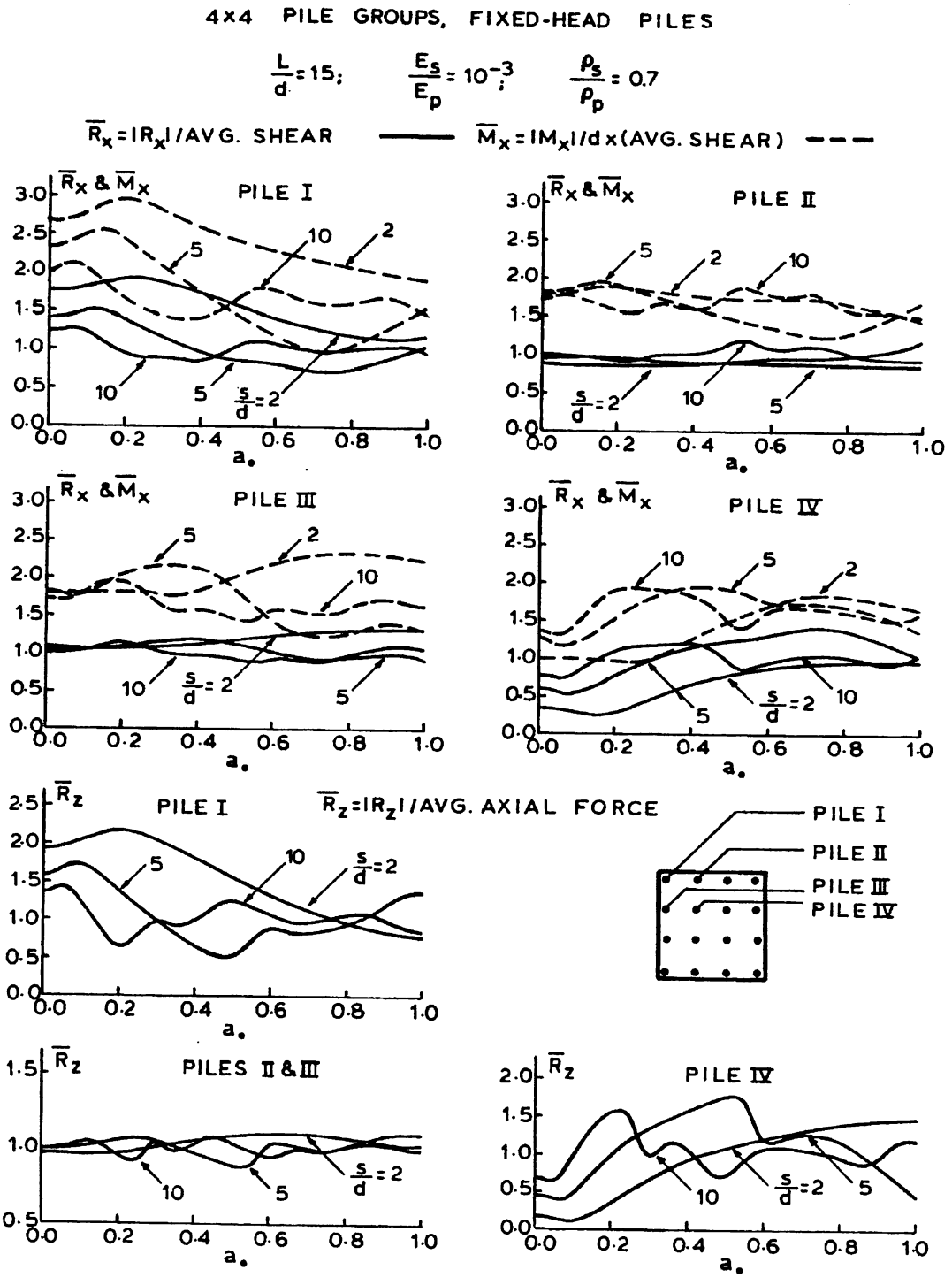

Fig. 2.16 Distribution of horizontal and vertical forces in 4x4 pile group in soft soil medium (after Kaynia and Kausel, 1982)

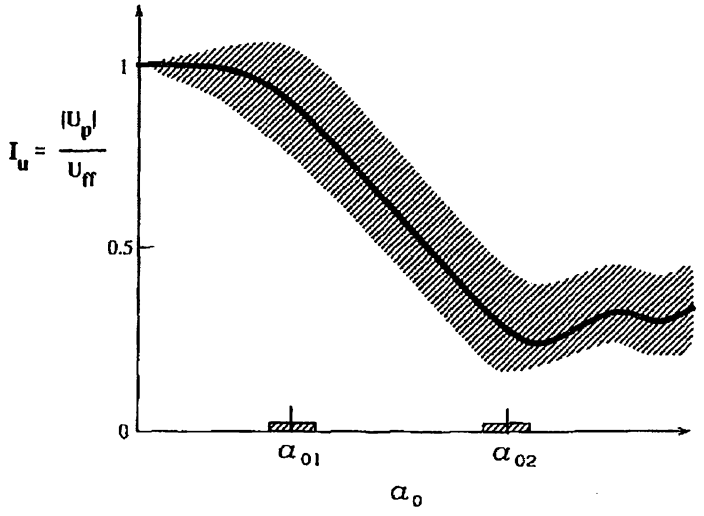

Fig. 2.17 Generalized pile-head/free-field transfer function for kinematic interaction (after Fan and Gazetas, 1991)

The elastic continuum method for pile foundations is based on the work of Mindlin (1936). The pile is idealized as a thin beam, with horizontal pile deflections evaluated from integration of the classic Mindlin equation for horizontal subsurface loading. The Mindlin equation is used to solve for horizontal displacements caused by a horizontal point load within the interior of a semi-infinite elastic-isotropic homogeneous mass. Solutions are obtained by integrating the equation over a rectangular area within the mass. The accuracy of these solutions is directly related to the evaluation of the Young's modulus and the other elastic parameters of the soil. Also layered soil properties cannot be included and instead solutions for constant (Davies and Budhu 1986), linearly increasing (Budhu and Davies 1988), and parabolic variation (Gazetas 1991) of soil modulus with depth have been derived. True continuum models do have the advantage of intrinsically modeling the effects of radiation damping, whereas discrete models must artificially simulate this energy dissipation mode.

The first representations of soil-pile interaction using the elastic continuum theory were described by Tajimi (1969). Tajimi (1969) used a linear Kelvin-Voigt visco-elastic stratum to model the soil. Tazoh et al. (1988) modified and extended the work of Tajimi (1969) to include superstructure inertial effects.

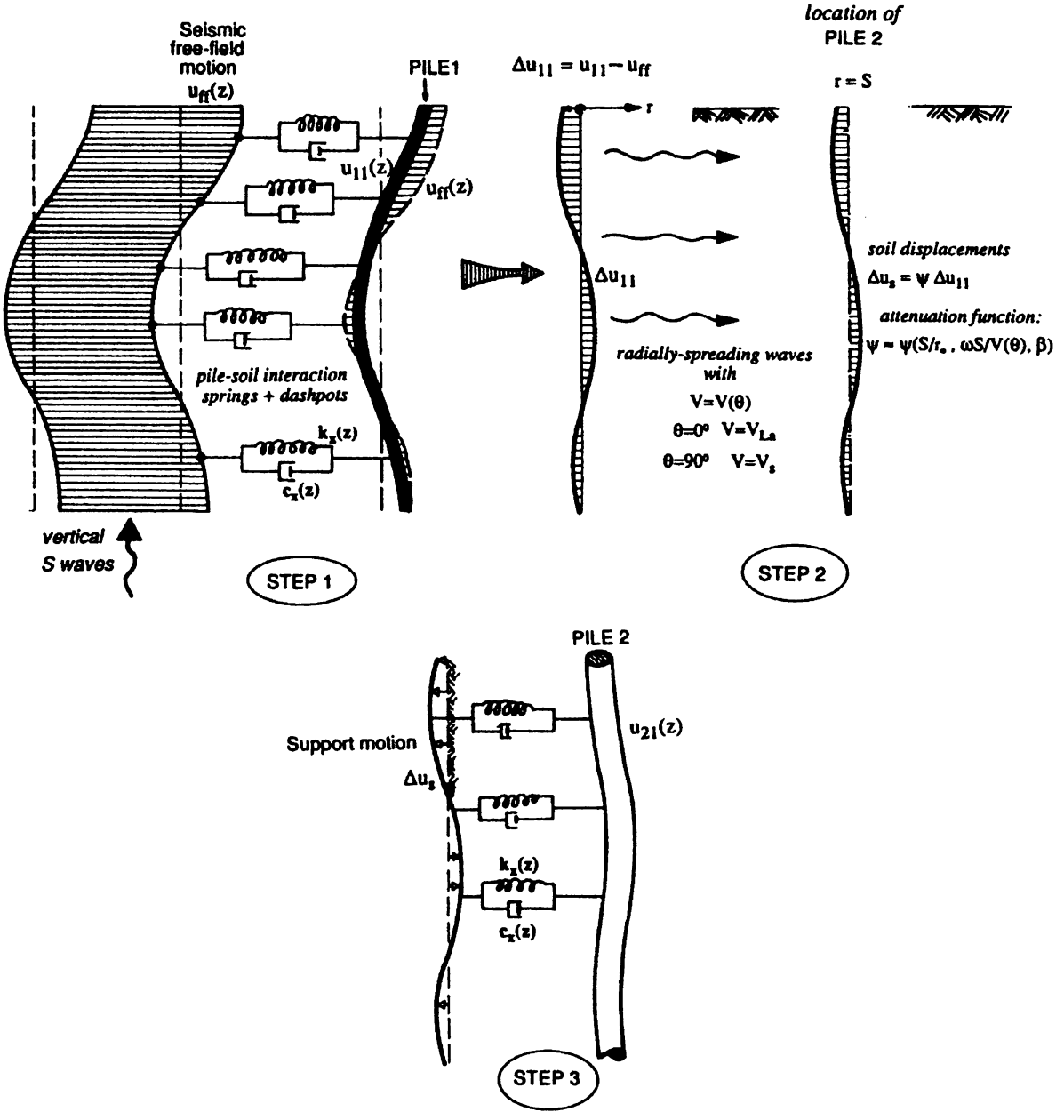

Fig. 2.18 Schematic of three-step procedure for computing pile-soil-pile interaction (after Makris and Gazetas, 1992)

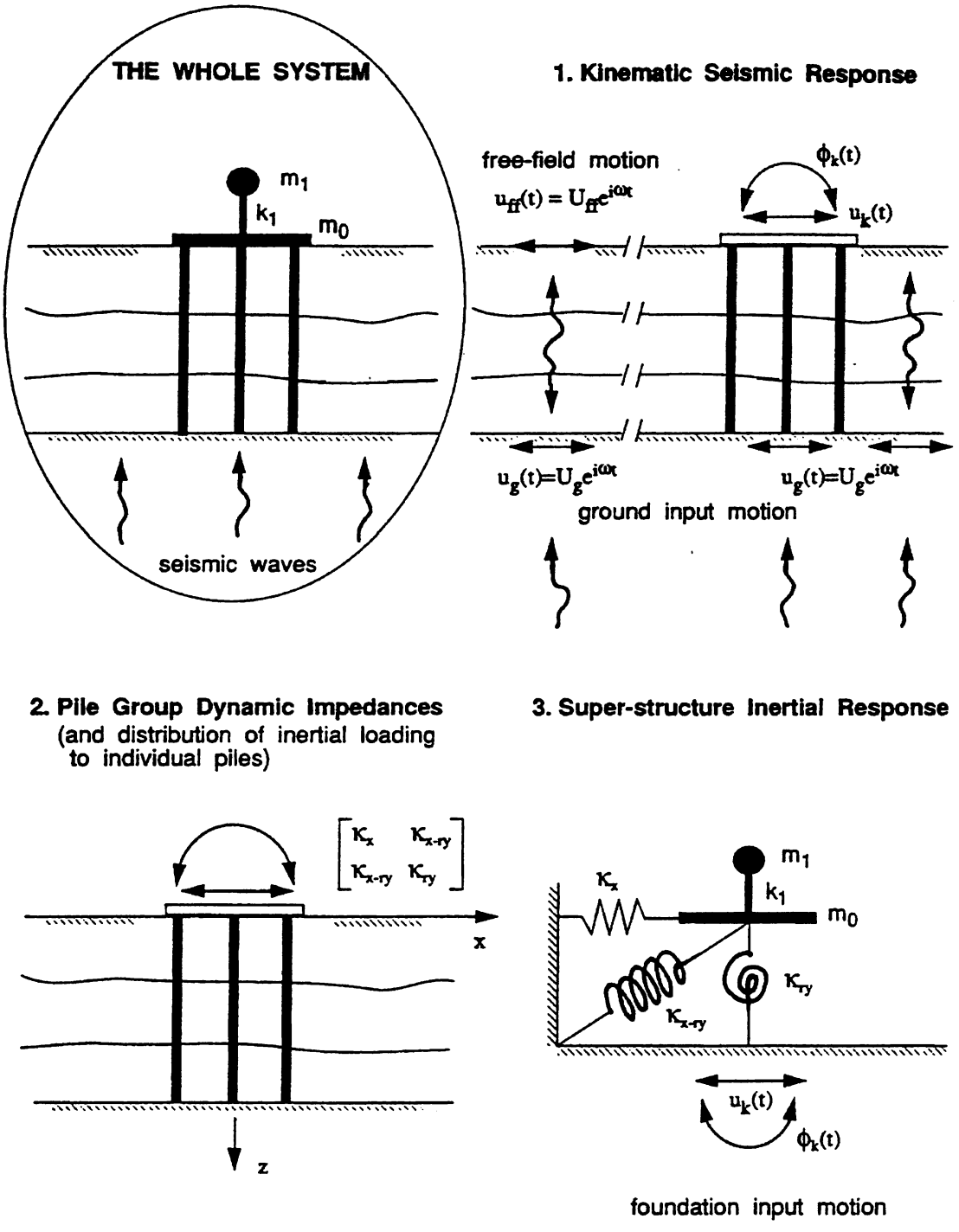

Fig. 2.19 Substructuring method for seismic soil pile superstructure interaction analysis (after Gazetas et al., 1992)

Poulos (1971a, b) presented the first systematic approach for analyzing the behavior of laterally loaded piles and pile groups using the theory of elasticity. Poulos and Davis (1980) used the elastic continuum approach to present a comprehensive set of analysis and design methods for laterally loaded piles. The approach assumes that both the pile and the soil have elastic properties, and flexibility coefficients were used to determine displacements of the pile-head due to applied loads. Solutions were provided for different functions of soil modulus versus depth below the ground surface. Poulos (1982) described a procedure for degradation of soil pile resistance under cyclic lateral loading and compared it to several case studies.

Characterization of the radiation damping of a pile foundation has been carried out by multiple researchers. Berger et al. (1977) assumed that a pile moving horizontally would generate only one dimensional (1D) P-waves in the direction of shaking and 1D S-waves perpendicular to shaking as indicated by Fig. 2.20(a).

Novak et al. (1978) proposed his thin slice elasto-dynamic solution in which a rigid cylindrical rod representing the pile is surrounded by soil that extends to infinity. Horizontal and vertical oscillations were applied to the system to determine its characteristics. The form of their solution to the radiation damping characteristics is shown in Fig. 2.20(b).

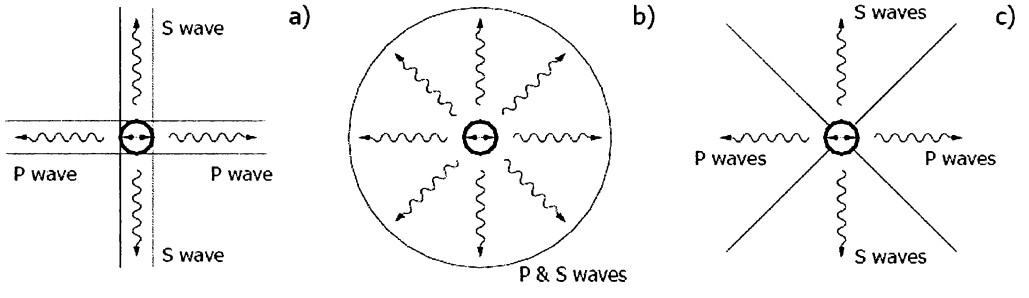

Fig. 2.20 Radiation damping of a horizontally vibrating pile a) Berger et al. 1977; b) Novak et al. 1978; c) Gazetas and Dobry 1984.

Gazetas and Dobry (1984) discuss the radiation damping and hysteretic action that is created in soil deposits due to dynamic loading and developed elastic solutions for lateral pile vibration. The energy developed from wave propagation increased damping due to the flexibility of the system, and the soil allowed for the radiation of energy away from the structure. Their solution is much simpler than that of Novak et al. (1978) and assumes that compression-

extension waves develop in the two quarter planes in the direction of shaking and shear waves in the planes perpendicular to shaking. This is indicated in Fig. 2.20(c), in which Lysmer's wave velocity is used instead of the compression wave velocity.

2.3.2.2 Finite element methods

The FEM potentially provides the most powerful means for conducting SSI analyses, but is has not yet been fully realized as a practical tool. The advantages of a FEM include the capability of performing the SSI analysis of pile groups in a fully-coupled manner, without resorting to independent calculations of site or superstructure response, or application of pile group interaction factors. It is of course possible to model any arbitrary soil profile, and to study 3D effects. Challenges to successful implementation of this technique lie in providing appropriate soil constitutive models that can model small to very large strain behavior, rate dependency, degradation of resistance, and still prove practical for use. Special features to account for pile installation effects and soil-pile gapping should also be implemented (Meymand 1998).

Yegian and Wright (1973) and Thompson (1977) were some of the first to implement FEM in the study of pile behavior using a 2D model. Yegian and Wright used a nonlinear soil representation to model the lateral displacement characteristics of pile foundations in soft clays. Thompson compared full-scale testing results to models using nonlinear soil materials, obtaining good agreement between the two near the ground surface. Emery and Nair (1977) studied an axisymmetric FEM that incorporated non-symmetric free-field acceleration boundary excitations from wave propagation analyses. Randolph (1977 and 1981) developed 3D FEM in conjunction with Fourier techniques. These models used linear soil elements and were used to develop simple design charts. Kay et al. (1983) promoted a site-specific design methodology for laterally loaded piles consisting of pressuremeter test data as input to an axisymmetric FE program. Lewis and Gonzalez (1985) compared field test results of drilled piers to a 3D FE study that included nonlinear soil response and soil-pile gapping.

As computers have become more powerful FEM has become more viable as an analysis method. Nonlinear 3D modeling was used in research by (Brown and Shie 1990 and Trochanis et al. 1991), and has indicated a good comparison between FE results and experimental studies. Brown and Shie used elasto-plastic soil models to develop p-y curves for comparison with field test results. Trochanis et al. used a yield surface soil model in their simplified analysis of the

lateral response of piles during monotonic and cyclic loading. Anandarajah and Zhang (2000) developed a simplified FEM to analyze the nonlinear dynamic pile-soil interaction for a single pile. This model was verified with data from a centrifuge test performed by Wilson (Wilson 1998, Boulanger, et al. 1999). This analysis was performed using the fully coupled method (Zienkiewicz and Shiomi 1984), where deformation and pore water pressure variations were simulated by modeling the pore pressure build-up and dissipation simultaneously. This soil model has the capability to describe the stress strain behavior of liquefiable sand. Beam elements were used to model the pile and the soil was model with 8 node elements. A special radiation boundary was used to simulate the infinite medium. A scaled version of a recording from the Kobe event (Event J) was considered as an input motion. Results from the FEM and the centrifuge tests agree well.

Maheshwari et al. (2004) developed a 3D FEM to examine the effects of soil plasticity (including work hardening) and separation at the soil-pile interface on the dynamic response of a single pile and pile groups. The pile was modeled with a linear elastic material and the soil was modeled with an advanced plasticity-based, hierarchical single surface (HISS) model. Only one fourth of the model was constructed by considering symmetry and anti symmetry. Kelvin elements (spring and dashpot) were used in all three directions (i.e., X, Y and Z) to simulate the infinite soil medium. The model was loaded (at the base, which is assumed to represent bed rock) with the El Centro (north-south component) acceleration record from the 1940 El Centro Earthquake. Furthermore, harmonic motion was used to find the transfer and impedance functions for the foundation. Pile-soil separation was considered only in the loading direction while the pile and soil were assumed to be in contact in the direction perpendicular to the motion. Friction between pile and soil were neglected. In every Gaussian point normal stress in soil elements (in the direction of loading) and confining pressure at that depth were compared for every time step and at every iteration within a time step. Separation was assumed when tensile normal stress was higher than confining stress. Numerical analyses by Maheshwari et al. (2004) reveal that nonlinearity reduced the real and imaginary part of the impedance function for the pile system. Moreover, soil nonlinear response in the soil-pile system has significant effect for low excitation frequencies.

Karthigeyan et al. (2006 and 2007) studied the influence of vertical loads on the lateral response of single piles installed in sandy and clayey soils through 3D FEM. In their numerical

model, the pile was treated as a linear elastic material and the soil was idealized using the Drucker-Prager constitutive model with a non-associated flow rule. The results of these FEM show that the presence of vertical loads increases the lateral load capacity of piles in sandy soils by as much as 40% depending on the level of vertical load. On contrary, the presence of a vertical load marginally reduces the lateral capacity of piles in clayey soils for vertical load levels up to 0.6 P_u and by as much as 20% for higher vertical load levels.

Rovithis et al. (2009 and 2011) studied the elastodynamic response of coupled soil-pile-structure systems to seismic loading using rigorous 3D FEM, emphasizing on the vibrational characteristics of the soil-structure system and the dynamic bending of the pile. The results demonstrate the strong influence on f_{SSI} of the foundation properties and the crucial importance of cross swaying-rocking stiffness of the pile. Furthermore, the notion of a *pseudo-natural SSI frequency* (f_{pSSI}) is introduced, as the frequency where pile-head motion is minimized with respect to free-field surface motion.

2.3.2.2.1 Pile group complete dynamic analyses

Wolf and von Arx (1978) generalized the solution of Blaney et al. (1976) to publish the first pile group complete dynamic response analysis method. They considered a horizontally layered visco-elastic soil deposit with piles of equal diameter and length, either floating or end bearing, in any group configuration. They used an axisymmetric FEM to calculate the Green's functions producing the displacements at any point in the soil mass given a ring load applied at a discrete layer. The Green's functions were then used to compute the flexibility matrix of the soil at each frequency, and the dynamic stiffness matrix of the complete system was then assembled. The results displayed strong dependence on frequency, number of piles, and pile spacing. Wolf (1980) detailed procedures for calculating the dynamic stiffnesses of groups of battered piles. Most recently, Wolf et al. (1992) described simplified but reasonably accurate cone models for single pile and pile group dynamic response. Waas and Hartmann (1981) analyzed pile groups arrayed in concentric rings, and assumed that the radial, vertical, and tangential components of displacement were proportional to the direction of applied loading. They substructured the problem (see Fig. 2.21) and determined the flexibility matrix of the visco-elastic soil deposit with applied point and ring loads, for coupling to the structure/pile stiffness matrix. They suggested that nonlinear soil behavior could be modeled by an equivalent linear analysis, and that

rectangular pile groups could be transformed into equivalent circular groups amenable to their analysis technique. Their analysis clearly demonstrated the effects of kinematic and inertial interaction as shown in Figs 2.22a - d (Meymand 1998).

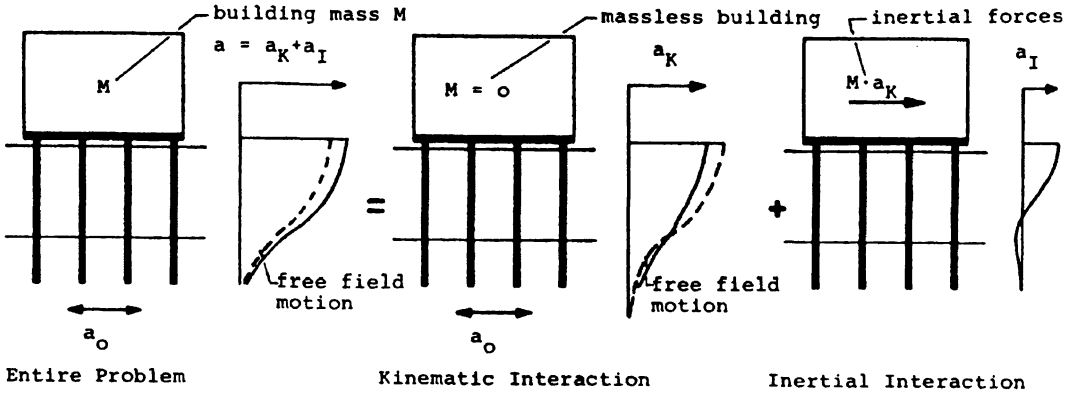

Fig. 2.21 Separation of SSI analysis into kinematic and inertial interaction components (after Waas and Hartmann, 1981).

The complex response method FE computer programs FLUSH (Lysmer et al., 1975), through principally designed SSI analyses, do have the capability of modeling SSPSI as a complete analysis, but are not well equipped to deal with strong soil-pile nonlinearity, gapping, etc. The generalized FE code DRAIN2D-X (Prakash et al., 1993) has also been used by a number of researchers as a platform for SSPSI analyses.

Lu et al, (2005) propose a 3D FE analysis of the SPSI system. The analysis is based on data from shaking table model tests made in the State Key Laboratory for Disaster Reduction in Civil Engineering, Tongji University, China. The general FE program ANSYS is used in the analysis. The surface-to-surface contact element is taken into consideration for the nonlinearity state of the soil–pile interface, and an equivalent linear model is used for soil behavior. A comparison of the results of the FE analysis with the data from shaking table tests is used to validate the computational model. It shows that separation, closing, and sliding exist between the pile foundation and the soil. The lateral acceleration response at the top of the superstructure is determined by the rocking and swing of the foundation and the deformation of the structure of a SSI system have been conducted by combining the results of a general FE program with the experimental results from shaking table tests. By comparing calculated and test results, it was

verified that the modeling method is rational. The model is suitable for the numerical analysis of a SSI system under small and strong ground motions.

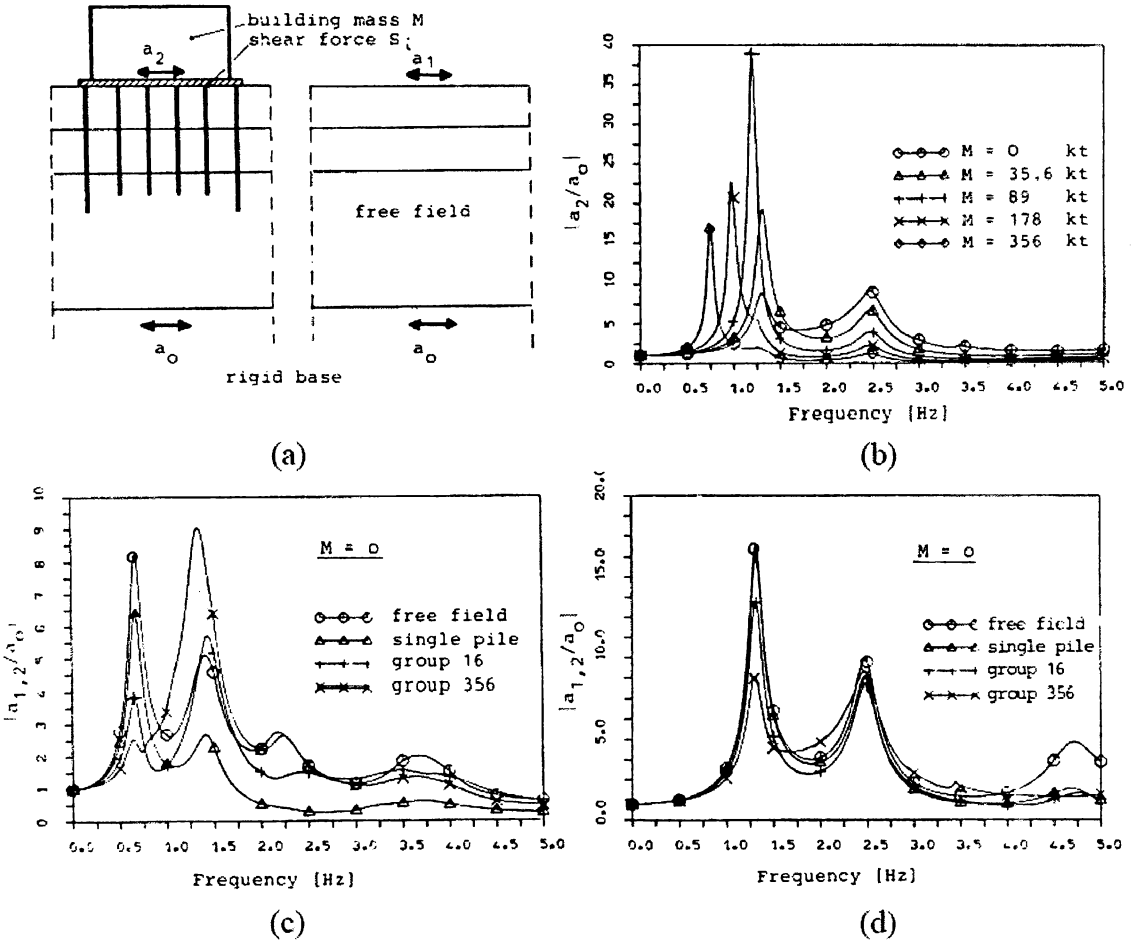

Fig. 2.22 a) Definition of transfer function; b) transfer function without building mass for soft soil; c) transfer function without building mass for stiff soil; d) transfer function for different building masses in stiff soil (after Waas and Hartmann, 1981)

Important conclusions that can be drawn from the computational analysis that is consistent with those that can be drawn from the test are as follows:

- The lateral displacement of the superstructure is composed of the deformation of the structure itself and that caused by the rocking and swing of the foundation.
- The deformation of the structure is the main component of the structural response, and the rocking and swing of the foundation take second place.

- With increasing input acceleration, the amplification factor of the acceleration peak value is reduced because of the nonlinearity of the soil.
- Vertical excitation has little effect on the response of the dynamic SSI.
- The distribution of the strain amplitude along the pile shows that large strains occur at the top of the pile and small strains occur at the tip.
- The distribution of the contact pressure on the pile-soil interface shows that a high pressure is present at both ends of the pile and that low pressure is present at the middle of the pile.

Important results from the calculations that cannot be made from the test are as follows:

- The computational analysis shows that a significant error will occur in the calculation for soft soil if the nonlinearity of the soil and the nonlinearity of the soil-structure interface are not taken into consideration.
- The phenomena of separation, closing, and sliding occur between the pile foundation and the soil under severe seismic input.
- The strain amplitude of the pile at the corner is bigger than that of the middle pile in the side row and that of the pile at the center.
- The sliding at the pile in the side row is larger than that at the piles in the middle row along the vibrating direction.

Dezi et al., (2007) propose a numerical procedure to evaluate the effects of kinematic and inertial interactions on pile groups by using a FEM. The method is used to calibrate Lumped Parameter Models (LPMs) which can be implemented in commercial FE programs to perform time domain analyses. The procedure is employed to study the spatial dynamic response of the railway bridge on the Tronto River (Marche region, Italy) which, due to the particular stiffness of substructures and deck, is an interesting case study. The seismic analysis is carried out in the time domain considering several real accelerograms. The results are compared with those obtained from the fixed base model by showing the importance of SSI in the actual design of the bridge. The main conclusions are:

- Foundation flexibility increases the fundamental periods of the system and alters the shape of the vibration modes with respect to the fixed base structure;
- The SSI analysis allows the design optimization of longitudinal seismic restraints;

- The 3D modeling of the bridge was found critical in accounting for the complex effects of the mutual interaction between the deck and the substructures and for considering their influences on transversal seismic response.

2.4 Full-scale tests

Carefully performed and well-instrumented full-scale tests on piles and pile groups provide the best and the accurate means of investigating the lateral loaded piles behavior because they simulate actual conditions. They are also the most expensive and the most difficult to perform. Therefore fewer full-scale tests have been conducted. They are limited in the sense that loading is applied only at piles-heads levels, concentrating the effects of soil-pile inertial interaction and ignoring the effects of kinematic interaction.

The first research conducted on laterally-loaded piles was done by Feagin (1937). The tests were conducted to provide design data for the design of the pile foundations for Lock and Dam 26 on the Mississippi River at Altona, Illinois, USA. Full-scale tests were conducted on timber and concrete single piles as well as various pile group configurations. The soil conditions at this site were sandy alluvium, and the piles were installed by a combination of jetting and driving. Feagin observed that the average soil resistance per pile decreased as more piles were added to the group. Feagin also concluded that group effects were only significant at large deflections and that at deflections of less than 6 mm group effects did not occur.

O'Halloran (1953) reported tests that were conducted in 1928 for a large paper mill located in Quebec City, Canada, along the banks of the St. Charles River. Load tests performed in conjunction with the Arkansas River Navigation Project provided significant amounts of noteworthy design and research data, which contributed to advancements in the state of practice in the early 1970's.

Further full-scale testing was done by Kim and Brungraber (1976) on 2×3 pile groups and isolated single piles at a site at Bucknell University campus farm near Lewisburg, Pennsylvania, USA. Their intent is to simulate loads occurring on bridge abutment foundations. Steel H-piles with approximately 12.2 meters in length were used. They compared the pile group per pile performance (fixed-head condition) to single (free-head) and computed pile group efficiencies in excess of unity, contrary to conventional notation. The group piles were joined by a pile cap, the bottom of which was cast against the ground surface, which introduced a potential

for pile cap base frictional contribution to lateral resistance. These tests noted that with increased lateral load, compressive stresses increased in the front row piles and decreased in the back row piles. It was determined that this was a result of the fixed-head condition of the pile group and that the front row piles were resisting rotation and thus had increased compressive stresses.

Holloway et al. (1982) revisited Lock and Dam No. 26 on the Mississippi River at Altona, Illinois, USA, in a study of rehabilitation schemes for the facility. They installed timber piles with the same construction techniques as originally used in the 1930's, and tested a 2x4 pile group to failure. One of the key results was experimental evidence of pile group "shadowing", i.e. the preferential load carrying capacity of piles in front of the line of loading, thereby reducing load on piles at the rear of the line of loading.

Meimon et al. (1986) conducted full-scale lateral load tests at a site in Brittany, France on a 6-pile group as well as a single pile. The pile group was composed of six piles hinged in a rigid cap and aligned in two rows spaced three pile diameters a part center-to-center. Within each row, the spacing was two pile diameters. Each pile was driven to a depth of 7.5 m. The initial soil profile consisted of high and low plasticity clays underlain with silt. The water table was located at the ground surface. They confirmed what had been observed by Feagin (1937) in that group effects increased with larger deflections. Meimon also noted what Kim and Brungraber (1976) had observed in that front row piles had greater resistance and also developed greater moments for a given pile group deflection. Neither Feagin (1937) nor Kim and Brungraber (1976) directly measured load on each pile group. Meimon et al. (1986) was the first to do this, which leads the way to further establishments in load distribution.

Brown et al. (1987) conducted full-scale tests in stiff clay and agreed with the results of Barton (1984) through centrifuge model tests that the elastic theory did not address what he saw to be the key factor in predicting pile group response; ultimate soil resistance. Brown set out to devise a new method to predict soil resistance and the very next year he revolutionized the design of pile groups with the concept of p-multipliers (Brown et al, 1988). Brown returned to do more tests on the same pile group tested in 1987, this time replacing the clay around the piles with sand. Brown saw the same results, that soil resistance per pile within the pile group was less than the single isolated pile and was primarily affected by spacing and by which row the pile was located in. All piles within the same row showed about the same resistance.

The results from Brown et al. (1988) can be seen in Fig. 2.23 where the decrease in load resistance per row is compared to the single pile. Noted in is the fact that first row loads are almost the same as the single pile loads and resist the most loads within the group, while trailing row piles carry substantially lower values. The normalized bending moment versus depth curves in Fig. 2.24 show how decreased resistance in trailing rows results in larger bending moments as well. The bending moment curves that are not normalized show that bending moment decreased in trailing rows as a result of less load being applied. Brown et al (1988) suggested *p*-multipliers to account for the reduction in resistance in each row. These *p*-multipliers act as reduction factors that scale down the actual *p-y* curves of the isolated single pile model, thus accounting for all nonlinearity in the soil profile.

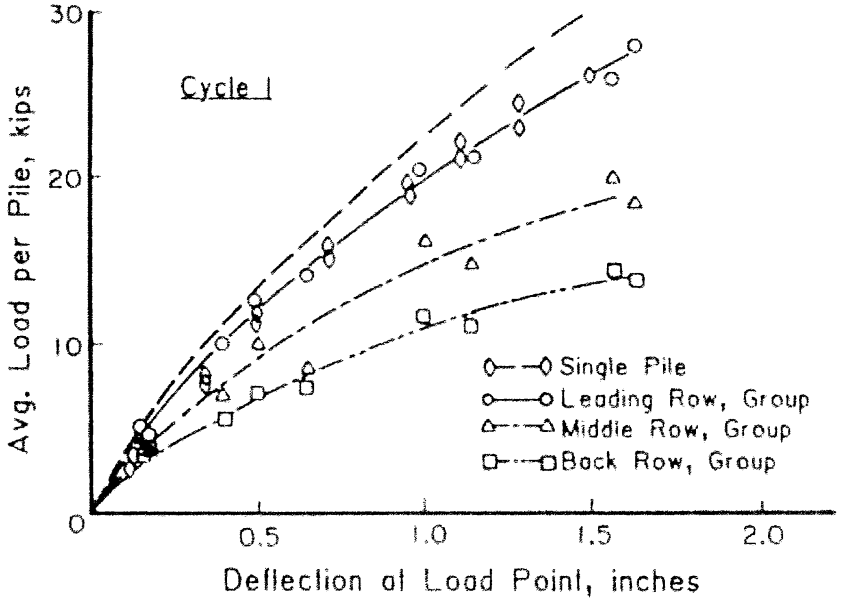

Fig. 2.23 Pile-head load resistance versus deflection for single pile and group by row position (Brown et al., 1988).

Ruesta and Townsend (1997) performed full-scale tests in sand in order to compare results with full-scale tests done by Brown et al. (1988) and centrifuge tests done by McVay et al. (1995). The tests conducted by Ruesta and Townsend were the first full-scale tests to have more than three rows and were unique in that they had four piles in each row. The piles were much larger than other tests and were made of reinforced concrete rather than steel. Their

conclusions suggested *p*-multipliers that are very similar to those suggested by these other tests. They also saw that outside piles took more load than inside piles within a row and attributed this to shadow effects and pile driving sequence. Rollins et al. (1998) did full-scale testing on steel piles in clay. This test resulted in more suggested *p*-multipliers that were slightly lower than those suggested for 3x3 pile groups in previous testing.

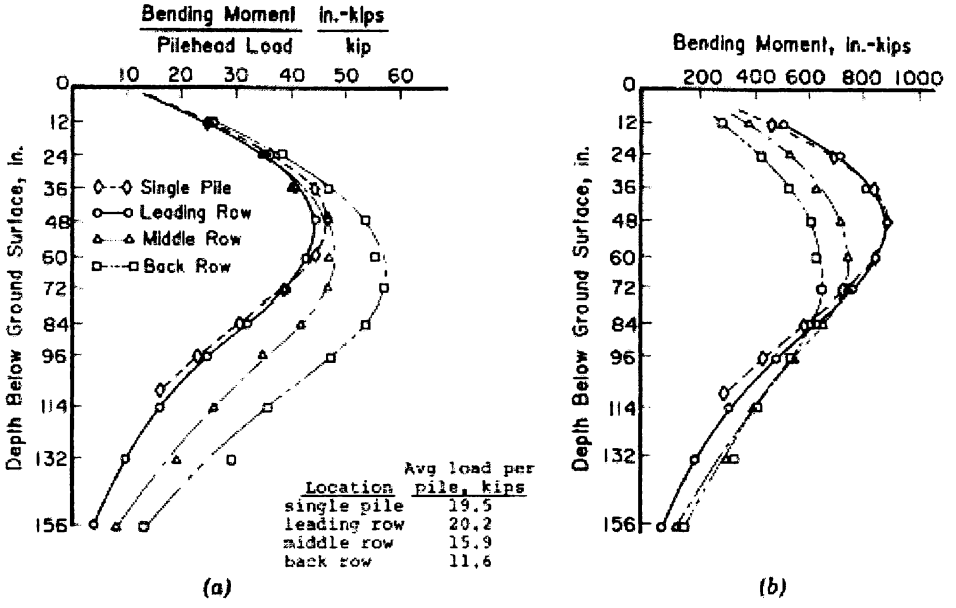

Fig. 2.24 Bending moment versus depth (Brown et al., 1988).

Huang et al. (2001) performed full-scale testing on both bored and driven pre-cast piles groups in order to compare the two and investigate the effects that pile installation had on pile group response. Huang found that installation procedures can have a significant effect on lateral soil resistance. Driven pile installation causes the soil to become denser and increases group interactions, while bored pile installation loosens the soil and decreases group interactions.

Rollins et al. (2003a) did further testing on the same site tested in 1998 with two new pile groups that were driven at the site, spaced at 2.8 and 5.65 pile diameters. This study concluded that *p*-multipliers are higher in the pile group spaced at 5.65 diameters than at 2.8 diameters and that pile interaction decreased with spacing as expected. However, group interaction was still fairly significant at 5.65 diameters and it was concluded that interaction remained significant up to spacing of about 6.5 pile diameters, after which group effects can be neglected. Rollins et al.

(2003b) did further full-scale testing in clay at a different site in Salt Lake City, USA on four pile groups spaced at 3.0, 3.3, 4.4, 5.6 pile diameters. The results of this these tests suggested *p*-multipliers similar to those previously suggested. It was also observed that, contrary to what Ruesta and Townsend (1997) observed in sand, outside piles within a row in clay did not resist more load than inside piles. Also, similar to what McVay et al. (1998) concluded, in pile groups with greater than three rows the trailing row carried higher loads than previous rows.

Rollins et al. (2005) performed a full-scale test on a 3x3 pipe pile group in loose to medium dense sand at 3.3D spacing. This study observed that within a row the outside piles consistently resisted more load than the inside piles. This same effect was observed in sand by Ruesta and Townsend (1997), but was not observed in clay by Rollins et al. (2003b). This result was attributed to the wider failure wedges that exist in adjacent piles in sand compared to those that develop in cohesive soils. More *p*-multipliers were suggested in this study and can be seen in together with all *p*-multipliers that have been suggested from the research reviewed in this chapter.

Weaver et al. (2001) conducted full-scale cyclic loading tests in the field on a 0.6 m diameter cast-in steel-shell (CISS) pile in liquefied soil to assess the accuracy of the *p-y* type of analysis. The test site is on Treasure Island in San Francisco Bay, USA which is the location of the National Geotechnical Experimentation Site. Therefore soil conditions at the site are very well known. Liquefaction was caused by blasting and the cyclic loading was conducted using a high speed hydraulic actuator. The back figured *p-y* curves for the liquefied sand differed significantly in shape from the standard *p-y* curves modified by the *p*-multiplier. The shape of the back-calculated *p-y* curves are shown in Fig. 2.25. The standard *p-y* curves including the *p*-multiplier effect are also shown for comparison. The two sets of *p-y* curves have distinctly different shapes and give different estimates of soil resistance. The slope of the standard *p-y* curve is greatest at small displacements and eventually decreases to zero at large displacements. The back calculated *p-y* curves show no resistance for a range of displacements between 20 and 50 mm. The soil resistance increased thereafter and was still increasing after 150 mm.

Rollins et al. (2006) conducted another study to investigate group interaction effects with respect to the pile spacing on laterally loaded pile groups. In order to evaluate the behavior, full-scale cyclic lateral load tests were performed on 3x5, 3x4 and 3x3 pile groups in stiff clay with 3.3D, 4.4D and 5.65D pile spacing respectively. The soil profile generally consists of stiff clay

layers with sand layers that were in a medium compact density state (Dr=60%), to a depth of 5m. These soils were underlain by sensitive clay, silty clay and sand layers. Similar to the other studies, lateral load tests were performed on single piles in order to provide comparison to the pile group test results. For the tests, closed-end steel pipe piles with an outer diameter of 0.324m and 9.0mm wall thickness were chosen.

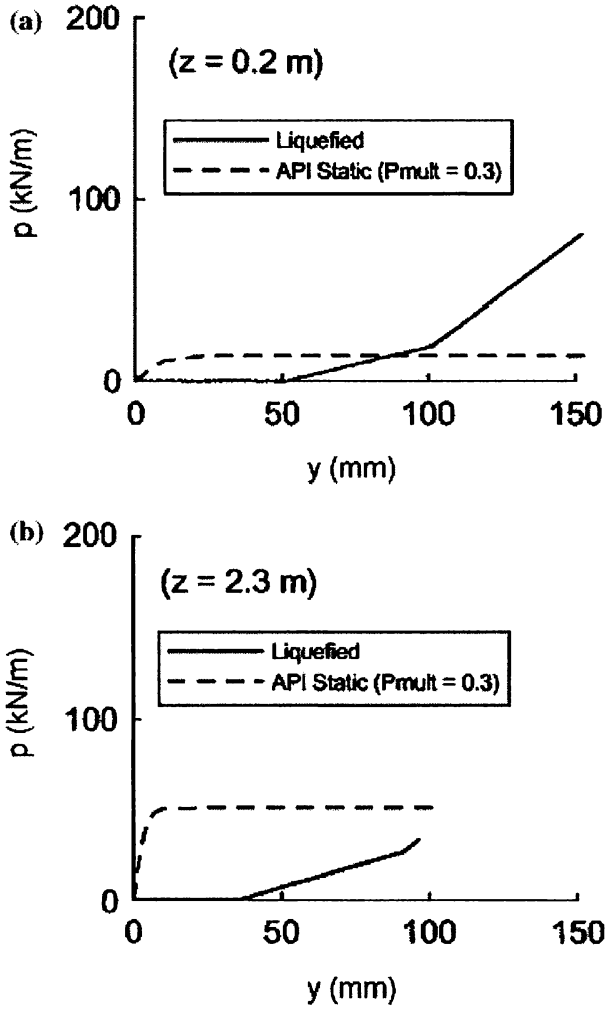

Fig. 2.25 Comparison of standard p–y curves with curves back-figured from test data at depths of (a) 0.2m and (b) 2.3m from a full-scale pile test (Weaver et al., 2001).

Rollins et al. (2006) concluded that, lateral load resistance was a function of pile spacing. While decreasing the pile spacing from 5.65D to 3.3D, group interaction effects became

progressively more important. Furthermore, the leading row (first row) piles in the group carried the greatest load, while the trailing row piles (second, third, fourth and fifth row piles), carried smaller loads for the same displacement level. For these pile groups driven in clay, row location within the group had more significant effect on the lateral resistance than the location within a row. Rollins et al. concluded that, for the same load level, the maximum moment in the trailing row piles were greater than in the leading row piles, due to the group interaction effects.

2.5 Centrifuge model tests

Centrifuge studies of scale model piles have provided a valuable means for understanding various aspects of soil-pile and soil-pile-structure interactions that are not readily accomplished by other experimental methods. A centrifuge apparatus consists of a rotating arm with an experiment package fixed to a swivel at one end; the centrifugal acceleration of the rotating arm induces an elevated gravitational field onto the model, which swivels to a position normal to the arm. Figure 2.26 shows representation of Centrifuge Testing Scheme (after Scott, 1994). The principle behind centrifuge testing is to use scale model piles and subject them to an artificially high acceleration field. This field reproduces the *in-situ* stresses that the full-scale pile would experience. This consideration is crucial when testing cohesionless soils whose stress-strain behavior is a function of confining pressure. In cohesive soils, where overburden stresses are not as significant, the centrifuge does offer the important capability of consolidating the deposit during spin-up, thereby achieving a more realistic soil strength profile. Centrifuge tests of model piles have been conducted with applying loads at pile-heads or pile caps, either statically or dynamically, or base excitation of the whole model by shaker devices (Meymand 1998).

The first centrifuge tests on model pile groups were performed by Barton (1984) on groups consisting of 2, 3, and 6 piles at various spacings and orientations with respect to the direction of load. Zhang and Hu (1991) examined the effect of residual stresses on the behavior of laterally loaded piles and pile groups. Adachi et al. (1994) examined pile-soil-pile interaction effects by testing two piles at various spacings and orientations. In these three studies, the soil was placed and the piles were installed prior to starting the centrifuge (i.e., pile installation occurred at 1g). Barton (1984) concluded that soil nonlinearity must be accounted for in pile group design and that the elastic theory did not account for this nonlinearity. Elastic methods underestimated the interactions within closely spaced pile group while overestimating the

interaction with pile groups at greater spacing. Barton also determined that the amount of total load carried by each pile within the group was not evenly distributed (as estimated by the elastic theory) and depended on spacing. Separate model tests were done in the same year by Cox et al. (1984) in soft clay. These tests were performed on piles in a line with lateral loads both parallel and perpendicular to the line of piles. Cox found that when load was placed perpendicular to the line of piles, group effects did not occur in spacing greater than 3 diameters. When the load was parallel with the line of piles, group effects were increased and efficiency decreased with the number of piles in the line.

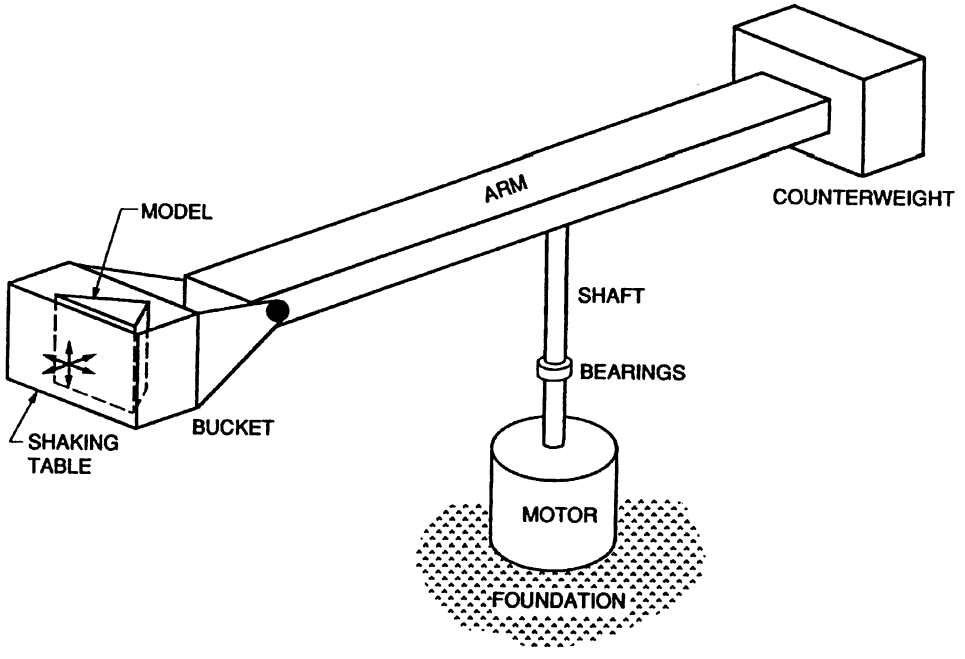

Fig. 2.26 Representation of Centrifuge Testing Scheme (after Scott, 1994)

Gohl (1991) provided a detailed examination of the complete series of centrifuge model pile group tests, with the conclusion that elastic interaction factors underestimated group deflections at close spacings (S/D < 4) and overestimated interaction for larger spacings. He also compared cyclic *p-y* curves to those constructed according to API recommendations, with the latter implying substantially stiffer response, particularly at depth. Simulation of the single pile experimental results with the computer code SPASM 8 was very successful.

Hamilton et al. (1991) were the first to report on centrifuge tests of laterally loaded piles in clay. Much of their analysis focused on the computation of ultimate soil resistance, incorporating mechanisms of soil-pile suction and adhesion in their model. Normalized experimental *p-y* curves were compared with curves constructed by Matlock's soft clay criteria (1970).

Kotthaus et al. (1994) used a centrifuge and small aluminum piles to conduct tests that simulate prototype concrete piles in sand. Kotthaus et al. observed that row efficiency decreased with trailing rows, defining efficiency as the ratio of the group load to the single pile load. Similar to the observation made by Brown et al. (1988), Kotthaus et al. (1994) found that the first row efficiency was close to 1.0, indicating that the resistance was about the same as the isolated single pile under the same loading.

While Kotthaus et al. (1994) focused on row efficiency; McVay et al. (1994) did similar centrifuge research that same year exploring the influence of soil density on pile group interactions in sand. McVay observed that the soil density did have an impact on the group interactions of the piles and that average load resistance increased with an increase in soil density, although the increase was not very large. McVay also saw that increased spacing resulted in greater pile capacity. McVay did more centrifuge testing the following year to further investigate the influence of pile spacing in sand. McVay et al. (1995) discovered that although density did have an influence on pile group interactions, pile spacing was actually much more influential. McVay concluded that the *p*-multiplier approach suggested by Brown et al. (1988) was a very good method of matching total group load and individual row distribution, and suggested some *p*-multipliers for spacing of 3 diameters and 5 diameters. McVay decided to further investigate larger pile groups of up to seven rows in order to obtain more comprehensive *p*-multipliers. McVay et al. (1998) found that load resistance continues to decrease until about the fourth row, after which it seems to stabilize. McVay also found that the load developed by the trailing row is about the same regardless of the number of rows in the pile group.

Wilson et al. (1995) performed model tests of pile supported structures in liquefiable sands on the large centrifuge facility at U.C. Davis. This machine is equipped with a 1-D base shaker, an "equivalent shear beam" laminar box to suppress boundary effects, and special container end conditions to provide complementary shear stresses and reduce unintended vertical accelerations. There is however no capability for driving piles in flight. An extensive series of

tests was made of single piles and small groups in saturated sands with a range of shaking intensities and development of very high excess pore pressure ratios, and in some cases consequent liquefaction. Pile motions were dominated by inertial forces from the superstructure, pile cap embedment had a significant effect on response, and peak pile bending moments during liquefaction events occurred close to the soil surface. Further work is reported by Wilson (1998) including the successful derivation of *p-y* curves from the experimental data and the favorable comparison of the tests results to the Caltrans pseudo-static analysis method.

Remaud et al. (1998) investigated the methods used by McVay et al. (1995) and did similar centrifuge testing in an attempt to obtain *p*-multipliers in a different method; attaching strain gages to the piles to obtain *p-y* curves from the bending moment profiles. Although Remaud's methods were different he saw similar results, that group effects were not evident in pile spacing greater than 6 diameters.

Much of the centrifuge model studies on laterally loaded pile groups were conducted with soil profile consist of sand layers. Ilyas et al. (2004) is one of the relatively few studies on laterally loaded pile groups in clay. Centrifuge model tests were performed both in normally consolidated and overconsolidated kaolin clay. The piles were arranged symmetrically and the groups consist of 2, 2x2, 2x3, 3x3, and 4x4 piles with 3D and 5D spacing. In tests, hollow aluminum square tube piles having 12 mm width and 260 mm length were used. These model piles correspond to the prototype piles having 840 mm width and 18.20 m length. All the tests were performed at 70 g on the National University Singapore Geotechnical Centrifuge. Ilyas et al. (2004) concluded that, while increasing the number of piles in group, the average lateral load per pile decreased. For piles installed in overconsolidated clay, the reduction of group effect was less clear than for piles installed in normally consolidated clay. Furthermore, for pile groups having 3D pile spacing installed both in normally consolidated clay and overconsolidated clay, group effect decreased as the number of piles increased. However, for larger spacings (5D), group effect became recessive. Ilyas et al. (2004) also concluded that, the "shadowing" effect was occurred on lead piles over trailing piles and this effect increased as the number of piles in group increased. Thus, higher lateral loads were carried by the lead row piles. When the average load per pile was compared among the piles within a row, the centre piles carried much less load and bending moment than the outer piles.

Based on the literature review, the previous studies on lateral behavior of single and group piles described above currently faces the following three problems:

(1) Level of loadings assumed for the previous study is often for the condition of moderate strain level induced in the ground. Lateral behavior of piles at extensive nonlinearity induced in the ground, such as for liquefaction or soil-pile gap formation, as encountered in recent strong earthquakes, is not fully studied.

(2) In the conventional study, the lateral behavior of piles has been studied independently from the vertical resistance of piles. Interaction between the lateral and vertical loads is not fully studied.

(3) In the seismic loading condition, soil-pile-structure interaction becomes the primary mechanism for lateral behavior of piles. The previous studies on the soil-pile interaction are limited for evaluating the effects of input frequency on soil-pile-structure interaction.

These three issues need to be addressed by further research on laterally loaded single and group piles.

References

1. Adachi, T., Kimura, M., and Kobayashi, H. 1994. Behavior of laterally loaded pile groups in dense sand, *Intl. Conf. Centrifuge 94*, Singapore, 509-514.
2. Allotey, N. and El Naggar, M.H. 2008. Generalized Dynamic Winkler model for nonlinear soil-structure interaction analysis. *Canadian Geotechnical Journal*, 45(4), 560-573.
3. American Petroleum Inst. 1993. Recommended practice for planning, designing, and constructing fixed offshore platforms - working stress design, Rpt. RP 2A-WSD, 20th Edition, July.
4. Anagnostopoulos, S. A., 1983. Pile foundation modelling for inelastic earthquake analyses of large structures, *Engineering Structures*, 5(3) 215-222.
5. Anandarajah, A. and Zhang, J. 2000. Simplified finite element modeling of nonlinear dynamic pile-soil interaction, Retrieved February 10, 2005, from http://www.ce.utexas.edu/em2000/papers/AAnand_2.pdf.
6. Barton, Y.O. 1984. Response of pile groups to lateral loading in the centrifuge, *Proceedings, Symposium on the Application of Centrifuge Modeling to Geotechnical Design*, W.H. Craig, ed., A.A. Balkema, Rotterdam, Netherlands, pp. 457-473.
7. Berger, E., Mahin, S.A., and Pyke, R. 1977. Simplified method for evaluating soil-pile structure interaction effects, *In Proceedings of the 9th Offshore Technology Conference*, OTC Paper 2954, Houston, Texas, 589-598.

8. Blaney, G., Kausel, E., and Roesset, J. 1976. Dynamic stiffness of piles, *Proc. 2nd Intl. Conf. on Numerical Methods in Geomechanics*, Blacksburg, Vol. 2, 1001-1012.
9. Bogard, D. and Matlock, H. 1980. Simplified calculation of p-y curves for laterally loaded piles in sands, Unpublished report, Earth Technology Corp.
10. Boulanger, R.W., Wilson, D.W., Kutter, B.L., and Abghari, A. 1999. Soil-pile-superstructure interaction in liquefiable sand, *Transportation research record* 1569, pp. 55-64.
11. Brown, D. and Shie, C. 1991. Modification of p-y curves to account for group effects on laterally loaded piles, *In Proceedings of the Geotech. Eng. Congress, Vol. 1, ASCE* Spec. Pub. 27, 479-490.
12. Brown, D., Reese, L., and O'Neill, M. 1987. Cyclic lateral loading of a large scale pile group, *J. Geotechnical Engineering, ASCE,* 113(11), 1326-1343.
13. Brown, D.A. and Bollman, H.T. 1996. Lateral behavior of a pile group in sand. *Journal of Geotechnical Engineering, ASCE,* 114(11), 1261–1276.
14. Brown, D.A., Morrison, C., and Reese, L.C. 1988. Lateral load behavior of pile group in sand, *Journal of Geotechnical Engineering, ASCE,* 114(11), 1261-1276.
15. Budhu M. and Davis T.G. 1988. Analysis of laterally loaded piles in soft clays, *Journal of Geotechnical Engineering, ASCE,* 114(1), 21-39.
16. Carter, D. 1984. A nonlinear soil model for predicting lateral pile response," Rpt. 359, Dept. of Civil Eng., Univ. of Auckland.
17. Chang, Y.L. 1937. Lateral pile loading tests. *Transactions of the American Society of Civil Engineers, ASCE* 102, 273–276.
18. Cox, W. R., Reese, L.C., and Grubbs, B.R. 1974. Field testing of laterally loaded piles in sand, *Proc. Offshore Technology Conf.*, Houston, Texas, Paper No. 2079, 459-472.
19. Cox, W.R., Dixon, D.A., and Murphy, B.S. 1984. Lateral load tests of 5.4 mm diameter piles in very soft clay in side-by-side and in-line groups, Laterally loaded deep foundations: analysis and performance, ASTM, West Conshohocken, Pa.
20. Davies, T. G. and Budhu, M. 1986. Non-linear analysis of laterally loaded piles in heavily overconsolidated clays, *Geotechnique*, 36(4), 527-538.
21. Dezi F., Dall'Asta A., Leoni G., Scarpelli G. 2007. Influence of the soil-structure interaction on seismic response of railway bridge, *Proc. 4th Int. Conf. on Earthquake Engineering*, Thessaloniki, Greece.
22. Dobry, R. and Gazetas, G. 1988. Simple method for dynamic stiffness and damping of floating pile groups, *Geotechnique*, 38(4), 557-574.
23. El-Naggar, M.H. and Novak, M. 1995. Nonlinear lateral interaction in pile dynamics, *Soil Dynamics and Earthquake Engineering*, 14(2), 141-157(17

24. Emery, J. and Nair, G. 1977. Dynamic response of a single pile, *In Proceedings 10th Specialty Session, 9th Intl. Conf. Soil Mechanics Fdn. Eng.,* Tokyo, 151-158.
25. Fan, K. and Gazetas, G. 1991. Seismic response of single piles and pile groups, Rpt. NCEER-91-0003, Dept. of Civil Eng., SUNY Buffalo, January.
26. Feagin, L.W. 1937. Lateral pile loading tests. *Transactions of the American Society of Civil Engineers, ASCE* 102, 236-254.
27. Finn, W.D.L. 2005. A study of piles during earthquakes: issues of design and analysis. *Bulletin of Earthquake Engineering,* 3, 141-234.
28. Gazetas, G. 1991. Foundation Vibrations, in Foundation Engineering Handbook, 2nd Ed., H.Y. Fang, Ed., Van Nostrand Reinhold.
29. Gazetas, G. and Dobry, R., 1984. Horizontal response of piles in layered soils, *J. Geotechnical Engineering, ASCE,* 110(1), 20-40.
30. Gazetas, G. and Makris, N. 1991. Dynamic pile-soil-pile interaction - part I: analysis of axial vibration, *Earthquake Engineering and Structural Dynamics,* 20(2), 115-132.
31. Gazetas, G., Fan, K., Tazoh, T., and Shimizu, K. 1993. Seismic response of the pile foundation of ohba-ohashi bridge, *Proc. 3rd Intl. Conf. on Case Histories in Geotech. Eng.,* St. Louis, Vol. 3, 1803-1809.
32. Gazetas, G., Fan, K., Tazoh, T., Shimizu, M., Kavvadas, M., and Makris, N. 1992. Seismic pile-group-structure interaction, in Piles Under Dynamic Loads, *Geotech. Spec. Pub. 34, ASCE,* 56-93.
33. Gazioglu, S.M. and O'Neill, M.W. 1984. An evaluation of p-y relationships in cohesive soils. In: J.R. Meyer (ed.), *Proceedings of the ASCE Symposium on Analysis and Design of Pile Foundations, ASCE National Convention*, San Francisco, California, Oct. 1–5.
34. Gohl, W. 1991. Response of pile foundations to simulated earthquake loading: experimental and analytical results, Ph.D. Dissertation, Univ. of British Columbia.
35. Hamilton, J., Dunnavant, T., Murff, J., and Phillips, R. 1991. Centrifuge study of laterally loaded behavior in clay, *Proc. Intl. Conf. Centrifuge '91*, Boulder, 285-292.
36. Hetenyi, 1946. Beams on elastic foundations, University of Michigan Press.
37. Holloway, D., Moriwaki, Y., Finno, R., and Green, R. 1982. Lateral load response of a pile group in sand, *Proc. 2nd International Conference on Numerical Methods in Offshore Piling*, Austin, 441-456.
38. Huang, A. B., Hsueh, C. K., O'Neill, M. W., Chern, S., and Chen, C. 2001. Effects of construction on laterally loaded pile groups. *Journal of. Geotechnical and Geoenvironmental Engineering., ASCE,* 127(5), 385–397.

39. Ilyas, L., Leung, C.F., Chow, Y.K., Budi, S.S. 2004. Centrifuge model study of laterally loaded pile groups in clay. *Journal of. Geotechnical and Geoenvironmental Engineering., ASCE,* 130(3), 274-283.

40. Karthigeyan S, Ramakrishna VVGST, and Rajagopal K. 2006. Influence of vertical load on the lateral response of piles in sand. *Computers and Geotechnics*, 33(2), 121–131.

41. Karthigeyan S, Ramakrishna VVGST, and Rajagopal K. 2007. Numerical investigation of the effect of vertical load on the lateral response of piles. *Journal of Geotechnical and Geoenvironmental Engineering, ASCE,* 133(5), 512–521.

42. Kay, S., Kolk, H., and van Hooydonk, W. 1983. Site specific design of laterally loaded piles, *In Proceedings of the Conf. Geotech. Practice in Offshore Eng.*, ASCE, Austin, 557-580.

43. Kaynia, A. and Kausel, E. 1982. Dynamic stiffness and seismic response of pile groups, Rpt. R82-03, Massachusetts Inst. of Technology, Cambridge.

44. Kim, J.B., and Brungraber, R.J. 1976. Full-scale lateral load tests of pile groups, *Journal of the Geotechnical Engineering Division, ASCE,* 102(1), 87-105.

45. Kishida, H., Suzuki, Y., and Nakai, S. 1985. Behavior of a pile under horizontal cyclic loading, *Proc. 11th Intl. Conf. Soil Mech. Fdn. Eng., San Francisco,* Vol. 3, 1413-1416.

46. Kotthaus, M., Grundhoff, T., and Jessberger, H. L. 1994. Single piles and pile rows subjected to static and dynamic lateral load. *Centrifuge 94,* editors: Leung, Lee and Tan, Balkema, Rotterdam, The Netherlands, 497-502.

47. Lee, I.K. and Harrison, H.B. 1970, Structures and foundation interaction theory, *J. Structural Division. ASCE,* 96(2), 177-198.

48. Lewis, K. and Gonzalez, L. 1985. Finite element analysis of laterally loaded drilled piers in clay, *In Proceedings of the 12th Intl. Conf. Soil Mechanics Fdn. Eng.,* Rio de Janiero, Vol. 2, 1201-1204.

49. Lu, X.L., Li, P.Z., Chen, B. et al. 2005. Computer simulation of the dynamic layered soil-pile-structure interaction system. *Canadian Geotechnical Journal* 42(3), 742-751.

50. Lysmer, J., Udaka, T., Tsai, C-F., and Seed, H. 1975. FLUSH - A Computer program for approximate 3-D analysis of soil structure interaction problems," Rpt. No. UCB/EERC-75/30, Earthquake Eng. Research Ctr., Univ. of California.

51. Maheshwari, B.K., Truman, K.Z., Naggar, M.H.EI., and Gould, P.L. 2004. Three dimensional finite element nonlinear dynamic analysis of pile groups for lateral transient and seismic excitations, *Canadian Geotechnical Journal*, 41, 118-133.

52. Makris, N., and Gazetas, G. 1992. Dynamic pile-soil-pile interaction - Part II: Lateral and Seismic Response, *Earthquake Engineering and Structural Dynamics*, 21(2), 145-162.

53. Matlock, H. 1970. Correlations for design of laterally loaded piles in soft clay, *Proc. 2nd Offshore Technology Conf.*, OTC 1204, Houston, Vol. 1, 577-594.

54. Matlock, H., Foo, S.H.C. and Bryant, L.M. 1978. Simulation of lateral pile behavior under earthquake loading. *In Proc., Earthquake Engineering and Soil Dynamics, ASCE Specialty Conference*, 601–619, Pasadena, California.

55. McClelland, B. and Focht, J. 1958. Soil modulus for laterally loaded piles, *Transactions of the American Society of Civil Engineers, ASCE,* 123, 1049-1086.

56. McVay, M., Bloomquist, D., Vanderlinde, D., and Clausen, J. 1994. Centrifuge modeling of laterally loaded pile groups in sands. *ASTM Geotechnical Testing Journal,* 17, 129-137.

57. McVay, M., Casper, R. and Shang, T.I. 1995. Lateral response of three-row groups in loose to dense sands at 3D and 5D spacing, *Journal of Geotechnical Engineering, ASCE,* 121(5), 436-441.

58. McVay, M., Zhang, L., Molnit, T., and Lai, P. 1998. Centrifuge testing of large laterally loaded pile groups in sands. *Journal of Geotechnology and Geoenvironmental Engineering, ASCE*, 124(10), 1019–1026.

59. Meimon, Y., Baguelin, F., and Jezequel, J.F. 1986. Pile group behaviour under long time lateral monotonic and cyclic loading, *Proceedings, 3rd International Conference on Numerical Methods in Offshore Piling, Inst.* Francais du Petrole, Nantes, France, 285-302.

60. Meymand, P. J., 1998. Shaking table scale model tests of nonlinear soil-pile superstructure interaction in soft clay, PhD, University of California, Berkeley.

61. Mindlin, R.D. 1936. Force at a point in the interior of a semi-infinite solid, *Physics* 7, 195-202.

62. Mostafa, Y.E., and El Naggar, M.H. 2002. Dynamic analysis of laterally loaded pile groups in sand and clay. *Canadian Geotechnical Journal*, 39 (6), 1358-1383.

63. Mylonakis, G., Nikolaou, A., and Gazetas, G. 1997. Soil-pile-bridge seismic interaction: kinematic and inertial effects. Part I: Soft Soil, *Earthquake Engineering and Structural Dynamics,* 26(3), 337 359.

64. Nogami, T. and Konagai, K. 1988. Time domain flexural response of dynamically loaded single pile, *J. Engineering Mechanics Division, ASCE*, 114(9): 1512-1525.

65. Nogami, T., Konagai, K., and Otani, J. 1988. Nonlinear pile foundation model for time domain dynamic response analysis, *Proc. 9th World Conf. Earthquake Eng.,* Tokyo, Vol. 3, 593-598.

66. Nogami, T., Konagai, K., Otani, J., and Chen, H.L. 1992. Nonlinear soil-pile interaction model for dynamic lateral motion. *Journal of Geotechnical Engineering, ASEC,* 118(1), 106-116.

67. Nogami, T., Otani, J., and Konagai, K. 1991. Nonlinear time domain numerical model for pile group under transient dynamic forces, *Proc. 2nd Intl. Conf. on Recent Advances in Geotech. Eng. and Soil Dyn.,* St. Louis, Vol. 3, 881-888.

68. Novak, M. 1991. Piles under dynamic loads, *Proc. 2nd Intl. Conf. on Recent Advances in Geotech. Eng. and Soil Dyn.,* St. Louis, Vol. 3, 2433-2456.

69. Novak, M., Nogami, T. and Aboul-Ella, F., 1978. Dynamic reactions for plane strain case, J. *Geotechnical Engineering, ASCE,* 104(4), 953-959.

70. O'Neill, M. and Murchison, J. 1983. An evaluation of p-y relationships in sands, Rpt. GT-DF02-83, Dept. of Civil Eng., Univ. of Houston, May.

71. O'Halloran, J. 1953. The lateral load capacity of timber pile groups. No. 154, *ASTM Special Publication.*

72. Parker, F. and Reese, L. 1970. Experimental and analytical study of behavior of single piles in sands under lateral and axial loading," Rpt. 117-2, Ctr. For Highway Research, Univ. of Texas, Austin, November.

73. Pender, M. and Pranjoto, S. 1996. Gapping effects during cyclic lateral loading of piles in clay, *Proc. 11th World Conf. Earthquake Eng.,* Acapulco, Paper No. 1007.

74. Penzien, J., Scheffy, C., and Parmelee, R. 1964. Seismic analysis of bridges on long piles, *J. Engineering Mechanics Division, ASCE,* 90(3): 223-254.

75. Pinto, P., McVay, M. and Lai, P. 1997. Centrifuge testing of plumb and battered pile groups in sand. *In Proc., Transportation Research Board, 17th Annual Meeting,* pp. 1–17, Washington, Disrict of Columbia, Paper No. 551.

76. Poulos, H. 1971 (a). Behaviour of laterally loaded piles: part 1 - single piles, *J. Soil Mechanics and Foundation Division, ASCE,* 97(5), 711-731.

77. Poulos, H. 1971 (b). Behaviour of laterally loaded piles: part 2 - group piles, *J. Soil Mechanics and Foundation Division, ASCE,* 97(5), 733-751.

78. Poulos, H. G., and Davis, E. H. 1980. Pile foundation analysis and design. John Wiley and Sons, Inc., NY.

79. Poulos, H.G. 1982. Developments in the analysis of static and cyclic lateral response of piles, In *Proceedings of the 4th International Conference on Numerical Methods in Geomechanics*, Canada, 1117-1135.

80. Prakash, S., Seerama, K., and Puri, V.K. 1992. Dynamics pile-soil-pile interactions, *Proc. of the seminar on Soil Dynamics and Geotechnical Earthquake Engineering*, Lisboa, Portugal, 253-386.

81. Prakash, V., Powell, G. 1993. DRAIN-3DX: base program description and user guide, version 1.10, Rpt. UCB/SEMM-94/07, Dept. of Civil Eng., Univ. of California, Berkeley.

82. Prater, E. G., 1979. Analysis of laterally loaded piles, *3rd International Conference on Numerical Methods in Geomechanics*, Aachen, April 2-6, 1087-1096.

83. Randolph, M. F., 1977. A theoretical study of the performance of piles, PhD, University of Cambridge.

84. Randolph, M.F. 1981. The response of piles to lateral loading, *Geotechnique* 31(2): 247–259.

85. Reese, L. C. 1984. Handbook on Design of Piles and Drilled Shafts under Lateral Load. U.S. Department of Transportation, Federal Highway Administration.

86. Reese, L. C., Isenhower, W. M., and Wang, S.T. 2006. Analysis and design of shallow and deep foundations, John Wiley & Sons, Inc.

87. Reese, L.C., and Wang, S.T. 1996. Technical manual of documentation of program GROUP 4.0 for Windows, Ensoft, Inc., Austain, Texas.

88. Reese, L.C., Cox, W., and Koop, F. 1974. Analysis of laterally loaded piles in sand, *Proc. 6th Offshore Technology Conf., OTC 2080*, Houston, Vol. 2, 473-483.

89. Reese, L.C., Cox, W., and Koop, F. 1975. Field testing and analysis of laterally loaded piles in stiff clay, *Proc. 7th Offshore Technology Conf., OTC 2312*, Houston, Vol. 2, 671-690.

90. Remaud, D., Garnier, J., Frank, R. 1998. Laterally loaded piles in dense sand: group effects, *Proceedings, 1998 International Conference on Centrifuge,* T. Kimura, O. Kusakabe, J. Tekamura, eds., A.A. Balkema, Rotterdam, Netherlands, 533-538.

91. Rollins, K.M., Johnson, S.R., Petersen, K.T., and Weaver, T.J. 2003 (a). Static and dynamic lateral load behavior of pile groups based on full-scale testing, *13th International Conference on Offshore and Polar Drilling, International Society for Offshore and Polar Engineering*, paper 2003-SAK-02, 8 pp.

92. Rollins, K.M., Lane, J.D., and Gerber, T.M. 2005. Measured and computed lateral response of a pile group in sand, *Journal of Geotechnical and Geoenvironmental Engineering, ASCE,* 131(1), 103-114.

93. Rollins, K.M., Olsen, R.J., Egbert, J.J., Jensen, D.H., Olsen, K.G., and Garrett, B.H. 2006. Pile spacing effects on lateral pile group behavior: analysis. *Journal of. Geotechnical and Geoenvironmental Engineering., ASCE,* 132(10) 1272-1283.

94. Rollins, K.M., Olsen, R.J., Egbert, J.J., Olsen, K.G., Jensen, D.H., and Garrett, B.H. 2003 (b). Response, analysis, and design of pile groups subjected to static and dynamic lateral loads, Utah Department of Transportation Research and Development Division, Report No. UT-03.03.

95. Rollins, Kyle M., Peterson, Kris T. and Weaver, Thomas J. 1998. Lateral load behavior of full-scale pile group in clay. *Journal of Geotechnology and Geoenvironmental Engineering, ASCE*, 124(6), 468–478.

96. Rovithis, E.N., Pitilakis, K.D., Mylonakis, G.E. 2009. Seismic analysis of coupled soil-pile-structure systems leading to the definition of a pseudo-natural SSI frequency, *Soil Dynamics and Earthquake Engineering*, 29(6), 1005-1015.

97. Rovithis, E.N., Pitilakis, K.D., Mylonakis, G.E. 2011. A note on a pseudo-natural SSI frequency for coupled soil-pile-structure systems, *Soil Dynamics and Earthquake Engineering*, 31(7), 873-878.

98. Ruesta, P. and Townsend, F. 1997. Evaluation of laterally loaded pile group at Roosevelt bridge, *Journal of Geotechnical and Geoenvironmental Engineering, ASCE,* 123(12), 1153-1161.

99. Scott, R.F. 1994. Review of progress in dynamic geotechnical centrifuge research. Dynamic Geotechnical Testing II, ASTM STP 1213, R.J. Ebelhar, V.P. Drnevich, and B.L. Kutter, Eds., American Society for Testing and Materials, Philadelphia, 305-329.

100. Swane, I. and Poulos, H. 1984. Shakedown Analysis of Laterally Loaded Pile Tested in Stiff Clay, *Proc. 4th Australia-New Zealand Conf. on Geomechanics*, Perth, Vol. 1, 165-169.

101. Tajimi, H. 1969. Dynamic analysis of a structure embedded in an elastic stratum, *In Proc. 4th World Conf., Earthquake Engineering*, Santiago, Chile, III(A-6), 53-69.

102. Tazoh, T., Wakahara, T., Shimizu, K., and Matsuzaki, M. 1988. Effective motion of group pile foundations, *In Proc., 9th World Conf. on Earthquake Engineering*; Tokyo, 3, 587-592.

103. Thompson, G. 1977. Application of finite element method to the development of p-y curves for saturated clays. Thesis, University of Texas-Austin.

104. Trochanis, A.M., Bielak, J. and Christiano, P. 1991. Three dimensional nonlinear study of piles. *Journal of Geotechnical Engineering, ASCE*, 117(3), 429-447.

105. Waas, G. and Hartmann, H.G. 1981. Analysis of pile foundation under dynamic load, *Conf. of Struct. Mech. in Reactor Tech.*, Paris, France, K 5/2, 1-8.

106. Weaver, T.J., Ashford, S.A. and Rollins, K.M. (2001) Development of p–y curves for a 0.6m diameter CISS pile in liquefied sand, *CDROM Proc. 6th CALTRANS Seismic Research Workshop*, Sacramento, CA.

107. Welch, R. C., and Reese, L.C. 1972. Laterally loaded behavior of drilled shafts, Research report No. 3-5-65-89, Center for highway research, University of Texas at Austin.

108. Wilson, D., Boulanger, R., Kutter, B., and Abghari, A. 1995. Dynamic centrifuge tests of pile supported structures in liquefiable sand, Univ. of California, Davis.

109. Wilson, D.W.1998. Soil-pile-superstructure interaction in liquefying sand and soft clay. PhD Thesis, Department of Civil and Environmental Engineering, University of California, Davis

110. Wolf, J. 1980. Dynamic stiffness of group of battered piles, *J. Geotechnical Engineering, ASCE,* 106(2), 198-203.

111. Wolf, J. and von Arx, G. 1978. Impedance functions of a group of vertical piles, *Proc. ASCE Conf. Earthquake Eng. Soil Dyn.*, Pasadena, Vol. 2, 1024-1041.

112. Wolf, J., Meek, J., and Sung, C. 1992. Cone models for a pile foundation, in Piles Under Dynamic Loads, *Geotech. Spec. Pub. 34, ASCE,* 94-113.

113. Wotherspoon, L. M., 2009. Integrated modelling of structure-foundation systems, PhD, University of Auckland.

114. Yegian, M. and Wright, S.G. 1973. Lateral soil resistance-displacement relationships for pile foundations in soft clays. *In Proceedings of 5th Annual Offshore Technology Conference*, Houston, TX.

115. Zhang, L., and Hu, T. 1991. Modeling of residual stresses of large piles in centrifuge. *Centrifuge 91,* Balkema. Rotterdam, The Netherlands, 237-243.

116. Zienkiewicz, O.C. and Shiomi, T. 1984. Dynamic behavior of saturated porous media: The generalized biot formulation and its numerical solution, *International Journal for Numerical and Analytical Methods in Geomechanics,* 8, 71-96.

CHAPTER 3

Modeling of Soil-pile Interaction in Horizontal Plane

Contents

3.1 Introduction

A proper numerical modeling for any physical problem requires a sufficient understanding of all aspects of this problem. An efficient way to get information leads to better understanding of problems that involve the interaction of soils and piles is to conduct model tests, centrifuge tests or even full-scale tests if necessary. This chapter presents 2D model tests on a horizontal cross section of a soil-pile system performed at disaster prevention research institute (DPRI), Kyoto University, to evaluate local soil displacement field in the vicinity of the piles associated with a global displacement of soil around the pile foundation. A 2D effective stress analyses in horizontal plane performed to generalize the findings from the model tests is also presented. The results of the model tests and the associated numerical analyses formed the basis to propose a simplified approach for idealizing the soil-pile interaction in horizontal plane in terms of a nonlinear soil-pile interaction spring. At the end of this chapter, some comments on the soil-pile interaction spring are elucidated.

3.2 Model Tests for Soil Deformation around Piles

The objective of the model tests is to evaluate a local soil displacement field in the vicinity of piles such as that illustrated in Fig. 3.1. The model tests were performed using an aluminum container (inner dimensions: 800 mm long, 500 mm wide, 40 mm high), a cylindrical pile model made of Teflon, 40 mm high with a diameter of 50 mm, was embedded in a sand deposit formed in the container as shown in Fig. 3.2. The sand deposit was formed by air pluviation for dry condition, and by pouring a slurry mixture of sand and viscous fluid (120cSt) for saturated condition. Silica sand No.7 was used. Relative densities of the sand deposits were about 70% for dry condition and about -150% (negative relative density) for saturated condition. After the sand deposit was formed, an acrylic plate was placed on the surface on the sand deposit. Displacement was induced to the pile model by pulling a wire attached to the mid portion of the pile model at the rate of 7.2 mm/min. Although the pile model was moved in the model tests, the primary interest of the model tests was to measure the displacement field of soil relative to the movement of the pile. Thus, the results of the model tests are readily applicable to the conditions when the global soil movement is induced around the pile foundation as shown in Fig. 3.2(b) (Iai et al. 2010).

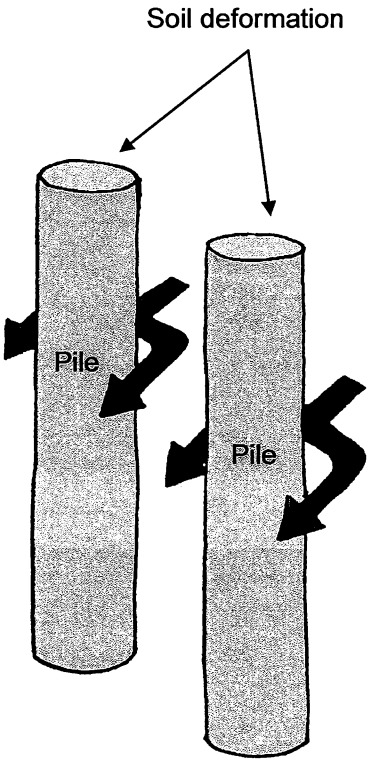

Fig. 3.1 Schematic figure of soil deformation around piles

The local displacement field monitored through a video-camera was plotted in terms of displacement vectors at nodes of the grid formed by colored sand markers. Under dry condition, the displacement vectors were directed away from the front of the pile in a pattern of a fan as shown in Fig. 3.3. The displacement vectors at pile side rapidly decreased with an increasing distance from soil-pile interface. A void was formed behind the pile following the movement of the pile. Under saturated condition, vortexes were formed at pile side as shown in Fig. 3.4. Void formation was not observed behind the pile under saturated condition. Displacement distribution in the vicinity of soil-pile interface was obtained as shown in Figs. 3.5(a) and (b) for dry and saturated soil conditions, respectively (Iai et al. 2010).

3.3 Soil-pile Interaction in Horizontal Plane: Numerical Analysis

2D analyses of a horizontal cross section of the soil-pile system were performed under pseudo-static conditions. An effective stress model based on multiple shear mechanism was used through

a computer code FLIP (Iai et al, 1992). In what follows, the core of the modeling is briefly introduced. Details are found in Ozutsumi (2003).

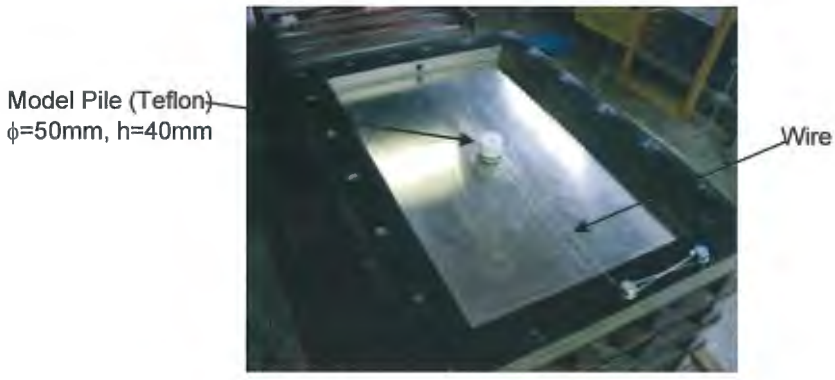

(a)

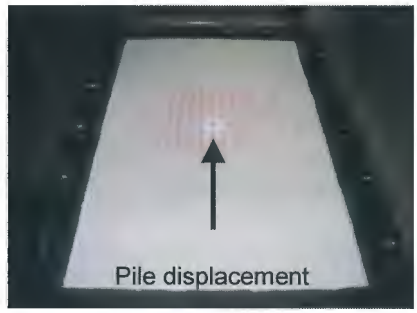

(b)

Fig. 3.2 Apparatus for model tests for soil-pile interaction in horizontal plane: (a) before sand poring (b) after forming sand deposit.

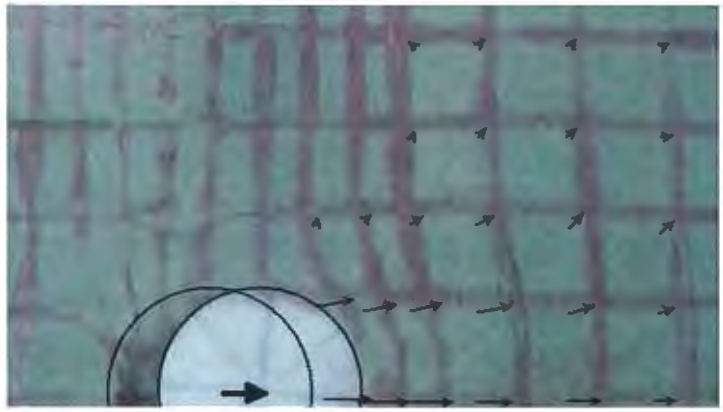

Fig. 3.3 Measured displacement field: pile displacement 11 mm, load = 20 N (dry condition)

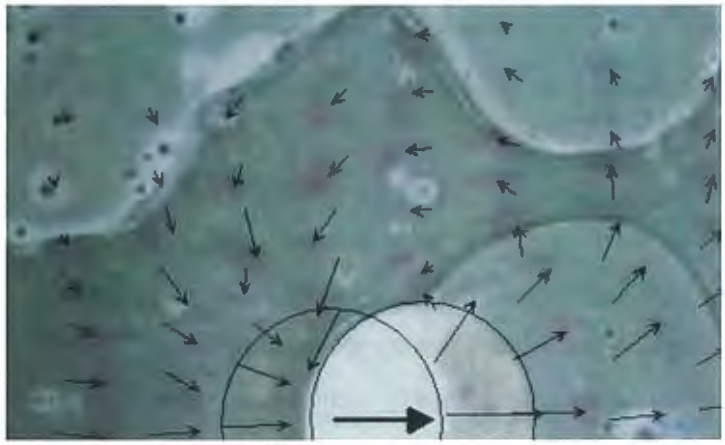

Fig. 3.4 Measured displacement field: pile displacement 21 mm, load = 6 N (saturated condition)

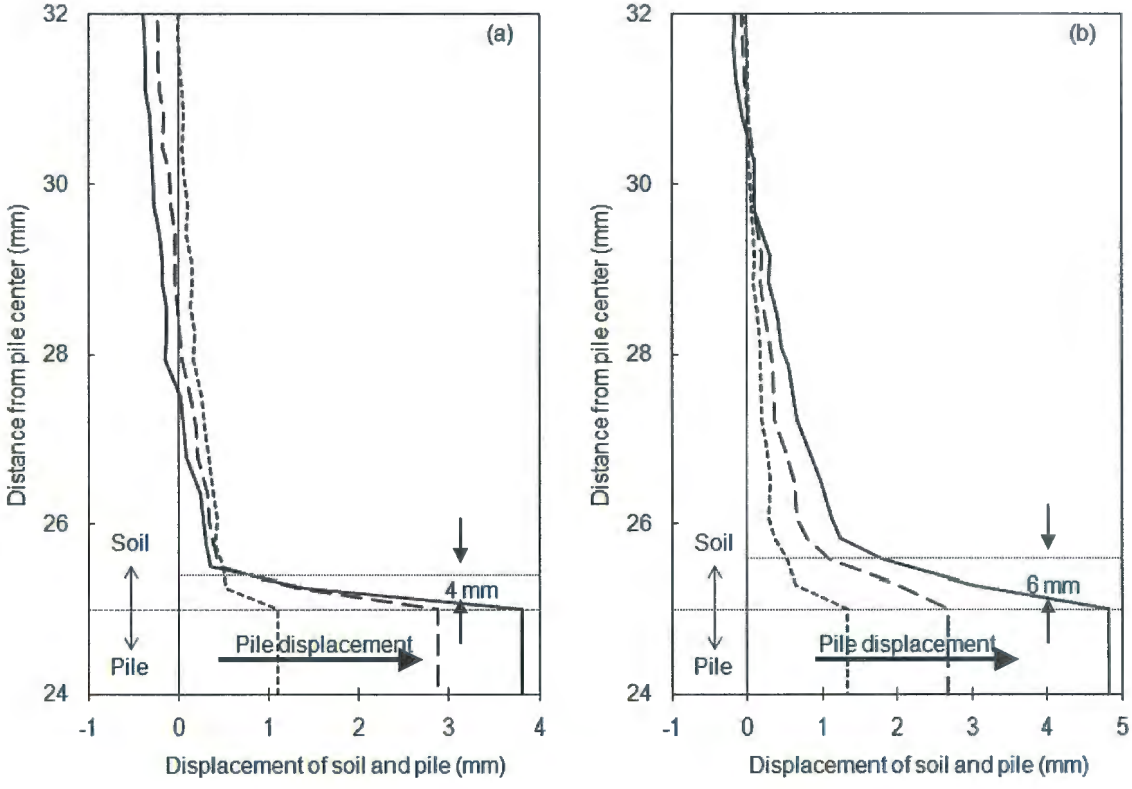

Fig. 3.5 Displacement distributions in the vicinity of soil-pile interface for: (a) dry and (b) saturated sand deposits

3.3.1 Soil model

The model is formulated based on the concept of contact forces in granular media. The model was originally proposed by Towhata and Ishihara (1985). As shown in Fig. 3.6, the model is represented by a movable point located within the circular fixed boundary defined in shear strain space and connected to the boundary with an infinite number of virtual springs. Each spring corresponds to a virtual simple shear mechanism having a various orientation. The relationship between force and displacement of each spring follows the hyperbolic type load displacement. The displacement of the movable point from the center represents the mobilized shear strain and the resultant of forces acting on the point represents the shear stress induced in the soil.

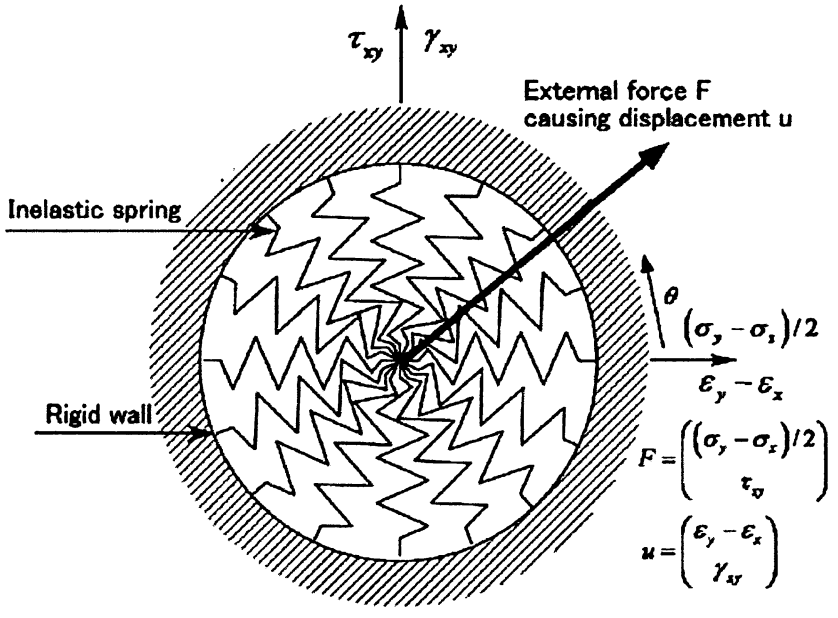

Fig. 3.6 Schematic view of the multiple simple shear mechanism (after Towhata and Ishihara 1985, Iai et al. 1992).

Let us consider the following vectors of stresses and strains:

$$\{\sigma'^T\}=\{\sigma'_x \quad \sigma'_y \quad \tau_{xy}\} \tag{3.1}$$

$$\{\varepsilon^T\}=\{\varepsilon_x \quad \varepsilon_y \quad \gamma_{xy}\} \tag{3.2}$$

in which compressive stress and contractive strain will assumed positive and the strains will be given from displacements u and v in x and y directions by

$$\varepsilon_x = \frac{\partial u}{\partial x}, \qquad \varepsilon_y = \frac{\partial v}{\partial y}, \qquad \gamma_{xy} = \frac{\partial u}{\partial y} + \frac{\partial v}{\partial x}. \tag{3.3}$$

It is assumed in the following discussion that σ'_z can be approximated by $(\sigma'_z + \sigma'_z)/2$. The basic form of the constitutive relation in an integrated form is given by

$$\left\{\sigma'^{T}\right\} = \sigma'_m \left\{n^{(0)}\right\} + \sum_{i=1}^{I} q^{(i)} \left\{n^{(i)}\right\} \Delta\theta \tag{3.4}$$

and in an incremental form as a derivative of Equation (2.4) by

$$\{d\sigma'\} = [D](\{d\varepsilon\} - \{d\varepsilon_p\}) \tag{3.5}$$

where ε_p= the plastic volumetric strain generated by the transient and cyclic loads. The tangential stiffness matrix $[D]$ is given by

$$[D] = K\left\{n^{(0)}\right\}\left\{n^{(0)}\right\}^T + \sum_{i=1}^{I} G_{L/U}^{(i)} \left\{n^{(i)}\right\}\left\{n^{(i)}\right\}^T \tag{3.6}$$

where the first terms in Equations (2.4) and (2.6) represent the volumetric mechanism with effective mean stress $\sigma'_m=(\sigma'_1+ \sigma'_3)/2$ in Equation (2.4) and elastic tangent bulk modulus of soil skeleton $K=dp/d\varepsilon$ in Equation (2.6) and the direction vector given by

$$\left\{n^{(0)}\right\}^T = \{1 \quad 1 \quad 0\} \tag{3.7}$$

and the second terms in Equations (3.4) and (3.6) represent the multiple shear mechanism without volume change. Each mechanism i=1,….,I, where I is the number of multiple shear mechanisms assumed for computation, represents a virtual simple shear mechanism, with each simple shear plane oriented at an angle $\theta_i/2+\pi/4$ relative to the x axis, whereθ_i is the angle of virtual shear mechanism i in $[(\varepsilon_x - \varepsilon_y) - \gamma_{xy}]$ plane and $\Delta\theta$ is the differential angle. The direction vectors $\left\{n^{(i)}\right\}$ for the multiple shear mechanism are given by

$$\{n^{(i)}\}^T = \{\cos\theta_i \quad -\cos\theta_i \quad \sin\theta_i\} \qquad \text{(For } i=1,\ldots..,I\text{)} \tag{3.8}$$

$$\theta_i = (i-1)\Delta\theta \qquad \text{(For } i=1,\ldots..,I\text{)} \tag{3.9}$$

$$\Delta\theta = \pi / I \qquad \text{(For } i=1,\ldots..,I\text{)} \tag{3.10}$$

The loading L and unloading U for shear mechanism are separately defined for each mechanism by the sign of

$$d\gamma^{(i)} = \{n^{(i)}\}^T \{d\varepsilon\} \tag{3.11}$$

in which

$$\gamma^{(i)} = \{n^{(i)}\}^T \{\varepsilon\} = (\varepsilon_x - \varepsilon_y)\cos\theta_i + \gamma_{xy}\sin\theta_i \tag{3.12}$$

where $\gamma^{(i)}$ is the virtual shear strain of the mechanism i=1,.....,I. Each tangent modulus $G_{L/U}^{(i)} = \dfrac{dq^{(i)}}{d\gamma^{(i)}}$ depends on the present state and the history of each virtual simple shear strain $\gamma^{(i)}$. The virtual shear stress $q^{(i)}$ is introduced as shear resistance variable to be defined per unit angle θ for mechanism i.

When the inherent soil fabric is assumed to be isotropic, the virtual simple shear mechanism is defined by a hyperbolic relation under a constant confining stress as

$$q^{(i)} = \frac{\gamma^{(i)} / \gamma_v}{1 + \left|\gamma^{(i)} / \gamma_v\right|} q_v \tag{3.13}$$

where q_v and γ_v are the parameters for defining the hyperbolic relationship and called the virtual shear strength and virtual reference strain, respectively. The virtual tangent shear moduli are obtained for the initial loading as

$$G_{L/U}^{(i)} = \frac{\gamma^{(i)} / \gamma_v}{\left(1 + \left|\gamma^{(i)} / \gamma_v\right|\right)^2} \frac{q_v}{\gamma_v} \Delta\theta \tag{3.14}$$

The relationships between the parameters q_v and γ_v and the macroscopic shear strength $\tau_m = (\sigma_1' - \sigma_3')/2$ and shear modulus G_m can be written as

$$G_m = \frac{q_v}{\gamma_v} \sum_{i=1}^{I} sin^2 \theta_i \Delta\theta \tag{3.15}$$

$$\tau_m = q_v \sum_{i=1}^{I} sin^2 \theta_i \Delta\theta \tag{3.16}$$

The shear modulus G_m, which corresponds to effective mean stress $\sigma'_m = p$, is related to the initial shear modulus G_{ma}, which corresponds to initial effective mean stress σ'_{ma}, as

$$G_m = G_{ma} \left(\frac{\sigma'_m}{\sigma'_{ma}}\right)^{0.5} \tag{3.17}$$

The shear strength is related to angle of internal friction ϕ_f and cohesion c as

$$\tau_m = c \cos\phi_f + \sigma'_m \sin\phi_f \tag{3.18}$$

3.3.2 Finite elements

In the analysis, a single row of equally spaced pile group deployed perpendicular to the direction of load as shown in Fig. 3.7(a), while Fig. 3.7(b) shows a simplified model for a single pile in the group.

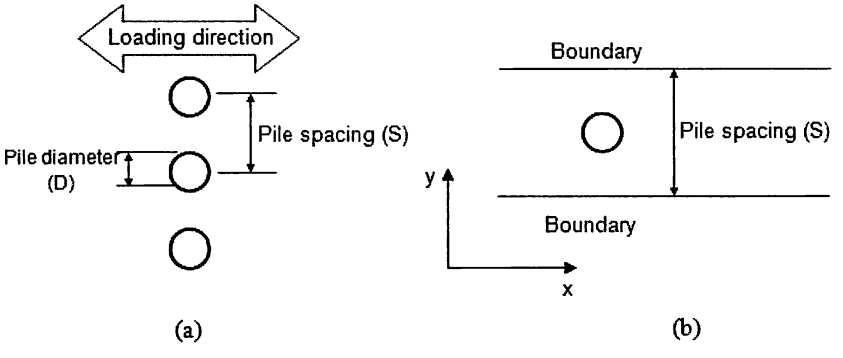

Fig. 3.7 Soil-pile system in horizontal plane: (a) single row of equally spaced pile group (plane view); (b) analysis domain for a single pile in the group

The analysis domain of the simplified model is defined by the periodic boundaries that run parallel to the load direction and go through the centers of pile spacing. The FE mesh used for the analysis has a unit thickness with pile spacing of S = 10D and a pile diameter D = 5 cm is shown in Fig. 3.8 for the area ranging from S = -5D to +5D. At the right and left side boundaries, displacements were fixed. At the other two boundaries, displacements were fixed in y direction and soil nodes with the same x-coordinate were assigned same displacements in x-direction (see Fig. 3.8) (Iai et al. 2006). In the analysis, whole soil-pile system was initially consolidated with a confining pressure of 0.28 kPa for simulating the confining condition at the middle depth of the model sand deposit (i.e. 2 cm from the surface). The cylindrical pile section was idealized using linear solid elements having a rigidity equivalent to that if concrete but this pile section was replaced by the soil elements in the initial phase of analysis for consolidation in order to avoid artificial stress concentration. Following this initial phase, the piles were loaded either monotonically or cyclically load. Soil deformation around the cylindrical cross section of the pile was computed in drained and undrained conditions. Parameters for sand used for the analysis were determined referring to the results of laboratory tests on Silica sand No.7 as shown in Table 1.

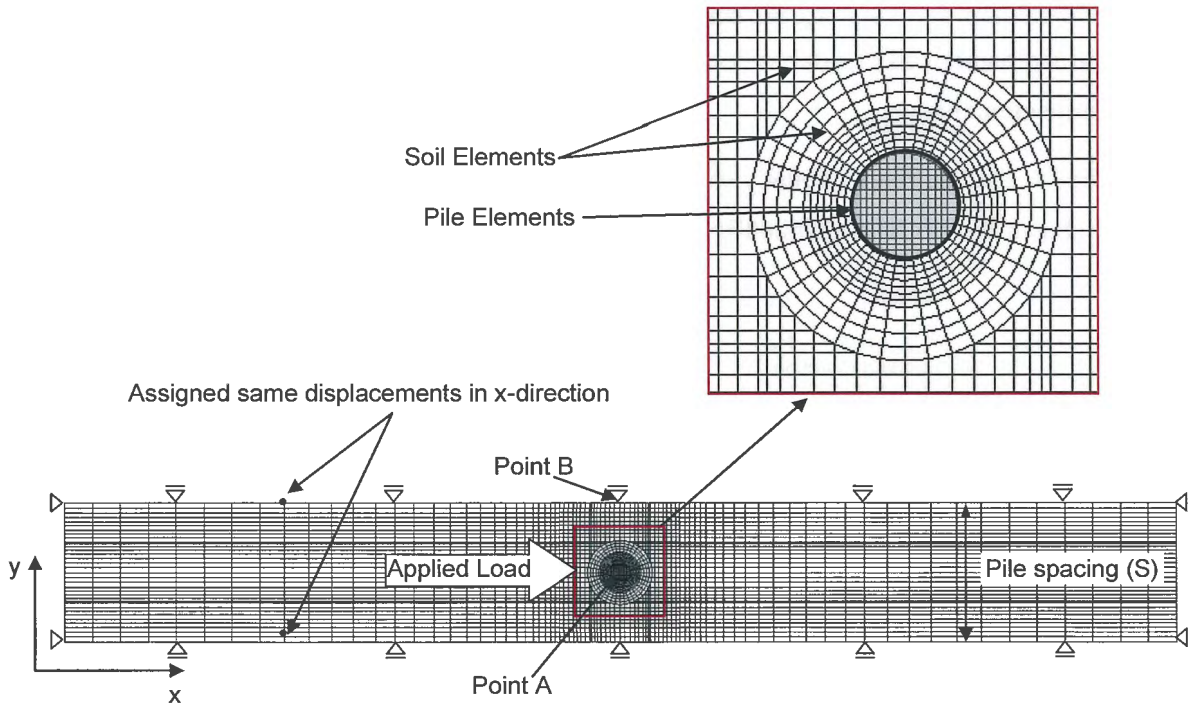

Fig. 3.8 Finite element mesh used for the analyses

Table 1 Parameters for silica sand No.7 in FLIP analysis

ρ_t (t/m^3)	G_{ma} (kPa)	υ	σ_{ma}' (kPa)	ϕ_f (degree)	H_{max}
2.0	3760	0.33	0.28	35	0.24

3.3.3 Computed results

The computation was performed in a numerically stable manner even at the large displacements in the order-of-magnitude displacement comparable to that of pile diameter. Numerical stability occurred only when the ultimate state of soil was reached either when the load resistance curve reached plateau, or when there is instability in the soil under drained condition.

Computed displacement field for the dry and saturated condition are shown in Figs. 3.9 and 3.10. In the dry condition, the displacement vectors are directed away from the front of the pile in a pattern of a fan. The displacement vectors at the pile side rapidly decreases with an increasing distance from the soil-pile interface. For the saturated condition, displacement vectors beside the pile shows vortexes as shown in Fig. 3.10. These displacement fields are basically consistent with those measured in the laboratory and shown in Figs 3.3 and 3.4. Only difference is noted with respect to the formation of voids behind the pile in the model tests. No void was formed in the analysis probably because the confining stress in the analysis was more uniform than the one in the model tests where the stress field became 3D when the void began to form.

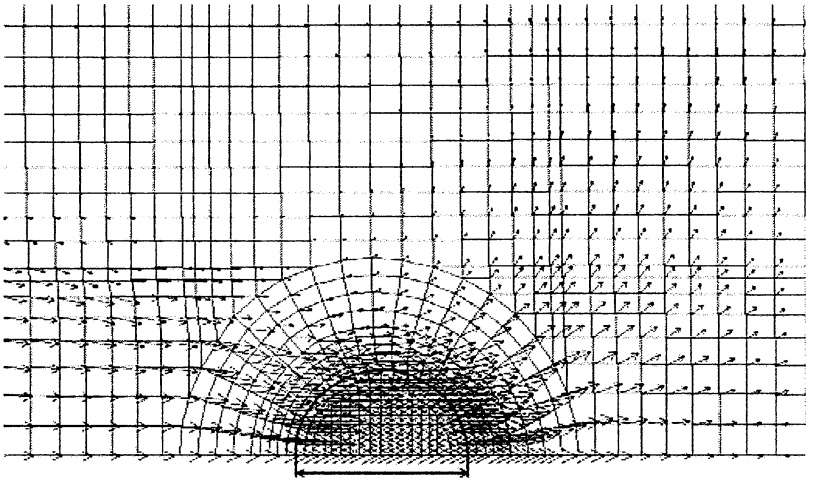

Fig. 3.9 Computed displacement field around pile (dry)

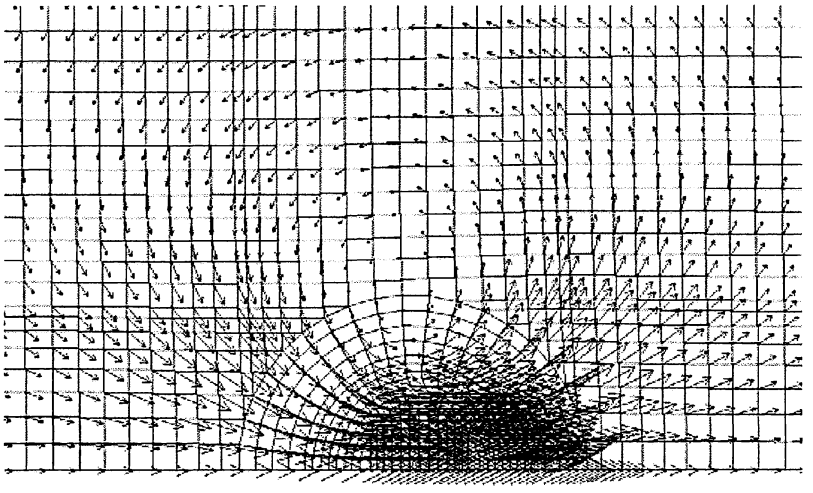

Fig. 3.10 Computed displacement field around pile (saturated)

In order to clearly show the displacement distribution between the piles, horizontal components of the displacements are plotted in Fig. 3.11. These results are basically consistent with those measured and shown in Fig. 3.5.

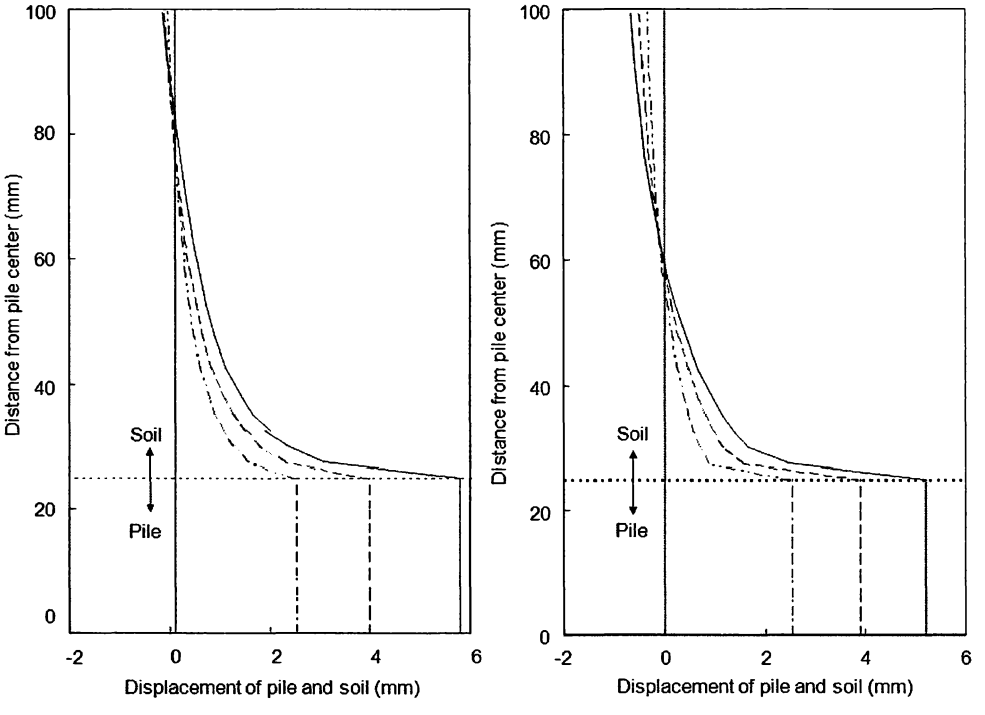

Fig. 3.11 Computed displacement distributions between the piles: (a) dry, (b) saturated

3.4 Soil-pile Interaction Spring

By using the same mesh and parameters, the load displacement relationship of a pile is computed for the horizontal cross section shown in Fig. 3.8 for different geotechnical conditions (i.e. sand/clay and dry/saturated). Because the limitation of space, only the analyses of dry sand will be discussed here. The pile was loaded with monotonic static and cyclic loads and the corresponding relative displacement was computed. The relative displacement (u) is defined as that of the pile relative to that of the soil at the periodic side boundary that is located at the pile to pile center (u_A- u_B) as shown in Fig. 3.8. Figure 3.12 shows an example of soil deformation around the pile after it was loaded laterally. The load (F) -relative displacement (u) curves for both monotonic static and cyclic loads are shown in Figs 3.13(a) and 3.13(b), respectively. As a comparison, simple shear tests of a single element of the soil were simulated using the same parameters. The relationship between shear stress (τ_{xy}) and shear strain (γ_{xy}) obtained from these simple shear tests under both monotonic and cyclic loads are shown in Figs 3.14(a) and 3.14(b), respectively.

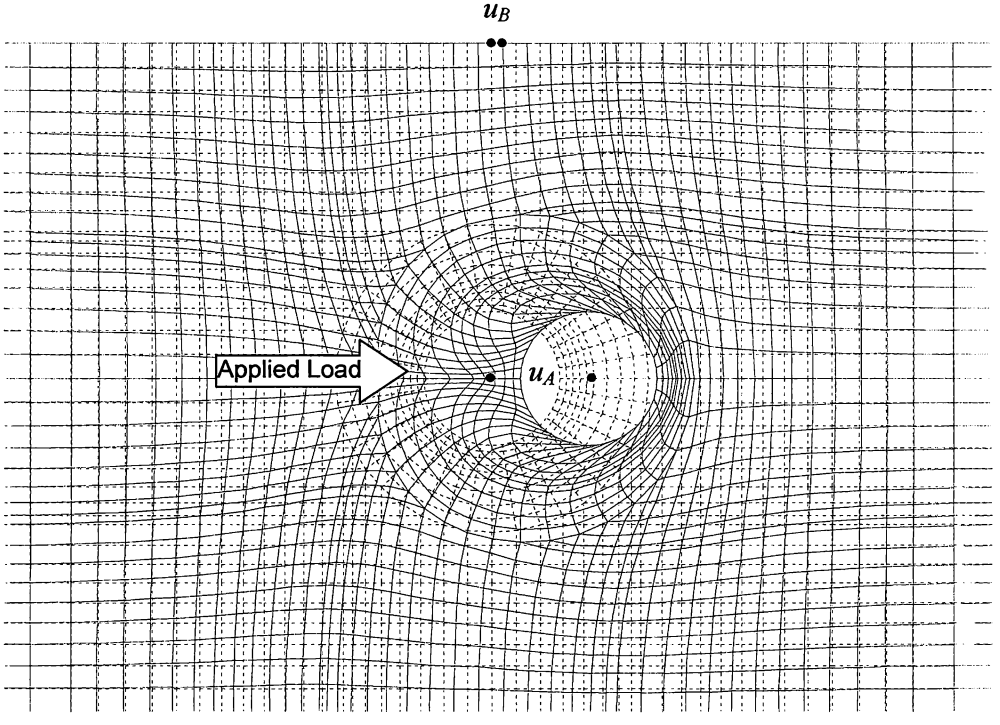

Fig. 3.12 Soil deformation around the pile: S/D = 5.0, D = 1.0 m

Although the mechanisms involved in the load-displacement curves are the results of complicated soil-pile interactions, the load-displacement curves shown in Figs 3.13(a) and 3.13(b) have practically the same shapes as those of stress-strain curves of the single soil element shown in Figs 3.14(a) and 3.14(b), respectively. This similarity is confirmed for a wide range of pile spacing and geotechnical conditions (Ozutsumi. 2003). Based on the above similarity, the amplitudes of relative displacements of the pile are normalized by the amplitudes of shear strains of the single soil element. The normalized relative displacement ($\beta_p = u / \gamma_{xy}$) is plotted against the current load of the pile relative to its ultimate load for different values of S/D in Fig. 3.15. The amplitudes of pile loads are also normalized by the amplitudes of soil shear stresses. The normalized pile load ($\alpha_p = F / \tau_{xy}$) is plotted against S/D as shown in Fig. 3.16. Note that α_p and β_p shown in Figs. 3.15 and 3.16 were obtained for D = 1m and soil thickness (L) of 1 m. Ozutsumi (2003) used α_p and β_p explained above to get generalized expressions for the relative displacement and pile load (spring force) as follow:

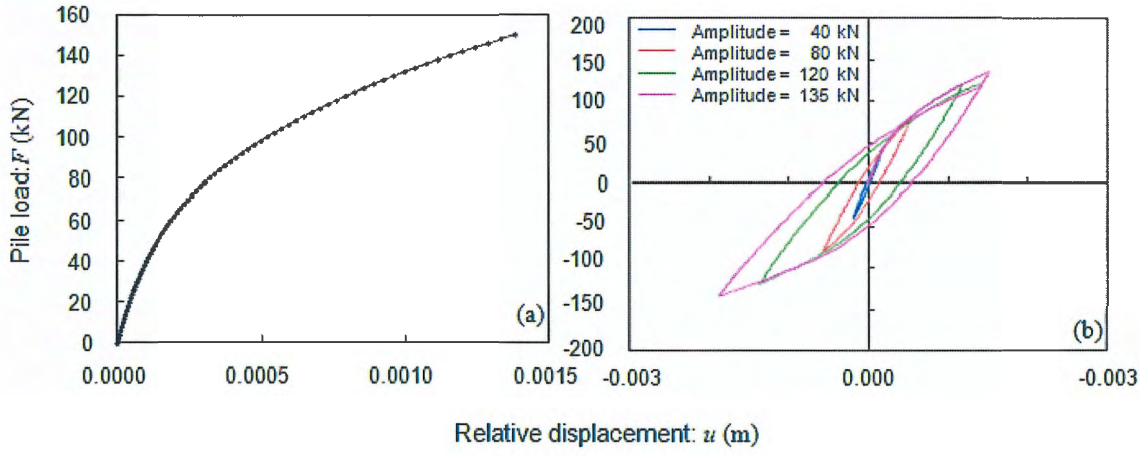

Fig. 3.13 Load-relative displacement relationship of the soil-pile system in the simplified model (S/D = 5.0): (a) monotonic static load; (b) cyclic load

$$\gamma_{xy} = (\text{Relative displacement}) / (D \times \beta_p) \tag{3.19}$$

$$\text{Spring force} = (L \times D \times \alpha_p) \times \tau_{xy} \tag{3.20}$$

$$\tau_{xy} = f(\gamma_{xy}) \tag{3.21}$$

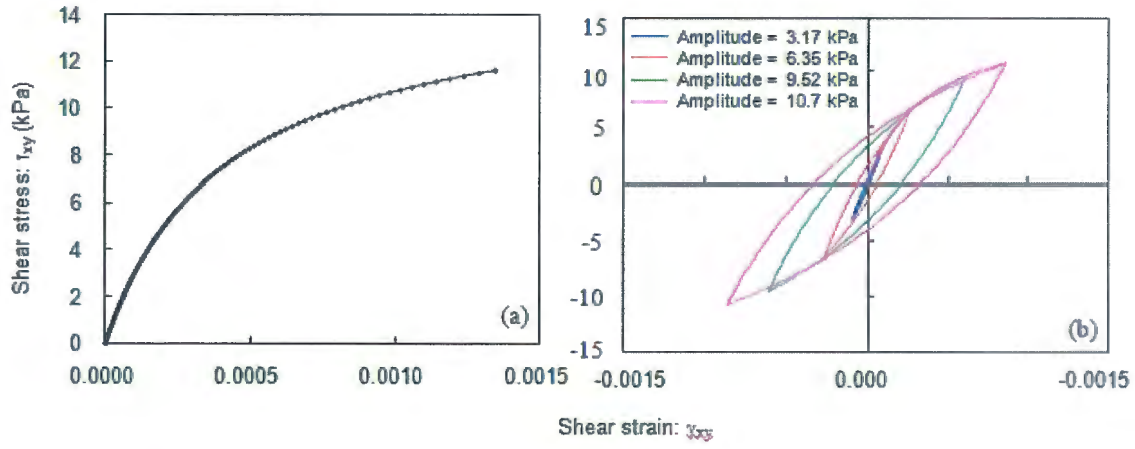

Fig. 3.14 Shear stress-shear strain relationship of a single soil element: (a) monotonic static; (b) cyclic simple shear

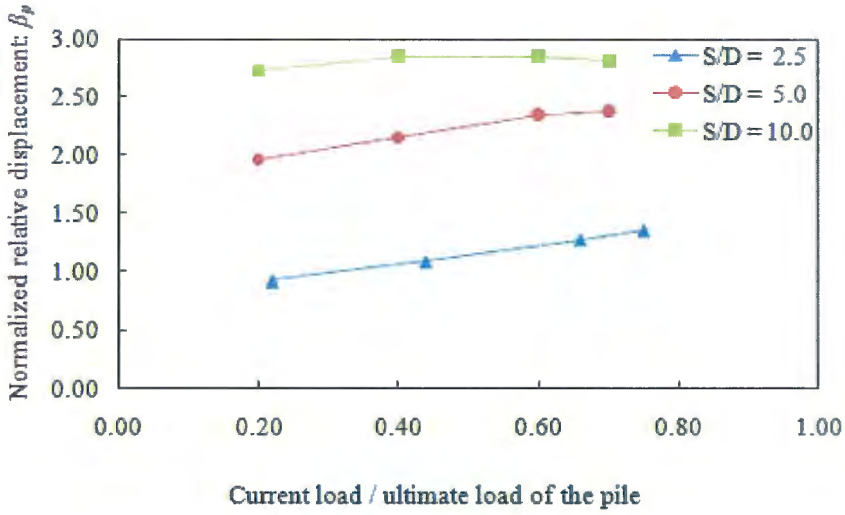

The path dependent function f in Equation (3.21) is given by using a fictitious single soil element of a multiple shear mechanism model.

For the analysis of soil-pile interaction, 2D analysis domains are set for a vertical cross section of soil-pile system. In this analysis, the soil-pile interaction in horizontal plane formulated through Equations (3.19) through (3.21) is idealized as a soil-pile interaction spring element as shown in Fig. 3.17.

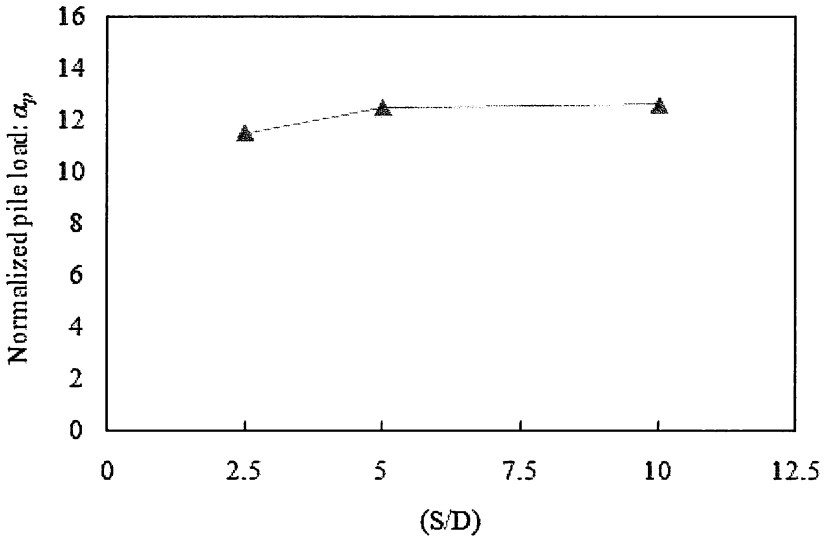

Fig. 3.16 Normalized pile load (α_p) variation with (S/D): dry sand

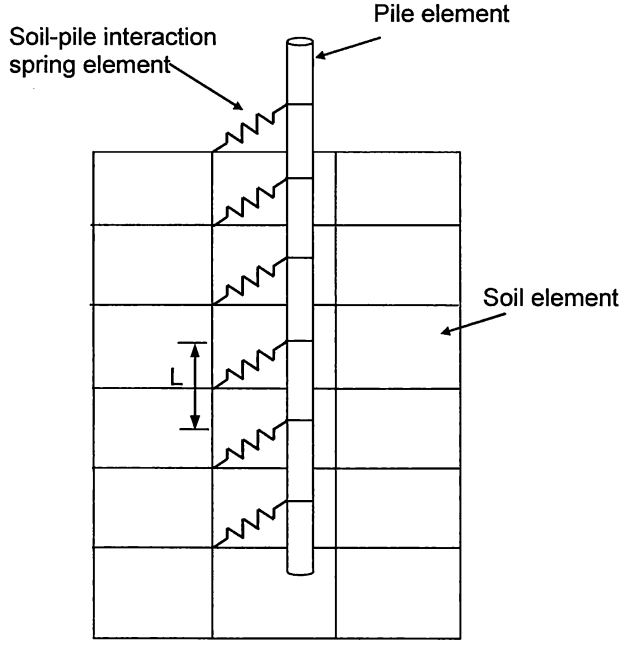

Fig. 3.17 Concept of the soil-pile interaction spring element

3.5 Some Comments on Soil-pile Interaction Spring

I. While the conventional spring elements used in the analysis of soil-pile interaction is embedded in the same plane of the two dimensional finite element analysis domain, the soil-pile interaction spring defined in this study is used as a spring that connects a free pile to a two dimensional cross section of soil between the piles.

II. The resistance of the soil-pile interaction spring (spring force) and consequently the lateral carrying capacity of the pile are dependent on the effective mean stress (confining pressure) of the surrounding soil at a specified relative displacement of the pile. The mechanism of this dependency can be described as follows:

1- In Equation (3.20), the spring force is proportional to the shear stress of soil τ_{xy}.

2- In Equation (3.4), the second term (the multiple shear mechanism without volume change) indicates that shear stress of soil τ_{xy} is proportional to the virtual shear stress $q^{(i)}$.

3- In Equation (3.13), the virtual shear stress $q^{(i)}$ is proportional to parameter q_v.

4- In Equation (3.16), parameter q_v is proportional to the shear strength of soil τ_m.

5- In Equation (3.18), the shear strength of soil τ_m is proportional to the effective mean stress σ'_m. Thus, there is a direct relationship between the confining pressure of the soil surrounding the pile and the pile lateral resistance.

III. In practice, gapping occurs at the rear of a laterally loaded pile shafts in cohesive soil. In pseudo random back-and-forth cyclic loading, such as occurs in an earthquake, gapping will occur near the ground surface on both sides of the pile shaft. Although the importance of soil-pile gap (separation) in the static and dynamic lateral resistance of single and group piles, this effect is not considered during modeling the soil-pile interaction spring.

IV. When the pile is subjected at its head to vertical loads or overturning moments, relative sliding between the pile and the surrounding soil will take place when the soil at the interface is sheared to a certain limit. Soil-pile sliding is also not considered during modeling the soil-pile interaction spring.

An attempt to model the effect of soil-pile separation and sliding in the analysis of lateral loaded piles using soil-pile interaction springs is done and details are given in the next section.

3.5.1 Soil-pile separation and sliding mechanisms

Subjecting a pile in cohesive soil to lateral loading caused the soil on the passive side (compression side) to move with the pile, but as previously mentioned, the soil on the active side (extension side) might not move with the pile. Hence, a gap occurred between the soil and pile surface on the active side (Tuladhar et al. 2008) as depicted in Fig. 3.18(a). To simulate this phenomenon, joint elements were used at the soil-pile interface. As shown in Fig. 3.18(b), the separation-contact model of the compression side was idealized using a high rigidity spring (Kn) between the pile and soil elements to avoid the overlapping of the elements during compression. Two cases, with and without separation, were considered on the tension side. In the separation case, no stress will transfer between the pile and the soil at any tension stress value, whereas the second case (without separation case) allows stress, including tensile stress, to transfer between pile and soil.

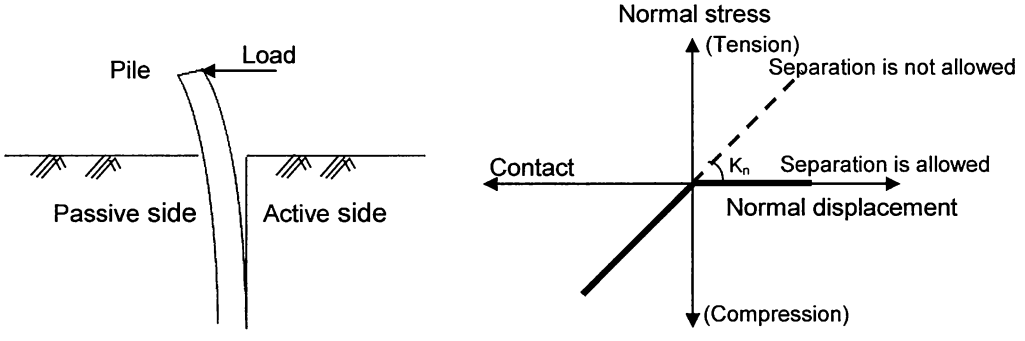

(a) (b)

Fig. 3.18 Separation-contact model for joint element between pile and soil.
(a) Gap formation behind a pile; (b) separation-contact model

Figure 3.19 shows the mechanism of sliding at the interface. Figure 3.18 indicates that sliding will initiate when the shear stress at the interface exceeds a certain value of τ_f given by the equation:

$$\tau_f = c_J + \sigma \tan\phi_J \tag{3.22}$$

where c_J and ϕ_J are shear strength parameters of soil at the interface.

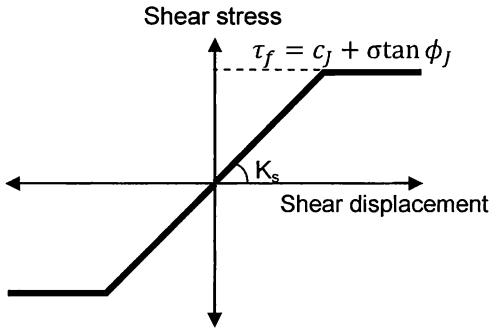

Fig. 3.19 Sliding mechanisms at the soil-pile interface

The effect of soil-pile separation on the behavior of single and grouped piles under both static and dynamic loads will be discussed in details in the next chapter.

3.6 Conclusions

The chapter presents recent developments on the soil-pile interaction in horizontal plane. The primary conclusions may be summarized as follows:

1. Local displacement field of soil in the vicinity of a pile associated with global displacement of soil around pile foundation shows vortexes at the pile side. Displacement at the pile side shows strain localization at the soil-pile interface, indicating a mechanism similar to a sliding. This fact implies that the finite element mesh size should be sufficiently small in the vicinity of the pile in order to represent these essential features of the local displacement field.
2. Computed local displacement field of soil through a multiple shear mechanism model in a horizontal plane are basically consistent with those measured. The computed load-displacement curves indicates that, for dry sand, the curves have similar shapes to those currently used in design practice in terms of *p-y* curve.
3. Although the mechanisms involved in the load displacement curve are the results of complicated soil-pile interaction as exemplified by the local displacement field described above, the load-displacement curves have practically the same shapes as those of the shear stress-shear strain of a single soil element under static and cyclic simple shear. Based on this

finding, the soil-pile interaction in horizontal plane is idealized as a soil-pile interaction spring element using a fictitious single soil element.

4. In addition to the soil-pile interaction spring, a joint element is used to idealize the soil-pile interface effect, including soil-pile separation and sliding effects.

References

1. Iai, S., Matsunaga, Y., and Kameoka, T. 1992. Strain space plasticity model for cyclic mobility. *Soils and Foundations*, 32(2): 1–15.
2. Iai, S., Tobita, T., Hussien, M.N., Rollins, K. M., and Ozutsumi, O. 2010. Soil-pile interaction under lateral load. *Soil-Foundation-Structure Interaction*. Orense, Chouw& pender (eds), London, 101–108.
3. Ozutsumi, O. 2003. Numerical studies on soil-structure systems on liquefiable deposit during earthquakes, Doctors Dissertation, Kyoto University.
4. Towhata, I. and Ishihara, K. 1985. Modeling soil behaviour under principle stress axes rotation, *Proceeding of the 5th International conference on Numerical methods in Geomechanics*, Vol. 1, 523-530.
5. Tuladhar, R., Maki, T., Mutsuyoshi, H. 2008. Cyclic behavior of laterally loaded concrete piles embedded into cohesive soil. *Earthquake Engineering and Structural Dynamics*, 37(1): 43–59. doi: 10.1002/eqe.744.

CHAPTER 4

Effect of Soil-Pile Separation on Performance of Pile Group

Contents

4.1 Introduction

Soil-pile separation is one aspect of SSI that is still not fully understood and poses a challenge to geotechnical engineers. When a pile in a cohesive soil deposit is subjected to lateral loading, the soil on the compression side moves with the pile whereas the soil on the extension side might not move together with the pile. Thus, a gap forms at the soil-pile interface on the extension side (Tuladhar et al. 2008). Two primary variables of the soil-pile system must be carefully evaluated in this situation. One is the deformation of soil due to pile displacement. This variable has to be evaluated even when the soil-pile separation occurs. The other is the soil-pile gap formation, especially the threshold level of displacement or the triggering level of the gap formation. These two variables might be relatively easy to analyze based on the appropriate FE modeling of a coupled soil-pile system. A sophisticated level of analysis might be based on 3D FE techniques that incorporate nonlinear behaviors of the soil (e.g., Brown and Shie 1991; Kimura and Zhang 2000; Tahghighi and Konagai 2007). However, the analysis becomes more challenging when the effect of soil-pile separation is studied on pile groups or when a dynamically loaded pile group associated with dynamic soil response is involved. In these situations, which are complex but of the utmost importance in practical design, how soil-pile separation can be simulated and how this separation affects the performance of the lateral loaded pile group remain issues to be studied.

In this chapter, the effect of soil-pile separation is studied with respect to the performance of a laterally loaded pile group. Full-scale tests consisting of a combination of a single and 3 × 5 group pile under static and dynamic lateral loads at a clayey site presents a unique opportunity for this end and allows a rigorous study while restricting the arbitrary back-fitting of parameters that would be necessary if only a partial combination of the test data were available. The 2D FE analysis based on the multi-shear mechanism constitutive relationship, **FLIP** (Iai et al. 1992), is used to analyze the results of this series of full-scale tests. In this study, two cases of numerical simulation were considered. The first case involves soil-pile separation if tension stress is generated at the soil-pile interface, while in the second, soil-pile separation does not occur even if there is tension stress at the soil-pile interface. Herein the effect of soil-pile separation on the overall behavior of laterally loaded pile groups under static and dynamic lateral load is studied in detail.

4.2 Lateral Load Test of a Full-Scale Single Pile and 3×5 Pile Group

4.2.1 Test site

The test site is located approximately 300 m north of the Federal Aviation Administration (FAA) control tower in a large unused lot owned by the Salt Lake City International Airport, USA. The site is a prime location for geotechnical investigations as well as foundation testing because of the relative seclusion and free space for easier access and mobilization of construction and testing equipment. Figure 4.1 shows the idealized soil profile at the test site. Although the soil profile contained some sand layers, the first three meters were composed mostly of soft clays and silts. The water table was at the ground surface. Soil samples were collected using hand augers and drill rigs. Cohesionless soil samples were obtained using a standard 50.8 mm diameter split spoon sampler. Thin-walled Shelby tubes, 76 mm in diameter, were used to collect undisturbed cohesive soil samples. Five laboratory tests were performed: particle size distributions, Atterberg limits, soil classification, shear strength, and consolidation test. Five in situ tests were also performed at the site: cone penetration test, dilatometer test, pressure meter test, standard penetration test, and vane shear test (Snyder 2004).

4.2.2 Single pile test layout

For proper assessment of the pile group performance, single pile test was conducted as a reference. A single pile was installed just west of the 3×5 pile group. The test pile had a 0.324 m outside diameter and wall thickness of 9.5 mm. The pile conformed to ASTM 252 Grade 3 specifications. The steel pipe pile was driven closed end to an embedment depth of 11.6 m. Figure 4.2 illustrates the layout of the single pile load test. A W760×284 (AISC Shape W30×191) reaction beam was placed against the west column of piles from the 3×5 pile group. A 1.34 MN hydraulic jack was placed between the beam and a channel section welded to the pile. A hemispherical swivel plate was placed between the channel section and the jack to allow for free rotation preventing any eccentric loading on the pile. A lateral load was applied 495 mm above the ground surface. Instrumentation was used to measure load, pile-head deflection, and strain with depth. Bending moments were computed from the recorded data. The load was measured with a 1.34 MN load cell placed between the jack and the swivel plate as shown in Fig.

4.2. The strain of the pile was measured by electrical resistance type strain gages made by Texas Measurement, Inc. (model WFLA-6-12). A total of 38 strain gages (19 on each side of the pile) were placed at regular intervals of 0.405 m to a 5.5 m depth, 0.91 m to a 9.14 m depth, and 1.2 m to the end of the pile. A string potentiometer with an accuracy of 0.25 mm was used to measure the pile-head deflection at the load point. (Snyder 2004).

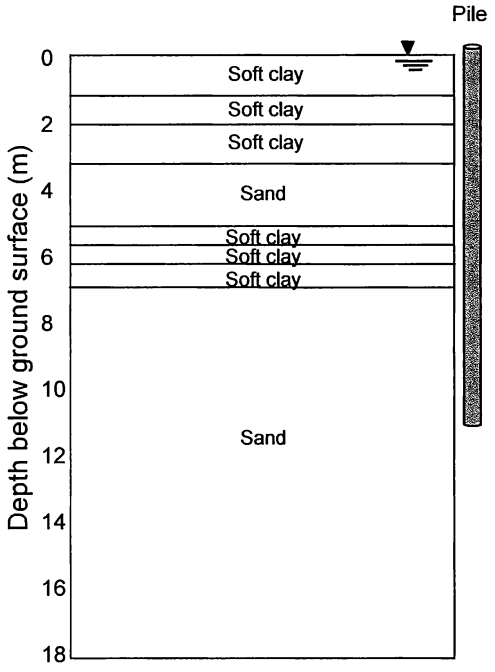

Fig. 4.1 Idealized soil profile at the Salt Lake City International Airport

4.2.3 Pile group test layout

The piles in the group were driven in a 3×5 pattern with a nominal spacing of a 3.92-pile diameter from center to center in the loading direction and of a 3.29-pile diameter perpendicular to the loading direction. The test piles in the group had the same sectional and material properties as the single pile. Figure 4.3 shows a photograph of the overall layout of the single pile and the 15-pile group. The single pile was driven about six pile diameters west of the 15-pile group. The single pile was located with the intent that it be close enough that the soil properties would be similar but far enough away that it would not be affected by the testing of the pile group. Two reinforced concrete drilled shafts (1.22 m diameter) were installed 7.92 m north of the front or northernmost row of the 15-pile group. These drilled shafts were required to provide a sufficient

reaction to load the pile group to high enough deflection levels so that group effects could be observed. The load was applied either statically or dynamically 495 mm above the ground surface. For static loading, the load was applied by two 1.34 MN hydraulic jacks powered by a hydraulic pump with a maximum pressure of 69,000 kPa. One jack was placed between each of the drilled shafts and a W760×284 (AISC Shape W30×191) reaction beam as shown in Fig. 4.4. Hemispherical swivel plates were attached to the face of the shaft as well as the beam for the jacks to bear on. This allowed for rotation preventing any eccentric loading on the drilled shafts (Snyder 2004).

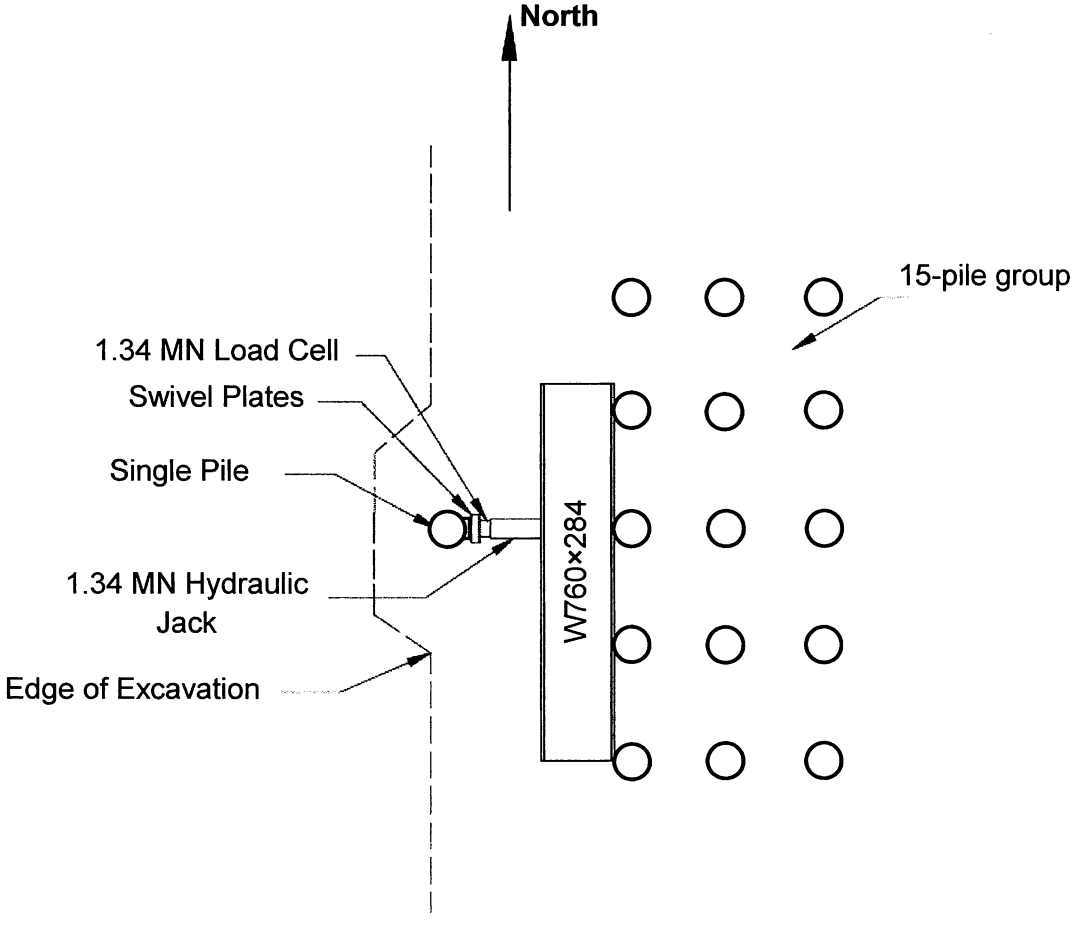

Fig. 4.2 Plan view of the test layout for the single pile

Fig. 4.3 Photograph of the full-scale lateral load test layout

Figure 4.5 illustrates the load frame setup for the 15-pile group. Two T-sections, welded to the beam, had four holes each in which eight Dywidag (Dywidag was a construction company based in Munich) bars were connected between the reaction beam and another two T-sections welded to another identical reaction beam. This beam was attached to a steel load frame assembled in a manner to provide the correct spacing for the piles. The Dywidag bars used were #9 (32 mm diameter) with a yield strength of 517,000 kN/m^2. Tie-rods were pin-connected to steel channel sections welded to each pile with the center of the section at 495 mm above the ground surface. The tie-rods were then attached to the pile group load-frame so that each pile was constrained to have the same deflection. The basic path of load transfer began with the jacks pushing on the drilled shafts and a reaction beam transferring the load through the Dywidag bars that pulled another reaction beam connected to the load frame. The load was then transferred from the load frame through the tie-rods into the piles. Figure 4.6 shows a photograph of the overall loading system for the 15-pile group. The load frame was designed to be essentially rigid relative to the piles so that each pile was constrained to have the same deflection for a given load (Rollins et al. 2006). The load frame had six wheels welded to the bottom to minimize friction and loss of load transfer. The wheels rolled across steel beams resting on the excavated ground

surface that acted as runners. This same system of wheels and runners were used underneath the other reaction beam (Snyder 2004).

Fig. 4.4 Photograph of hydraulic jack with hemispherical swivel plates on each end loading against the drilled shaft cap and the W760×284 reaction beam: static loading test

For dynamic loading, a 311 kN statnamic device consists of a load cell, piston with a combustion chamber, reaction mass, and exhaust vent (silencer) is used. The reaction mass is composed of several rings of concrete assembled together with a silencer running through the center of the rings. Figure 4.7 shows a photograph of the statnamic device used in the tests. The statnamic test is performed by launching the reaction mass and silencer away from the pile group. This is done by igniting a solid fuel propellant (fuel pellets) inside the combustion chamber. The fuel, once ignited, causes a sudden expansion of high pressure gas that rapidly applies a large force to the pile group and propels the reaction mass in the opposite direction. The force developed is determined by the quantity of fuel pellets placed inside the piston. The test layout of the dynamic test is provided in Fig. 4.8. The same load frame and tie rod load cells that were used in the static tests on the pile group were used for the dynamic tests. However, the Dywidag bars were disconnected from the load frame eliminating the drilled shafts from the test setup. The transfer of load through the frame was the same as the static load test.

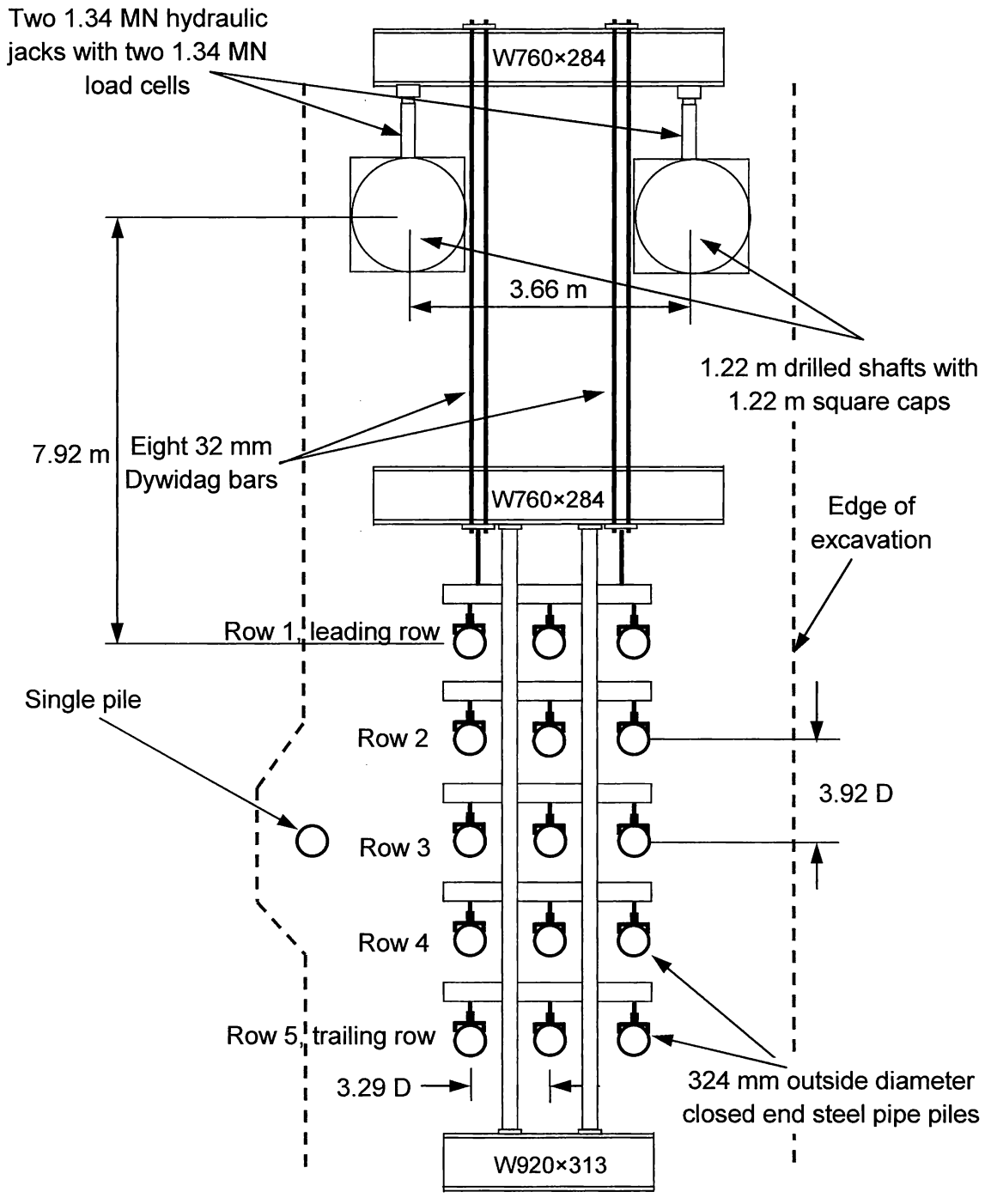

Fig. 4.5 Plan view of loading system for the 15-pile group and drilled shafts: static loading test

Fig. 4.6 Photograph of the overall view of the loading system from north of the 15-pile group: static loading test.

Fig. 4.7 Photograph of the statnamic device used to dynamically load the 15-pile group

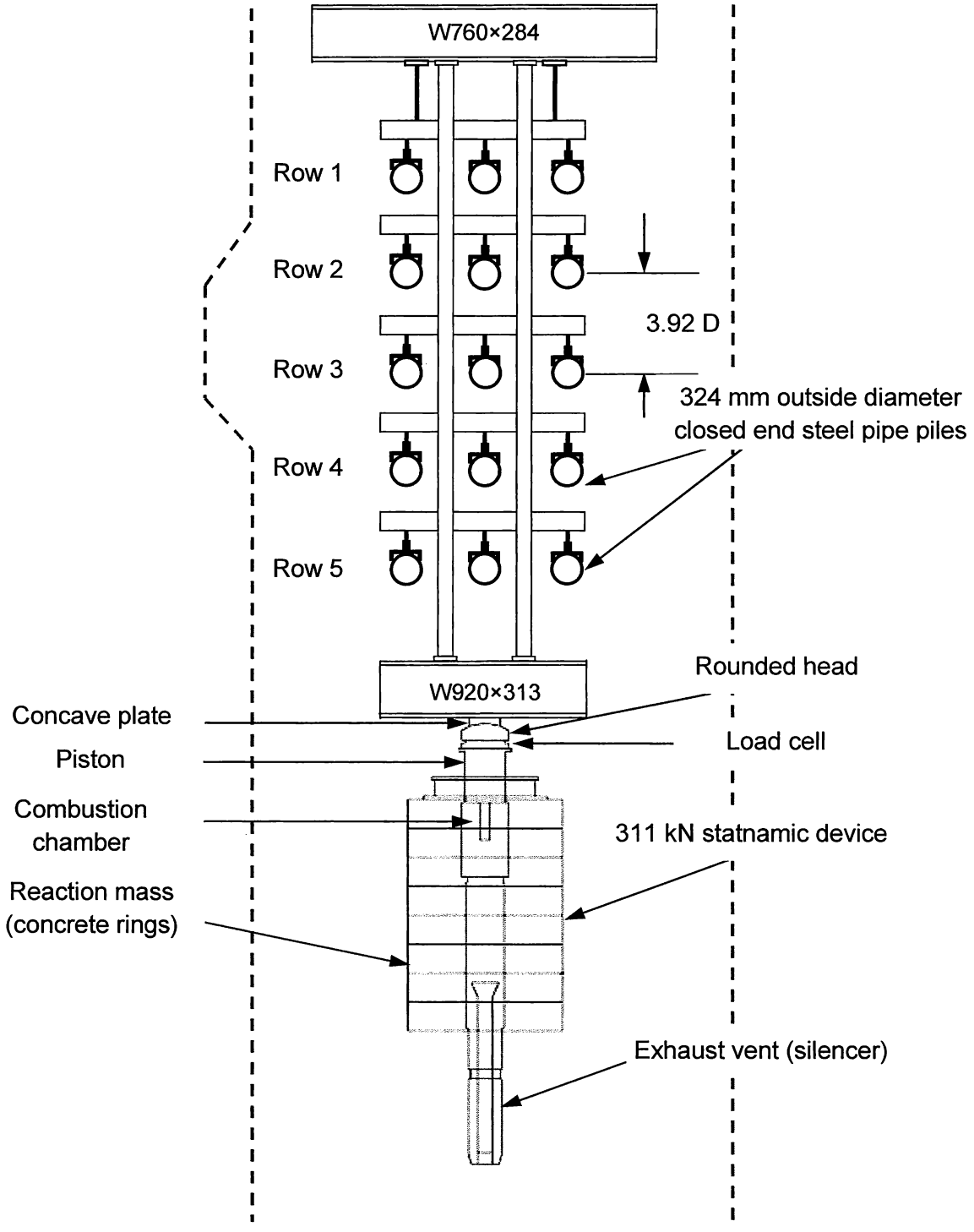

Fig. 4.8 Plan view of loading system for the 15-pile group: dynamic loading test

The tested piles were loaded in the same direction as the static tests. The statnamic sled was supported upon two 7.9 m long W920×223 beams, which were laid on their weak sides. Railroad ties were laid on the beams in between the flanges to provide a clear path of movement for the statinamic device. The steel beams were in turn supported by four H-piles which were driven approximately 7.6 m below the base of the beams to utilize the bearing capacity of a dense sand layer at that depth eliminating any settlement issues with the 311 kN statnamic device aided in maintaining the required elevation of the device to load the piles at 495 mm above the excavated ground surface around the piles. This prevented any eccentric loading on the pile group and allowed for a tight fit between the concave plate and the rounded head (Snyder 2004).

The instruments in the 15-pile group measured pile-head deflection, applied load, and strain versus depth. Individual pile loads were measured by strain gage pairs attached to tie-rods, which functioned as load cells. The tie-rods connected the piles to the load frame using a pinned connection to produce a zero moment free-head boundary condition. For static loading, two 1.34 MN load cells were placed on each of the hydraulic jacks to measure load applied to the drilled shafts. This allowed comparisons to be made between the total measured load on the pile group compared to the drilled shafts as a check for consistency and accuracy. The average difference between the total measured loads was 4.9% at peak loads with a maximum difference of 8.6%. For dynamic loading, additional load cell is placed between the piston and the head of the statnamic device as shown in Fig. 4.8. This load cell was used to measure the total applied force and provided a comparison to the sum of the load measured from all the group piles. Seventeen linear variable differential transformer (LVDT) transducers, which had an accuracy of 0.127 mm, were used to measure pile-head deflections. The center piles of each of the five rows were monitored by 30 electrical resistance type strain gages (15 on each side) placed at regular intervals of 0.61 m to a 4.88 m depth, 0.91 m to a 7.62 m depth and 1.22 m to the end of the pile (Snyder 2004).

4.3 Finite Element Modeling and Parameter Identification

4.3.1 Finite elements

The 2D FE program FLIP was employed to simulate the full-scale lateral load tests of the single and group piles. The analysis focused on the five piles in the middle row of the 3x5 pile group. Figure 4.9 shows the general layout and meshing of the FE model. The same meshing of the soil

profile was used to analyze the single pile. The analysis is conducted under undrained conditions. Side boundary displacements were fixed in the horizontal direction, while those at the bottom boundary were fixed in both the horizontal and vertical directions. The top and bottom of the piles were set as displacement and rotation free to simulate the condition of the full-scale tests.

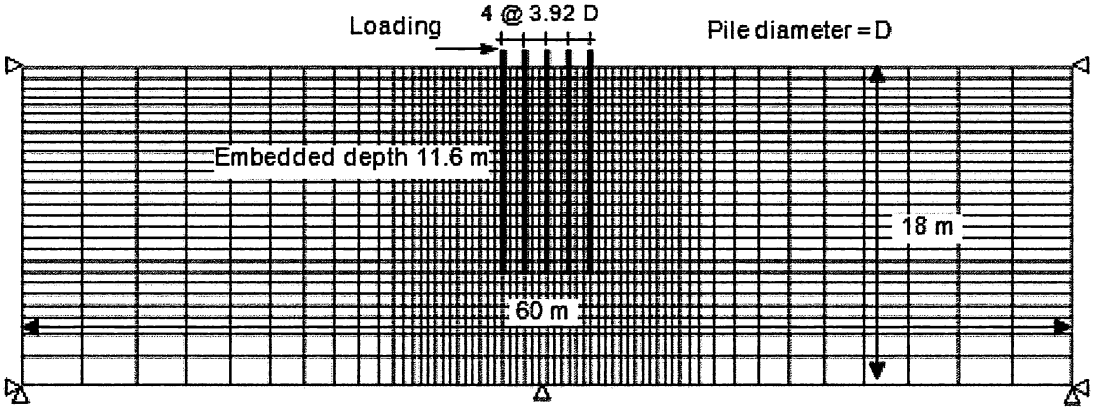

Fig. 4.9 General layout and meshing of the FE model

4.3.2 Soil model

The soil model used in this study consists of a multiple shear mechanism (Iai et al. 1992). The analysis adopted the idealized soil layers shown in Fig. 4.1. Soil properties were obtained from geotechnical investigation data at the site, which included standard laboratory tests, unconsolidated-undrained (UU) traixial tests, consolidation tests, and in situ tests such as the cone penetration test, pressure meter test, and standard penetration test. Figure 4.10 reports the shear strength values for the test site determined from laboratory and in situ tests conducted in 1996, 2002, and 2003. The 1996 tests showed evidence of stiff clay in the upper 1 m of the profile. However, this stiff layer was not encountered in any of the shear strength tests performed much closer to the 3×5 group pile in 2002 and 2003. At a depth of 1 m, the shear strength from 2003 unconfined test turned out to be about 27 kPa, which is not close to the strength observed in 1996 tests. As shown in Fig. 4.10, the shear strength profile defined in this study is consistent with shear strengths determined from laboratory and in situ tests conducted in 2002 and 2003. Except for the reduced shear strength of the first three meters of the profile, the defined profile is identical to the detailed profile used in the analysis reported by Snyder (2004).

The elastic shear modulus G_{ma} for cohesive soil was determined using an undrained shear strength based on the correlation provided by Jamiolkowski et al. (1979), while that for cohesionless soil was determined using

$$G_{ma} = \rho V_s^2 \tag{4.1}$$

where ρ is soil density and V_s is shear wave velocity calculated using SPT data based on the correlation provided by Ohata and Goto (1978).

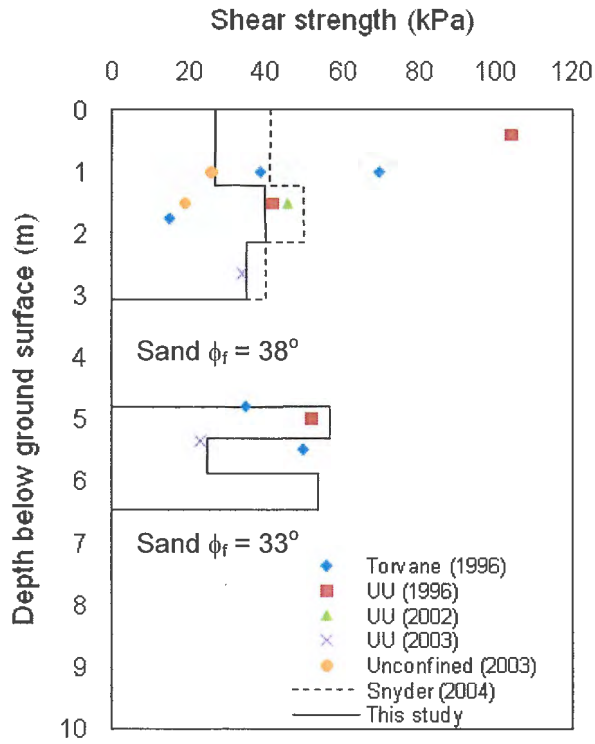

Fig. 4.10 Shear strength parameters for the soil profile used in this study compared to shear strengths determined from field and laboratory tests.

Variation of shear modulus in depth is consistent with the variation of tip resistance and sleeve friction of the CPT test results reported in Snyder (2004). The bulk modulus of the soil skeleton K_{ma} was determined assuming a Poisson's ratio υ of 0.33. Table 4.1 lists the model

parameters for the soil elements used in this study. Values of these parameters pertain only to the 1st cycle. As described later, degradation effects were considered upon applying a cyclic load.

4.3.3 Pile model

Bilinear 1D beam elements with three degrees of freedom per node were used to model the piles. Normal force, shear force, and bending moment of each element were obtained directly from the finite element program. Table 4.2 defines the model parameters of pile elements. The parameters for piles were obtained from the industrial standard (Tobita et al. 2006).

Table 4.1 Idealized soil layers and model parameters for soil elements

Soil layer	Depth (m)	Saturated unit weight, γ_{sat} (t/m^3)	σ'_{ma} (kPa)	G_{ma} (kPa)	υ	K_{ma} (kPa)	ϕ_f (degrees)	c (kPa)	Max damping ratio, (h_{max})
Soft clay	0-1.22		36.72	12,200		31,720		27	
Soft clay	1.22-2.14	1.92	41.98	18,000		46,800		40	
Soft clay	2.14-3.06		47.35	15,800		41,080		35	
Sand	3.06-4.80	1.83	52.93	161,000		418,600	38		
Soft clay	4.80-5.33		62.62	34,100	0.33	88,660		56.9	0.20
Soft clay	5.33-5.87	1.92	67.83	15,000		39,000		25	
Soft clay	5.87-6.48		67.83	32,400		84,240		54	
Sand	6.48-11.6	1.83	77.67	127,000		330,200	33		
Sand	11.6-18.00		85.5	40,600		105,560	33		

Table 4.2 Model parameters for pile element

Shear modulus, Gs (kPa)	Poisson's ratio (υ)	Density, ρ (t/m^3)	Area/unit width	Initial flexural rigidity (kPa)	Flexural rigidity after yield (kPa)	Plastic bending moment (kN·m)
77,500,000	0.29	7.9	0.02897	108,671	65,200	875

4.3.4 Soil-pile separation and sliding mechanisms

Subjecting a pile in cohesive soil to lateral loading caused the soil on the passive side (compression side) to move with the pile, but as previously mentioned, the soil on the active side (extension side) might not move with the pile. Hence, a gap occurred between the soil and pile surface on the active side (Tuladhar et al. 2008) as depicted in Fig.4.11 (a). To simulate this phenomenon, joint elements were introduced at the soil-pile interface. As shown in Fig.4.11 (b), the separation-contact model of the compression side was idealized using a high rigidity spring

(Kn) between the pile and soil elements to avoid the overlapping of the elements during compression. Two cases, with and without separation, were considered on the tension side. In the separation case, no stress will transfer between the pile and the soil at any tension stress value, whereas the second case (without separation case) allows stress, including tensile stress, to transfer between pile and soil.

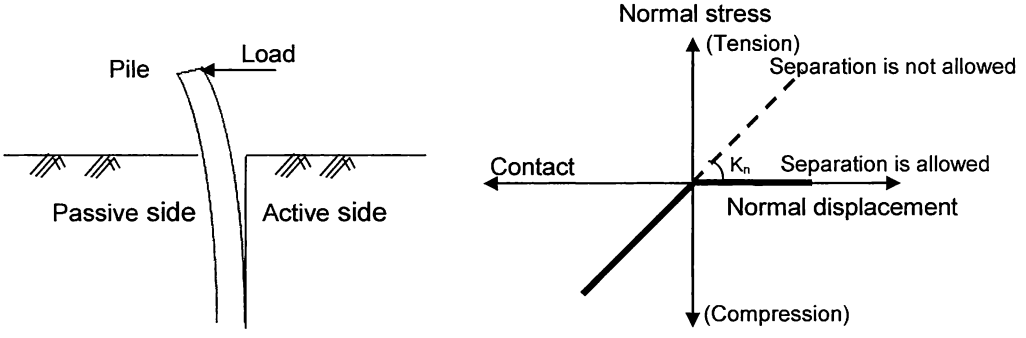

Fig. 4.11 Separation-contact model for joint element between pile and soil. (a) gap formation behind a pile; (b) separation-contact model

Figure 4.12 shows the mechanism of sliding at the interface. Figure 4.12 indicates that sliding will initiate when the shear stress at the interface exceeds a certain value of τ_f given by the equation:

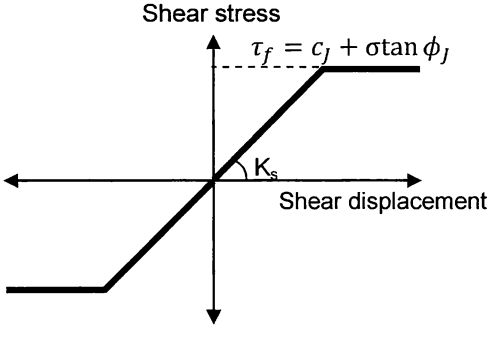

Fig. 4.12 Sliding mechanisms at the soil-pile interface

$$\tau_f = c_J + \sigma \tan \phi_J \tag{4.2}$$

where c_J and ϕ_J are shear strength parameters of soil at the interface. The shear strength of the interfaces was defined with zero cohesive strength and 2/3 of the friction angle for sandy soils. In the case of clayey soils, the interfaces were assumed to have zero frictional strength and the same cohesive strength of the surrounding soil. The interface strength values depend very much on the type of pile material (wood, steel, or concrete) and method of installation (driven or bored). The interface strength properties selected for the analyses fall within the range of properties recommended for estimating the skin friction capacity of piles (Bowles 1988). The normal stiffness and shear stiffness of the interface elements were initially set to 10^6 kN/m^2 /m. These values were decided after performing several analyses with different interface stiffness values (see Appendix A2). Table 4.3 defines the model parameters for the joint elements.

Table 4.3 Model parameters for joint element

Interface angle of friction (ϕ_J)	Cohesion(c_J)	Normal stiffness (kN/m^3)	Tangential stiffness (kN/m^3)
2/3 ϕ_f	c	1,000,000	1,000,000

4.3.5 End bearing spring

The axial soil reactions at pile tips were simulated using nonlinear spring elements (Q-z curve). The nonlinear spring at the pile tip can be represented according to Zhang et al. (1999) as

$$z = \frac{Q_b(1-\upsilon)}{4r_o G_{ma}(1-\frac{Q_b}{Q_f})} \tag{4.3}$$

where Q_f is ultimate tip resistance (force). G_{ma} and υ are initial shear modulus and Poisson's ratio of the soil at the pile tip, respectively. r_o is pile radius and Q_b is mobilized tip resistance (force) for a given displacement z.

4.3.6 Soil-pile interaction spring

The interaction between a pile and the surrounding soil in 3D type is idealized in the 2D analysis using nonlinear soil-pile spring elements that described in Chapter 3.

4.4 Single Pile under Static Load

In the analysis of a single pile under static load, the lateral load was statically applied at the pile head (0.495 m above the ground surface) until a displacement of 90 mm at the loading point was achieved. Figure 4.13(a) shows the computed and measured load deflection curves at the pile head with and without soil-pile separation. The analysis without separation greatly overestimated the lateral load-carrying capacity of the pile. In fact, the soil-pile gap was observed *in situ* at the full-scale tests as shown in Fig. 4.14. In contrast, the analysis considering soil-pile separation provided an improved load-deflection curve and agreed well with the field results. As previously demonstrated, the separation between the soil and pile occurred in the analysis when normal stress at the interface was changed from compression to tension.

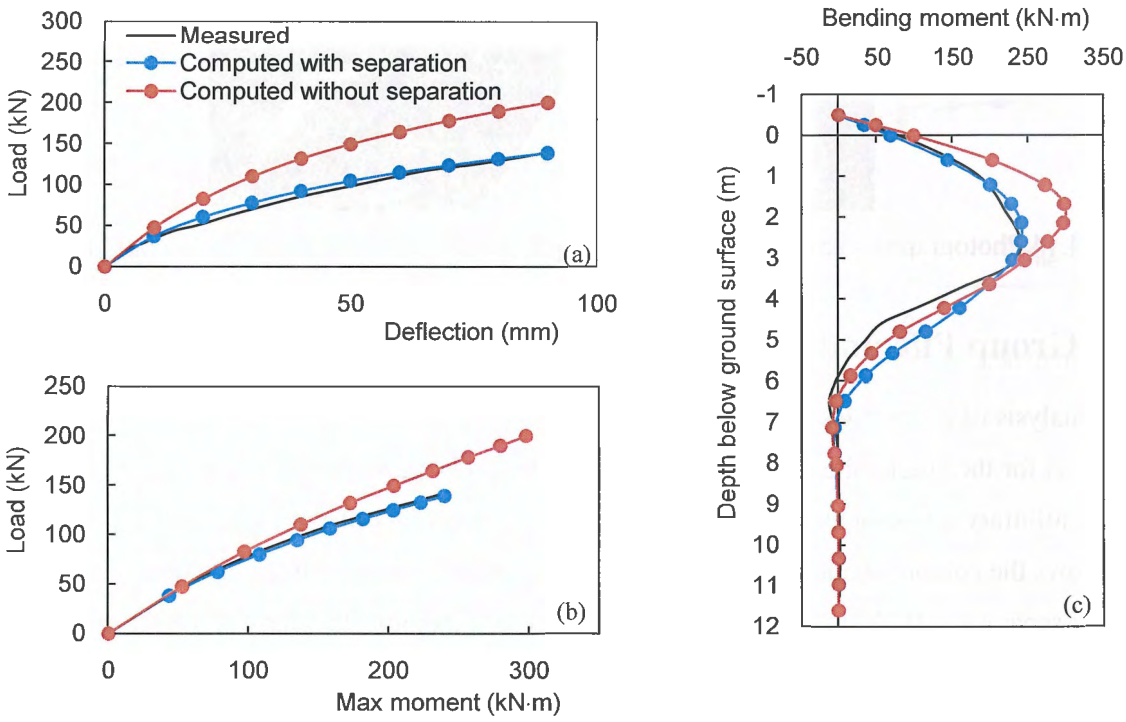

Fig. 4.13 Single pile response under a static load: (a) load-deflection curve, (b) load-maximum moment curve, and (c) moment versus depth below ground surface curve.

The computed load-maximum moment curve and moment profile, which corresponded to a pile head deflection of 89 mm, with soil-pile separation also agreed well with the measured

curves as shown in Figs. 4.13(b) and 4.13(c). At the same load level, the analysis without soil-pile separation underestimated both the deflection and maximum bending moment. The percentage of underestimation increased as the load increased and reached, at the maximum applied load, 50% for deflection and 22% for maximum moment. At a target deflection of 90 mm, ignoring soil-pile separation led to a 43% overestimation of the ultimate lateral load-carrying capacity of the pile.

Fig. 4.14 Photograph of gap formation behind a pile when the pile is deflected laterally to the

4.5 Group Pile under Static Load

In the analysis of group piles under static load, the lateral load was statically applied in the same manner as for the single pile. The same model parameters as those for the single pile were used without arbitrary adjustment or back-fitting to the measured data of the group pile test. Figure 4.15 shows the computed and measured average load per pile versus deflection with and without soil-pile separation. Both the measured and computed results indicated that the load distribution in the pile group was not uniform, but a function of the pile position. Both the analyses with and without soil-pile separation slightly overestimated the load carrying capacity of the leading pile (pile no. 1), whereas the computed loads of the second, third, and fourth piles agreed well with the measured ones. For the trailing pile (pile no. 5), the computed results of the analysis with separation agreed well with the measured one, but the computed results without separation overestimated the load carrying capacity of the trailing pile. Regardless of load level, analysis without soil-pile separation underestimated the deflection of the trailing pile. The percentage of

underestimation increased as the loading increased, and reached 70% at the maximum applied load. At the maximum target deflection of 83.4 mm, ignoring soil-pile separation overestimated the ultimate lateral load-carrying capacity of the trailing pile by 73%.

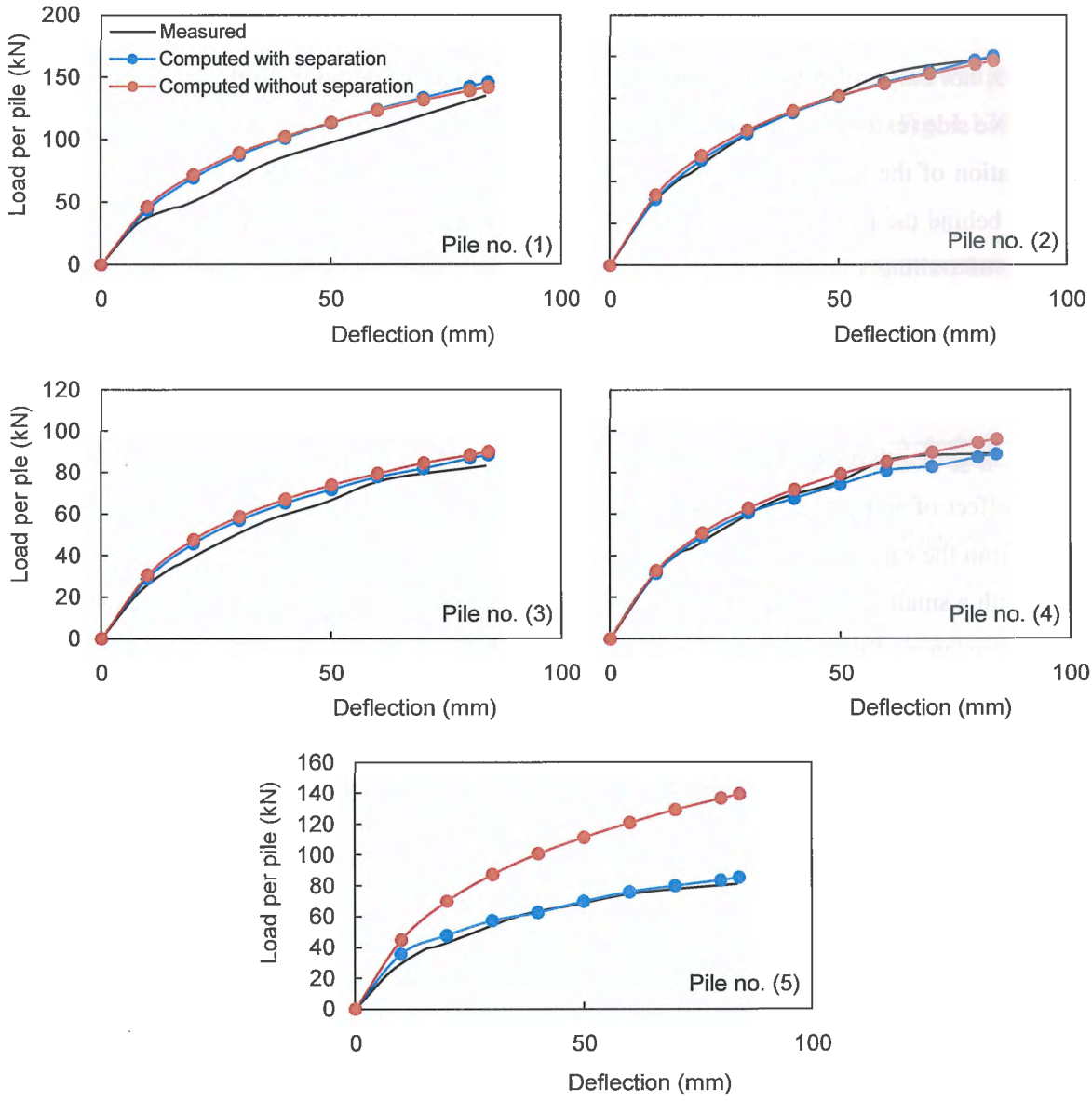

Fig. 4.15 Group pile response under a static load

The effect of soil-pile separation on the trailing pile was similar to that on the single pile, but the effect of soil-pile separation on the other piles in the group differed. This distinctive

effect of soil-pile separation on group piles was further examined by plotting the earth pressure (total horizontal soil stress) at points just at the back of and in front of each pile in the group. Figs 4.16(a) and 4.16(b) plot the variation of both earth pressure and pore pressure with deflection curves for piles 1, 3, and 5 at a depth of 0.30 m with separation and without separation, respectively. For piles 1 and 3, soil-pile separation show little effect on earth pressures not only in front of the piles but also at the back of the piles. In the analysis, soils on the active side (extension side) of each pile moved in the direction of pile deformation due to the deformation of the next column of pile behind the pile in question; therefore, a gap cannot be formed behind the pile in relatively closely spaced pile groups. Soil deformation due to the next column of trailing pile pushed on these piles, diminishing the potential for a soil-pile gap. However, the effect of soil-pile separation for the trailing pile (pile no. 5) differed from those for piles 1 and 3. Although the earth pressure-deflection curves from a point at the front of the pile showed similar trends in both analyses but the analysis with soil-pile separation induced a slightly larger earth pressure, the earth pressure at the back of the pile was significantly affected by the effect of soil-pile separation. In the analysis with soil-pile separation, the earth pressure began from the earth pressure at rest but gradually decreased to zero in the relative early loading stage with a small deflection. The extension zone at the back of the pile did not contribute to the lateral resistance of the pile when separation occurred. In contrast, the earth pressure at the back of the pile computed without separation progressively decreased to zero and then generated a negative earth pressure, which corresponded to the negative pore pressure built up behind the pile as shown in Fig. 4.16(b). In the analysis without soil-pile separation, the soil behind the pile pulled the pile opposite to the loading direction, resulting in an excessive increase in the overall soil resistance during pile deformation.

Figures 4.17(a) and 4.17(b) show the ratio of the computed and the measured loads of each pile relative to the load of the single pile at target deflections of 10 and 83.4 mm, respectively. Both the measured and computed load distributions among the piles were not uniform. The load distribution curve obtained from the FE analysis without soil-pile separation had a concave shape with maxima at both ends (the leading and trailing piles) and a minimum in the middle (pile no. 3). However, this type of load distribution was not observed in the field. The measured data for a given displacement showed that the leading pile carried the greatest load while piles 3 and 5 carried the lowest loads. Piles 2 and 4 carried loads somewhat higher than

piles 3 and 5, but were significantly less than the leading pile. Although the loads computed with soil-pile separation for piles 2, 3, and 4 at a low deflection level (10 mm) agreed well with the corresponding measured loads, the computed loads of the leading and the trailing piles were slightly overestimated (Fig. 4.17(a)). At the maximum deflection level (83.4 mm), the FE analysis with soil-pile separation agreed well with the field data (Fig. 4.17(b)). Except for the leading pile, the measured and the computed results with soil-pile separation showed that the load of each pile was smaller than that of the single pile at maximum deflection (Fig. 4.17(b)).

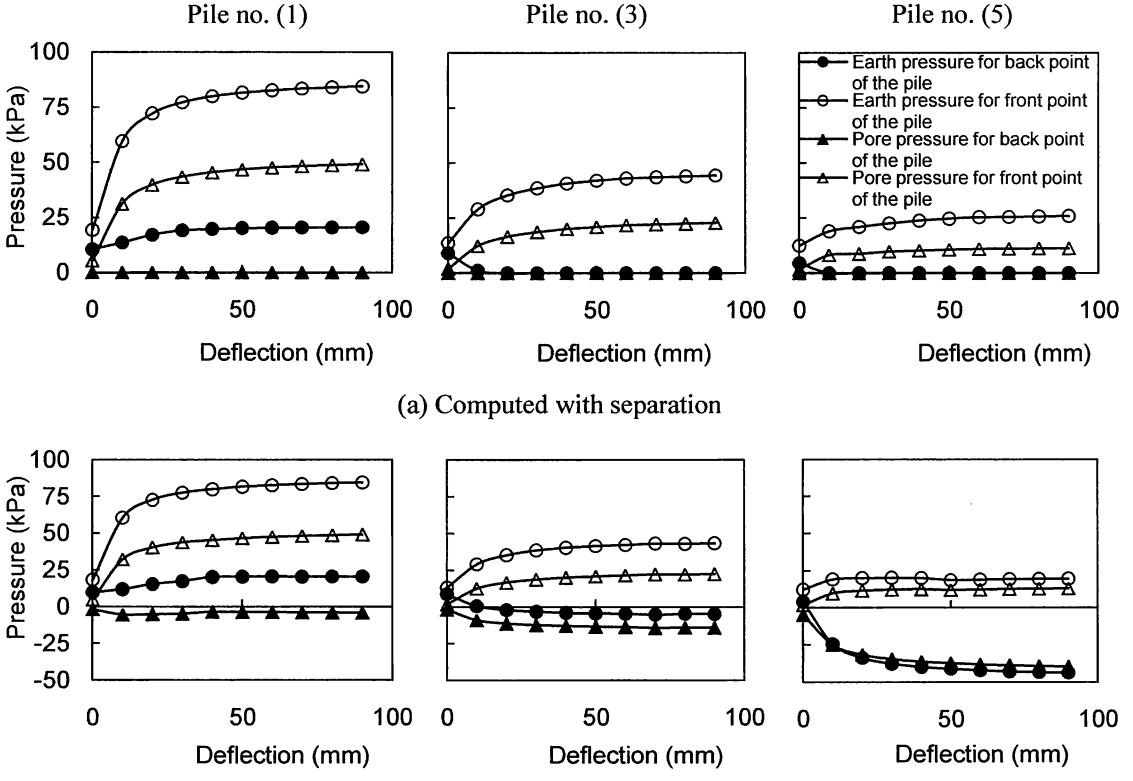

(a) Computed with separation

(b) Computed without separation

Fig. 4.16 Statically loaded pile group: Variation of earth pressure and pore pressure with deflection curves for two points in front and back of piles 1, 3, and 5 at a depth = 0.3 m. (a) Computed with and (b) without separation

Figure 4.18 plots the distribution of the bending moment over a depth for piles 1, 3, and 5 at deflections of 13, 25, 38, 64, and 89 mm. This figure compares the depths where the maximum moments were measured and computed. The analyses with and without soil-pile separation were

generally successful at predicting the depths of the maximum moments. The difference between the measured and computed depths of the maximum bending moment was within 1.0 m. Additionally, the computed depths where the bending moment returned to zero were consistent with the measured ones. The difference between the measured and computed depths was within 1.0 m. For pile 1, both the analyses with and without separation had a slightly larger bending moment than the measured one. Ignoring soil-pile separation did not affect the computed moments for piles 1 and 3. However, ignoring soil-pile separation for pile 5 overestimated the bending moment.

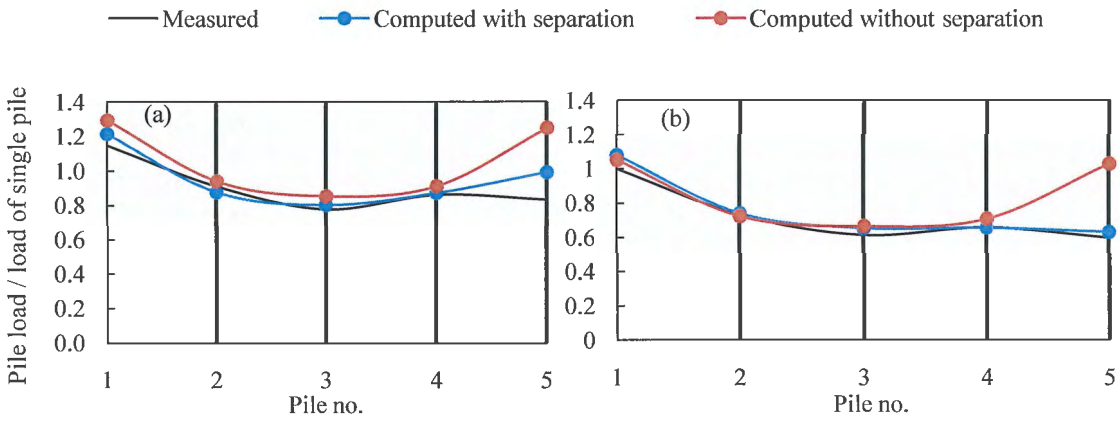

Fig. 4.17 Statically loaded pile group: Ratio of the computed and the measured loads of each pile relative to the load of the single pile; (a) target deflection = 10 mm, and (b) target deflection = 83.4 mm

4.6 Group Pile under Dynamic Load

In addition to static loading tests, full-scale statnamic tests were performed on the 3×5 pile group. For each series of the tests, first the pile group was cyclically loaded statically up to a certain target deflection followed by the statnamic test to the same target deflection. The statnamic test was performed as the 16th cycle for target deflections of 13 and 25 mm, 15th cycle for 38 mm, 11th cycle for the 64 mm, and 12th cycle for the 89 mm target deflection (Snyder 2004). In the FE simulation, five amplitudes of sequential statnamic loads were applied without the cyclic static load sequence (Fig. 4.19). The model parameters in the analysis were identical to those for the static load test without introducing arbitrary parameter adjustments or back-fitting

to the measured data. The only difference was the inclusion of the degradation factor which considered the effect of rapid cyclic loading of the shear modulus of clayey soil.

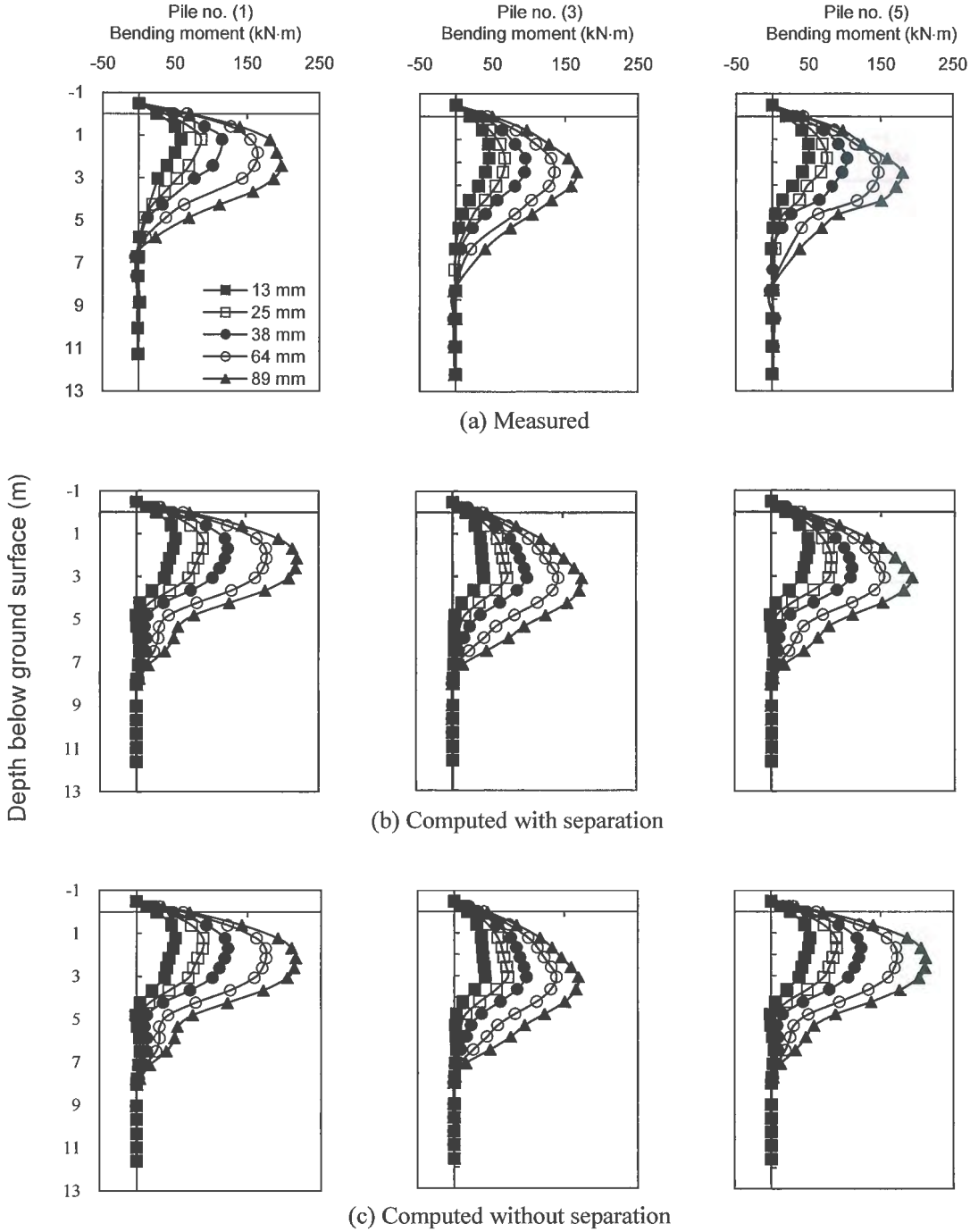

Fig. 4.18 Statically loaded pile group: Computed and measured bending moment versus depth for piles1, 3, and 5, and target deflections of 13, 25, 38, 64, and 89 mm.

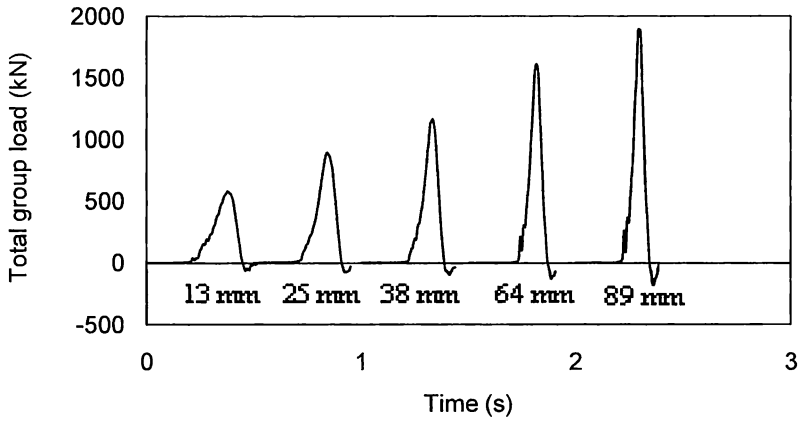

Fig. 4.19 Time sequence of the total load applied to the pile group in numerical analysis

For cohesive soils, the value of the shear modulus after N cycles (G_N) can be related to its value in the first cycle G_{ma} by (Idriss et al. 1978):

$$G_N = \delta G_{ma} \tag{4.4}$$

where the degradation index δ is given by $\delta = N^{-t}$ when t is the degradation parameter. In the analysis, a plasticity index of about 10 for the top layers of clay, which was obtained from a geotechnical investigation at the test site, and shear strains, which corresponded to all the target deflections and were obtained from the 1st cycle static load, were used (Vucetic and Dobry 1988) to determine the degradation parameter, t. Table 4.4 shows shear strains, degradation parameters, and degradation indices corresponding to the target deflections for the top clay layers. In the analysis, Rayleigh damping parameters were set as $\alpha = 0$ and $\beta = 0.0015$.

Figure 4.20 shows the load-deflection curves from the analyses with and without soil-pile separation compared to the measured ones for target displacements of 13, 25, 38, 64, and 89 mm. The analysis without soil-pile separation generally overestimated the total group load carrying capacity for both the loading and unloading phases. At the maximum applied load, the deflection obtained without soil-pile separation was smaller than that obtained from the field data. The percentages of reduction were 8.6, 16.0, 17.3, 21.8, and 23.3% for target deflections of 13, 25, 38, 64, and 89 mm, respectively, which strongly suggests that neglecting the effect of soil-pile separation leads to unconservative results in design practice.

Table 4.4 Shear strains, degradation parameters, and degradation indices corresponding to target deflections

Depth (m)	Target deflection														
	13 mm			25 mm			38 mm			64 mm			89 mm		
	Shear strain (%)	t	δ	Shear strain (%)	t	δ	Shear strain (%)	t	δ	Shear strain (%)	t	δ	Shear strain (%)	t	δ
0-1.22	0.13	0.05	0.88	0.23	0.08	0.81	0.43	0.13	0.71	0.74	0.19	0.63	1.00	0.24	0.56
1.22-2.14	0.11	0.04	0.9	0.28	0.09	0.78	0.39	0.12	0.73	0.69	0.18	0.64	0.95	0.23	0.57
2.14-3.06	0.08	0.03	0.92	0.20	0.07	0.83	0.35	0.11	0.75	0.66	0.18	0.65	0.94	0.23	0.57

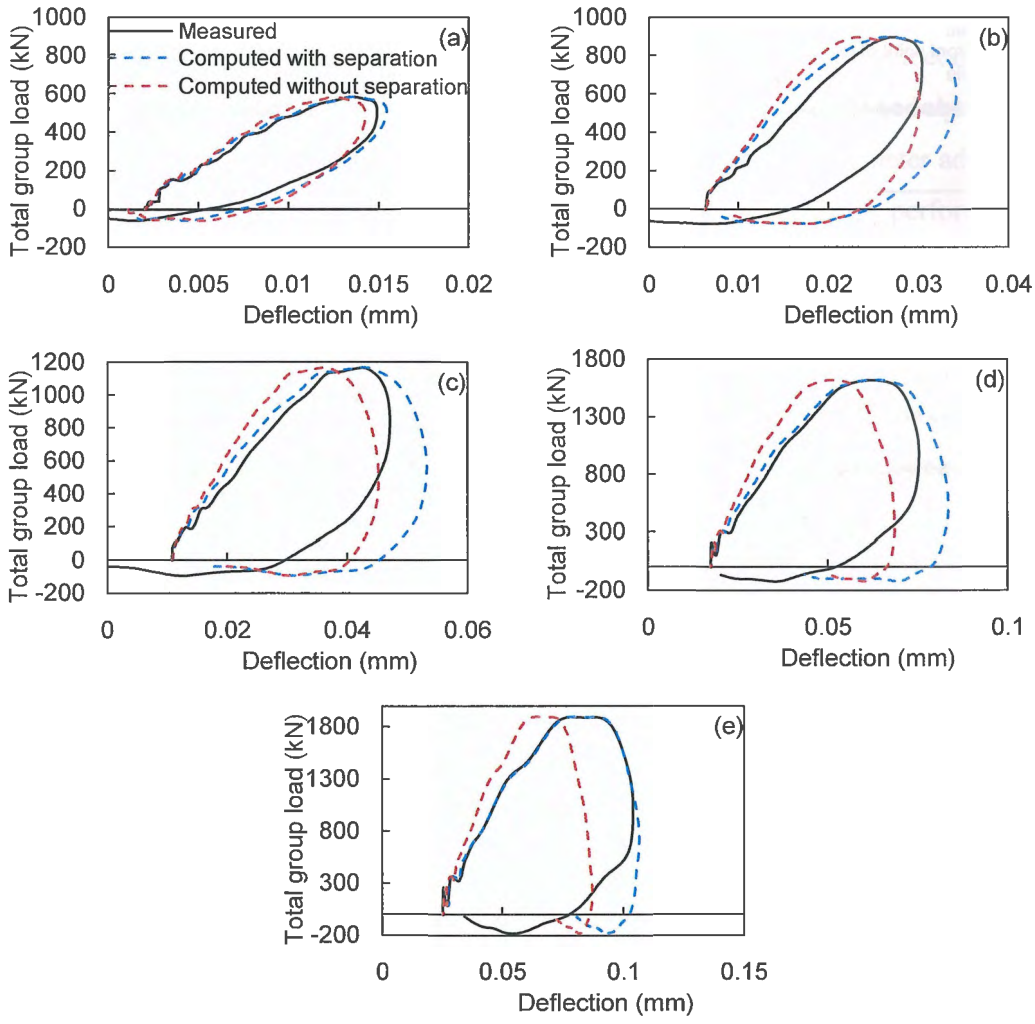

Fig. 4.20 Dynamically loaded pile group: Computed and measured bending moment versus depth for piles1, 3, and 5 with target deflections of 13, 25, 38, 64, and 89 mm

Figure 4.21 plots the time histories of earth pressure corresponding to the target deflection of 89 mm in front of and at the back of the trailing pile at a depth of 0.30 m. Although the earth pressure-deflection curves from the front point of the pile displayed approximately the same trend in both analyses, the earth pressure at the back of the pile was significantly affected by the soil-pile separation. The computed results without separation gave a negative earth pressure, which increased the ultimate load carried by the group at the same deflection level.

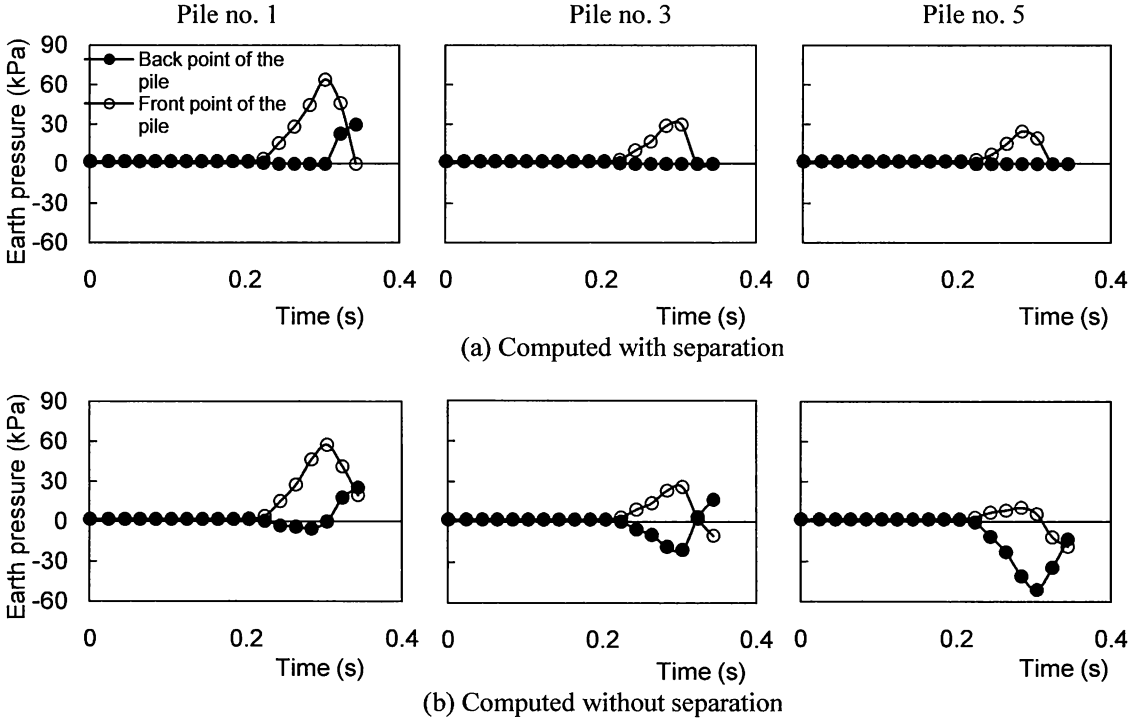

(a) Computed with separation

(b) Computed without separation

Fig. 4.21 Dynamically loaded pile group: The time histories of earth pressure for two points in front and back of piles 1, 3, and 5 at a depth = 0.3 m and a target deflection = 89 mm; (a) with and (b) without separation

Figure 4.22 plots the distribution of bending moment with depth for piles 1, 3, and 5. These bending moment curves corresponded to the maximum load applied to the group pile. Unlike the static load case where the depth corresponding to the maximum bending moment progressively increased with increasing deflection, the change in the depth of the maximum bending moment was negligible in the dynamic load tests. This trend was clear in both the measured and computed bending moment distributions. Both analyses, with and without

separation, successfully predicted the depths of the maximum moments. The difference between the computed and measured depths was 1.0 m or less. Additionally, the computed depths where the bending moment returned to zero agreed well with the measured one as the difference was less than 1.0 m. Although the computed bending moments obtained from the analysis with separation agreed well with the field data for all piles and target deflections, the analysis without separation generally underestimated the bending moments.

4.7 Conclusions

The main objective of this study is to explore the effect of soil-pile separation on the performance of a laterally loaded pile group. This study takes full advantage of a comprehensive set of full-scale tests, consisting of a single and 3x5 group pile under static and dynamic loads and thereby reduces the limitations that were often caused by arbitrary parameter adjustment or back-fitting to the measured data. Two dimensional finite element analyses performed in this study lead to the following conclusions:

1. For a statically loaded single pile, at the same load level, the analysis without soil-pile separation underestimates both deflection and maximum bending moment. The percentage of underestimation increases with the progress of loading and reaches, at the maximum applied load, 50% for deflection and 22% for maximum moment. At a target deflection of 90 mm, ignoring soil-pile separation leads to 43% overestimation of the ultimate lateral load-carrying capacity of the pile.
2. For a statically loaded pile group, the effect of soil-pile separation is most distinctive at the trailing pile. The effect of soil-pile separation is not significant for other piles in the group including the leading pile. The potential soil-pile gap for these piles appeared to be closed by the soil deformation pushed forward by the next column of pile trailing behind. In the analysis without soil-pile separation, the soil behind the trailing pile pulls back the pile opposite to the loading direction and resulting in the excessive increases in the overall soil resistance during pile deformation. At any load level, the analysis without soil-pile separation underestimates the deflection of the trailing pile. The percentage of underestimation increases with the progress of loading and reaches to 70% at the maximum applied load. At a maximum target deflection of 83.4 mm, ignoring soil-pile separation leads to 73% overestimation of the ultimate lateral load-carrying capacity of the trailing pile.

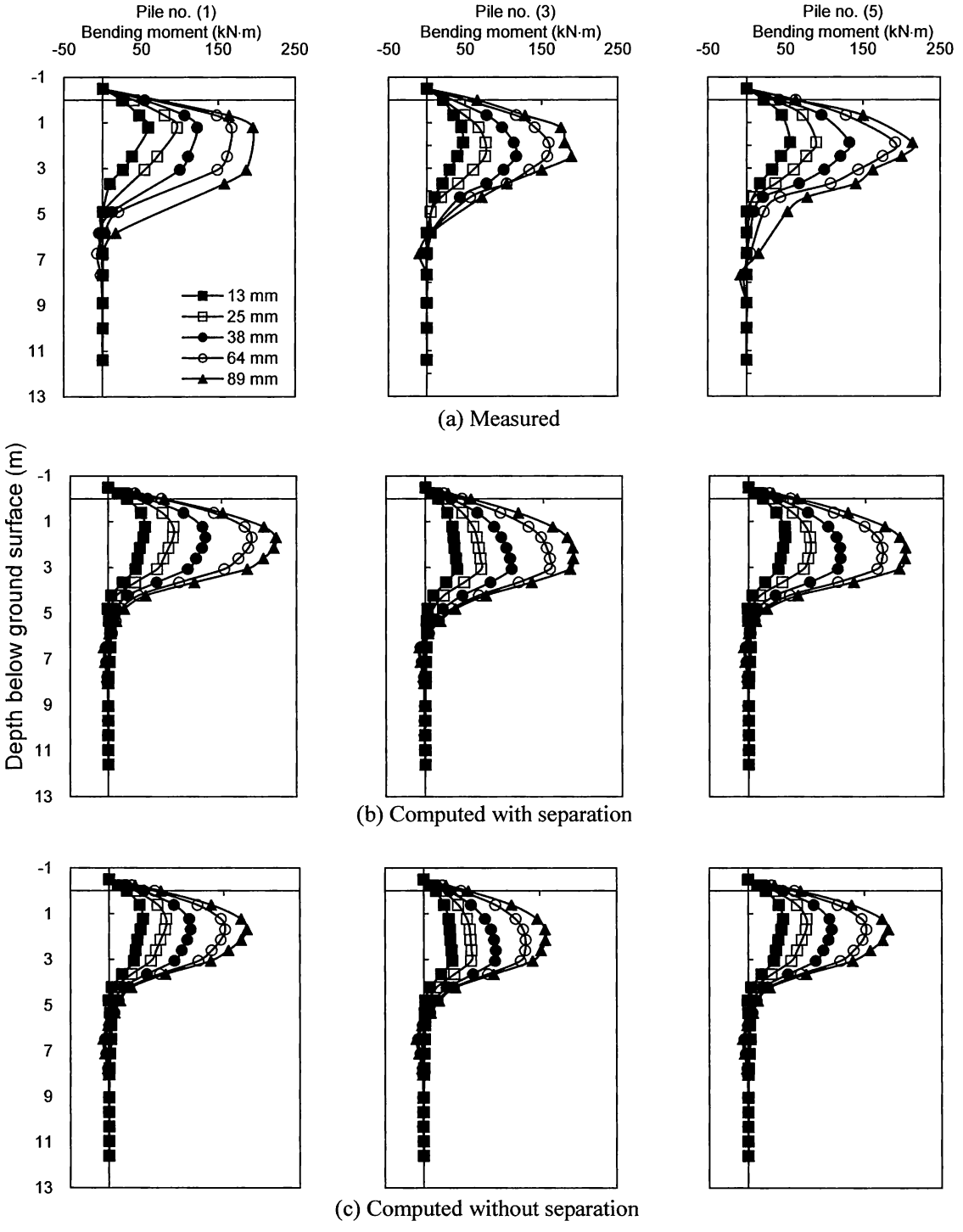

Fig. 4.22 Dynamic loaded pile group: Measured and computed load-deflection curves of group pile: target deflection of 13mm (a), 25 mm (b), 38 mm (c), 64 mm (d), and 89 mm (e)

3. The effect of soil-pile separation significantly affects the group action in terms of overall load carrying capacity and bending moment, as well as the load distribution among the piles in pile group. The load distribution curve obtained from the FE analysis without soil-pile separation has a concave shape with the maximum at both ends (leading and trailing pile) and the minimum in the middle (pile no 3). Measured data show that, for a given displacement, the leading pile carried the greatest load whereas piles 3 and 5 carried the lowest loads. Piles 2 and 4 carried loads somewhat higher than piles 3 and 5 but significantly less than the leading pile. At a low deflection level (10 mm), while the computed loads with soil-pile separation for piles 2, 3, and 4 are in good agreement with the corresponding measured loads, the computed loads for leading and trailing piles are slightly overestimated. At the maximum deflection (83.4 mm), the FE analysis with soil-pile separation shows good agreement with the field data. The measured and the computed results with soil-pile separation show that, except for the leading pile, the load of each pile is smaller than that of the single pile at maximum deflection. The good agreement between the FE results with soil-pile separation and the field data is obtained her under a certain soil and pile properties and also certain pile group configuration.
4. For dynamically loaded pile group, the effect of soil-pile separation is significant not only in the loading phase but also in the unloading phase. At maximum applied load, the deflection obtained without separation is smaller than that obtained from field data. The percentages of reduction were 8.6, 16.0, 17.3, 21.8, and 23.3% for target deflections of 13, 25, 38, 64, and 89 mm, respectively. Ignoring the effect of soil-pile separation significantly underestimates both deflection and bending moment values, leading to unconservative design of group piles.

References

1. Brown, D. A., and Shie, C. F. 1991. Some numerical experiments with a three dimensional finite element model of a laterally loaded pile. *Computers and Geotechnics*, 12: 149–162. doi:10.1016/0266-352X(91)90004-Y.
2. Iai, S., Matsunaga, Y., and Kameoka, T. 1992. Strain space plasticity model for cyclic mobility. *Soils and Foundations*, 32(2): 1–15.
3. Idriss, I.M., Dobry, R., and Singh, R.D. 1978. Nonlinear behavior of soft clays during cyclic loading. *Journal of the Geotechnical Engineering Division, ASCE*, 104(12): 1427–1447.

4. Jamiolkowski, M., Lancellotta, R., Marchetti, S., Nova, R., and Pasqualini, E. 1979. Design parameters for soft clays. *In Proceedings of the 7th European Conference on Soil Mechanics and Foundation Engineering*, Brighton, 5, pp. 27-57.
5. Kimura, M., and Zhang, F. 2000. Seismic evaluations of pile foundations with three different methods based on three-dimensional elasto-plastic finite element analysis. *Soils and Foundations*, 40(5): 113–132.
6. Ohta, Y., and Goto, N., 1978. Empirical shear wave velocity equations in terms of characteristic soil indexes. *Earthquake Engineering and Structural Dynamics*, 6(2):67–187.
7. Rollins, K.M., Olsen, R.J., Egbert, J.J., Jensen, D.H., Olsen, K.G., and Garret, B.H. 2006. Pile spacing effects on lateral pile group behavior: load tests. *J. Geotechnical and Geoenvironmental Engrg., ASCE,* 132,(10) 1262-1271.
8. Snyder, J., L. 2004. Full–scale lateral–load tests of a 3x5 pile group in soft clays and silts. M.Sc. thesis, Brigham Young University, Provo, Utah, United States.
9. Tahghighi, H., and Konagai, K. 2007. Numerical analysis of nonlinear soil–pile group interaction under lateral loads. *Soil dynamic and Earthquake Engineering*, 27(5): 463–474. doi:10.1016/j.soildyn.2006.09.005.
10. Tobita, T., Iai, S., and Rollins, K. M. 2006. Numerical analysis of full–scale lateral–load tests of a 3 × 5 pile group. *In Proceeding of the 1st European Conference on Earthquake Engineering and Seismology*, Geneva, Switzerland.
11. Tuladhar, R., Maki, T., Mutsuyoshi, H. 2008. Cyclic behavior of laterally loaded concrete piles embedded into cohesive soil. *Earthquake Engineering and Structural Dynamics*, 37(1): 43–59. doi: 10.1002/eqe.744.
12. Vucetic, M., and Dobry, R. 1988. Degradation of marine clays under cyclic loading. *Journal of the Geotechnical Engineering*, 114(2): 133–149.
13. Zhang, L., McVay, M. C., and Lai, P. 1999. Numerical analysis of laterally loaded 3×3 to 7×3 pile groups in sands. *Journal of Geotechnical and Geoenvironmental Engineering*, 125(11), 936–946. doi 10.1061/(ASCE)1090-0241(1999)125:11(936).
14. Bowles, J. E. 1988. Foundation analysis and design, 4th Ed., McGraw-Hill, New York.

CHAPTER 5

Effect of Vertical Loads on Lateral Resistance of Pile Group

Contents

5.1 Introduction

Studies on piles and pile groups over 70 years may be categorized into those on the behavior of pile foundations under vertical loads (e.g., Whitaker 1957, Ottaviani 1975, Randolph and Wroth 1978, Xu and Poulos 2000, Zhu and Chang 2002,) and those under pure lateral loads (e.g., Matlock and Reese 1960, Poulos 1971a, 1971b, Rollins et al. 1998, 2005, Basu and Salgado 2007,). The former category of studies led to the methodologies to evaluate bearing capacities and settlements of piles, while the latter to evaluate bending moments and deflections. The results of these extensive studies have formed the basis for the current design practice of pile foundations, where vertical and lateral loads were assumed to act independently and the interaction between these loads was not significant. However, Meyerhof et al. (1983) and Meyerhof and Yalcin (1984) investigated through model tests the effects of lateral loads and bending moments on the vertical bearing capacity of single and group piles and they suggested a significant decrease in the vertical bearing capacity due to the presence of lateral loads or bending moments.

The results available in the literature with respect to the effects of vertical loads on the lateral response of single piles (e.g., McNulty 1956, Sorochan and Bykov 1976, Anagnostopoulos and Georgiadis 1993,) suggested a significant increase in the lateral resistance of piles in the presence of vertical loads. Other related research on single piles includes (Zhukov and Balov 1978 and Zhang et al. 1999,). Zhang et al. (2002) through centrifuge experiments on 3×3 and 4×4 fixed-head battered pile groups concluded that the effects of vertical load on the lateral resistance of 3×3 pile groups were not significant. For 4×4 pile groups however, the lateral resistances increased significantly with vertical loads.

In recent studies by Karthigeyan and Ramakrishna (2005) and Karthigeyan et al. (2006, 2007,) the authors showed through a series of 3D FE analyses on single piles that the presence of vertical loads increases the lateral load capacity of piles in sandy soils by as much as 40 %. There is a strong need to pursue these recent developments in the studies on pile behavior. In fact, the scopes of these recent studies that indicate the significance of the load interaction mentioned earlier were limited to the behavior of single piles. Little work has been devoted to the behavior of pile groups subjected to the combined effects of vertical and lateral loads.

In this chapter, the effect of vertical loads on the lateral resistance of a single pile and a pile group is studied using 2D FEM. After the description of FE modeling and material

properties, the chapter then presents the effect of vertical loads on the lateral resistance of a single pile, to be followed by the main part of the study with respect to the behavior of a 3 ×5 pile group under combined loads.

5.2 2D Profile of Soil-pile System for FE Analysis

The 2D FE program FLIP (Iai et al. 1992) was employed to study the behavior of a pile group under combined loading. Same pile configuration and material properties described in Chapter 4 are used in this chapter. The 2D FE analysis focused on the five piles in the middle row of the group. Figure 5.1 shows the general layout and meshing of the FEM. Side boundary displacements were fixed in the horizontal direction, while those at the bottom boundary were fixed in both the horizontal and vertical directions. The top and bottom of the piles were set as displacement and rotation free. In the analysis, a uniform layer of sand was used as the soil profile. Model parameters of the sand layer are shown in Table 5.1.

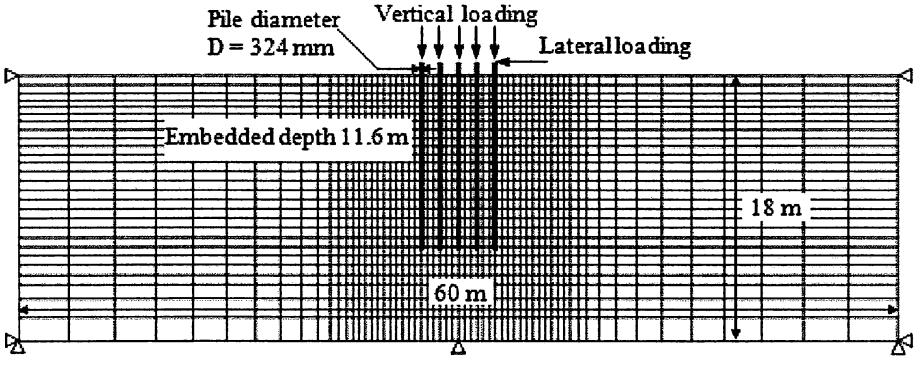

Fig. 5.1 General layout and meshing of the finite element model

Table 5.1 Model parameters of the sand layer

Saturated unit weight, γ_{sat} (t/m^3)	σ'_{ma} (kPa)	G_{ma} (kPa)	υ	K_a (kPa)	ϕ_f (degrees)	c (kPa)	Max damping ratio, (h_{max})
1.83	98	43,500	0.33	114,000	33		0.20

Prior to the analysis of pile group behavior, analysis of a single pile was performed as a reference in order to discuss the specific behavior of the pile group under combined loads. The

same meshing of the soil profile was used to analyze the single pile. A total of 4 cases including single and group piles were considered. Pure lateral loads were considered in half of these cases while a combination of vertical and lateral loads was considered in the others. In the analysis of piles subjected to combined load, a vertical displacement (V) of 0.1D (D = pile diameter) (i.e. vertical load = 75 % of the ultimate vertical capacity of the pile (P_u), details of the calculation of ultimate vertical capacity of the pile is given in Appendix A1) was applied on the pile-head prior to the application of lateral loads for both the single and the grouped piles then lateral loads were statically applied until a target lateral displacement of 60 mm was achieved. The maximum vertical applied displacement at the pile-head was kept constant during the application of the lateral displacement.

5.3 Behavior of a Single Pile under Combined Loads

5.3.1 Preliminary analysis

As described at the introduction, recent studies on piles under combined loads (Karthigeyan and Ramakrishna 2005, Karthigeyan et al. 2006, 2007,) indicated that the presence of vertical loads on single piles increases the lateral resistance of the pile in sand deposit. Prior to the main part of this study on pile groups described later, a preliminary analysis of a single pile was performed in order to confirm these recent developments through the analysis model used in this study. In this preliminary analysis, the lateral resistance of a single 10-m-long, 1.2 x 1.2- m^2 concrete pile embedded in a sandy soil layer 34-m deep was analyzed with and without a vertical load of 384 kN in order to reproduce the recent analysis results by Karthigeyan et al. (2007) (to be called the previous analysis). Details of pile and soil properties used in the previous analysis are given in Table 5.2.

The comparison between the present 2D load-deflection curve up to a lateral displacement of 120 mm and the 3D results provided by the previous analysis with and without vertical loads are shown in Figs 5.2(a) and 5.2(b). In particular Fig. 5.2(a) shows load-deflection curves obtained from the previous analysis, while Fig. 5.2(b) shows load-deflection curves obtained from this study. Both figures declared an increase of the pile lateral resistance due to the application of vertical loads with percentages of increase at 120 mm lateral deflection of 6 and 7% respectively. Although initial slopes of the present load-deflection curves obtained from the analyses with and without vertical loads were about 0.76 and 0.69 of the corresponding

curves provided by the previous analysis as a result of the difference in soil modeling (i.e., for the previous analysis, the Drucker-Prager constitutive model with non associated flow rule for sandy soils were used to predict the stress-strain behavior), loads at maximum deflections agree well with each other. The present FE prediction matches reasonably well with that provided by the previous analysis. Thus, the analysis model used in the present study has the capability to reproduce the results consistent with the recent studies on the pile behavior under the combined action of vertical and lateral loads.

Table 5.2 Pile and soil Properties used in the analysis provided by Karthigeyan et al. (2007)

Pile details	Soil details
Size: 1200 × 1200 mm^2	ϕ = 36
Length: 10 m	C = 0
Type of pile: Concrete	E_s = 50 Mpa
Young's modulus E_p: 25,000 MPa	γ_p = 20 kN/m^3
Unit weight (γ_p): 24 kN/m^3	μ_s = 0.15
Poisson's ratio μ_p: 0.15	

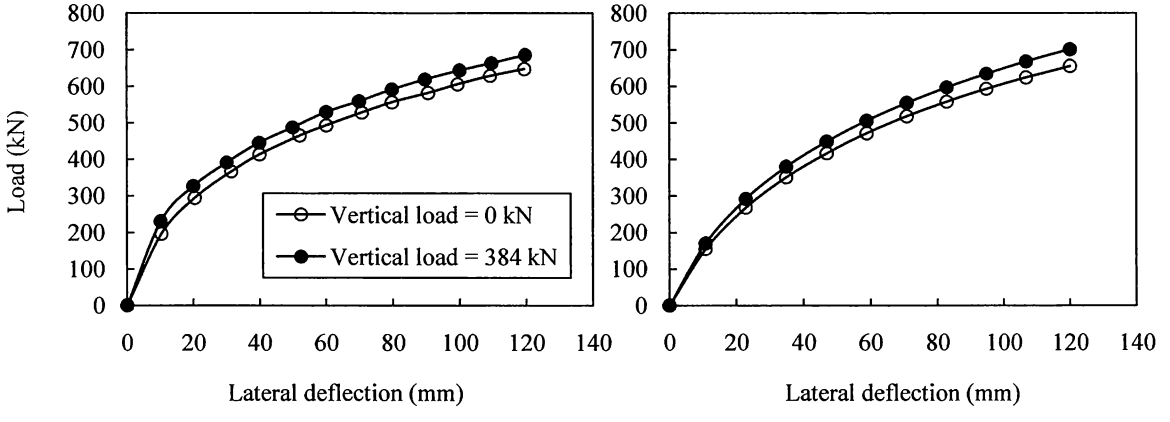

Fig. 5.2 Load-lateral deflection curves of the single pile for the analyses with and without vertical loads: (a) 3D by Karthigeyan et al. 2007; (b) This study

5.3.2 Single pile response under combined loads

In order to study the behavior of pile groups under combined loads, analysis of a single pile under combined load was performed as a reference. The soil profile and material parameters described in Section 5.2 were used for the analysis. Results of the analysis on single pile response under both lateral and combined loads, shown in Fig. 5.3, indicate that a vertical load inducing a vertical displacement (V = 0.1D) of the pile head increases the lateral load-carrying capacity of the pile at a lateral deflection of 60 mm by 8 %. Similar percentages of increase were induced in the maximum shear force and bending moment in the pile.

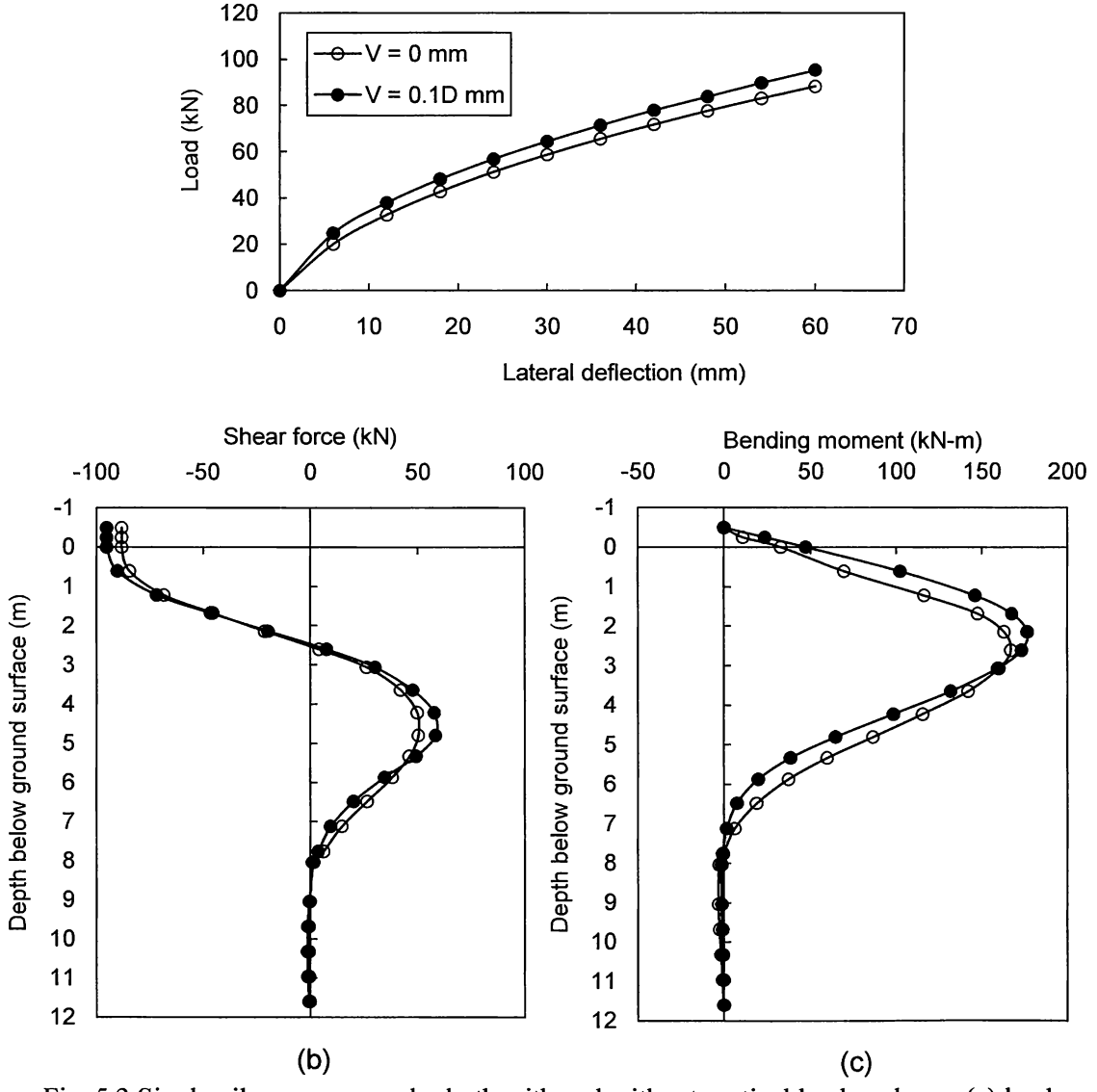

Fig. 5.3 Single pile response under both with and without vertical load analyses: (a) load-deflection curve; (b) shear force profile; and (c) bending moment profile

An attempt to identify the mechanism of the increase in the lateral resistance of a single pile subject to a vertical load was made by studying deformation and stress changes induced in soil due to the vertical load. The downdrag of the soil by the vertical loaded pile as it moves down is shown in Fig. 5.4. In this figure, displacement field was scaled by 20 times relative to that of the geometric scale. The vertical load on a single pile drags down the soil surrounding the pile because of the effect of skin friction of the pile.

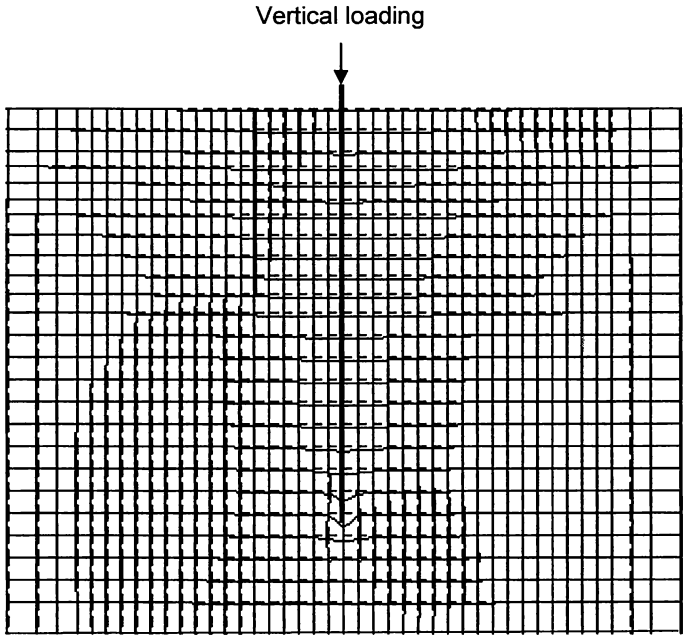

Fig. 5.4 Soil deformation associated with a vertical load applied to the head of the single pile

Soil displacement field is shown in Fig. 5.5(a). Due to the symmetry of the soil displacement relative to the pile longitudinal axis, only the right part of Fig. 5.5(a) will be considered in this discussion. Figure 5.5(a) shows that soil rotates counter clockwise due to the action of the vertical load on the pile head and the centre of rotation is located just below the ground surface and at some distance right to the pile. As a result of this rotation, in the vicinity of the pile, the displacement vectors of soil at shallow depths (up to 10D) are directed towards the pile whereas those at deeper depths are directed away from the pile. Figure 5.5(b) shows clearly the difference in horizontal components of soil displacement directions with respect to the pile depth. The resulting lateral displacement of soil at shallow depths pushes the soil toward the pile, inducing an increase in the lateral stress (σ'_x) in the soil. Moreover, the displacement field also

increases the vertical stress (σ'_y) in the soil in the vicinity of the pile because of the presence of the foundation layer as represented by the fixed displacement boundary at the bottom of the analysis domain. These stress changes results in the increase in the confining pressure in the soil in the vicinity of the pile as shown in Fig. 5.6. The increase in the confining stress of soil, then, increases the resistance of soil-pile interaction spring through the mechanism incorporated in the modeling of the spring as described in Chapter 3.

Figure 5.7 shows stress paths of soil elements attached to the pile shaft and at different depths. All these paths initiate from K_o line and move in the direction shown in Fig. 5.7 indicating that the increase in the effective vertical stress of the soil element due to the application of vertical load is accompanied by an increase in the corresponding soil horizontal stress.

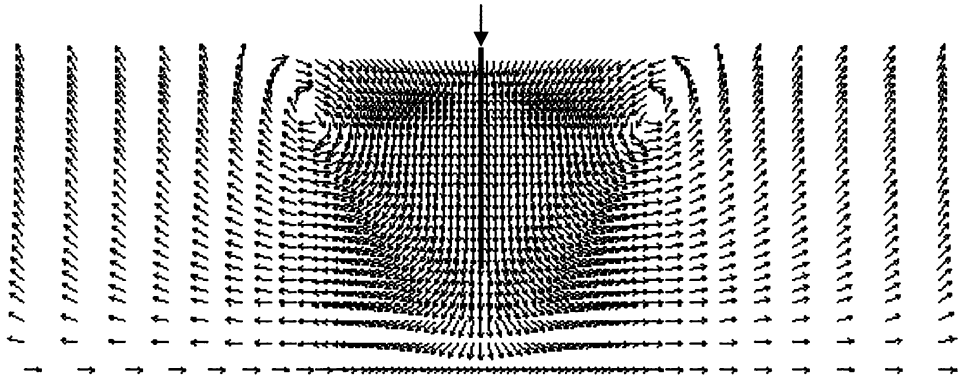

(a)

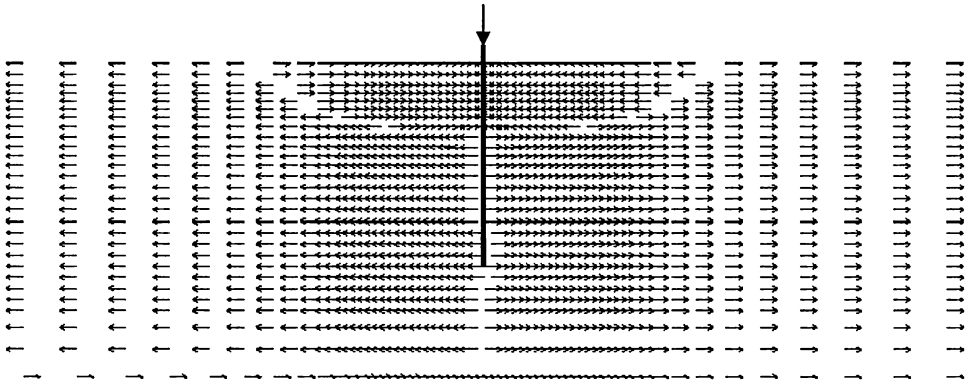

(b)

Fig. 5.5 Soil displacement field due to a vertical load on the pile head: (a) total soil displacement; (b) horizontal soil displacement

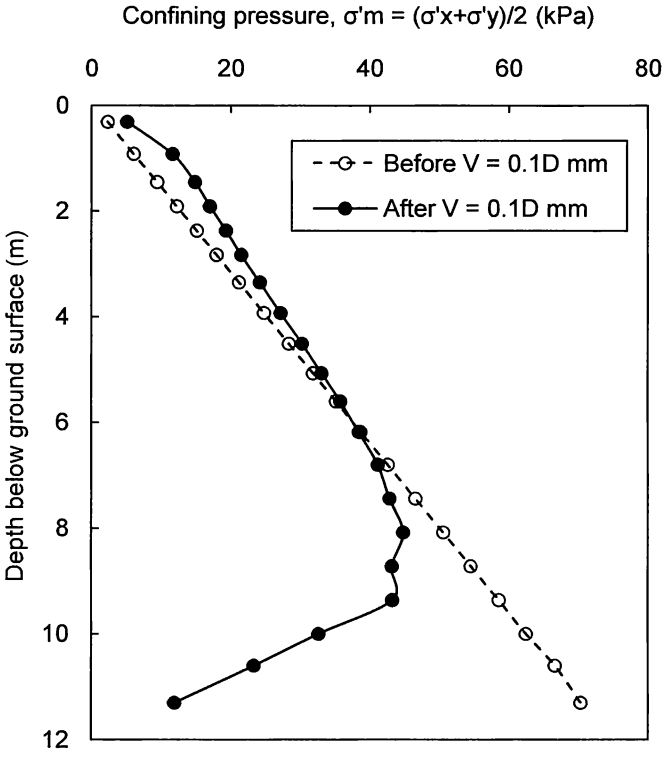

Fig. 5.6 Variation of the confining pressure along the pile depth before and after the application of the vertical load

Figure 5.8 shows the variation of horizontal soil stresses of soil elements along the depth of the pile before and after the application of lateral loads for the analyses with and without vertical loads. In particular, the soil stress at the back side of the pile was plotted in Fig. 5.8(a), whereas that at the front side was plotted in Fig. 5.8(b). Moreover, horizontal soil stress profiles induced before and after the application of vertical loads were introduced for comparison purposes. These figures show that the inclusion of vertical loads prior to lateral loads increases the horizontal stress of soil elements along the depth of the pile not only at the front side but also at back side of the pile. The enhanced soil reaction is counterbalanced to some extent by a loss of a horizontal soil stress that occurs in the region approximately 6D above the pile tip. This is due to the interaction of the pile base movement and of the soil just above the pile base elevation. Loukidis and Salgado (2008) have reported similar findings for a pile in sandy soils through FE analysis. Figure 5.8 also indicates that the effect of vertical loads on the induced horizontal soil stresses lasts even after the application of lateral loads.

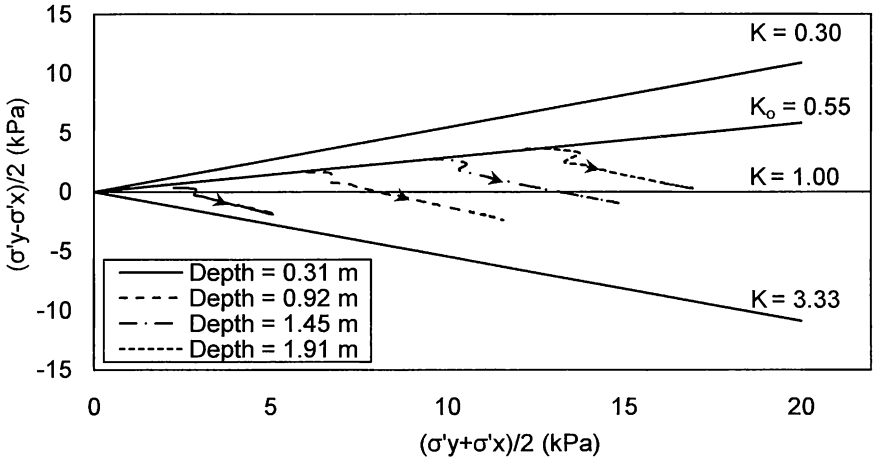

Fig. 5.7 Stress paths of soil elements attached to the pile shaft

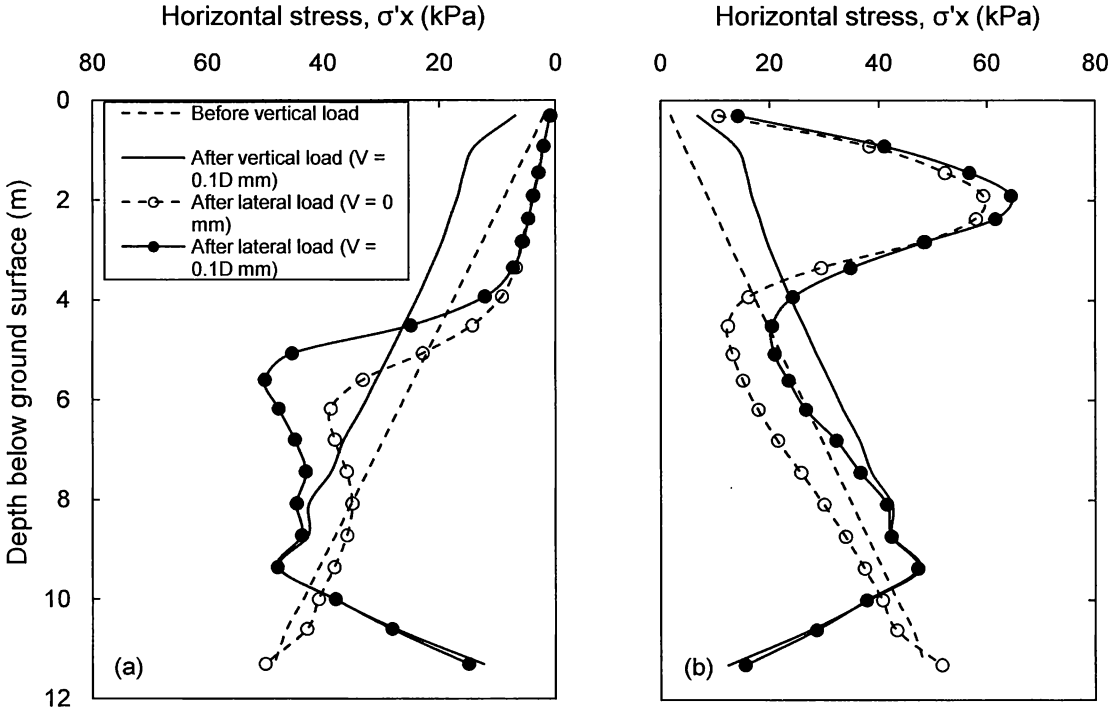

Fig. 5.8 Horizontal soil stresses along the depth of the pile at different loading stages and conditions: (a) back side; (b) front side

The net horizontal soil stress at a 60 mm lateral deflection, to be defined as the stress difference in front and at the back of the pile, was plotted against the pile depth as shown in Fig. 5.9. The influence of vertical loads is to increase the net horizontal stresses of soil especially at shallow depth (the upper portion of the subsurface (5 to 10D in depth) is of predominant importance in soil-pile interaction due to lateral loading as suggested by Rees and Van Impe (2001)). This increase of the net horizontal soil stress is further examined through plotting the variation of the net horizontal stress for points at a depth of 1.91 m below the ground surface (the depth where maximum horizontal stresses occur, Fig. 5.9) with the corresponding lateral deflections of these points as shown in Fig. 5.10. Figure 5.10 confirms that the effect of vertical loads is to increase the net horizontal soil stress accompanied by the increase of the lateral load carrying capacity of the pile.

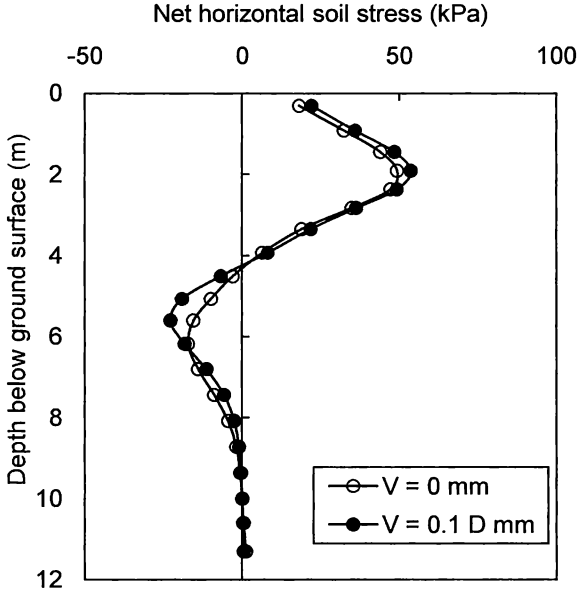

Fig. 5.9 Net horizontal soil stresses along the depth of the pile at a 60 mm lateral deflection

5.4 Behavior of Pile Groups under Combined Loads

5.4.1 Pile group response under combined loads

In the analysis of the pile group, loads were statically applied in the same manner as for a single pile. The same model parameters as those for the single pile were used. Figure 5.11 shows the total group load versus lateral deflections of piles heads with and without the presence of vertical

loads and at a pile spacing of 3.92-pile diameter. Similar to the single pile behavior, a vertical load inducing a vertical displacement of 0.1-diameter in piles leads to a 9 % increase in the lateral load-carrying capacity of the pile group.

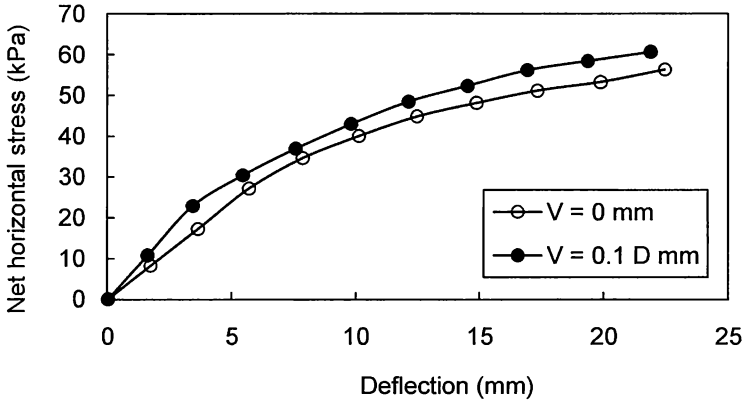

Fig. 5.10 Variation of the net horizontal stress with the corresponding lateral deflections at a depth of 1.91 m

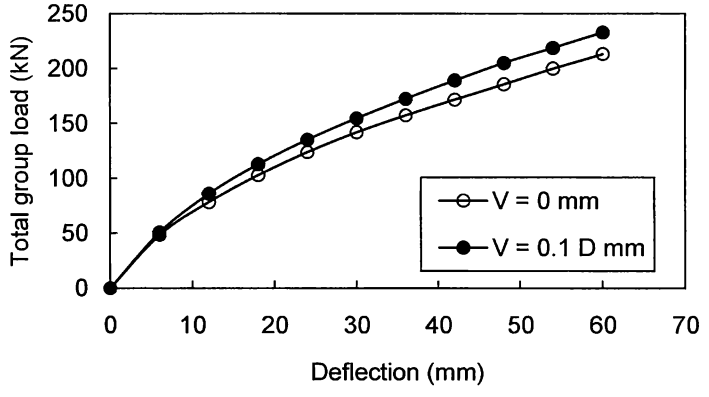

Fig. 5.11 Total lateral load-deflection curves of a pile group with 3.92-pile diameter spacing

5.4.2 Load distribution among piles in a group

Figure 5.12 shows load versus pile head deflection computed with and without the presence of vertical loads for each pile. As shown in this figure, the effect of vertical loads on the response of each pile in a group is not the same but is a function of the pile position. In the presence of vertical loads, the lateral load of the leading pile (pile 1) at all deflections is less than the

corresponding load developed under pure lateral loads. The percentage reduction reaches to a 10% at a 60 mm lateral deflection. For other pile including the trailing pile (pile 5), the influence of vertical loads is to increase the lateral loads at all deflections. The percentages of increase reach to 9, 14, 17, and 35% for piles 2, 3, 4, and 5, respectively. The influence of vertical loads on the lateral response of piles 1 and 2 seems to be rather limited; however, the effect on other piles can't be ignored in design practice.

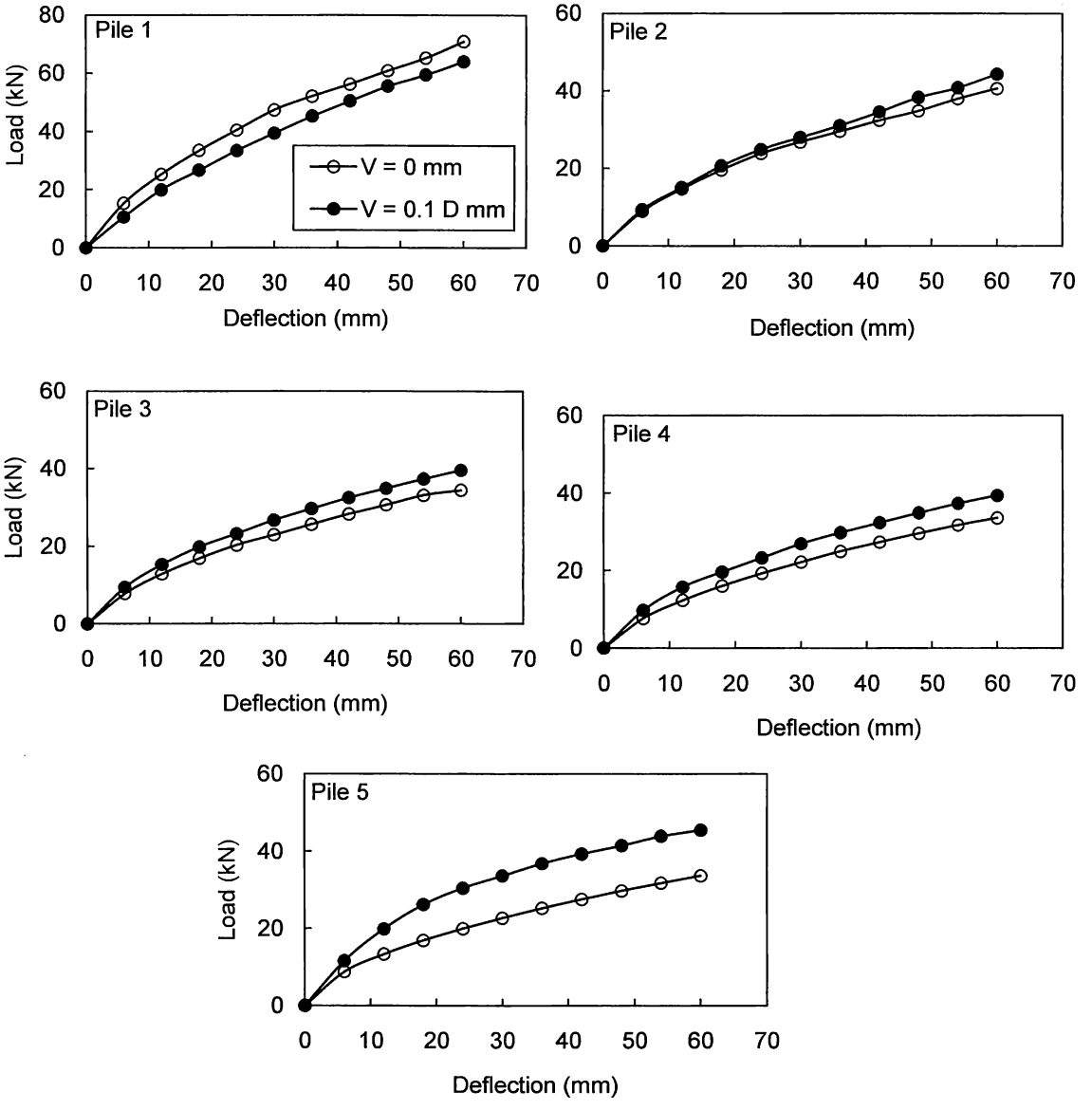

Fig. 5.12 Load-deflection curve of each pile in a group at 3.92-pile diameter spacing

In order to discuss the load distribution among piles in a group, the ratios of the lateral load of each pile relative to the corresponding load of the single pile are shown for deflections of 30 and 60 mm in Fig. 5.13. As shown in this figure, the presence of vertical loads on piles reduces the difference in pile loads especially for the leading piles. In accordance with the load distribution among piles in the pile group, differences in bending moments and shearing force induced in individual piles in the group are reduced as shown in Fig. 5.14 and Fig. 5.15, respectively. The reduction in the difference of loads of piles in the group may be beneficial with respect to the performance of pile groups under lateral loads. According to the current design practice of pile foundations under pure lateral loads, all piles are design assuming that they carry the maximum pile load in the group (the leading pile load). The current study demonstrates that when dead loads are considered, the load distribution between piles will be more uniform leading to a more economical foundation design.

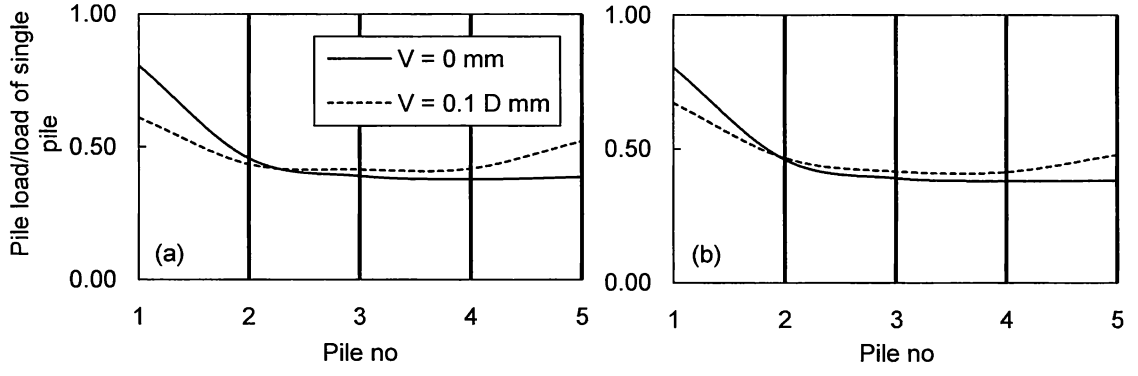

Fig. 5.13 Ratio of lateral loads computed with and without vertical loads of each pile in a group at 3.92-pile diameter spacing relative to the corresponding load of the single pile at target deflections: (a) 30 mm; (b) 60 mm

5.4.3 Mechanism of change in the lateral response of the pile group due to vertical loads

In order to discuss the mechanism of the change in the lateral response of the pile group due to vertical loads, soil deformations and stresses induced by vertical loads applied to piles were studied further. The downdrag of the soil by the vertical loaded piles as they move down is shown in Fig. 5.16. In this figure, the displacement field is scaled by 20 times relative to that of the geometric scale. The ground surface moves downward more in the portion confined by piles than elsewhere, but the movements also do occur away from the intermediate zone. As the single

pile case, the soil displacement field is shown in Fig. 5.17(a). Due to the symmetry, only the right part of Fig. 5.17(a) will be discussed here. This figure shows that soil rotates counter clockwise due to the action of vertical loads on piles heads and the centre of rotation was located just below the ground surface and at some distance right to the pile group. As a result of this rotation, just outside the pile group, the displacement vectors of soil at shallow depths were directed towards the pile group whereas those at deeper depths were directed away from it. Figure 5.17(b) show clearly the difference in horizontal components of soil displacement directions with respect to the pile depth. The depth at which the horizontal displacement vectors change their directions was much deeper than the corresponding depth in the single pile case.

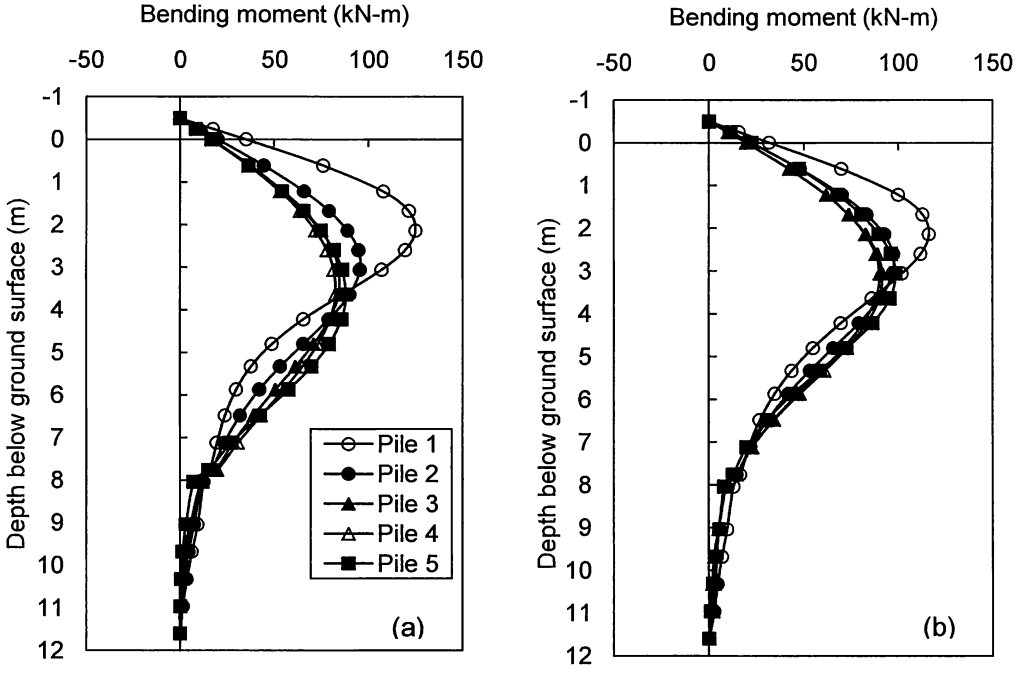

Fig. 5.14 Bending moment profiles of piles in the group under: (a) pure lateral; and (b) combined loads

The corresponding horizontal soil stresses along the first four meters on piles 1, 3, and 5 in the group are shown in Fig. 5.18, where the stresses at the back of and in front of the piles were separately plotted. For pile 3 (the middle pile), the increases in horizontal soil stress along the pile depth are the same for both sides of the pile. For pile 1 (the leading pile), the increase in

the horizontal stress at the back of the pile (inside the group) is larger than that in front of it (outside the group) due to the effect of the interaction of the next row of piles behind the leading pile. For Pile 5 (the trailing pile), opposite trend with the same magnitude is obtained. Net lateral stresses are shown in Fig. 5.19. For the middle pile, there is no net lateral stress induced by vertical loads. This means that the middle pile behaves approximately the same as the single pile (see Fig. 5.13). For the leading pile, the net horizontal stress due to vertical loads acts in the same direction with the prospective lateral load, leading to a decrease in the pile resistance to the subsequent lateral load. For the trailing pile, the net horizontal stress acts against the prospective lateral load, leading to an increase in the pile resistance to the subsequent lateral load.

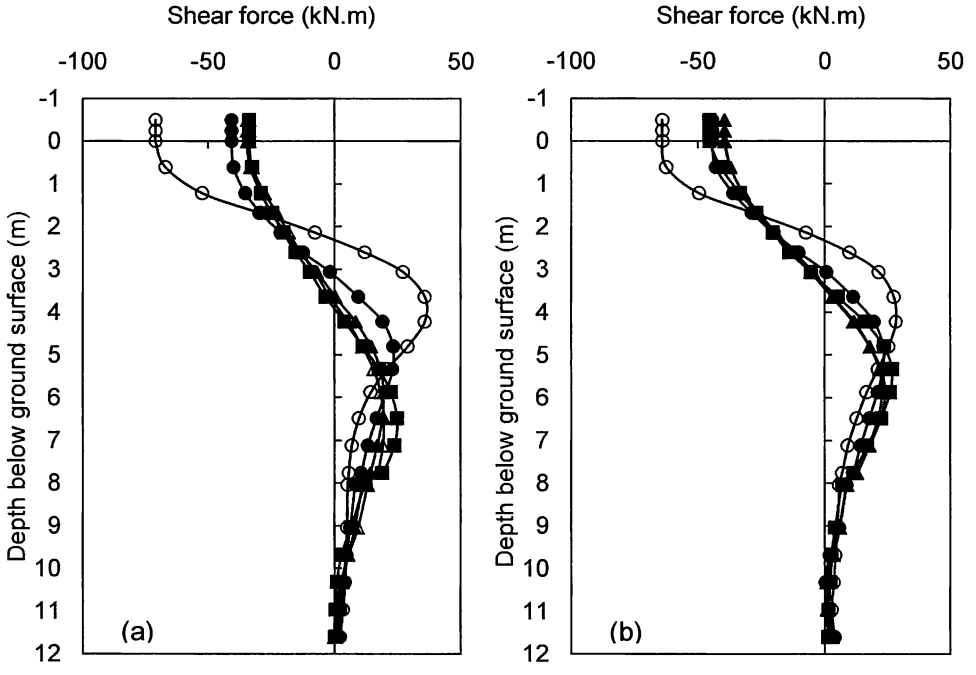

Fig. 5.15 Shearing force profiles of piles in the group under: (a) pure lateral; and (b) combined loads

When the lateral load is applied to the pile group, the lateral stresses discussed above will change in general. In order to study this aspect of soil behavior, variation of horizontal soil stresses for points at different depths with the corresponding lateral deflections is shown in Fig. 5.20. In this figure, positive sign of deflection indicates that the point is in front of the pile, while negative sign of deflection indicates that the point is back to the pile. For the leading pile,

although the horizontal soil stress-deflection curves in front points of the pile show approximately the same trend in both of the analyses with and without vertical loads, the horizontal soil stress at the back of the pile is significantly affected by the presence of vertical loads. In the analysis without vertical loads, the horizontal soil stress initiates from the earth pressure at rest and gradually increases especially at deeper depths. On the other hand, the horizontal soil stress obtained from the analysis with vertical loads initiates from the enhanced earth pressure due to the application of vertical loads and approximately remains constant. For a range of pile head deflection (60 mm) and for points back to the leading pile (especially at deeper depths) during the application of lateral load, there is a significant increase in the horizontal soil stress due to the pre-application of the vertical loads.

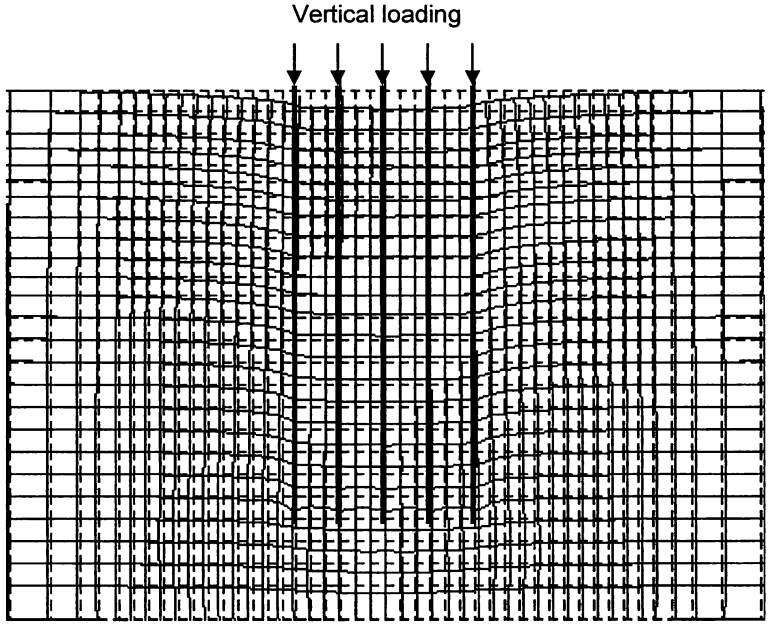

Fig. 5.16 Soil deformation corresponding to vertical loads applied to piles heads

For piles 3 and 5, the horizontal soil stress is significantly affected by the effect of vertical loads not only at the back of the piles but also in front of them. For front points, in the analysis without vertical loads, the horizontal soil stress initiates from the earth pressure at rest and gradually increases especially at deeper depths. In the analysis with vertical loads, the horizontal soil stress initiates from the enhanced earth pressure and remains constant or slightly decreases. For back points, there is somewhat difference in the behavior of piles 3 and 5. For pile

3, the horizontal soil stress obtained from the analysis without vertical loads initiates from at rest earth pressure and gradually increases with rate depends on the depth of the point under consideration. The horizontal soil stress obtained from the analysis with vertical loads shows different behavior, it initiates from enhanced earth pressure and gradually decreases due to the release of soil stress (as the pile deflects) in the zone behind the pile. Same behavior is captured for the trailing pile except that the horizontal soil stress obtained from the analysis without vertical loads at back points initiates from at rest earth pressure and remains constant and both of the analyses with and without vertical loads produce same soil stresses after lateral deflection of 20 mm.

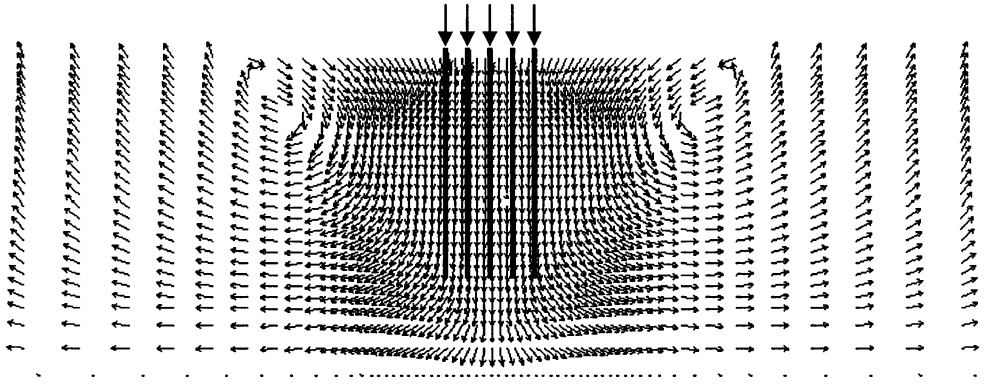

(a)

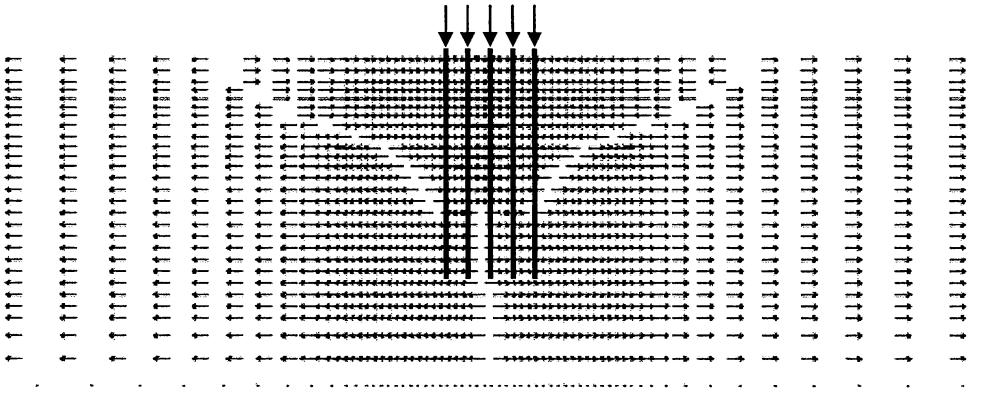

(b)

Fig. 5.17 Soil displacement field due to vertical loads on piles heads in a pile group: (a) total soil displacement; (b) horizontal soil displacement.

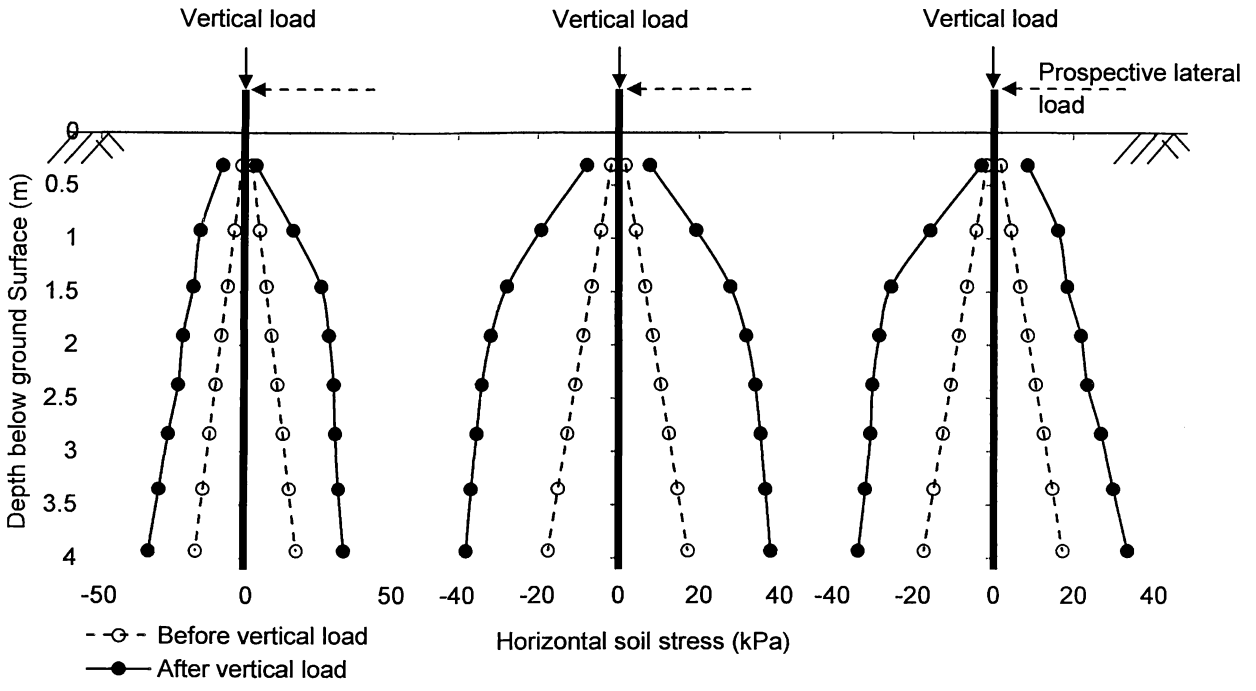

Fig. 5.18 Horizontal soil stresses before and after the application of vertical loads along the upper part of the pile depth just at the back of and in front of piles 1, 3, and 5.

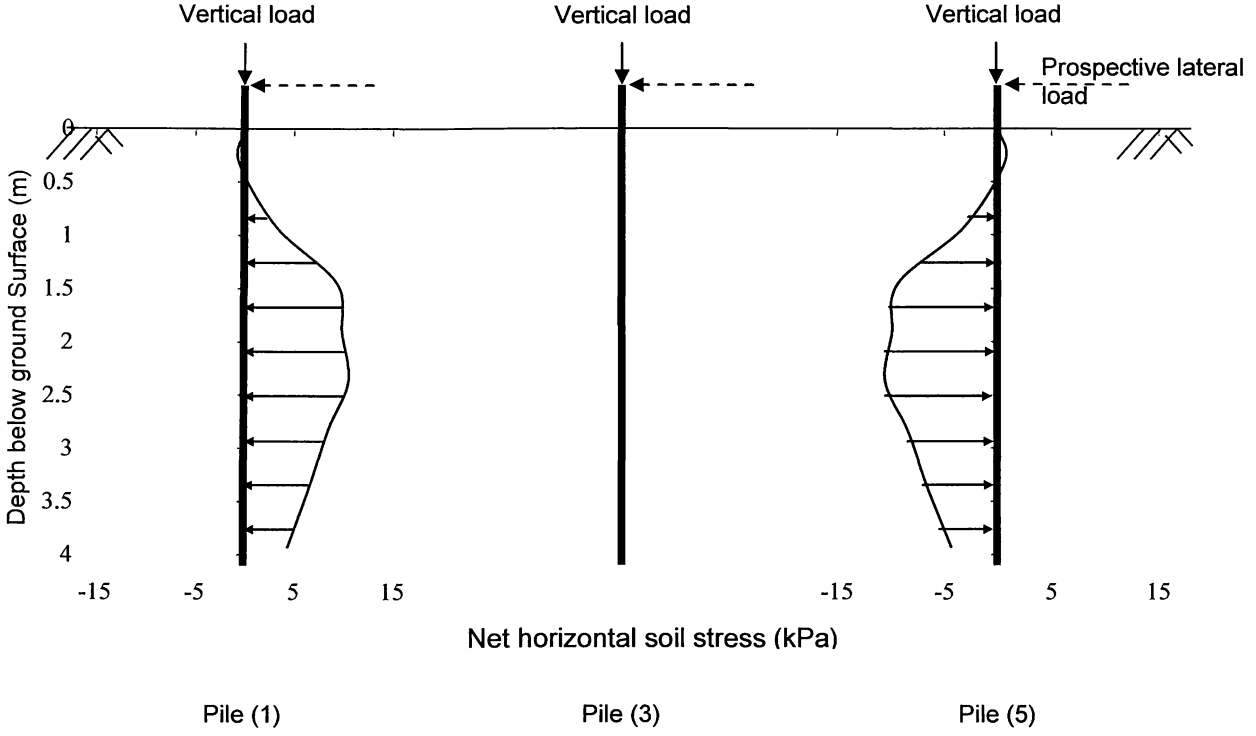

Fig. 5.19 Net horizontal soil stresses after the application of vertical loads along the upper part of the pile depth just at the back of and in front of piles 1, 3, and 5.

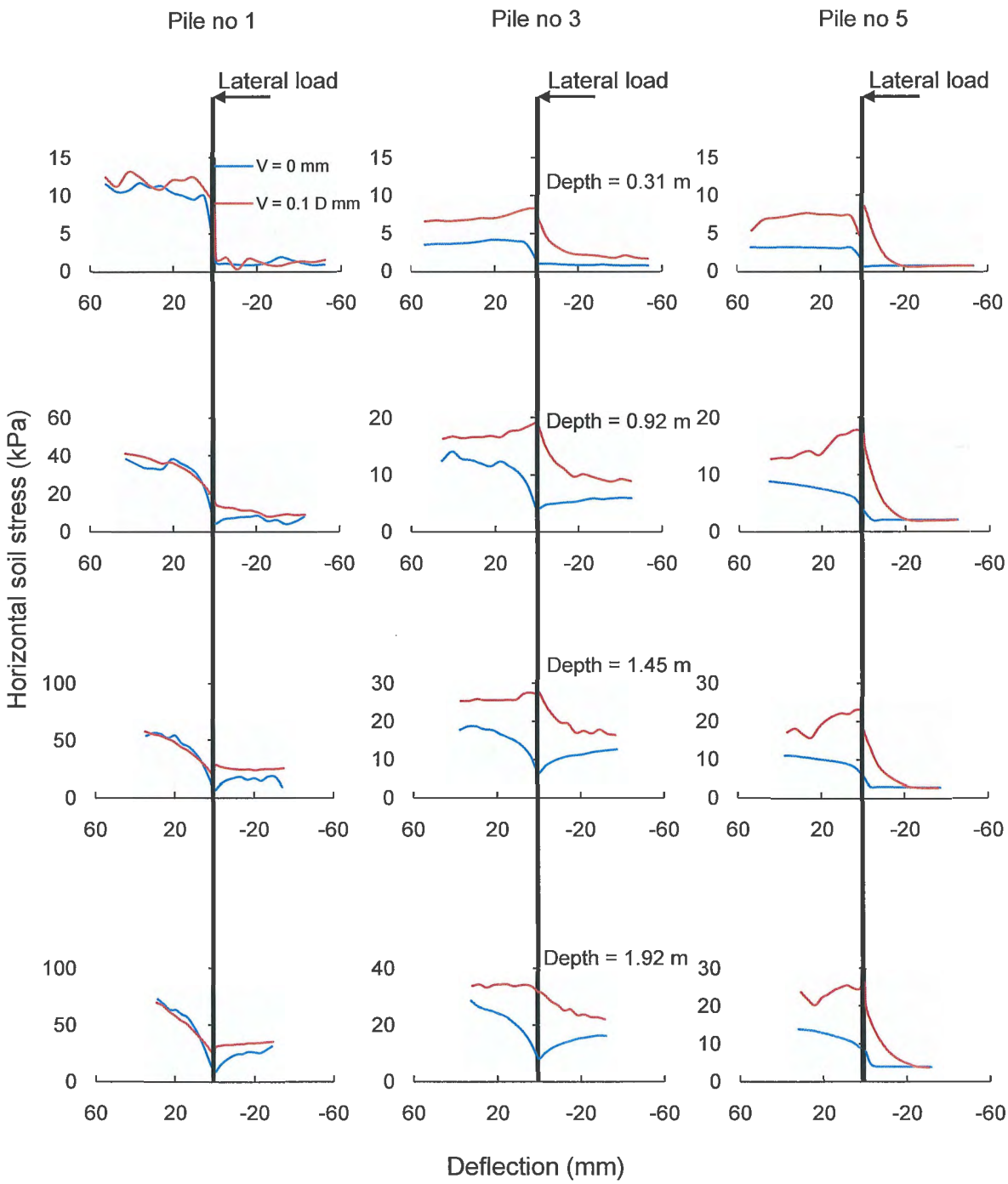

Fig. 5.20 Variation of horizontal soil stresses at different depths with the corresponding lateral pile deflections for both analyses with and without vertical loads for piles 1, 3, and 5.

The net horizontal soil pressure of piles 1, 3, and 5 at a lateral deflection of 60 mm were plotted against pile depth as shown in Fig. 5.21. For piles 3 and 5, the influence of vertical loads is to increase the net horizontal stresses of soil especially at shallow depths, which is the predominant factor of the increase of the lateral load carrying capacity of the pile. For the leading pile, the presence of vertical loads decreases the net horizontal stresses, leading to a reduction in lateral loading carrying capacity of the pile.

The net soil stress is further examined through the variation of the horizontal stress differences for points at a depth of 1.45 m below the ground surface (the depth where maximum horizontal stresses occurs, Fig. 5.21) with the corresponding lateral deflections of these points as shown in Fig. 5.22. Figure 5.22 confirms that the effect of vertical load on the group pile behavior is to decrease the net horizontal soil stress for the leading pile and increase the soil stress for other piles leading to the change in the lateral carrying capacity of the individual pile.

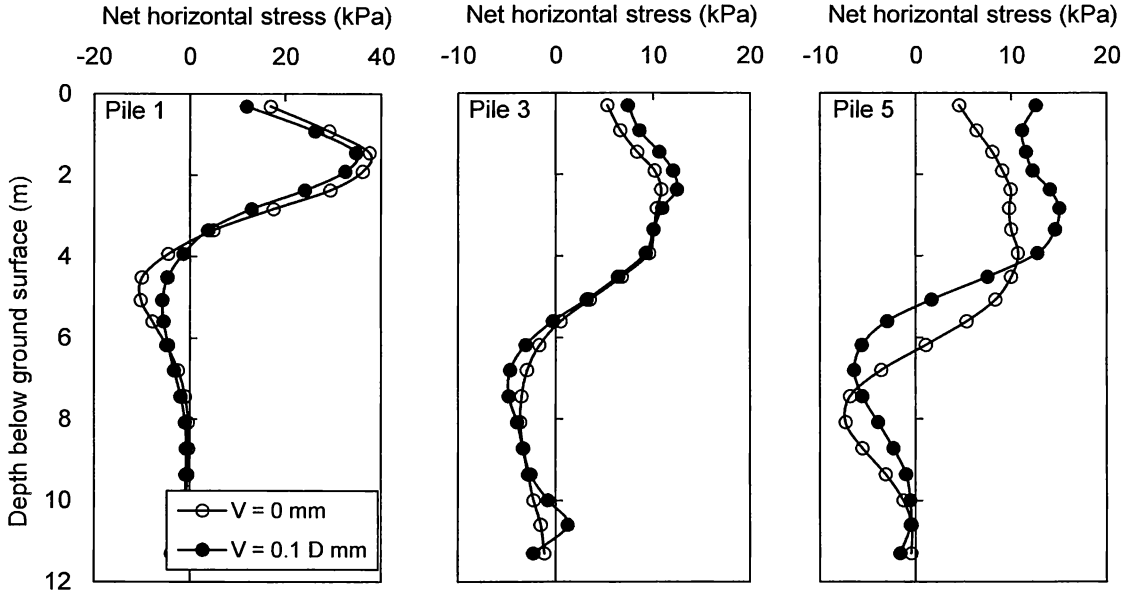

Fig. 5.21 Net horizontal soil stresses along the depth of piles 1, 3, and 5 at a 60 mm lateral deflection: (a) back side; (b) front side.

5.4.4 Effect of vertical load magnitudes

Figure 5.23 shows the variation of the percentage of change (increase or decrease) in lateral resistances of single and grouped piles with the magnitude of the applied vertical displacement (V). The vertical displacement ranged from 0 to 0.2D. In Fig. 5.23, the lateral resistances

increase (for piles 2, 3, 4, and 5) and decrease (for pile 1) gradually until a vertical load corresponding to V ≈ 0.05D, then the lateral resistances change little with vertical loads. These results declare that the maximum change in the lateral resistance of piles could be occurred during the working vertical loads and thus the corresponding percentages of changes can't be neglected.

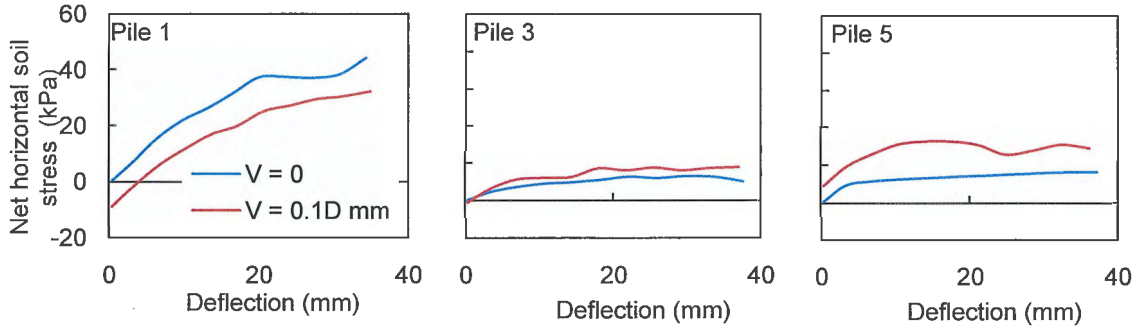

Fig. 5.22 Variation of net horizontal stress with the corresponding lateral deflections for piles 1, 3, and 5 at a depth of 1.45 m

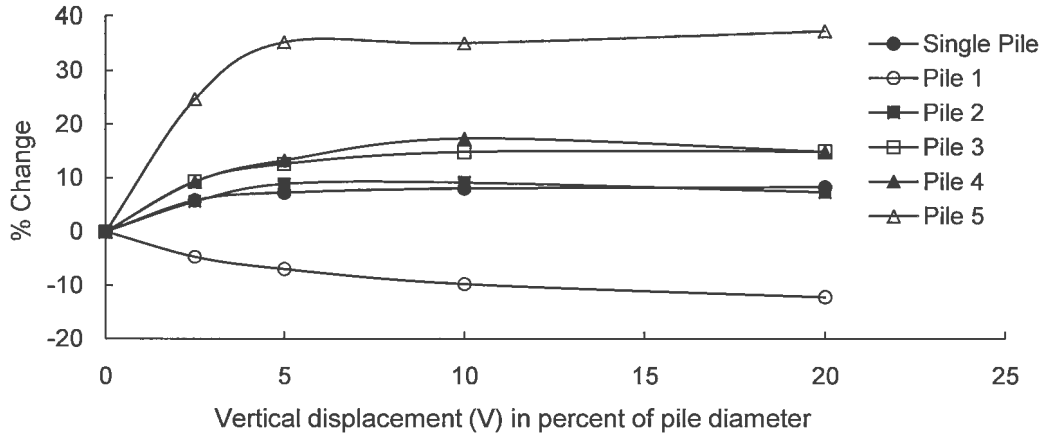

Fig. 5.23 Effect of vertical load magnitudes

5.5 Influence of Vertical Loads on Lateral Pile Group Response Considering Soil-pile-cap Interactions

In this section, a reinforced concrete pile cap is attached to the system at ground surface for both single and group piles cases. Dimensions of pile caps in both cases are shown in Fig. 5.24. The effect of vertical loads on the lateral responses of single and group pile considering soil-pile-cap interaction will be discussed in details in the following sub sections.

5.5.1 Pile Cap Model

Linear plan elements with two degrees of freedom per node were used to model the concrete pile caps. The Elastic modulus (E_c), Poisson's ratio (υ_c), and density (ρ_c) were set to be 40 GPa, 0.18, and 2.5 t/m^3, respectively. Joint elements with the properties shown in Table 4.3 in chapter 4 were used at soil-cap interface to represent sliding mechanism between them.

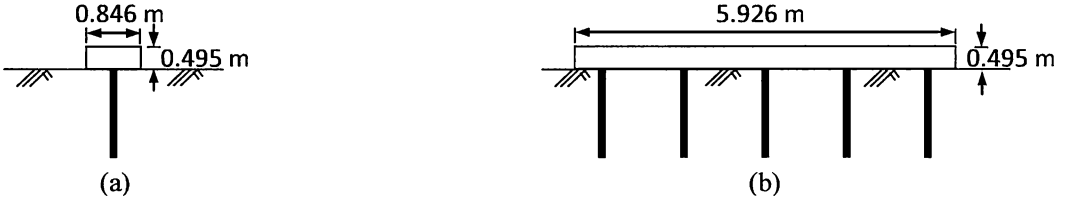

Fig. 5.24 Pile cap dimensions: (a) single pile; (b) pile group

5.5.2 Response of single pile with cap

Figure 5.25 shows the load versus lateral deflections of the single pile with cap for both analyses with and without the presence of a vertical load. Figure 5.25 indicates that the effect of a vertical load inducing a vertical displacement (V = 0.1D mm) to the pile cap is similar to that shown in Fig. 5.3 for a free head pile but with a higher percentage increase of the lateral-carrying capacity of the pile. At the maximum lateral deflection of 60 mm, the percentage of increase of the lateral-carrying capacity of the pile reaches 19 %.

An attempt to identify the mechanism of the increase in the lateral resistance in this case was made by studying deformations and stress changes induced in soil due to the vertical load. The downdrag of the soil by the vertical load applied at the pile cap as it moves down is shown in Fig. 5.26. In this figure, displacement field was scaled by 20 times relative to that of the

geometric scale. The vertical load on a pile cap drags down the soil surrounding the pile because of the down word movement of the cap in addition to the effect of skin friction of the pile.

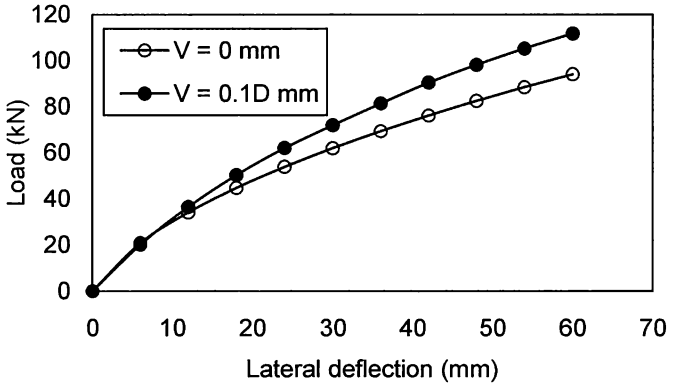

Fig. 5.25 Load-deflection curve of single pile with cap for both cases with and without vertical load

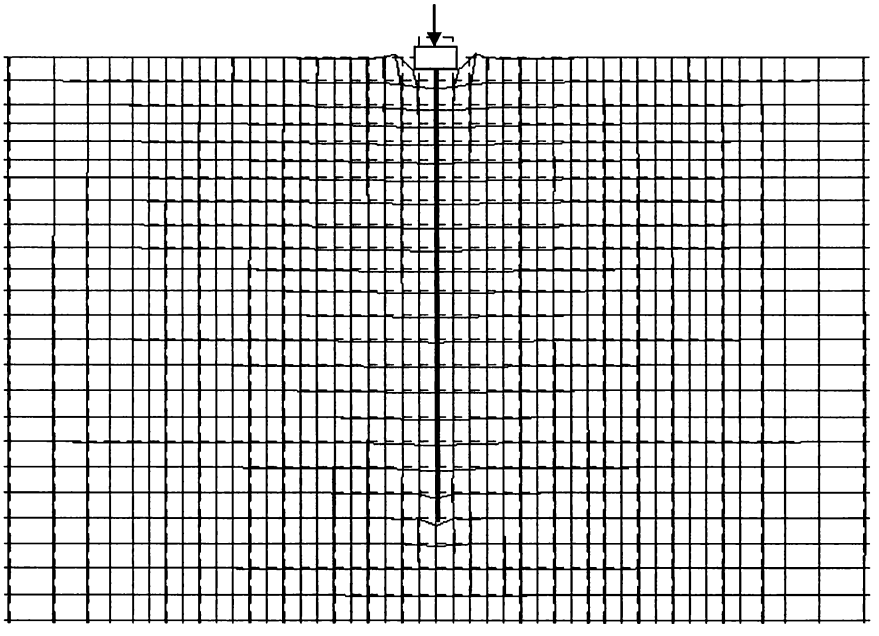

Fig. 5.26 Soil deformation associated with a vertical load applied to the pile cap

Soil displacement field is shown in Fig. 5.27. As stated earlier in the analysis of free head piles, due to the symmetry of the soil displacement relative to the pile longitudinal axis, only the

right part of Fig. 5.27 will be considered in this discussion. It should be noted from Fig. 5.27 that the displacement vectors of soil beneath the pile cap were directed away from the cap in a pattern of a fan. This displacement field increases the vertical stress (σ'_y) in the soil in the vicinity of the pile because of the presence of the foundation layer as represented by the fixed displacement boundary at the bottom of the analysis domain. Moreover soil rotates counter clockwise due to the action of the vertical load on the pile cap and the centre of rotation is located just below the ground surface and at some distance right to the pile. The displacement vectors of soil at shallow depths are directed towards the pile. The resulting lateral displacement of soil at shallow depths pushes the soil toward the pile, inducing an increase in the lateral stress (σ'_x) in the soil. These stress changes results in the increase in the confining pressure in the soil in the vicinity of the pile. The increase in the confining stress of soil, then, increases the resistance of soil-pile interaction spring through the mechanism incorporated in the modeling of the spring as described in Chapter 3.

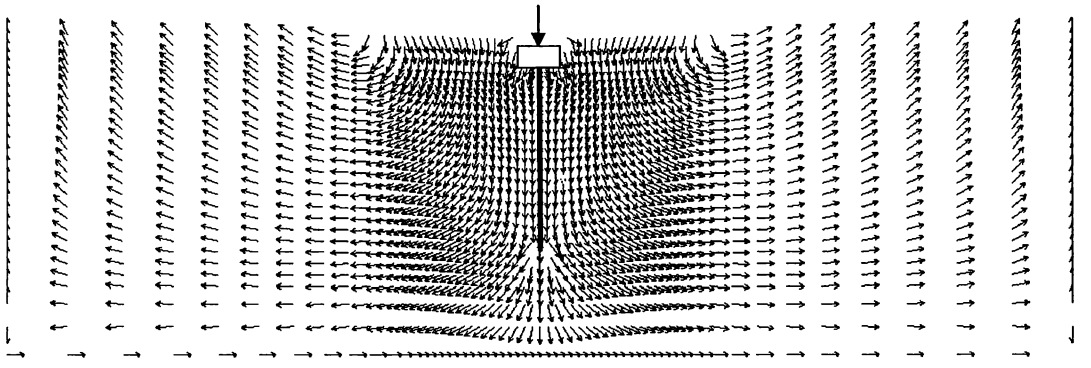

Fig. 5.27 Soil displacement field due to a vertical load on the pile cap

The difference in the increase in the lateral resistance of the single pile with and without a pile cap subject to a vertical load could be explained further by plotting the horizontal soil stress along the upper part of the pile. These horizontal stresses induced before and after the application of the vertical load for both analyses with and without a pile cap as shown in Fig. 5.28. Figure 5.28 declares that the inclusion of vertical loads prior to lateral loads increases the horizontal stress of soil elements along the upper part of the pile depth (4 m) for both cases with and without a pile cap and the shape of the horizontal stress profile after these increases differ. The horizontal stress profile induced after the application of the vertical load on the free head case is

affected only by the relative movement between the pile and the soil (soil-pile interaction), while the corresponding profile of the capped pile case is affected by the movements of both the pile and the cap relative to the soil movement (soil-pile and soil-cap interactions). As shown in Fig. 5.28, the free head stress profile starts at the ground surface (where the stress levels are smaller and the soil response exhibits a higher degree of softening) and propagates downwards as the vertical stress transfer from the pile to the surrounding soil. On the contrary, the capped pile stress profile starts at the ground surface with a high stress value due to the confinement condition of the soil comes from the downward movement of the cap then the horizontal stress gradually decreases with the depth and approaches the stress profile of the free head case as the effect of soil-cap interaction vanishes. The difference between the confining pressure profile in capped pile case and the corresponding profile of the free head case may explain the difference in the percentages of lateral load capacity increase in the two cases.

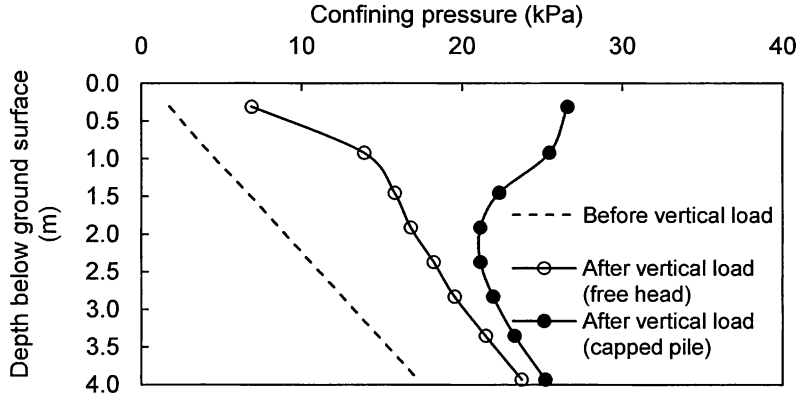

Fig. 5.28 Confining pressure along the upper part of the pile

The net horizontal soil stress at a 60 mm lateral deflection was plotted against the pile depth as shown in Fig. 5.29. As expected, the influence of vertical loads is to increase the net horizontal stresses of soil especially at shallow depth and the percentage of increase is higher than that of free head pile.

5.5.3 Response of group pile with cap

Figure 5.30 shows the piles loads versus deflection for the capped group with and without vertical loads. The lateral load-carrying capacity of each pile in the group (pure lateral load) was

slightly increased in the presence of the cap because of the friction between the bottom of the cap and the ground surface. The effect of vertical loads on the lateral load carrying capacity of each pile in the capped group is similar to the free head case but with higher percentages of decrease or increase. The percentage of decrease of the lateral load carrying capacity of pile 1 at a maximum lateral deflection of 60 mm was 28.44 % while the percentages of increase were 10.14, 36.91, 45.60, and 71.11 % for piles 2, 3, 4, and 5, respectively. The inclusion of the pile cap amplifies the effect of vertical loads on the subsequent lateral load response of piles.

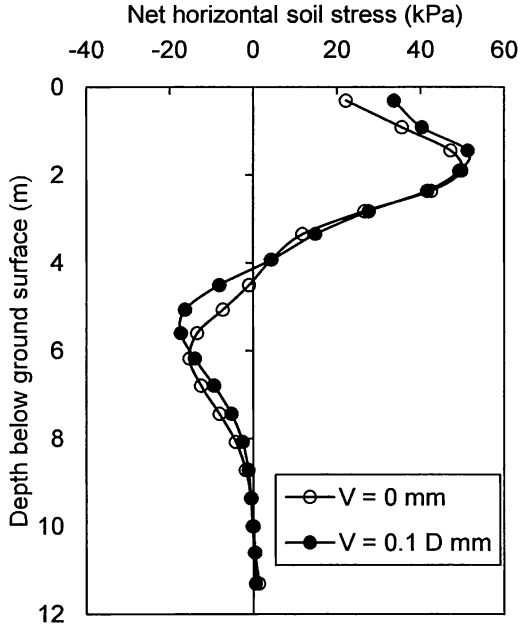

Fig. 5.29 Net horizontal soil stresses along the depth of the pile at a 60 mm lateral deflection

In order to discuss the effect of vertical loads on the load distribution among piles in the group for the analysis with a pile cap, the ratios of the lateral load of each pile relative to the corresponding load of the single pile are plotted for both analyses with and without vertical loads and are shown for deflections of 30 and 60 mm in Fig. 5.31. Similar to the free head pile group case, the load distribution among piles in a capped pile group without vertical loads at both deflections of 30 and 60 mm is not uniform and the leading pile carries the greatest load while other piles carried loads less than the leading pile. The presence of vertical loads on piles reverses the load distribution curve (i.e. the trailing pile carried the greatest load while other piles including the leading pile carried loads less than the trailing pile) at both deflections of 30 and 60

mm. In accordance with the load distribution among piles in the pile group, distributions of bending moments and shear induced in individual piles in the group tend to be uniform as shown in Fig. 5.32 and Fig. 5.33, respectively.

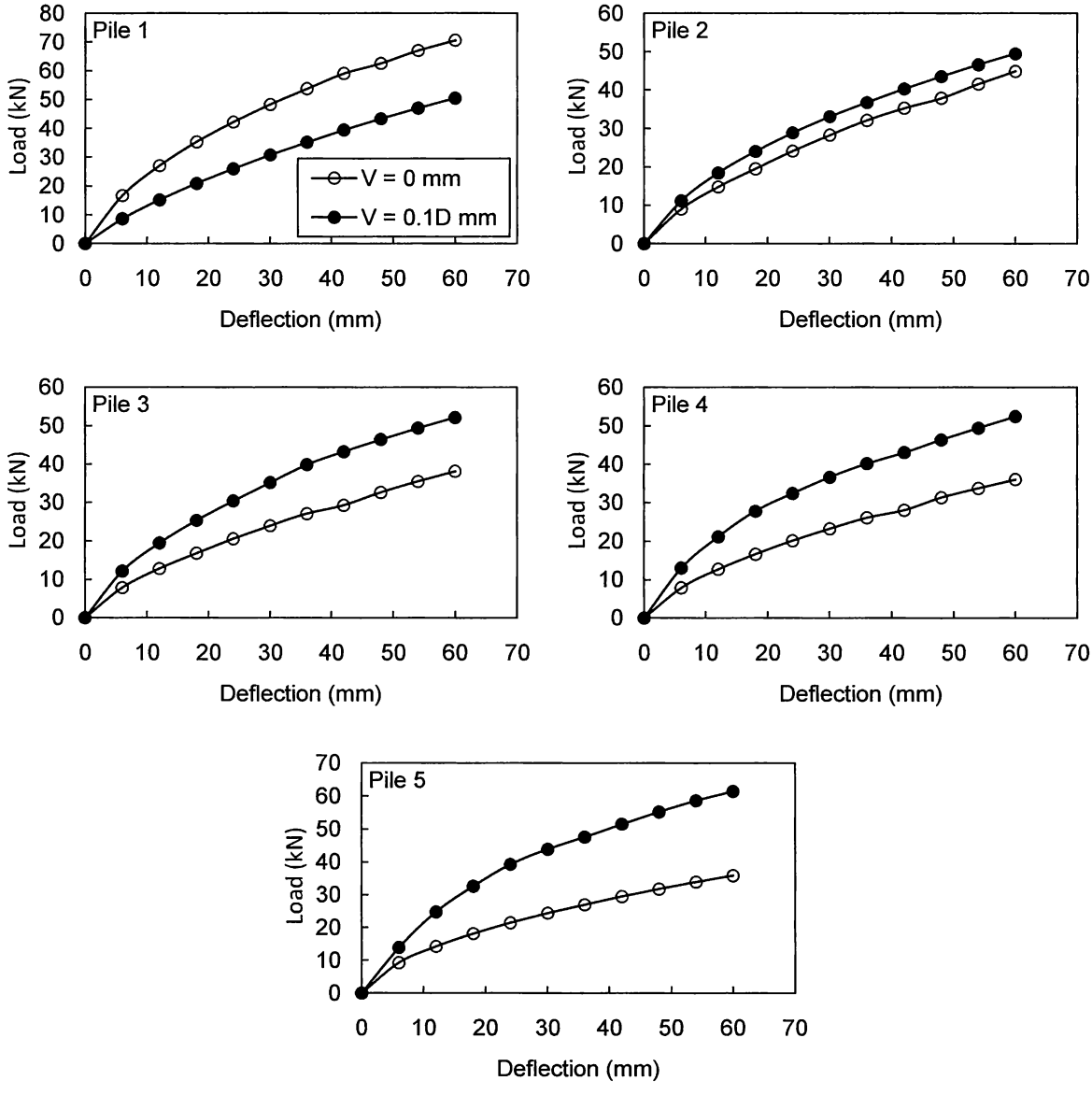

Fig. 5.30 Load-deflection curve of each pile in a group with a pile cap at 3.92-pile diameter spacing.

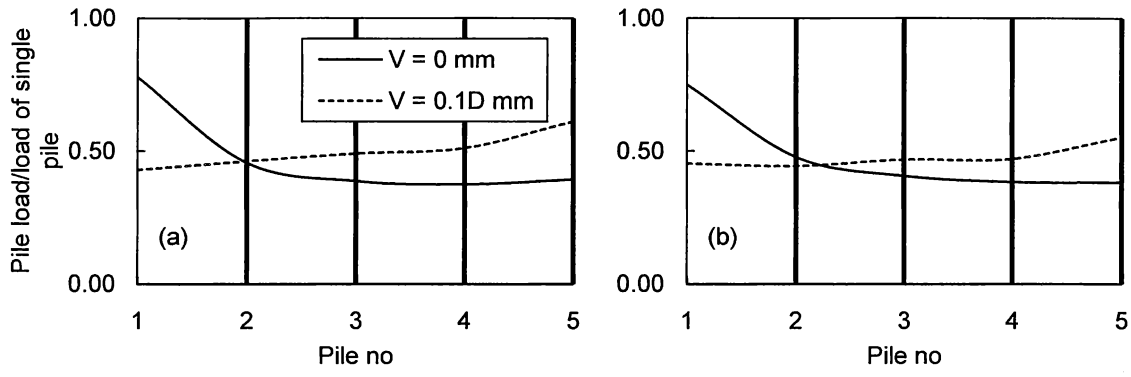

Fig. 5.31 Ratio of lateral loads computed with and without vertical loads of each pile in a group with a pile cap at 3.92-pile diameter spacing relative to the corresponding load of the single pile at target deflections: (a) 30 mm; (b) 60 mm.

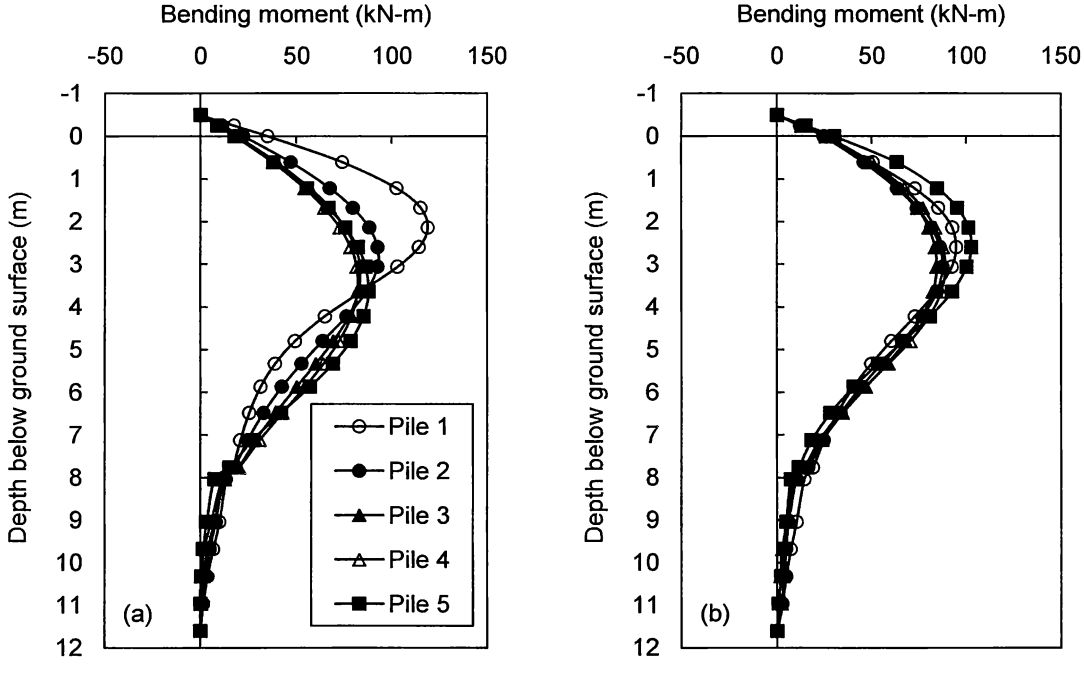

Fig. 5.32 Bending moment profiles of piles in the capped group under: (a) pure lateral; and (b) combined loads

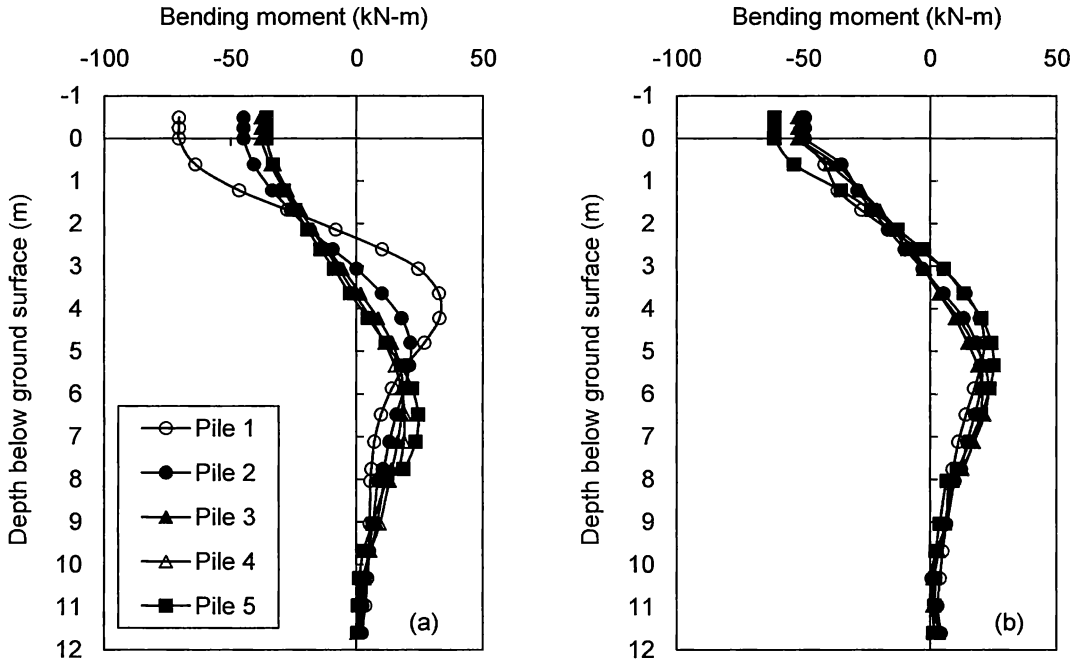

Fig. 5.33 Shearing force profiles of piles in the capped group under: (a) pure lateral; and (b) combined loads

The downdrag of the soil by the vertical load at the pile cap is shown in Fig. 5.34. In this figure, the displacement field is scaled by 20 times relative to that of the geometric scale. The ground surface moves downward more in the portion under the cap than elsewhere, but the movements also do occur away from the intermediate zone. The soil displacement field is shown in Fig. 5.35(a). Due to the symmetry, only the right part of Fig. 5.35(a) will be discussed here. This figure shows that soil rotates counter clockwise due to the action of vertical loads on the pile cap and the centre of rotation was located just below the ground surface and at some distance right to the pile group. As a result of this rotation, just outside the pile group, the displacement vectors of soil at shallow depths were directed towards the pile group whereas those at deeper depths were directed away from it. Figure 5.35(b) show clearly the difference in horizontal components of soil displacement directions with respect to the pile depth.

The corresponding horizontal soil stresses along the first four meters on piles 1, 3, and 5 in the group are shown in Fig. 5.36, where the stresses at the back of and in front of the piles were separately plotted. Figure 5.36 declares a highly uniform increase in the horizontal stresses of soil surrounding the piles after the application of vertical loads.

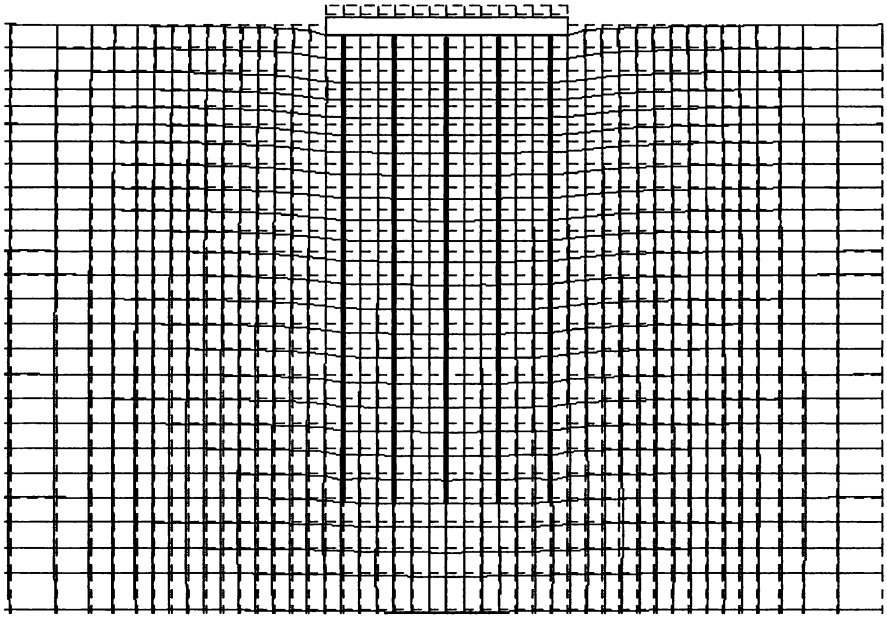

Fig. 5.34 Soil deformation corresponding to vertical loads applied to pile cap.

When the lateral load is applied to the pile group, the lateral stresses discussed above will change in general. In order to study this aspect of soil behavior, variation of horizontal soil stresses for points at different depths with the corresponding lateral deflections is shown in Fig. 5.37. In this figure, positive sign of deflection indicates that the point is in front of the pile, while negative sign of deflection indicates that the point is back to the pile.

For the trailing pile, the horizontal soil stress is significantly affected by the effect of vertical loads not only at the back of the piles but also in front of them. For front points, in the analysis without vertical loads, the horizontal soil stress initiates from the earth pressure at rest and gradually increases. In the analysis with vertical loads, the horizontal soil stress initiates from the enhanced earth pressure and approximately remains constant. For back points, the horizontal soil stress obtained from the analysis without vertical loads initiates from at rest earth pressure and gradually decreases (as the pile deflects). The horizontal soil stress obtained from the analysis with vertical loads shows similar behavior, it initiates from enhanced earth pressure and slightly decreases in the zone behind the pile. Both of the analyses with and without vertical loads produce same soil stresses after lateral deflection of about 30 mm.

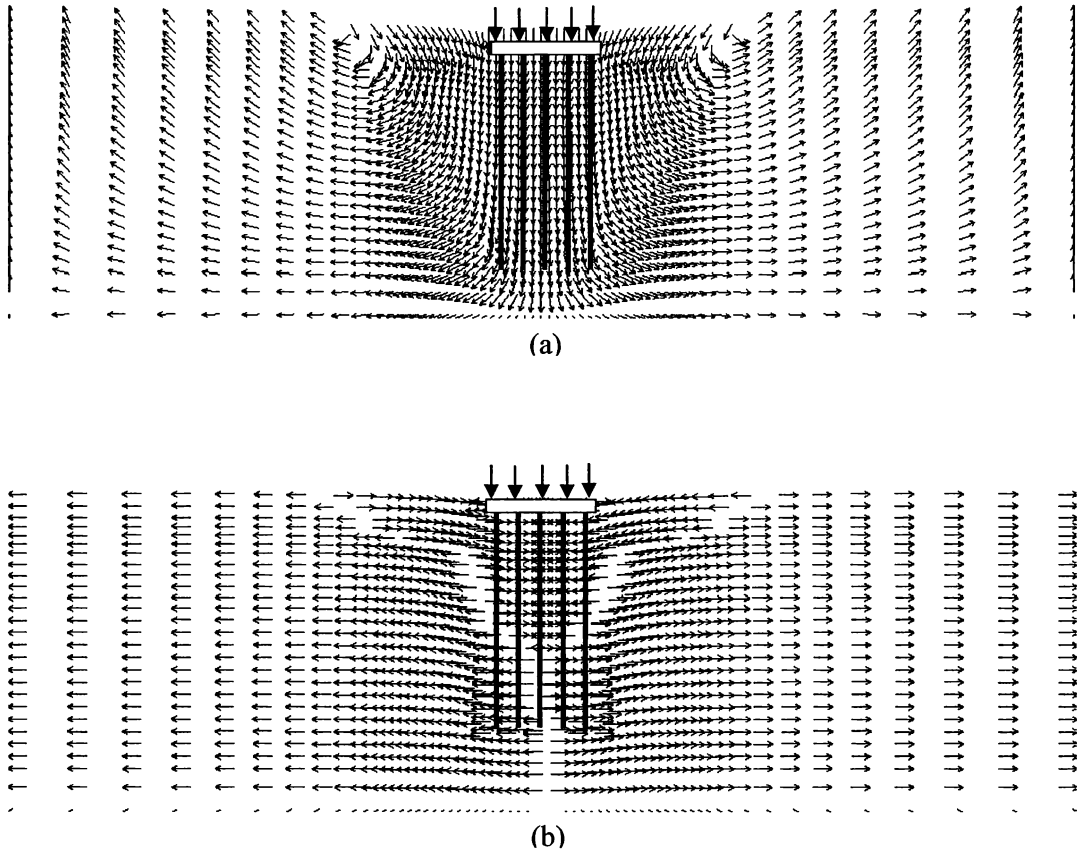

Fig. 5.35 Soil displacement field due to vertical loads on the pile cap in a pile group: (a) total soil displacement; (b) horizontal soil displacement.

For the middle pile, the horizontal soil stress is also significantly affected by the effect of vertical loads not only at the back of the piles but also in front of them. For front points, the horizontal soil stress initiates from the earth pressure at rest or the enhanced earth pressure for the analyses with and without vertical loads, respectively and gradually increases with rate depends on the depth of the point under consideration. For back points, the horizontal soil stress initiates from the earth pressure at rest or the enhanced earth pressure for the analyses with and without vertical loads, respectively and slightly increases or remains constant (as the pile deflects).

For the leading pile, the horizontal soil stress is significantly affected by the effect of vertical loads not only at the back of the piles but also in front of them. For back points, in the

analysis without vertical loads, the horizontal soil stress initiates from the earth pressure at rest and gradually increases. In the analysis with vertical loads, the horizontal soil stress initiates from the enhanced earth pressure and increases gradually. For front points, the horizontal soil stress initiates from the earth pressure at rest or the enhanced earth pressure for the analyses with and without vertical loads, respectively and gradually increases with rate depends on the depth of the point under consideration. Although, the horizontal soil stress-deflection curves in front points of the pile show approximately the same trend in both of the analyses with and without vertical loads at deeper depths, the horizontal soil stress at shallow depth of 0.31 m is significantly affected by the presence of vertical loads.

The net horizontal soil pressure of piles 1, 3, and 5 at a lateral deflection of 60 mm were plotted against pile depth as shown in Fig. 5.38. For piles 3 and 5, the influence of vertical loads is to increase the net horizontal stresses of soil especially at shallow depths, which is the predominant factor of the increase of the lateral load carrying capacity of the pile. For the leading pile, the presence of vertical loads decreases the net horizontal stresses, leading to a reduction in lateral loading carrying capacity of the pile.

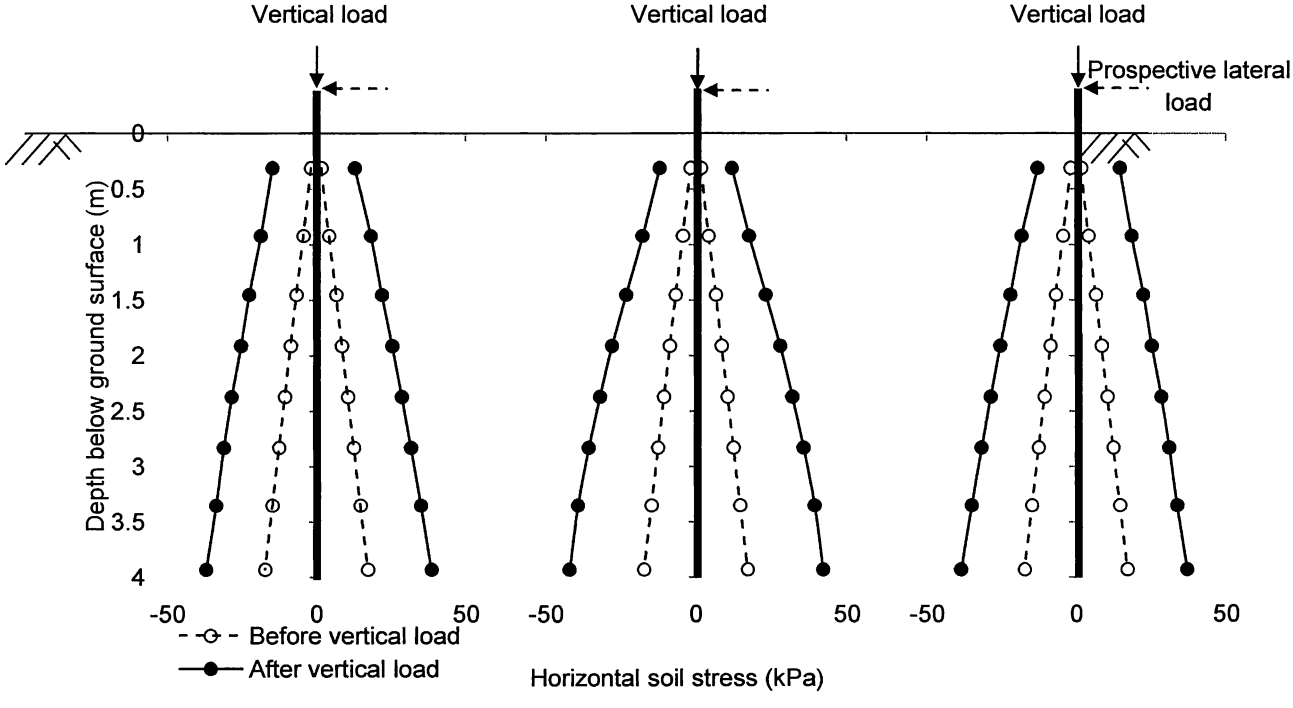

Fig. 5.36 Horizontal soil stresses before and after the application of vertical loads on the pile cap: along the upper part of the pile depth just at the back of and in front of piles 1, 3, and 5.

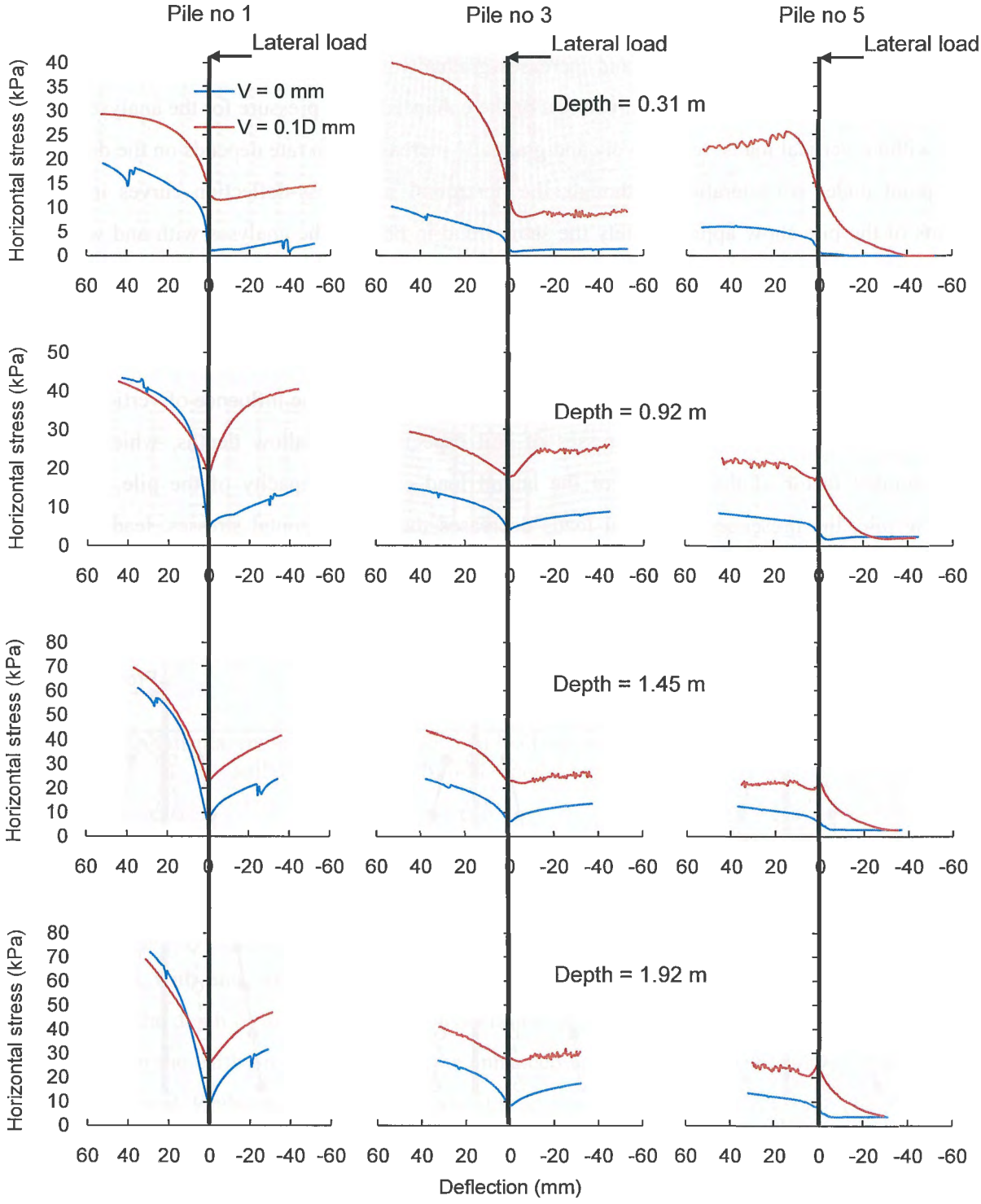

Fig. 5.37 Variation of horizontal soil stresses at different depths with the corresponding lateral pile deflections for both analyses with and without vertical loads for piles 1, 3, and 5.

The net soil stress is further examined through the variation of the horizontal stress differences for points at a depth of 1.45 m below the ground surface with the corresponding lateral deflections of these points as shown in Fig. 5.39. Figure 5.39 confirms that the effect of vertical load on the group pile behavior is to decrease the net horizontal soil stress for the leading pile and increase the soil stress for other piles leading to the change in the lateral carrying capacity of the individual pile.

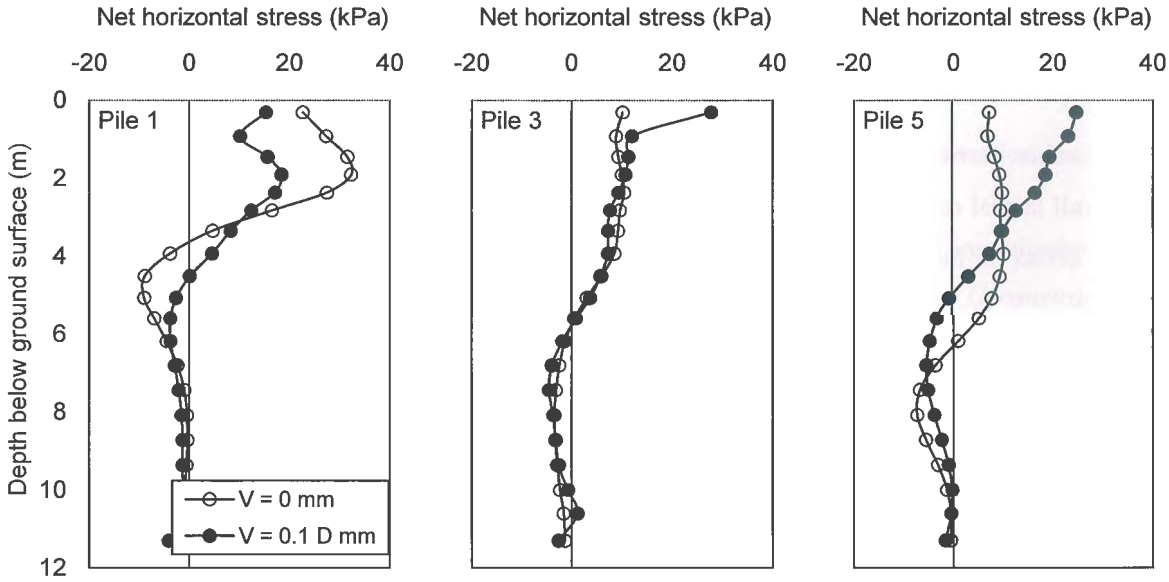

Fig. 5.38 Variation of horizontal soil stresses at different depths with the corresponding lateral pile deflections for both analyses with and without vertical loads for piles 1, 3, and 5.

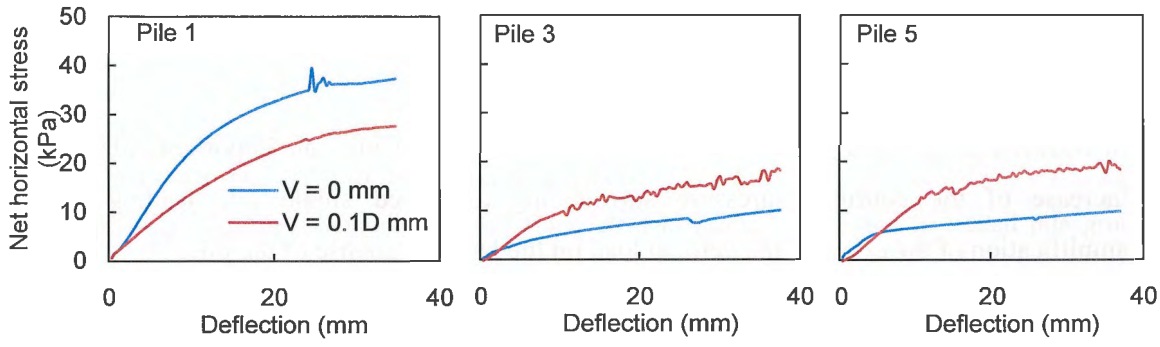

Fig. 5.39 Variation of net horizontal stress with the corresponding lateral deflections for piles 1, 3, and 5 at a depth of 1.45 m

5.6 Conclusions

The effect of vertical loads on the lateral response of a free head and capped pile group (3×5) embedded in sandy soil has been studied in this paper through a series of two-dimensional finite element analyses. Of the findings of this study, the following conclusions can be drawn:

1. The influence of vertical loads on the lateral response of piles is to increase the confining pressure in the sand deposit surrounding the pile, leading to an increase in the lateral pile resistance. A vertical load applied to a single pile with a vertical displacement of 0.1-pile diameter (D = 324 mm) increases the lateral pile resistance, at a 60 mm lateral deflection, by 8 %.
2. The same vertical load applied to a pile group spaced at 3.92-pile diameters increases the overall lateral resistance of the group by 9 %.
3. The effect on individual piles depends on the pile position. The vertical load leads to a 10 % decrease in the lateral resistance of the leading pile (pile 1) and 9, 14, 17, and 35 % increases in the lateral resistances of piles 2, 3, 4, and 5, respectively.
4. The vertical load applied on the pile group increases the confining pressures in the sand deposit confined by the piles but the rate of increase in those outside the group is relatively small, resulting in the difference in a balance of lateral soil pressures acting at the back of and in front of the individual pile.
5. The middle pile (pile 3) behaves approximately the same as the single pile as a result of no net lateral stress induced by the vertical load. For the leading pile (pile 1), the net horizontal stress due to the vertical load acts in the same direction with the prospective lateral load, leading to a decrease in the pile resistance to the subsequent lateral load. For the trailing (pile 5), the net horizontal stress acts against the prospective lateral load, leading to an increase of the pile resistance to the subsequent lateral load.
6. In addition to soil-pile interaction, soil-pile cap interaction play an important role in the increase of the confining pressure surrounding a capped single pile leading to an amplification of the effect of the vertical load on the lateral response of the pile.
7. The effect of vertical loads on the lateral load carrying capacity of individual pile in a capped pile group is similar to the free head case but with higher percentages of decrease or increase.

References

1. Anagnostopoulos, C. and Georgiadis, M., 1993. Interaction of axial and lateral pile responses. *Journal of Geotechnical Engineering* (ASCE), 119(4), 793–798.
2. Basu, D. and Salgado, R., 2007. Elastic analysis of laterally loaded pile in multi-layered soil. *Geomechanics and Geoengineering*, 2 (3), 183–196.
3. Iai, S., Matsunaga, Y. and Kameoka, T., 1992. Strain space plasticity model for cyclic mobility. *Soils and Foundations*, 32(2), 1–15.
4. Karthigeyan, S., and Ramakrishna, V.V.G.S.T., 2005. Interaction between vertical and lateral loads on the response of piles in soft clays. *Proceeding of the Sixteenth International Conference on Soil Mechanics and Geotechnical Engineering*, Osaka, 1997–2000.
5. Karthigeyan, S., Ramakrishna, V.V.G.S.T. and Rajagopal, K., 2006. Influence of vertical load on the lateral response of piles in sand. *Computers and Geotechnics*, 33(2), 121–131.
6. Karthigeyan, S., Ramakrishna, V.V.G.S.T. and Rajagopal, K., 2007. Numerical investigation of the effect of vertical load on the lateral response of piles. *Journal of Geotechnical and Geoenvironmental Engineering* (ASCE), 133(5), 512–521. Loukidis, D. and Salgado, R., 2008. Analysis of the shaft resistance of non-displacement piles in sand. *Géotechnique*, 58(4), 283–296.
7. Matlock, H. and Reese, L.C., 1960. Generalized solutions for laterally loaded piles. *Journal of the Soil Mechanics and Foundation Division* (ASCE), 86(5), 63–91.
8. McNulty, J.F., (1956). Thrust loading on piles. *Journal of the Soil Mechanics and Foundation Division* (ASCE), 82(2), 1–25.
9. Meyerhof, G.G. and Yalcin, A.S. 1984. Pile capacity for eccentric inclined load in clay. *Canadian Geotechnical Journal*, 21(3), 389-396.
10. Meyerhof, G.G., Yalcin, A.S., and Mathur, A.K. 1983. Ultimate pile capacity for eccentric inclined load. *Journal of Geotechnical Engineering, ASCE*, 109(3), 408-423.
11. Miura, K., Miura, S., and Toki, S. 1986. Deformation behaviour of anisotropic dense sand under principal stress axes rotation. *Soils and Foundations*, 26(1): 36–52.
12. Nakata, Y., Hyodo, M., Murata, H., and Yasufuku, N. 1998. Flow deformation of sands subjected to principal stress rotation. *Soils and Foundations*, 38(3): 115–128.
13. Ottaviani, M., 1975. Three-dimensional finite element analysis of vertically loaded pile groups. *Géotechnique*, 25(2), 159–174.
14. Poulos, H.G., 1971a. Behavior of laterally loaded piles: I-single piles. *Journal of the Soil Mechanics and Foundation Division* (ASCE), 97(5), 711–731.
15. Poulos, H.G., 1971b. Behavior of laterally loaded piles: II-group piles. *Journal of the Soil Mechanics and Foundation Division* (ASCE), 97(5), 733–751.

16. Randolph, M.F. and Wroth, C.P., 1978. Analysis of deformation of vertically loaded piles. *Journal of Geotechnical Engineering Division* (ASCE), 104(12), 1465–1488.
17. Reese, L.C. and Van Impe, W.F., 2001. *Single piles and pile groups under lateral loading.* Rotterdam, Netherlands: A.A. Balkema.
18. Rollins, K.M., Peterson, K.T. and Weaver, T.J., 1998. Lateral load behavior of full-scale pile group in clay. *Journal of Geotechnical and Geoenvironmental Engineering* (ASCE), 124(6), 468–478.
19. Rollins, K.M., Lane, J.D., and Gerber, T.M., 2005. Measured and computed lateral response of a pile group in sand. *Journal of Geotechnical and Geoenvironmental Engineering* (ASCE), 131(1), 103–114.
20. Snyder, J.L., 2004. *Full–scale lateral–load tests of a 3x5 pile group in soft clays and silts*. M.Sc. thesis. Brigham Young University.
21. Sorochan, E.A. and Bykov, V.I., 1976. Performance of groups of cast-in place piles subject to horizontal loading. *Journal of Soil Mechanics and Foundation Engineering*, 13(3), 157–161.
22. Symes, M.J., Gens, A., and Hight, D.W. 1984. Undrained anisotropy and principal stress rotation in saturated sand. *Géotechnique*, 34(1): 11–27.
23. Whitaker, T., 1957. Experiments with model piles in groups. *Géotechnique*, 7(4), 147–167.
24. Xu, K.J. and Poulos, H.G., 2000. General elastic analysis of piles and pile groups. *International Journal for Numerical and Analytical Methods in Geomechanics*, 24(15), 1109–1138.
25. Zhang, L., McVay, M.C. and Lai, P.W, 1999. Centrifuge modelling of laterally loaded single battered piles in sands. *Canadian Geotechnical Journal*, 36(9), 1074–1084.
26. Zhang, L., McVay, M.C. and Lai, P.W., 1999. Numerical analysis of laterally loaded 3×3 to 7×3 pile groups in sands. *Journal of Geotechnical and Geoenvironmental Engineering* (ASCE) 1999, 125(11), 936–946.
27. Zhang, L.M., McVay, M.C., Gardner, R., Han, Sanjoon, and Lai, Peter. 2002. Effects of dead loads on the lateral response of battered pile groups. *Canadian Geotechnical Journal,* 39(3), 561-575.
28. Zhao, X., and Evans, T.M. 2009. Discrete simulations of laboratory loading conditions. *International Journal of Geomechanics*, ASCE, 9(4): 169–178.
29. Zhu, H. and Chang, M.F., 2002. Load transfer curves along bored piles considering modulus degradation. *Journal of Geotechnical and Geoenvironmental Engineering* (ASCE), 128(9), 764–774.
30. Zhukov, N.V. and Balov I.L. 1978. Investigation of the effect of a vertical surcharge on horizontal displacements and resistance of pile columns to horizontal loads. *J Soil Mech Found Eng*, 15(10:16-

CHAPTER 6

Analyses of Coupled Soil-Pile-Structure System under Sinusoidal Excitations with Various Frequencies

Contents

6.1 Introduction

Estimation of the seismic response of piles and piles supporting structures has received large attention in recent years especially after the damages caused to pile foundations during recent destructive earthquakes (e.g. Niigata Earthquake of 1964, Kobe Earthquake of 1995, Chi-Chi Earthquake of 1999, Bhuj Earthquake of 2001, Tohoku Earthquake 2011,). The catastrophic losses in terms of human life and economic assets have emphasized the importance of understanding the seismic soil-pile-structure interaction (SSPSI) and motivated researchers to propose numerical and analytical solutions of SSPSI to revamp the design codes and building regulations trying to prevent or simply reduce such kinds of damages.

As stated in Chapter 2, the available procedures of analyzing SSPSI have included those based on simplified interactions models such as the beam on dynamic Winkler Foundation approach (Kagawa and Kraft 1980; Pender and Pranjoto 1996; Allotey and El Naggar 2008), as well as those based on more rigorous FEM (Blaney et al. 1976; Cai et al. 1995; Rovithis et al. 2009) or BEM (Kattis et al. 1999; Padrón et al. 2007) formulations. These methods utilize either simplified two-step methods that uncouple the structure and foundation portions (Gazetas 1984; Fan et al. 1991) or a fully coupled SSPSI system in a single step (Kaynia and Mohzooni 1996; Mylonakis et al. 1997; Guin and Banerjee 1998). Although the former provides insights as to the distinct role of inertial and kinematic interaction, the latter gives a direct and more convenient estimation of the complete system response. The coupled 3D FE approach is most representative of the SSPSI system. However, such these methods, even if available, have well-known limitations when used in seismic design. This particularly true if the seismic analysis using actual or simulated ground motions is to be performed in the frequency domain. Under these conditions, SSPSI must be computed for a large number of frequencies covering the frequency content of the seismic signal.

For this reason, a simplified model would be quite useful provided it had been shown to be in accord with the rigorous results for a wide range of soil profiles and excitation frequencies (Nikolaou et al. 2001). Several investigators attempted to propose procedures to simplify the rigorous 3D FE models. The proposed method by Ozutsumi et al. (2003) described in Chapter 3 is one of these simplified procedures. In this chapter, the applicability of the 2D FEM including soil-pile interaction spring proposed by Ozutsumi et al. (2003) to study SSPSI is verified. The system under investigation comprises a SDOF structure supported on an end-bearing single pile

embedded in a homogeneous dry sand layer over rigid rock (fully coupled system). This verification has been executed in this chapter assuming elasto-dynamic behavior of the soil and comparing the free-field, pile, and structure responses with those found in other established results from the literature. In addition, the effects of soil profile and nonlinear soil properties on the free-field response, kinematic soil-pile interaction as well as the effective natural frequency of the coupled system are elucidated.

6.2 Problem Definition

The SSPSI examined in this study comprises of an end-bearing single pile supporting a SDOF structure founded on a homogeneous dry sand layer of thickness (L) over rigid rock as shown in Fig. 6.1. The response of the SDOF structure to seismic loading depends basically on the structural characteristics, namely its mass m_{st} and stiffness k_{st} and the fixed base fundamental frequency of the structure can be given as:

$$f_{st.fixed} = \frac{1}{2\pi}\sqrt{\frac{k_{st}}{m_{st}}} \tag{6.1}$$

If the predominant frequency of the input motion is close to the fixed base frequency, the structure displacement would be maximized relative to the displacement of the input motion.

When the structure is founded on a compliant soil, not only the structural characteristics but also soil properties will control the response of the soil-structure system leading to the definition of the effective natural frequency (f_{SSI}). When the predominant frequency of input motion is close to this frequency, the structure displacement (U_s) will be maximized relative to the free field soil displacement (U_{ff}).

If the structure is supported by piles, both structural characteristics and foundation (soil + pile) properties will control SSPSI response. Not only the effective natural frequency (f_{SSI}) will characterize the response in this case but also a pseudo-natural frequency (f_{pSSI}) does. f_{pSSI} is first introduced by Rovithis et al. (2009) as the frequency at which the structure displacement is maximized relative to the pile-head displacement (U_p). The applicability of the current FE adopting the simplified model proposed by Ozutsumi et al. (2003) to predict the effective and the pseudo-natural frequencies will be focused on in this chapter.

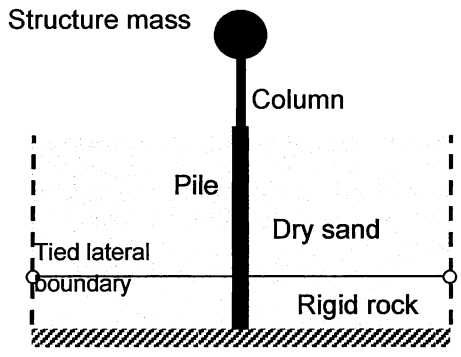

Fig. 6.1 A schematic view of the system under investigation

6.3 Finite Elements and Parameters Identification

The 2D effective stress FE analysis, FLIP (Iai et al. 1992), has been used to analyze the SSPSI problem. A 30 (m) thick soil stratum was meshed with quad plane elements. The length of each element was adequately defined according to the anticipated wavelength propagating in the soil. The maximum element size, E_{max}, was less than one-fifth to one-eighth the shortest wavelength (λ) to ensure accuracy (Kramer 1996).

The FE analyses were performed in two stages. In the first stage (self-weight analysis), the *in-situ* stresses were initialized in the soil due to the own weight of the soil. Properties of pile and soil-pile interaction spring were set to be zero during this stage of analysis. During the second stage of analysis (seismic response analysis), the actual properties of soil, pile, and soil-pile interaction spring were assigned. The total mesh size was extended to a horizontal distance from the pile of 30-pile diameter to prevent spurious wave reflections at the boundaries. Moreover, tied lateral boundary approach (a simpler alternative to the boundary approach suggested by Zienkiewicz et al. (1988) that illustrated in Fig. 6.1.) is used in the analysis. In this approach, the values of displacements, stresses, etc. are identical on both side boundaries. This condition is explicitly imposed in FLIP by an equivalent node concept, multiple points constrains (MPC).

All input motion are specified at bedrock level in the form of a harmonic horizontal displacement $U_g\ (t) = U_g.exp\ (i2\pi ft)$, where U_g = amplitude of the input bedrock displacement; f = frequency of excitation; $i^2 = -1$.

6.3.1 Soil model

In the description of the soil model given in Chapter 3, the shear modulus G_m corresponding to effective mean stress σ'_m is related to the initial shear modulus G_{ma} corresponding to initial effective mean stress σ'_{ma} as:

$$G_m = G_{ma}\left(\frac{\sigma'_m}{\sigma'_{ma}}\right)^{m_G} \tag{6.2}$$

where m_G is a parameter that controls the shear modulus distribution with the depth. If $m_G = 0$, the shear modulus will be constant with the depth and if $m_G = 0.5$, the shear modulus will be proportional to the square root of the depth as shown in Fig. 6.2. The verification process of the FE model will be based on a constant shear modulus distribution with the depth ($m_G = 0$) then the effect of the change in m_G will be discussed at the end of this chapter.

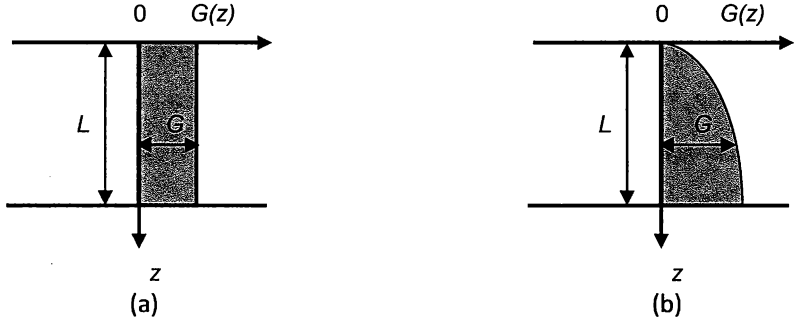

Fig. 6.2 Soil profiles studied in the analysis: (a) $m_G = 0$ and (b) $m_G = 0.5$

Parameters for dry sand used in the current FE analysis are shown in Table 6.1. The bulk modulus of the soil skeleton K was determined assuming a Poisson's ratio υ of 0.4. The initial shear wave velocity (Vs) is calculated using:

$$V_s = (G_{ma} / \rho_s)^{0.5} \tag{6.3}$$

and found to be = 200 m/s.

Table 6.1 Model parameters for soil

Density, $\rho_{t\ (t/m^3)}$	E_s(kPa)	G_{ma} (kPa)	υ	σ'_{ma} (kPa)
1.5	168,000	60,000	0.40	230

6.3.2 Pile column system

Linear elastic beam elements with three degrees of freedom per node are used for modeling pile and column. Normal force, shear force, and bending moment of each element are obtained directly from the used program. It is assumed that the pile has a circular cross-section of diameter D_p = 1.5 m, length L_p = 30 m (equal to the thickness of the soil stratum L), the pile slenderness ratio (L_p/D_p) = 20, Young's modulus E_p = 65 GPa (i.e E_p/E_s = 1000), Poisson's ratio υ_p = 0.3, and mass density ρ_p = 2.5 t/m^3. Same material properties were assigned for the column with only a change in the column Young's modulus.

6.3.3 Properties of the SDOF structure

The structural mass (M) and height (H_{st}) were assumed to be equal to 100 Mg and 10 m, respectively and the ratio EI_{st}/EI_p = 0.06, 0.66, and 1.85 leading to a fundamental frequency $f_{st,\ fixed}$ = 1.67, 5.0, and 8.4 Hz, respectively. These fixed-base frequencies (1.67, 5.0, and 8.4 Hz) of the structure are set to be equal the first (f_1), second (f_2), and third (f_3) natural frequencies of the soil layer, respectively.

The wave parameter ($w.p$) (Veletsos et al. 1974):

$$w.p = \frac{V_s}{f_{st.fixed}.H_{st}} \tag{6.4}$$

which is may be looked upon as a measure of the relative stiffness of the soil and the structure. When V_s and H_{st} are selected to be constants and equal to 200 m/s^2 and 10 m, respectively, ($w.p$) is inversely proportional to $f_{st.fixed}$. $1/w.p$ is equal to 0.083, 0.25, and 0.42 corresponding to $f_{st,\ fixed}$ = 1.67, 5.0, and 8.4 Hz, respectively.

6.4 Verification of the Finite Element Model

To assess the accuracy of the FE model used in this study, free field amplification, kinematic soil-pile interaction, kinematic bending moments, and the dynamic characteristics of the coupled

system were compared with those found using other established approaches. Verification has been performed in the frequency domain assuming elasto-dynamic behavior of the soil. Sample seismic signal is imposed at very low amplitude to ensure linear-elastic soil behavior.

6.4.1 Free field motion

Free-field displacements are motions of the soil that occur at a distance from the pile such that they are not affected by the presence of the pile or that would have occurred if the pile were not present (Byrne et al. 1984). Elastic response time histories for free-field were derived at different frequencies of excitations (0.5-10.5 Hz). From these time histories, the amplitude of steady-state response is noted and normalized with respect to the amplitude of input bedrock motion. Thus amplification of soil stratum is derived at different frequencies and compared with other approaches available in literature. In Fig. 6.3, amplification of the soil stratum obtained using the present 2D FE method is compared with that obtained using a simple 1D free-field analysis (in the frequency domain, Gazetas 1984) at different frequencies of excitation. Amplification for 1D analysis is given by:

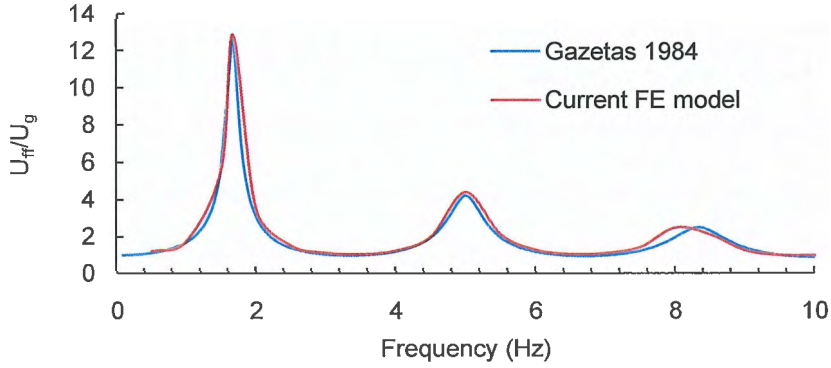

Fig. 6.3 Verification of the free-field amplification

$$\frac{U_{ff}}{U_g} = \frac{1}{\cos(qL)} \tag{6.5}$$

where

$$q = \frac{2\pi f}{V_s\sqrt{(1+2i\beta_s)}} \tag{6.6}$$

where L = height of soil stratum; f = frequency of excitation; V_s = S-wave velocity; β_s = hysteretic damping ratio; U_g and U_{ff} = amplitude of input bedrock displacement and free-field ground displacement, respectively. The comparison shows that there is an excellent agreement between the current FE method and free-field analysis conducted by Gazetas 1984 for all frequencies range covered in Fig. 6.3.

6.4.2 Kinematic soil-pile analysis

A seismic S-wave propagating vertically in a soil layer without any foundation causes only horizontal displacements in the free-field soil. A cylindrical pile tends to diffract the incident seismic waves, modifying the free-field soil motion, so that the horizontal displacement of the pile-head, U_p, will be different from the free-field surface motion U_{ff}, and a rotation ϕ_p of the pile-head will take place. This type of interaction between piles and soils is called kinematic interaction. This kinematic effect is usually assessed in terms of the kinematic interaction factors I_u and I_ϕ which are defined, respectively, as the maximum translation and rotation of the pile head normalized by the corresponding maximum displacement of the free field soil surface as:

$$I_u = \frac{U_p}{U_{ff}} \tag{6.7}$$

and

$$I_\varphi = \frac{\varphi_p \cdot D_p}{U_{ff}} \tag{6.8}$$

The kinematic interaction factors obtained by this study were compared to established results from the literature (Rovithis et al. 2009 and Fan et al. 1991). Both fixed and free conditions at pile head were considered.

The analytical solution for I_u is given by the expression (Markis and Gazetas 1992):

$$I_u = \Gamma = \frac{k + iwc}{E_p I_p (q^4 + 4\lambda^4)} \tag{6.9}$$

this was obtained through a properly calibrated dynamic Winkler model. The corresponding kinematic interaction factors for a free head pile are (Nikolaou et al. 2001):

$$I_u = \Gamma \left[1 + \frac{1}{2} \left(\frac{q}{\lambda} \right)^2 \right] \tag{6.10}$$

and

$$I_\varphi = \Gamma \frac{q^2 D_p}{\lambda} \tag{6.11}$$

in the above equations, $(k+iwc)$ denotes the so-called dynamic impedance of the Winkler bed, with k being the dynamic stiffness, c being the radiation damping, $w = 2\pi f$ being the cyclic vibrational frequency and i the imaginary unity; $q = w/V_s$ is the wave number of the harmonic SH waves in the soil; λ is the well-known Winkler wave number:

$$\lambda = \left\{ \frac{k + iwc - mw^2}{4E_p I_p} \right\}^{\frac{1}{4}} \tag{6.12}$$

Based on the comparative results shown in Fig. 6.4 that shows the variation of kinematic interaction factors with the normalized frequency:

$$a_0 = w^* D_p / V_s \tag{6.13}$$

It is established that the adopted FE model captures well the variation of kinematic pile response in wide range of frequency.

6.4.3 Kinematic pile bending moment

The verification process continues to include the kinematic pile bending moment arising from the passage of seismic waves through soil layer. As well known in linear analysis, all computed stress and strain quantities are proportional to the excitation intensity, expressed by the amplitude

of the bedrock acceleration $\ddot{U}_g = w^2 U_g$. The pile bending moments were normalized to the amplitude of bedrock acceleration (Kavvadas and Gazetas 1993, Rovithis et al. 2009):

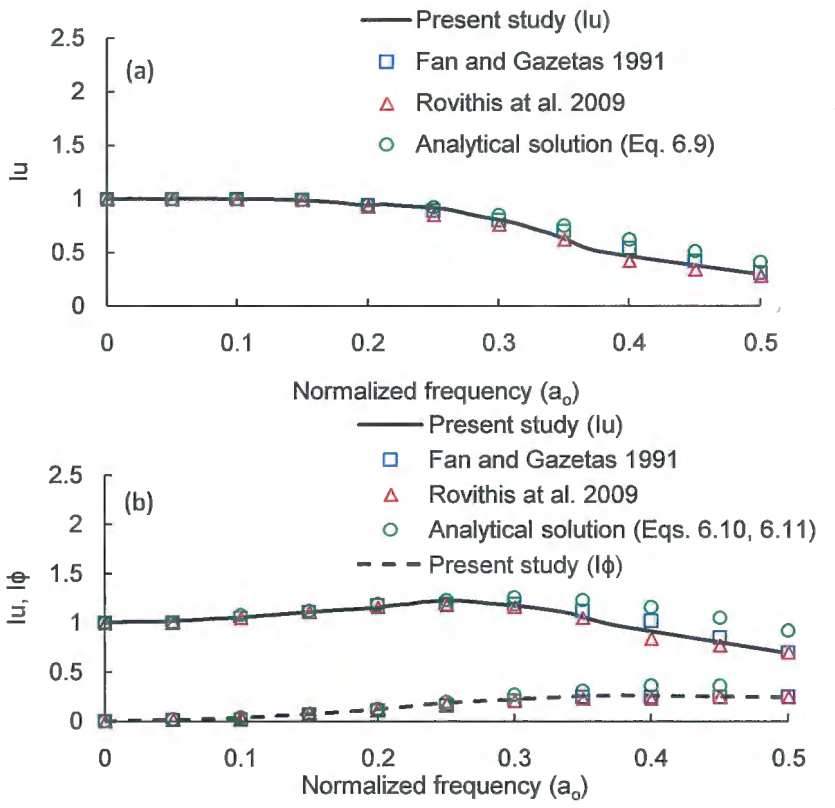

Fig. 6.4 Kinematic soil-pile interaction for: (a) fixed head and (b) free head conditions

$$M_{nor} = \frac{M}{\rho_p D_p^4 \ddot{U}_g} \tag{6.14}$$

Figure 6.5 presents the distribution of amplitudes of normalized steady state bending moments for the free and fixed pile head conditions at the first three fundamental frequencies of the soil deposit f_1, f_2 and f_3 calculated using the present FE method compared to those obtained by 3D FE analysis by Rovithis et al. (2009) with the same soil and pile conditions. Figure 6.5. implies that the current FE analysis reasonably reproduced normalized pile bending moment agree well previous established ones by Rovithis et al. (2009) for different fundamental frequencies of the soil.

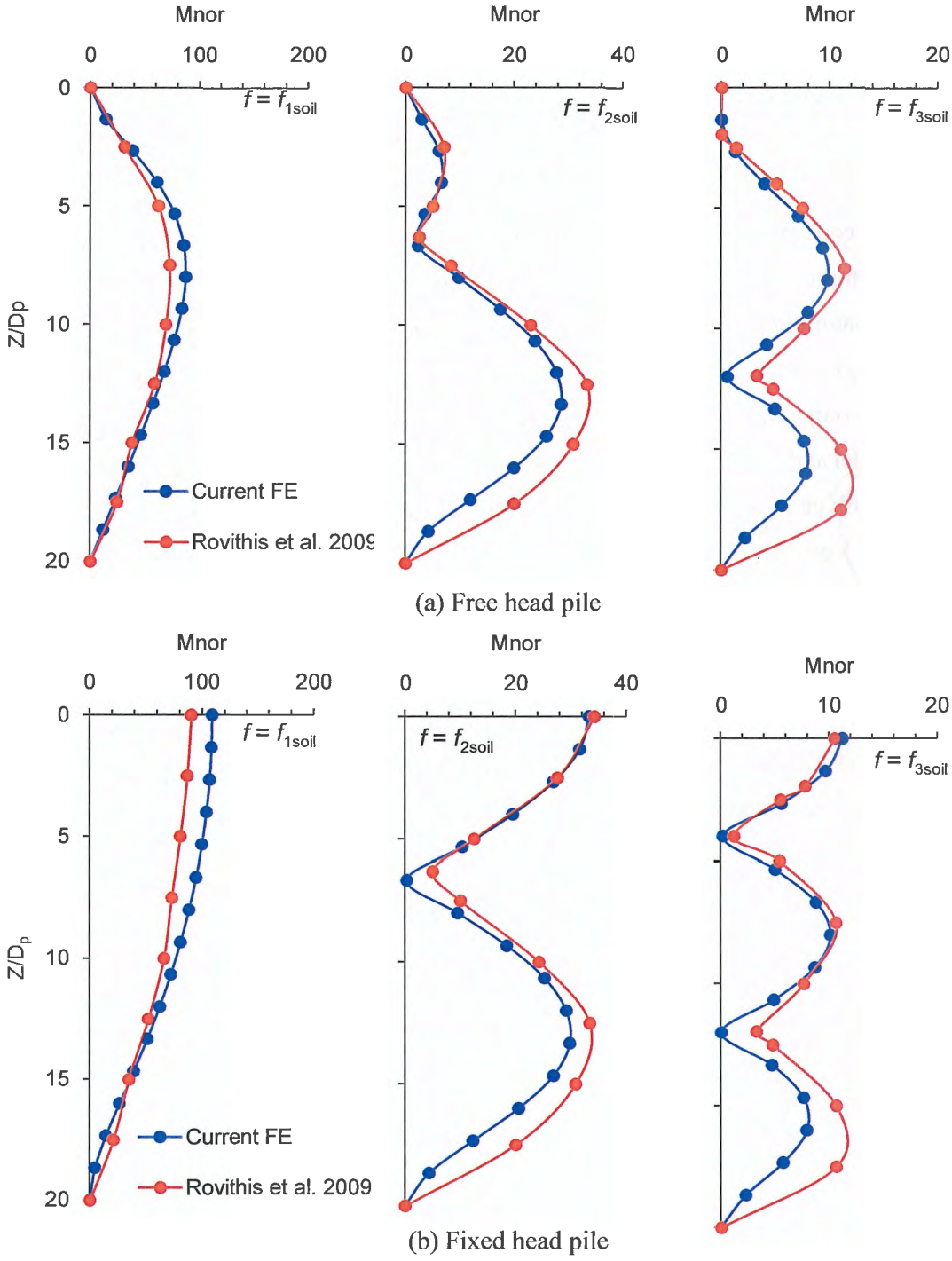

Fig. 6.5 Verification of normalized steady state bending moments at the first three fundamental frequencies of the soil deposits: (a) free head pile; (b) fixed head pile

Figure 6.6(a) and (b) shows the pile and ground deformations corresponding to normalized bending moments presented in Fig. 6.5(a) and (b), respectively , obtained using tje current FE model and at the first three fundamental frequencies of the soil deposits.

6.4.4 Dynamic characteristics of the coupled SPS system

In this step, a concentrated mass attached to the structural column is introduced to the model. The verification process in this stage focuses on evaluating the effective natural frequency (f_{SSI}). The effective natural frequency (f_{SSI}) of the coupled system is defined as the frequency at which the ratio (U_s/U_{ff}) is maximized, where U_s is the structure mass displacement. Verification was performed by comparing the effective natural period of the system (T_{SSI}) calculated using the current FE model at different values of parameter $1/w.p$ with the available analytical solutions as well as the 3D FE analysis by Rovithis et al.(2009). The available analytical procedures include:

1. Solution by Veletsos and Meek (1974):

$$T_{SSI} = T_{st,fixed}\sqrt{1+\frac{K_{str}}{K_x}\left(1+\frac{K_x H_{str}^2}{K_\theta}\right)} \tag{6.15}$$

where $T_{st,fixed}$ and K_{st} represent the fixed-base natural period and stiffness of the structure. K_x and K_θ denote the frequency-dependent foundation stiffness in translational and rocking oscillations, respectively.

2. Rigorous analytical solution by Maravas et al.(2007):

$$T_{SSI} = T_{st,fixed}\sqrt{\frac{K_{str}}{K_x}\left(\frac{1+4\zeta^2}{1+4\zeta_x^2}\right)+\frac{K_{str}H_{str}^2}{K_\theta}\left(\frac{1+4\zeta^2}{1+4\zeta_\theta^2}\right)+\left(\frac{1+4\zeta^2}{1+4\zeta_{str}^2}\right)} \tag{6.16}$$

where ζ_{str} and ζ represent the damping ratio of the fixed-base and flexibly supported structure, respectively, and ζ_x, ζ_θ the damping ratios in swaying and rocking of the foundation.

Comparison of the current FE model results against the aforementioned equations as well as the results obtained by Rovithis et al. (2009) is illustrated in Fig. 6.7. Figure 6.7 presents the ratio of the effective natural frequency of the system to the natural frequency of the fixed-base structure ($f_{SSI}/f_{str.,fixed}$) against the parameter ($1/w.p$). A very good agreement between the

numerical results and both the rigorous analytical solution of Maravas et al. (2007) and the 3D analysis of Rovithis et al. (2009) is evident confirming the accuracy of the FE model.

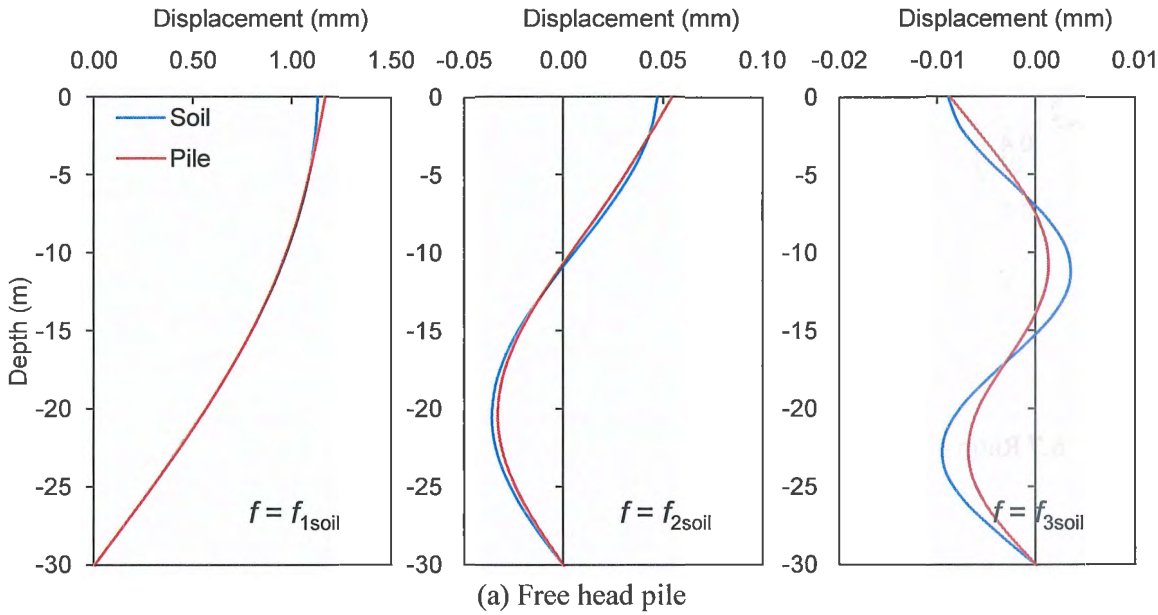

(a) Free head pile

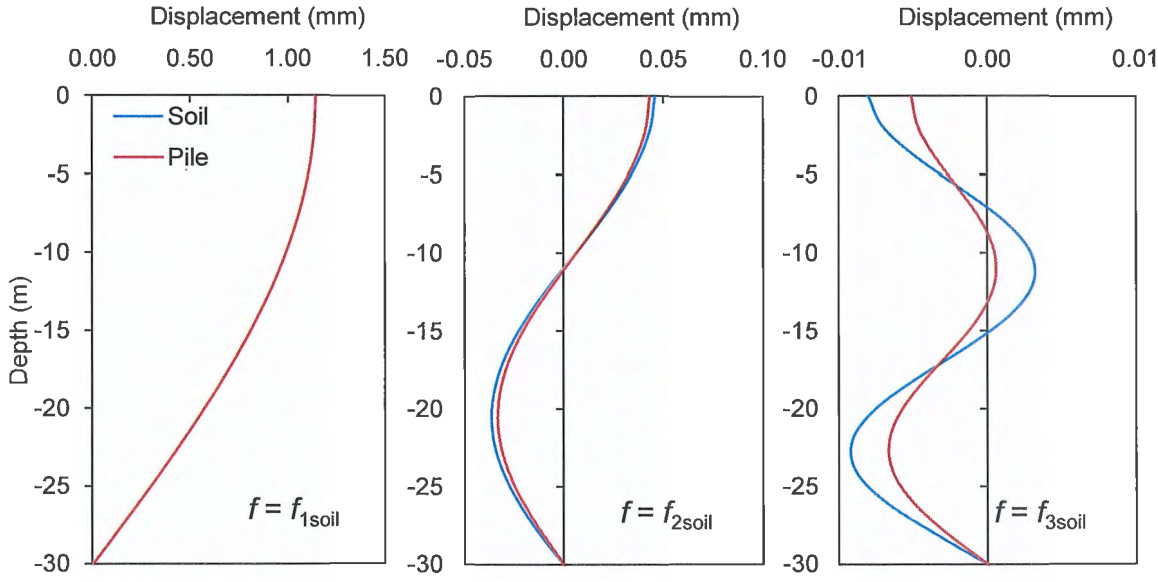

(b) Fixed head pile

Fig. 6.6 Horizontal displacements of the pile and the ground at the first three fundamental frequencies of the soil deposits: (a) free head pile; (b) fixed head pile

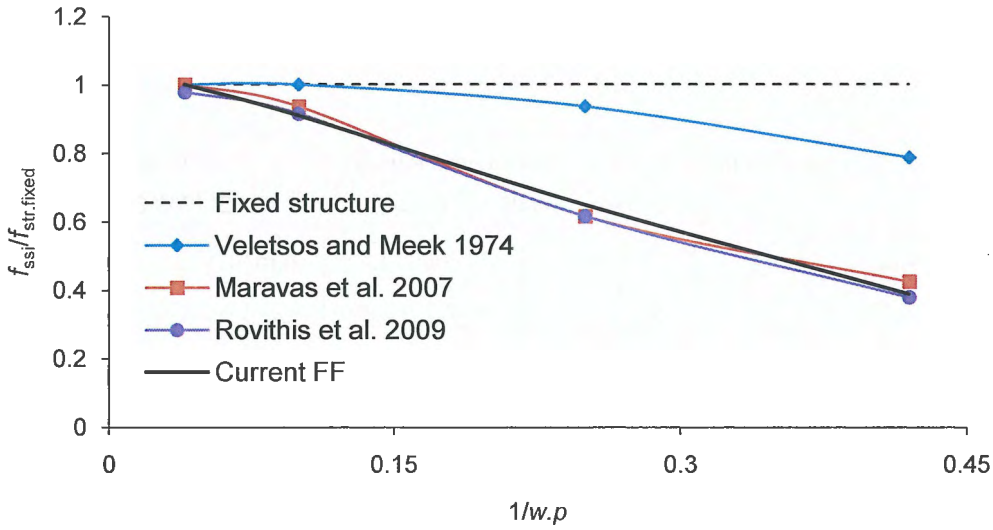

Fig. 6.7 Ratio of the effective natural frequency of the system to the structural fixed-base frequency against parameter $1/w.p$

Figure 6.8(a) shows the amplification ratios obtained from the current FE analysis of the coupled system, while Fig. 6.8(b) shows the corresponding ratios obtained from the 3D FE analysis by of Rovithis et al. (2009). Fig. 6.8 declares that not only the current FE model is successful in predicting the effective natural frequency (f_{SSI}), but it also predicts the pseudo-natural frequency (f_{pSSI}) very well. It should be noted from Figs. 6.8(a) and (b) that the pseudo-natural frequency (f_{pSSI}) is higher than the conventional effective natural frequency (f_{SSI}) of the system.

Based on Figs. 6.8(a) and (b), it is obvious that the current FE model is capable of predicting the fundamental frequencies that dominate the system response. It is observed that pile-head motion is substantially amplified at the effective natural frequency (f_{SSI}), where the response of the pile-structure system is maximized. It can also be seen that at the pseudo-natural frequency (f_{pSSI}) of the system, a significant de-amplification of pile-head motion occurs. Consequently, the pseudo-natural frequency possesses a double role: First, it defines the frequency where the motion of the superstructure is maximized relative to the translational motion of the pile head (i.e., U_s/U_p = max). Second, it is the frequency where the pile-head motion is minimized relative to the free field soil surface motion (i.e., U_p/U_{ff} = min).

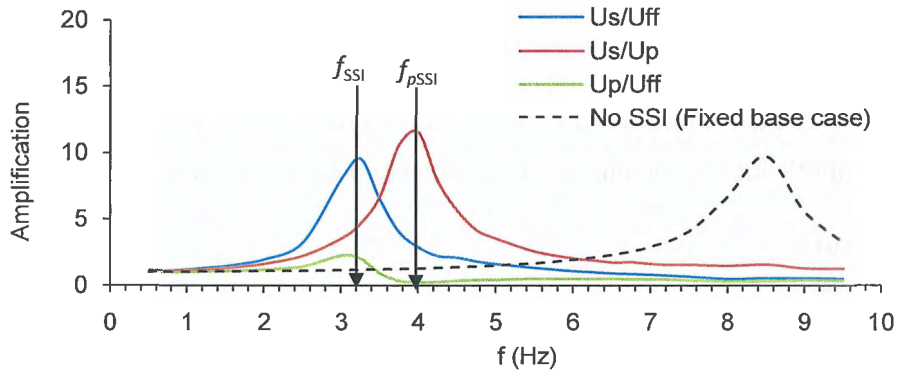

(a)

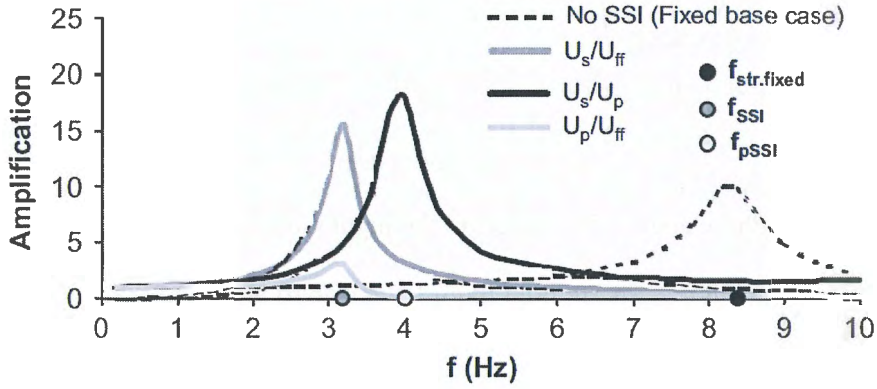

(b)

Fig. 6.8 Amplification ratios obtained from the analysis of the coupled system: (a) current FE; (b) Rovithis et al. (2009)

In order to investigate the physical meaning of this significant de-amplification, pile response is correlated with superstructure response in term of the phase angle with respect to the input motion at the bedrock level, as shown in Fig. 6.9. In addition to pile head, structure, and free field, phase angles of displacements of additional points on the pile (at depths of 2 and 4 m from ground surface) and column (at a height of 2 m) are given for comparison. The effect of inertial interaction on the phase angle of the pile-head motion is evident close to the frequencies (f_{SSI}) and (f_{pSSI}), it can be noticed that the pile head follows the superstructure motion until frequency reaches the effective natural frequency (f_{SSI}). At this particular frequency, the phase angle of the pile starts to deviate from that of the superstructure. When the frequency becomes

equal to the pseudo natural frequency (f_{pSSI}) of the system, the pile starts moving in the direction opposite to that of the superstructure. This implies that at the pseudo-natural frequency of the system, the superstructure movement has a restraining effect on the pile motion, justifying the significant de-amplification of the pile-head movement relative to the free field.

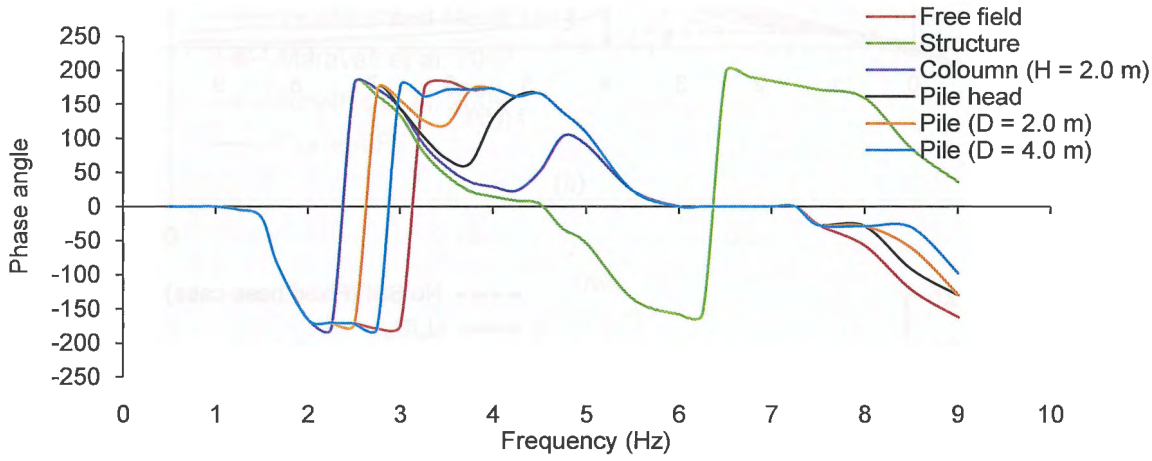

Fig. 6.9 Phase angle with respect to the input motion at bedrock level.

6.5 Effect of Soil Profile and Soil Nonlinearity

The effects of soil profile and material nonlinearity of the soil are a major concern. It is anticipated that the soil stratum plays a significant role in the response of the SSPSI system.

6.5.1 Effect on free-field response

The effect of soil profile on the free-field response is studied by changing the value of parameter m_G to be zero in Eq. (6.2) as stated earlier. The effect of nonlinearity of soil is also studied by changing the amplitude of the input acceleration (A). Figure 6.10 compares the variation of the free-field amplification with respect to bed rock motion versus frequencies of the input motion. The second and the third natural shear frequencies of the soil layer get closer to the first natural shear frequency as the soil shear modulus distribution with depth become not uniform (inhomogeneous), in agreement with the results obtained by Gazetas 1984. A substantial increase is observed in the peak amplification at the first, the second, and the third natural frequencies as the soil become inhomogeneous. Figure 6.10 shows also the fundamental periods lengthening

due to soil nonlinearity and the substantial reduction in the peak amplification accompanied with these periods lengthening.

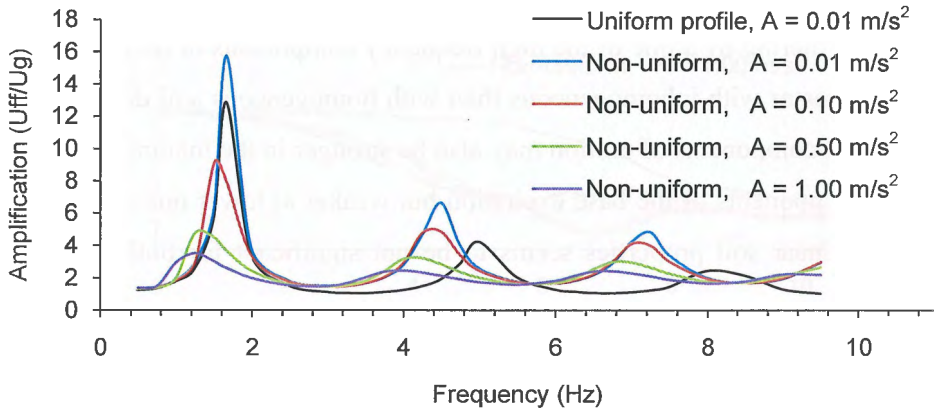

Fig. 6.10 Influence of soil profile and soil non-linearity on the free-field response

The strain level of the soil might be different with the change of the frequency of the input motion, even if the peak acceleration was constant. Figure 6.11 shows the variation of the shear strain of the ground with the frequency of input motions at constant values of the amplitude of input accelerations. As expected, a substantial increase is observed in the peak amplification of soil shear strain at the first, the second, and the third natural frequencies with the increase of the amplitude of the input motion.

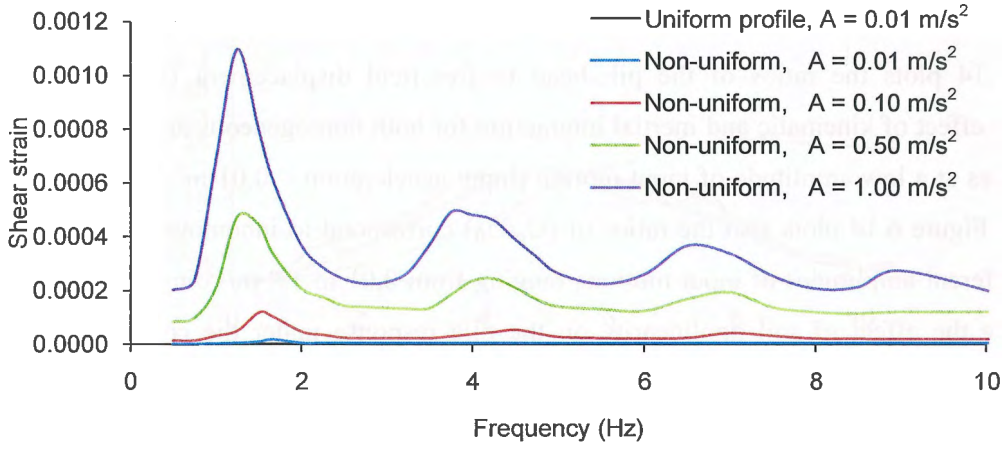

Fig. 6.11 Shear strain variation with frequency and amplitude of input motion.

6.5.2 Effect on kinematic soil-pile interaction

The influence of soil profile on kinematic interaction factors for both fixed and free-head conditions is portrayed in Fig. 6.12. Figure 6.12 declare that, in the frequency range studied (f = 0.5-10.5 Hz), the filtering by a pile of the high frequency components of the base excitation may be substantially greater with inhomogeneous than with homogeneous soil deposits. At the same time, the rotational components of motion may also be stronger in the inhomogeneous deposits at high frequency components of the base excitation but weaker at lower ones. On the other hand, the effect of nonlinear soil properties seems to be not significant for both interaction factors components.

6.5.3 Effect on the coupled soil-pile-structure interaction

The effect of soil profile on the effective natural frequency of a coupled soil-pile-structure system ($1/w.p$ = 0.42) is shown in Fig. 6.13. The fixed base fundamental frequency of the structure is also plotted as a reference. Figure 6.13 shows the strong effect on soil-pile-structure interaction resulting in a significant reduction of f_{SSI} with respect to the natural frequency of the structure under fixed base conditions. Figure 6.13 also illustrates a reduction in f_{SSI} corresponding to the change in soil profile from homogeneous to inhomogeneous soil profile. A reduction in f_{SSI} due to soil nonlinearity associated with substantial decrease in the peak amplification could be observed from Fig. 6.13.

6.5.4 Effect on the combined kinematic and inertial pile response.

Figure 6.14 plots the ratios of the pile-head to free-field displacement (U_p/U_{ff}) under the combined effect of kinematic and inertial interaction for both homogeneous and inhomogeneous soil profiles at a low amplitude of input motion (input acceleration = 0.01 m/s^2) to ensure linear behavior. Figure 6.14 plots also the ratios of (U_p/U_{ff}) correspond to inhomogeneous soil profile and at different amplitudes of input motions ranging from 0.01 to 1.0 m/s^2 input acceleration to investigate the effect of soil nonlinearity on the pile response under the combined action of kinematic and inertial interactions. It is worth to note that at least for all cases included in Fig. 6.14, the ratio U_p/U_{ff} seems to be dominated by two discrete frequencies: a lower frequency where the pile-head motion is amplified and a higher one where the response is suddenly de-amplified with respect to free-field motion.

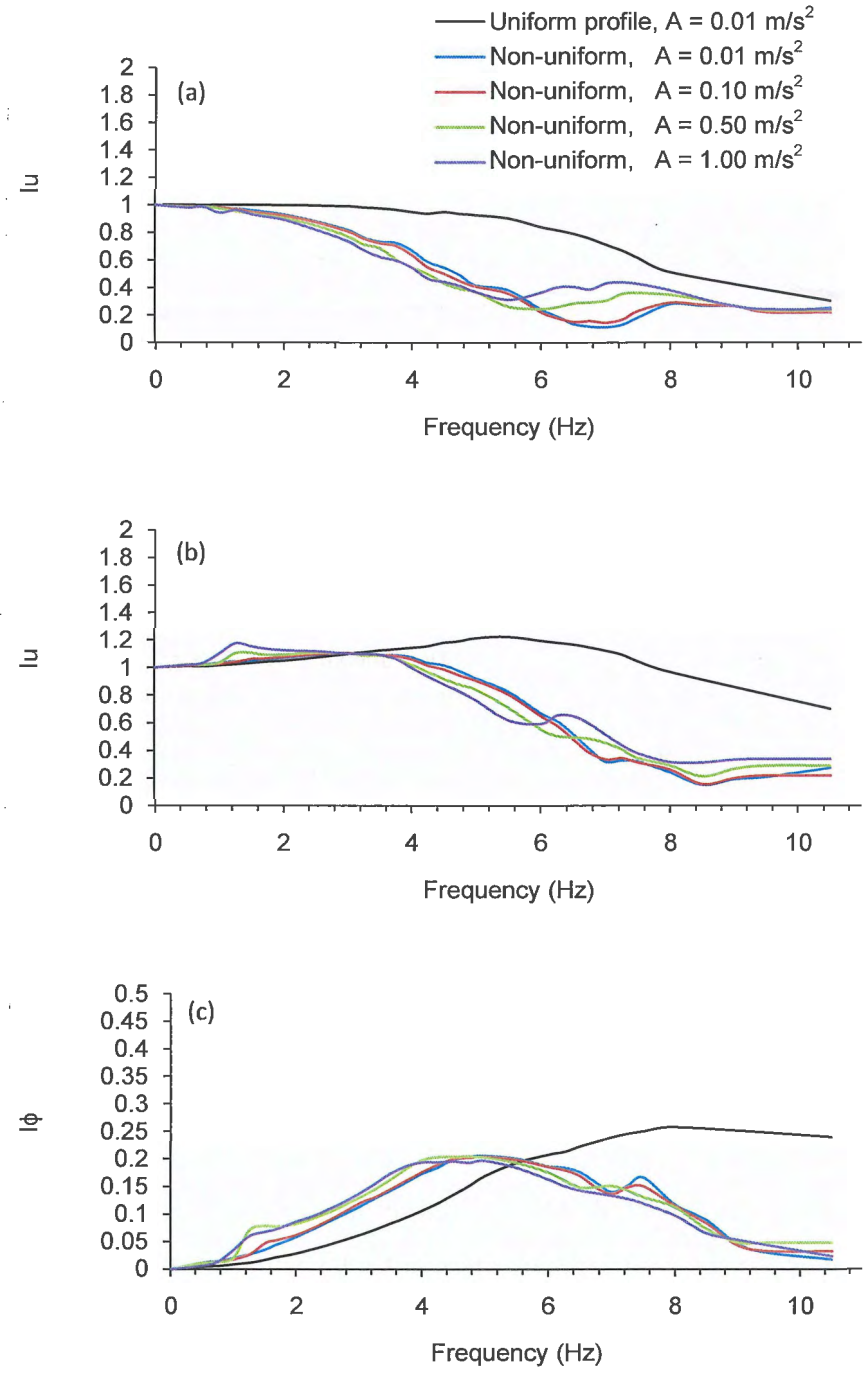

Fig. 6.12 Effect on the interaction factors: (a) I_u (Fixed head); (b) I_u (free head); and (c) I_ϕ (free head)

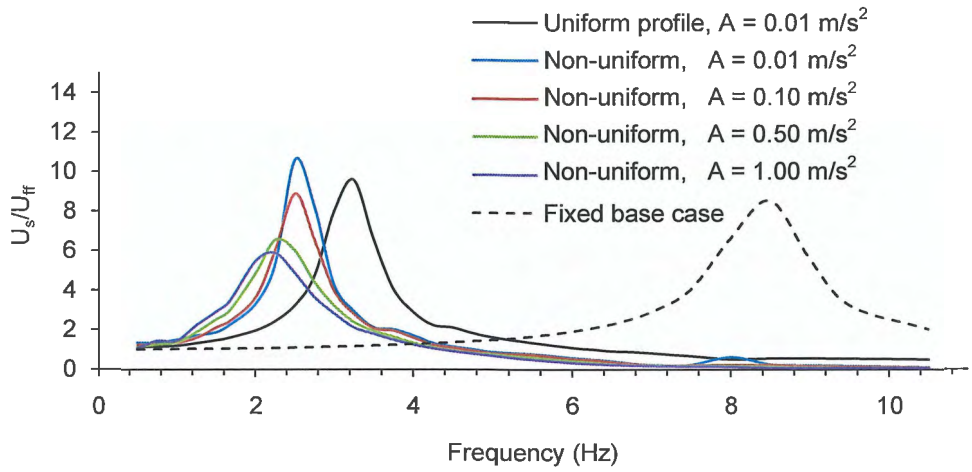

Fig. 6.13 Effect on effective natural frequency (f_{SSI}) of the soil-pile-structure system: $1/w.p = 0.42$

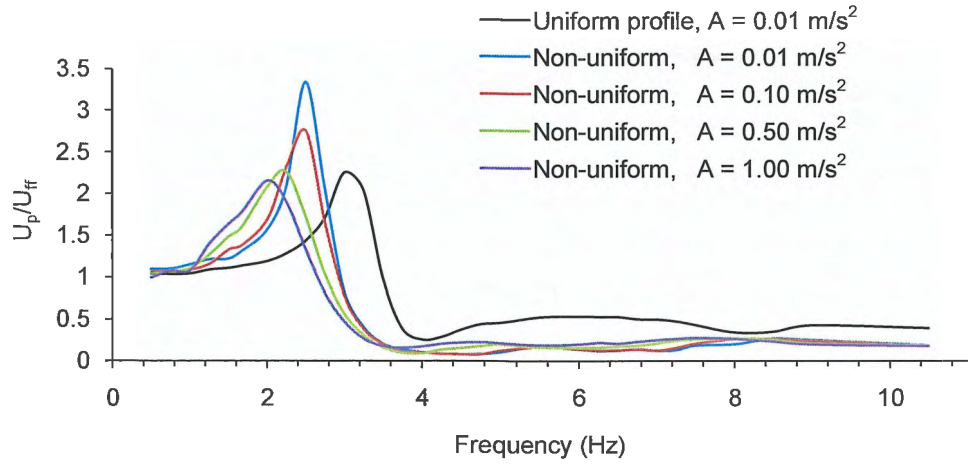

Fig. 6.14 Effect on pile-head to free-field displacement response of the coupled system

As observed by Rovithis et al. 2009, pile-head motion is substantially amplified at the effective natural frequency f_{SSI}, where the response of the pile-structure system is maximized. A pseudo-natural frequency (f_{pSSI}) is introduced by Rovithis et al. 2009 (using linear 3D FE analysis) as the frequency where the pile-head motion is minimized relative to the free-field soil surface motion. As shown in Fig. 6.14 there is some reduction in f_{pSSI} as the soil become inhomogeneous. In contrast to the clear effect of soil nonlinearity on f_{SSI}, f_{pSSI} seems to be not affected by soil nonlinearity.

6.6 Conclusions

Applicability of the simplified FE model, proposed by Ozutsumi et al. (2003), to the analysis of SSPSI in the frequency domain is examined. The verification process has been executed assuming elasto-dynamic behavior of the soil and comparing the results obtained using the simplified FE model with those found using other established results from the literature. Based on the comparative results in the paper, it is established that It has been shown that this procedure can be used successfully for a provision of the response of a single pile to inertial loading caused by the lateral forces imposed on the over structure and kinematic loading caused by the soil developed during an earthquake. In addition, the effects of soil profile and material nonlinearity of the soil on the kinematic and inertial interaction as affected by the frequency content of input motion are parametrically investigated and the following conclusions can be drawn from this study:

1. Kinematic soil-pile interaction: the filtering of pile to the high frequency components of the base excitation is substantially greater with inhomogeneous than with homogeneous soil deposits. On the other hand the effect of nonlinear soil behavior seems to be not significant.
2. Combiend kinematic and inertial interaction: a significant reduction in f_{SSI} due to soil inhomogeneity as well as soil nonlineartiy.
3. In contrast to the clear effect of soil nonlinearity on f_{SSI}, f_{pSSI} seems to be not affected by it.

References

1. Allotey, N. and El Naggar, M.H. (2008), "Generalized dynamic Winkler model for nonlinear soil-structure interaction analysis," *Canadian Geotechnical Journal*, 45(4), 560-573.
2. Blaney, G., Kausel, E., Roesset, J.,(1976) Dynamic stiffness of piles, *Proc. 2nd Intl. Conf. on Numerical Methods in Geomechanics, Blacksburg*, 1001-1012, 1976.
3. Byrne, P., Anderson, D., and Janzen, W. _1984_. "Response of piles and casings to horizontal free-field soil displacements." Can. Geotech. J., 21(4), 720–725.
4. Cai, Y., Gould, P., Desai, C. (1995), "Numerical implementation of a 3-D nonlinear seismic S-P-S-I methodology, in Seismic Analysis and Design for Soil-Pile-Structure Interactions, *Geotechnical Special Publication*, 70, ASCE, 96-110.
5. Fan, K and Gazetas, G. (1991) Seismic response of single piles and pile groups, Technical Report NCEER-91-0003.

6. Fan, K., Gazetas, G., Kaynia, A., Kausel, E., Ahmad, S. (1991), "Kinematic seismic response of single piles and pile groups," *Journal of Geotechnical Engineering*, 117(12), 557–74.
7. Gazetas, G. (1984), "Seismic response of end bearing single piles," Soil Dynamics and Earthquake Engineering, 3(2), 82–93.
8. Guin, J. and Banerjee, P. K., (1998) Coupled soil-pile-structure interaction analysis under seismic excitation. *Journal of Structural Engineering*, 124(4), 434–444.
9. Iai, S., Matsunaga, Y., Kameoka, T. (1992), "Strain space plasticity model for cyclic mobility," *Soils and Foundations*, 32(2), 1–15, 1992.
10. Kagawa, T. and Kraft, L. (1980), "Seismic P-Y responses of flexible piles," *Journal of Geotechnical Engineering*, ASCE, 106(8), 899-918.
11. Kattis, S.E., Polyzos, D., Beskos, D.E. (1999), "Vibration isolation by a row of piles using a 3-D frequency domain BEM," *International Journal for Numerical Methods in Engineering*, 64, 713-728.
12. Kaynia, A. M. and Mahzooni, S. (1996), "Forces in pile foundations under seismic loading," *Journal of Engineering Mechanics*, 122(1), 46–53.
13. Kavvadas, M., Gazetas, G. (1993) Kinematic seismic response and bending of free-head piles in layered soil. *Geotechnique*, 43(2), 207-22
14. Kramer, S.L.,(1996) *Geotechnical earthquake engineering*. Prentice Hall inc. Englewood Cliffs, N.J.
15. Maravas, A., Mylonakis, G. and Karabalis, D., (2007) Dynamic characteristics of simple structures on piles and footings. *In: Proceedings of the 4th international conference on earthquake geotechnical engineering.* Thessaloniki, Greece, paper no. 1672.
16. Markis, N. and Gazetas, G., (1992) Dynamic pile-soil-pile interaction, part II: Lateral and seismic response. *Earthquake Engineering and Soil Dynamics*, 20(2), 145–62.
17. Mylonakis, G., Nikolaou, A. and Gazetas, G. (1997) Soil-pile-bridge seismic interaction: kinematic and inertial effects. PartI : Soft soil. *Earthquake Engineering and Structural Dynamics*; 26 : 337 – 59.
18. Nikolaou, S., Mylonakis, G., Gazetas, G. and Tozoh, T., (2001) Kinematic pile bending during earthquakes: analysis and field measurements. *Geotechnique*, 51(5), 425–40.
19. Ozutsumi, O., Tamari, Y., Oka, Y., Ichii, K., Iai, S., Umeki, Y. (2003) "Modeling of soil–pile interaction subjected to soil liquefaction in plane strain analysis," *Proc. of the 38th Japan National Conference on Geotechnical Engineering*, Akita, 1899–1900.
20. Padrón, J.A., Aznárez, J.J., Maeso, O. (2007), "BEM–FEM coupling model for the dynamic analysis of piles and pile groups," *Engineering Analysis with Boundary Elements*, 31(6), 473-484.
21. Pender, M. and Pranjoto, S.,(1996) Gapping effects during cyclic lateral loading of piles in clay, *Proc. 11th World Conf. Earthquake Eng., Acapulco,* Paper No. 1007.

22. Rovithis, E.N., Pitilakis, K.D., Mylonakis, G.E. (2009), "Seismic analysis of coupled soil-pile-structure systems leading to the definition of a pseudo-natural SSI frequency," *Soil Dynamics and Earthquake Engineering*, 29(6), 1005-1015.
23. Veletsos, A.S. and Meek, J.W., (1974) Dynamic behavior of building-foundation systems. *Earthquake Engineering and Structural Dynamics*, 3, 121–38.
24. Zienkiewicz, O., Bicanic, N. and Shen, F., (1988) Earthquake input definition and the transmitting boundary conditions. In Doltsinis, I. S., editor, *Advances in Computational Nonlinear Mechanics*, Springer-Verlag, 109–138.

CHAPTER 7

Centrifuge Model Tests and Analyses of Nonlinear Seismic Response of Soil-Pile-Structure System

Contents

7.1 Introduction

The lack of well-documented and well-instrumented full-scale case history data and post-earthquake investigations of pile failures inhibits the further progress in the research field of seismic pile behavior, but it motivates researchers to perform physical modeling through centrifuge and shaking table model tests as an alternative technique to augment the field case histories with laboratory data obtained under controlled conditions. The results of these tests provide a good basis for calibration and validation of the available analytical methods developed for SSPSI problems. In this chapter, nonlinear seismic analyses using the 2D FE model adopting the proposed soil-pile spring proposed by Ozutsumi et al. (2003) and described in details in the previous chapter are compared to the results of shaking table centrifuge model tests of pile-supported structures in a dense sand profile over rigid rock. The model is shaken using sinusoidal accelerations with different amplitudes and different frequencies. A schematic view of the system under investigation is shown in Fig. 7.1. In the next sections, the principles of centrifuge modeling centrifuge facilities at Kyoto University, centrifuge test procedure, and FE models are described in detail. Then the results of the FE and centrifuge models are compared in terms of time histories of soil and structural responses. The test results of centrifuge are presented in terms of prototype unless otherwise stated.

7.2 Centrifuge Tests

In geotechnical centrifuge tests a model is rotated in a centrifuge device at a constant radius r around the central axis and thereby subjected to an outwards acceleration of $a = r\omega^2$ where ω is the eigen angular frequency of the rotation. Adjusting ω, the model can be exposed to a multiple of the gravitational acceleration whereby the self-weight of the soil proportionally increases. That is to say in a centrifuge the effective stress levels in the prototype can be actually modeled and unlike in 1 g tests the stress-strain behavior under high stresses can be directly observed. To do so, it is assumed that the model in a centrifuge behaves in the same way it would behave in an equivalent field of multiple gravity and that a model in an acceleration field of "N" times gravitational acceleration actually behaves similar to a prototype "N" times larger than the model (Tan and Scott 1985). The scaling law for the centrifuge tests for N g is summarized in Table 7.1. For additional information pertaining to centrifuge mechanics, the reader is referred to the

20th Rankine Lecture by Schofied (1980), which provides a detailed discussion of centrifuge testing principles.

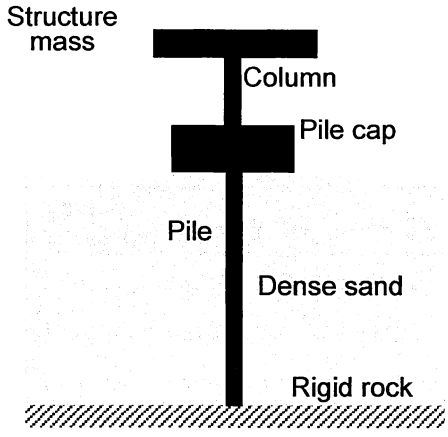

Fig. 7.1 A schematic view of the soil-pile-structure system under investigation

7.2.1 Centrifuge facility at Disaster Prevention Research Institute, Kyoto University

The author carried out all the centrifuge experiments described in this thesis, at the Disaster Prevention Research Institute, Kyoto University (DPRI-KU). The model is scaled down to 1/40. Thus, all model tests were carried out in the centrifugal acceleration field of 40 g (Table 7.1). A functional scheme of the centrifuge facility is given in Fig. 7.2. The centrifuge has an effective radius of 2.5 m. The rated experimental capacity is 24 g-tons with a maximum attainable centrifugal acceleration of 200 g, and the maximum model mass of 200 kg. The centrifuge model is normally prepared outside the centrifuge pit, and then transferred to the swinging platform (numbered 2 in Fig. 7.2) and mounted on the centrifuge using a crane. A motor (7) drives the rotating arm (1) through the shaft and bevel gear (8). The swinging platforms swing outwards and upwards as the centrifuge arm gains speed, so that the direction of the resultant acceleration field passes through the pivot and the centroid of the package. To compensate the unbalance emerging from the weight of the model placed on the platform, an equivalent platform swings on the opposite arm which can be loaded with an equivalent weight (3). A shake table driven unidirectionally by a servo hydraulic actuator is attached to a platform and it is controlled through a personal computer (PC) (6) on the centrifuge arm. It is fixed near to the axis to minimize the centrifugal force acting on the computer. All the equipment necessary for shake table control is put together on the arm. The PC is accessible during flight from a PC (12) in the

control room through wireless LAN and "Remote Desktop Environment". A second wireless LAN system connects the data loggers (5) with another PC (11) in the control room so the time response of the installed sensors can be monitored during flight. The shake table has the capacity of 15 kN, 10 g and ± 2.5 mm in maximum force, acceleration and displacement, respectively.

Table 7.1 Scaling law for centrifuge tests for N g

Quantity	Scaling Factor (prototype/model)
Length	N
Density	1
Time	N
Frequency	1/N
Acceleration	1/N
Velocity	1
Displacement	N
Stress	1
Strain	1
Stiffness	1
Pore pressure	1
Permeability	N
Bending moment	N^3
Shear force	N^2
Flexural rigidity	N^4
Viscosity of pore fluid	1/N

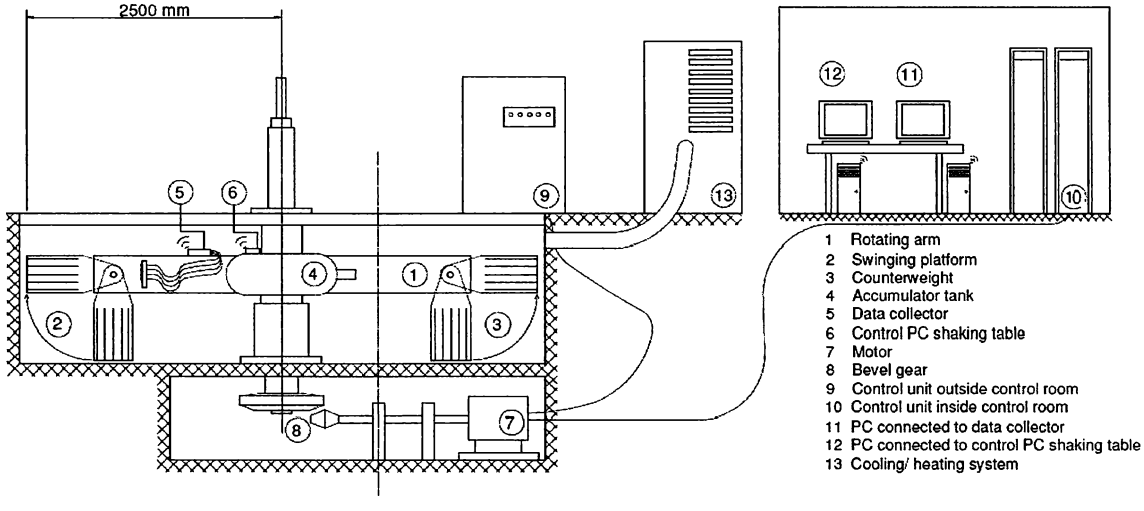

Fig. 7.2 Schematic view for centrifuge facility at the Disaster Prevention Research Institute, Kyoto University (DPRI-Ku)

7.2.2 Material properties and tests procedures

All tests were carried out in the centrifugal acceleration field of 40 g using a rigid soil container with inner dimensions of 0.45 m (L) × 0.15 m (W) × 0.29 m (H).

7.2.2.1 Material properties

Dry sand

The model ground in this study was made of Silica sand No. 7 having the physical and mechanical properties shown in Table 7.2 and the particle size distribution curve shown in Fig. 7.3. The soil is classified as "poorly graded sand (SP)". This sand is an industrial material so that consistency of the material properties throughout all models can be assured.

Table 7.2 Physical properties of Silica sand No. 7

e_{max}	e_{min}	D_{50} (mm)	U_c	G_s
1.19	0.71	0.13	1.875	2.66

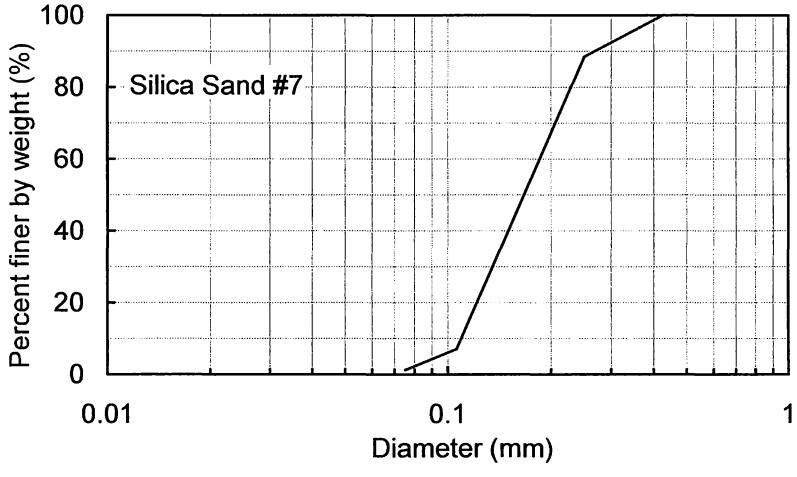

Fig. 7.3 Particle size distribution curve for Silica sand No. 7

Coupled pile-structure model

Assembly drawing and dimensions of the experimental apparatus of the coupled pile-structure model used in this study is given in Appendix B1. The tested steel model consists of a single pile

supporting a simple structure consisted of a pile cap, a column, and a superstructure mass as shown in Figs. 7.1.

Material properties of the model pile, pile cap, column, and superstructure mass used in this study are shown in Table 7.3, Table 7.4, Table 7.5, and Table 7.6 respectively. For the pile cap and the superstructure mass, the centrifuge scaling relations were applied based on mass and stiffness.

Table 7.3 Properties of pile modeling

	Steel tube		
	Model scale	Prototype scale	Units
Length	0.29	11.6	m
Outer diameter	10	400	mm
Wall thickness	0.75	30	mm
Young's modulus	206	206	GPa
2nd moment of inertia	2.35×10^{2}	6.00×10^{8}	mm^4
Bending stiffness	48.41	1.24×10^{8}	$MN\text{-}mm^2$

Table 7.4 Properties of pile cap modeling

	Steel plate		
	Model scale	Prototype scale	Units
Side length	40	1600	mm
Thickness	30	1200	mm
Mass	0.3792	24269	Kg
2nd moment of inertia	9.0×10^{4}	2.30×10^{11}	mm^4
Bending stiffness	1.85×10^{4}	4.75×10^{10}	$MN\text{-}mm^2$

Table 7.5 Properties of column modeling

	Steel tube		
	Model scale	Prototype scale	Units
Length	0.075	3.0	m
Outer diameter	10	400	mm
Wall thickness	0.75	30	mm
Young's modulus	206	206	GPa
2nd moment of inertia	2.35×10^{2}	6.00×10^{8}	mm^4
Bending stiffness	48.41	1.24×10^{8}	$MN\text{-}mm^2$

Table 7.6 Properties of superstructure mass modeling

	Steel plate		
	Model scale	Prototype scale	Units
Side length	50	2000	mm
Thickness	15	600	mm
Mass	0.297	19008	Kg
2nd moment of inertia	1.41×10^{4}	3.61×10^{10}	mm^4
Bending stiffness	2.90×10^{3}	7.42×10^{9}	$MN\text{-}mm^2$

7.2.2.2 Instrumentation

In a series of model tests in the present study, three types of electronic instruments were used to measure pile bending moments, displacements and accelerations of pile cap, displacements and accelerations of superstructure mass, and accelerations of ground. These instruments can be listed as:

(1) Accelerometers (SSK, A6H-50), to record dynamic motions of ground, pile cap, and structural mass.

(2) Laser displacement transducers (Keyence, LBP-080), to measure the lateral displacements of pile cap and the structural mass.

(3) Seven strain gauges (Foil strain gauge, FLK-2-17) were placed at different locations along the piles to measure pile bending moments.

The general locations of instruments and dimensions are shown in Fig. 7.4. All used sensors for instrumentation of the model are products of Tokyo Sokki Kenkyujo Co., Ltd. and calibrations factors are provided by the company. The specification for accelerometers, laser displacement transducers, strain gauges can be found in Appendix B2, B3, and B4, respectively.

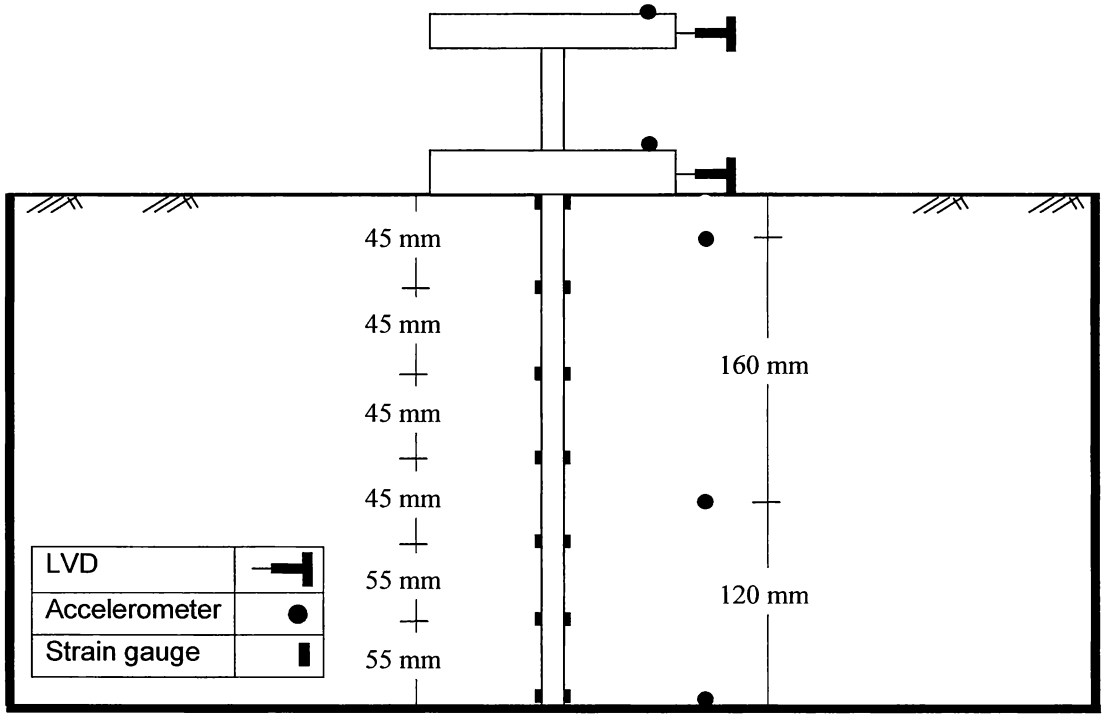

Fig. 7.4 Centrifuge model test set-up and instrumentation

7.2.2.3 Test setup and construction of the model ground

The centrifuge model is normally prepared outside the centrifuge pit, and then transferred to the swinging platform. After cleaning the box with Ethanol, A dry sand deposit was prepared by air pluvation as shown in Fig. 7.5. (Details of this method are given in Appendix B5). After fixing the pile in the bottom plate in the soil container base, silica sand was rained in 1 g field using a hopper fixed at the specified height (depending on the initial target relative density of 73.8 % used in this study, the falling height can be determined as described in Appendix B5) until the sand deposit formed 11.6 m thick deposit (290 mm in model scale). The pile was placed in the

model before the soil was pluviated, attempting to simulate a pile installed with minimal disturbance to the surrounding soil, as may be the case when a pile inserted into a pre-augered hole. Gaffer tape was used to supplementary fix the sensors in position as well as to fix the cables of the sensors to the back wall of the box to prevent unwanted influences on the sand deposit and movement of sensors. After the model ground is constructed, the pile cap was placed and fixed at the pile head directly on the ground surface, and then the column and the structural mass were added to the model. The completed model was then weighed and fixed on the swinging platform of the centrifuge arm and the counterweight on the opposite arm is adjusted.

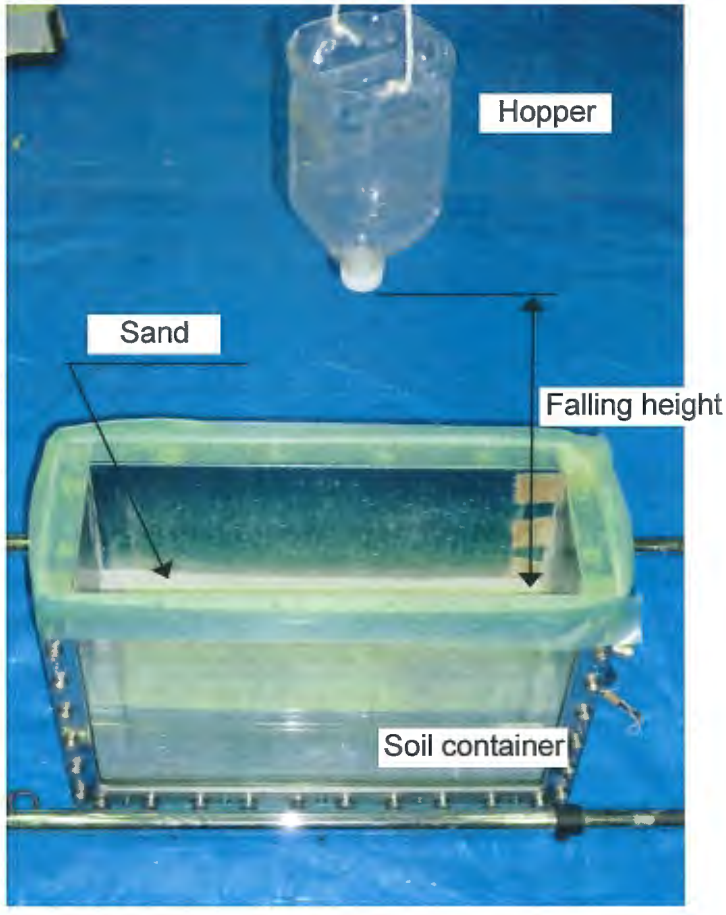

Fig. 7.5 Dry sand deposit preparation by air pluviation

7.2.2.4 Test procedures

After confirming that all equipments and sensors are well functioning without any abnormality, centrifugal acceleration was increased gradually up to 40 g. The sand deposit was then consolidated in 40 g centrifugal acceleration field for 5 min. By measuring the heights of the ground surface after the consolidation by a ruler, the actual relative density before shaking was obtained. The centrifugal acceleration is again increased up to 40 g to apply the dynamic motion to the model. Three sinusoidal waves as input base accelerations with different amplitudes and different frequencies as shown in Table 7.7 were applied in series (Each shaking event was stronger than the previous one) to the system without the superstructure mass. Then the superstructure mass was added and the three input base accelerations were applied to the system with the same previous manner.

Table 7.7 Input base motions

Base acceleration	Max amplitude (g)	Frequency (Hz)
1	0.005	0.1
2	0.084	0.5
3	0.317	1.0

7.3 Finite Element Model

7.3.1 Finite element

The 2D FE program FLIP (Iai et al. 1992) was employed in this study. Figure 7.6 shows the general layout and meshing of the FE model. Side boundary displacements were fixed in the horizontal direction, while those at the bottom boundary were fixed in both the horizontal and vertical directions to simulate the condition of the centrifuge tests.

7.3.1.1 Soil model

The soil continuum was modeled using 2D quad elements with a hyperbolic-type multiple shear mechanism (Iai et al. 1992). Parameters for sand used in the FE analysis were determined referring to the results of laboratory tests on Silica sand No. 7 as shown in Table 7.8. The bulk modulus of the soil skeleton K was determined assuming a Poisson's ratio υ of 0.33. Rayleigh damping parameters were set as $\alpha = 0$ and $\beta = 0.002$.

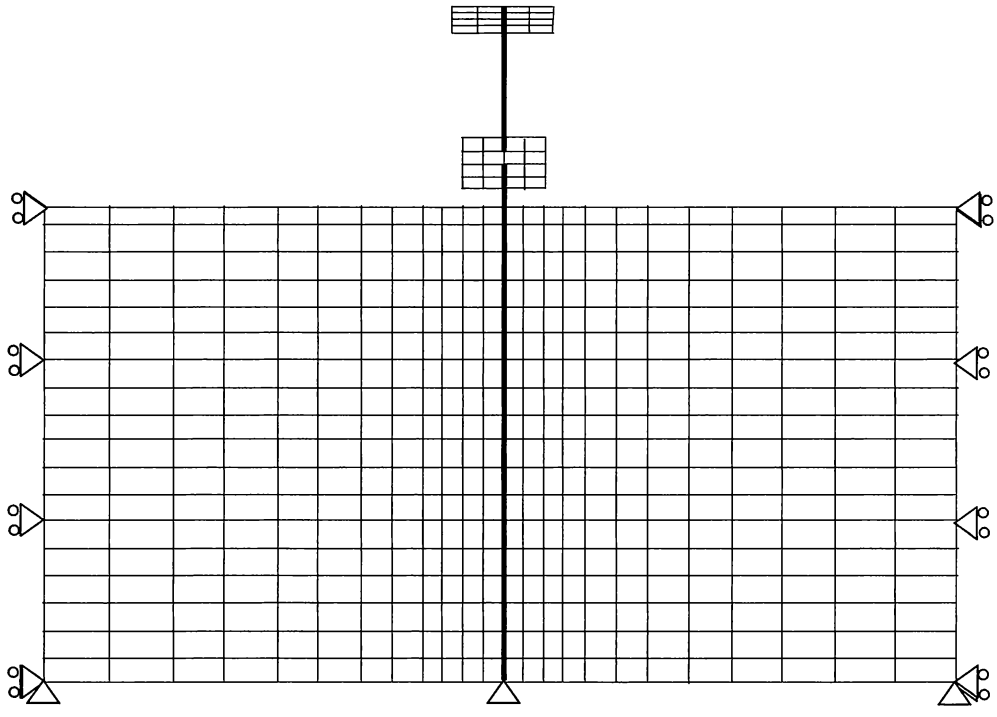

Fig. 7.6 General layout and meshing of the FE model

Table 7.8 Model parameters for soil elements

Density, ρ (t/m^3)	G_{ma} (kPa)	υ	σ'_{ma} (kPa)	φ_f (deg)	H_{max}
1.5	5.1×10^4	0.33	57.11	38	0.20

7.3.1.2 Pile and column model

Bilinear one-dimensional beam elements with three degrees of freedom per node were used to model the pile and the column. Normal force, shear force, and bending moment for each element were obtained directly from the finite element program. Table 7.9 defines the model parameters of pile and column elements. Parameters for the pile and the column were from the industrial standard.

Table 7.9 Model parameters for pile and column elements

Density, ρ (t/m^3)	G_{ma} (kPa)	υ	Initial flexural rigidity (kPa)	Flexural rigidity after yield (kPa)	Plastic moment (kN-m)
7.9	7.75×10^7	0.29	3.64×10^5	2.47×10^5	4163

7.3.1.3 Pile cap and superstructure mass model

Linear plane elements with two degrees of freedom per node were used to model the pile cap and the superstructure mass. Young's modulus of 206 GPa, Poisson's ratio of 0.3, and mass density of 7.9 t/m^3were used for both the pile cap and the superstructure mass.

7.4 Comparison of Calculated and Recorded Responses

The challenge for the FE models was to reasonably approximate the recorded responses for a total six cases (three input motion shaken the system with and without the superstructure mass) with same model and without arbitrary adjustment or back-fitting of the input parameters.

7.4.1 Time histories of the soil-pile-superstructure system

Recorded and calculated responses of soil and pile cap for input motions of 0.1, 0.5, and 1.0 Hz without the superstructure mass are compared in Figs. 7.7, 7.8, and 7.9, respectively. The computed time histories of ground acceleration, pile cap acceleration, and pile cap displacement are consistent with recorded ones in terms of their amplitudes and phases. Thus the FE analysis reproduced soil and pile cap responses' reasonably well.

Recorded and calculated responses of soil, pile cap, and superstructure mass for input motions of 0.1, 0.5, and 1.0 Hz after adding the superstructure mass are compared in Figs. 7.10, 7.11, and 7.12, respectively. The general trend of ground acceleration, pile cap acceleration, and pile cap displacement records was satisfactorily predicted in terms of their amplitudes and phases for all input motions. The computed time histories of superstructure acceleration are consistent with the recorded in terms of phase for all input motions. However, the FE slightly underestimated the amplitudes of superstructure acceleration for input motion of 1.0 Hz. For input motions of 0.1 and 0.5 Hz, the computed superstructure accelerations agree well with the recorded one.

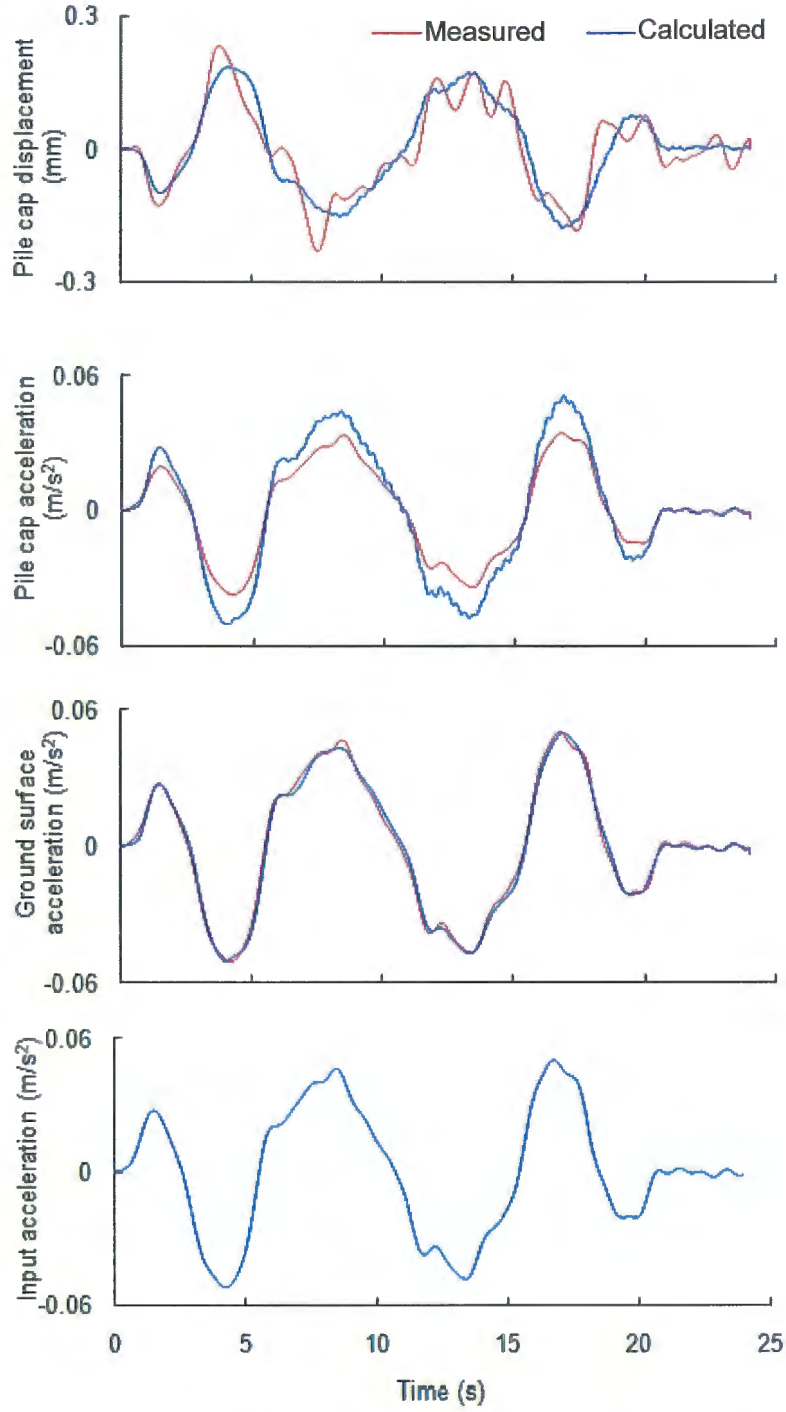

Fig. 7.7 Comparison of recorded and calculated ground and pile cap responses, without superstructure, 0.1 Hz

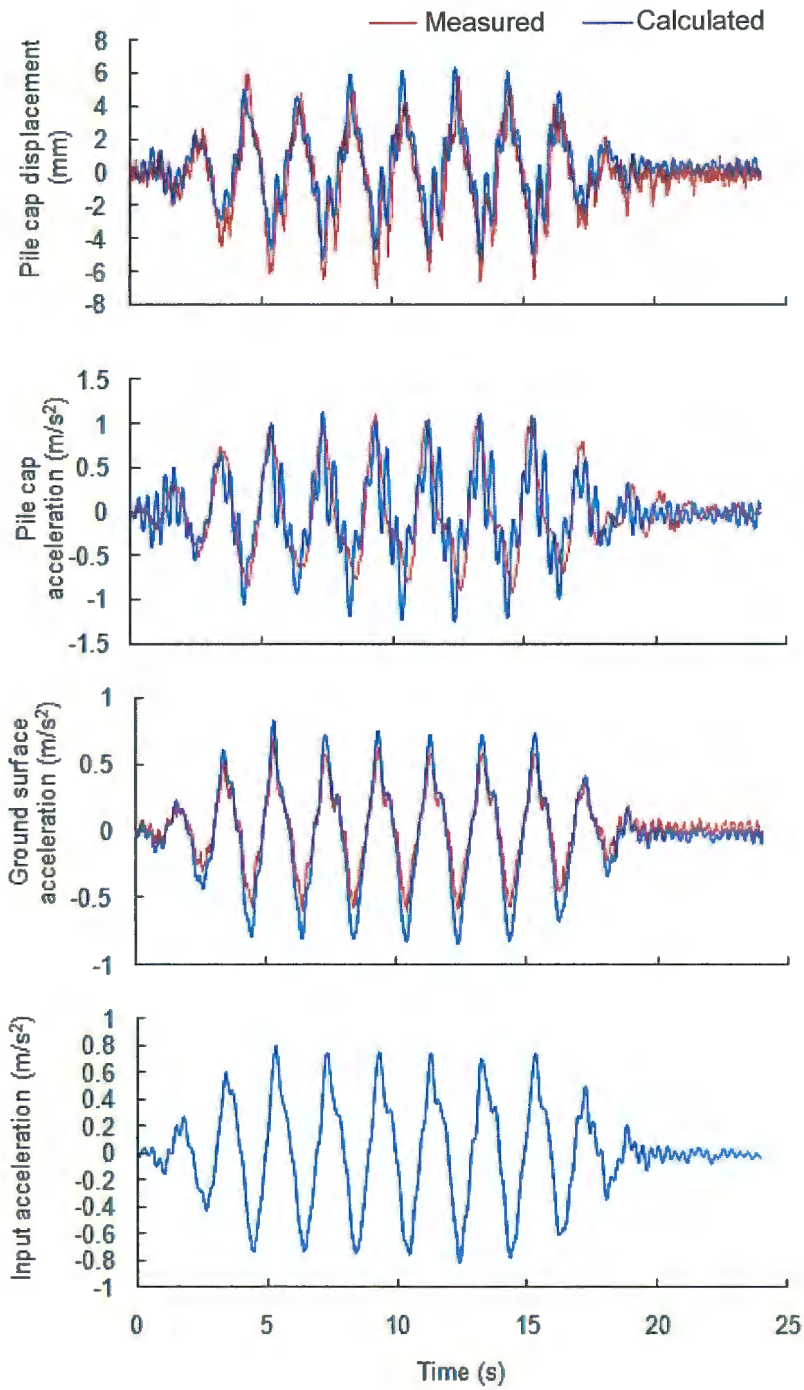

Fig. 7.8 Comparison of recorded and calculated ground and pile cap responses, without superstructure, 0.5 Hz

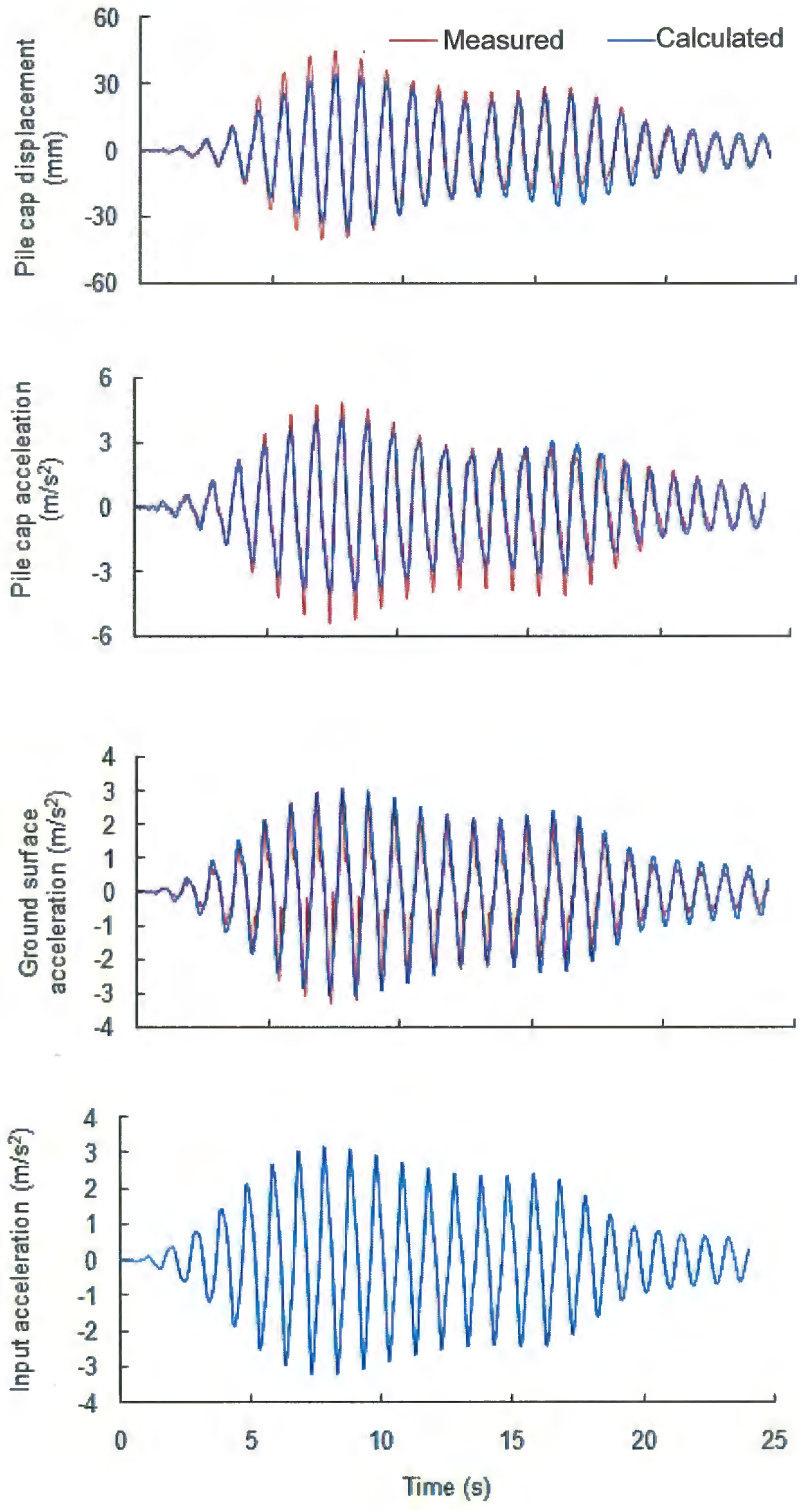

Fig. 7.9 Comparison of recorded and calculated ground and pile cap responses, without superstructure, 1.0 Hz

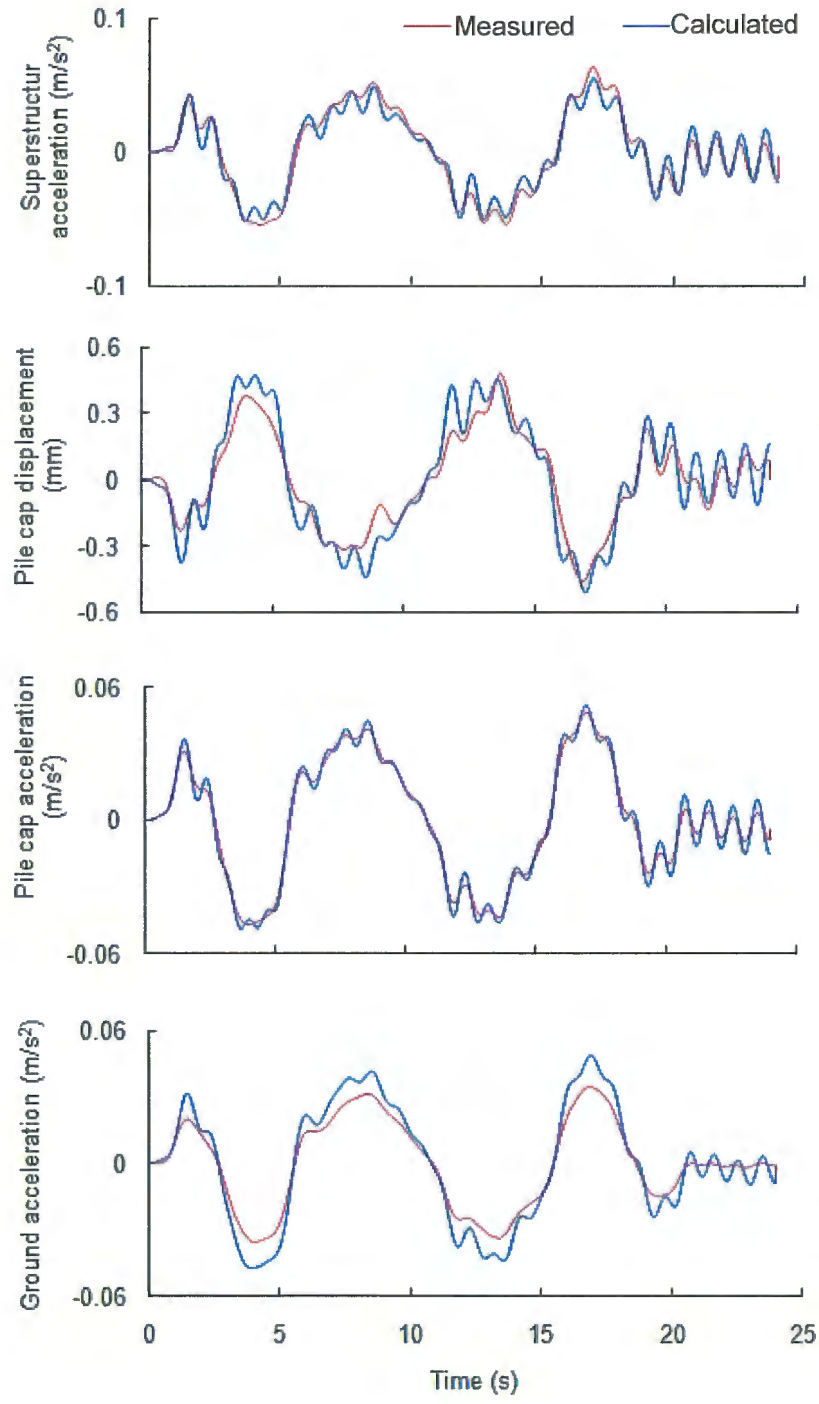

Fig. 7.10 Comparison of recorded and calculated ground and pile cap responses, with superstructure, 0.1 Hz

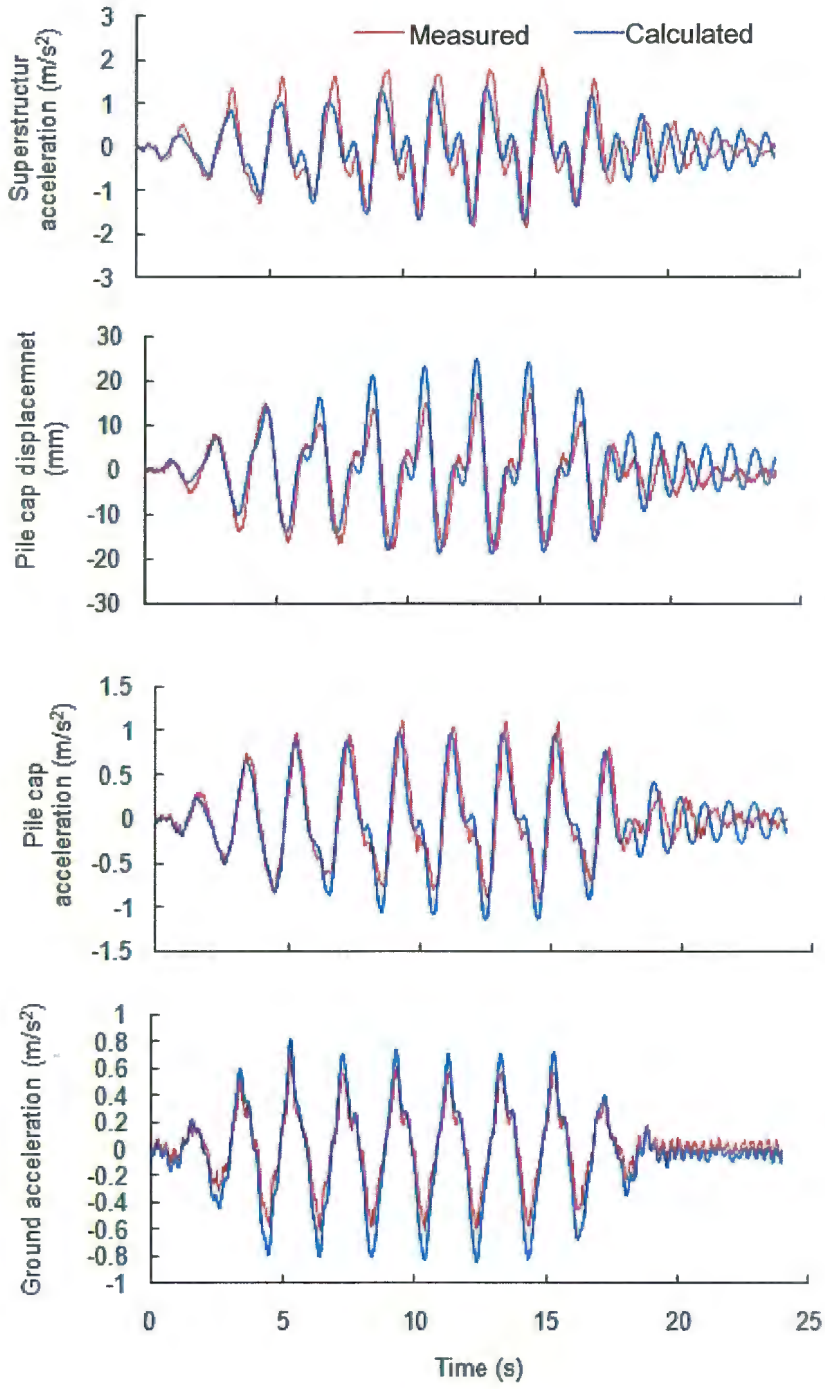

Fig. 7.11 Comparison of recorded and calculated ground and pile cap responses, with superstructure, 0.5 Hz

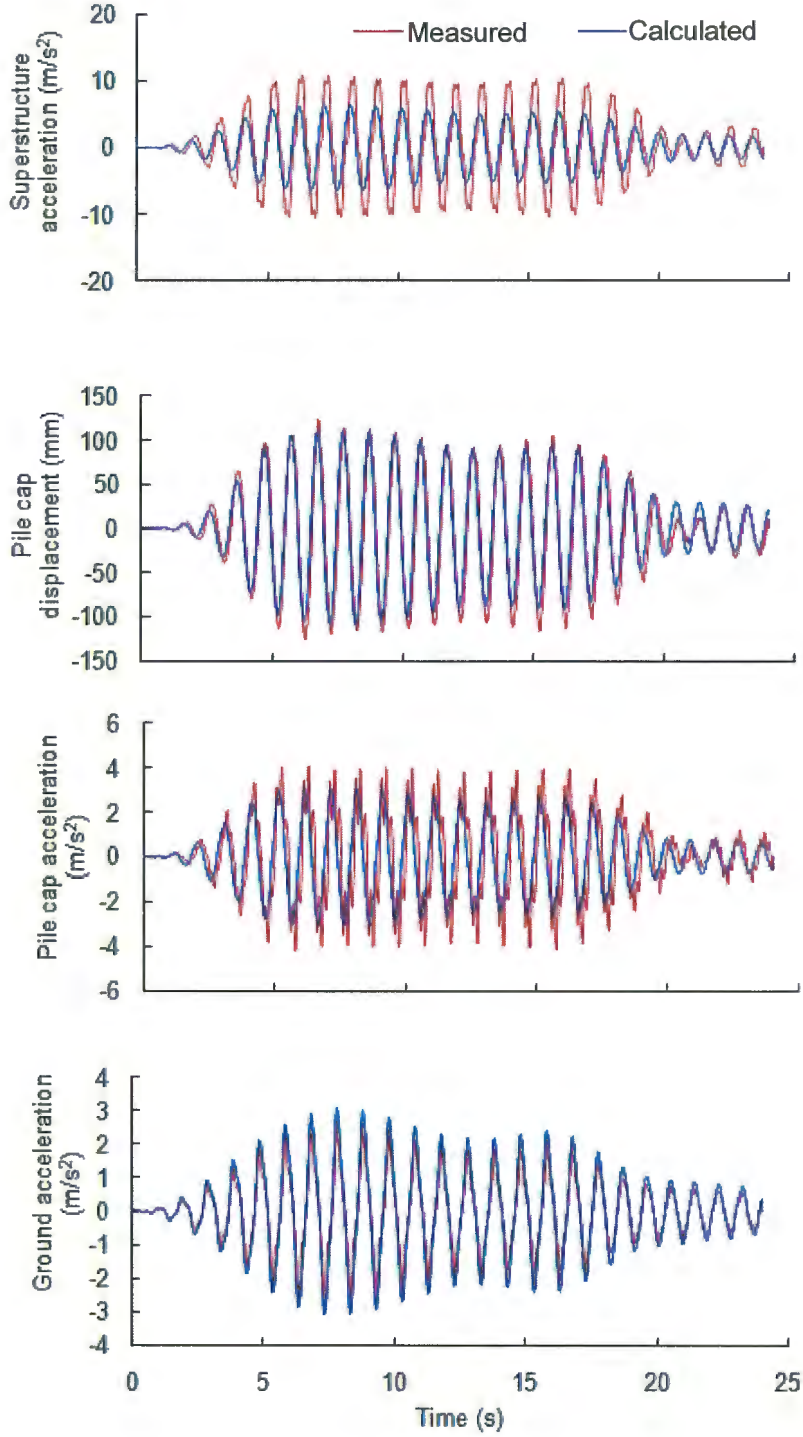

Fig. 7.12 Comparison of recorded and calculated ground and pile cap responses, with superstructure, 1.0 Hz

7.4.2 Fourier spectra of soil and structural responses

The recorded and measured soil and pile cap responses for input motions of 0.1, 0.5, and 1.0 Hz without the superstructure mass are presented in terms of Fourier spectra in Figs. 7.13, 7.14, and 7.15, respectively. Figurs 7.13, 7.14, and 7.15 shows that the FE analysis reproduced soil and structural accelerations that agree well with the measured data.

The recorded and measured soil, pile cap, and superstructure responses for input motions of 0.1, 0.5, and 1.0 Hz with the superstructure mass are presented in terms of Fourier spectra in Figs. 7.16, 7.17, and 7.18, respectively. Figures 7.16, 7.17, and 7.18 show that the FE analysis reproduced soil and structural accelerations that agree well with the measured data.

7.4.3 Peak bending moment profile

Figures 7.19 and 7.20 plot the peak bending moment profiles, calculated as extremes bending-moments at different depths along the pile for input motions of 0.1 and 1.0 Hz and for both cases with and without the superstructure mass.

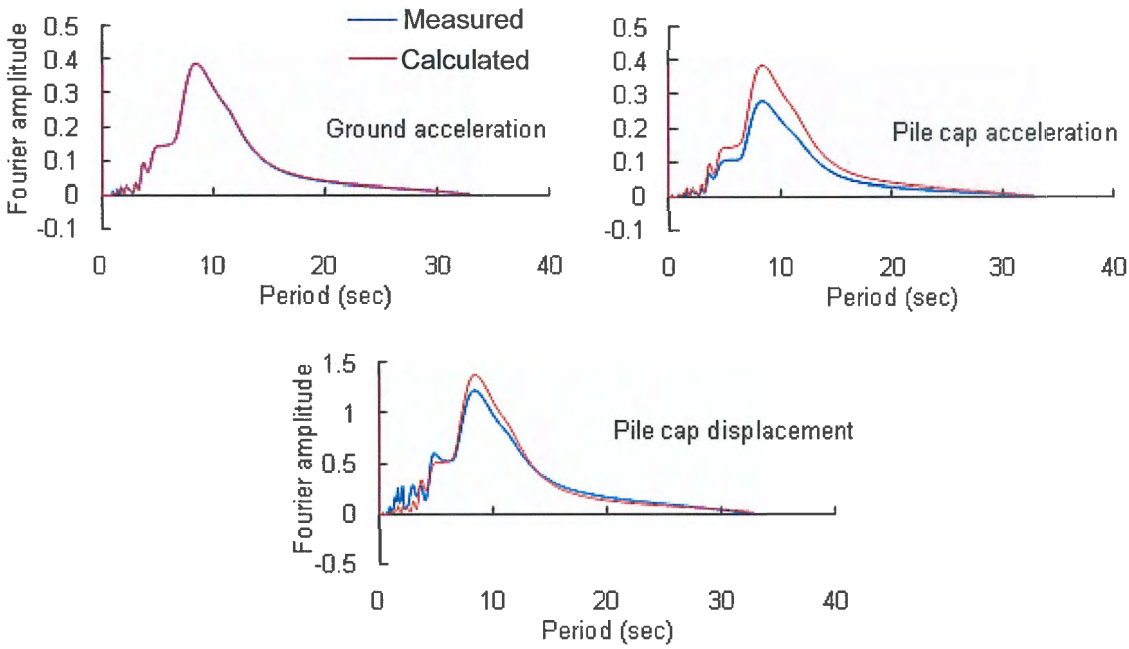

Fig. 7.13 Comparison of recorded and calculated Fourier spectra for ground and pile cap responses: without superstructure, 0.1 Hz

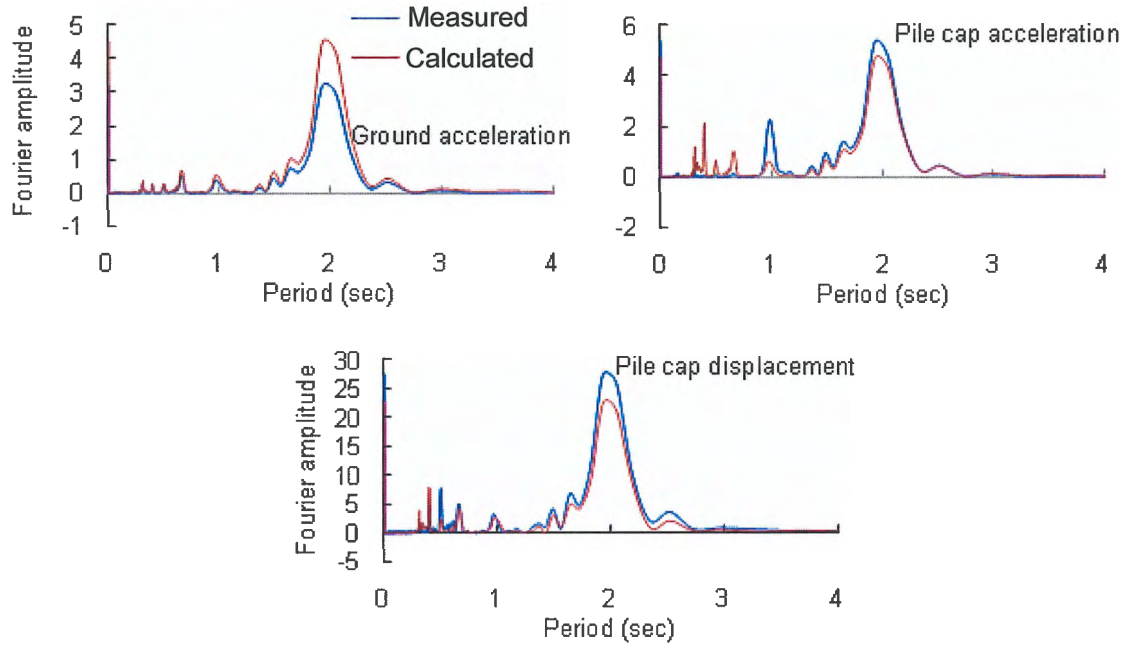

Fig. 7.14 Comparison of recorded and calculated Fourier spectra for ground and pile cap responses: without superstructure, 0.5 Hz

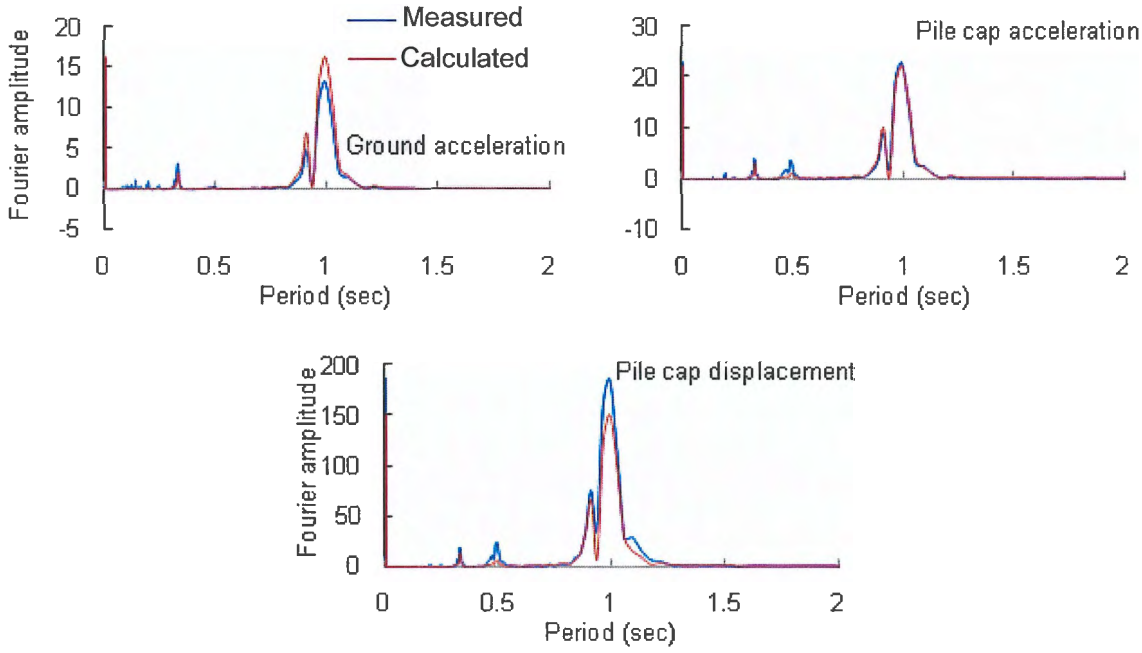

Fig. 7.15 Comparison of recorded and calculated Fourier spectra for ground and pile cap responses: without superstructure, 1.0 Hz

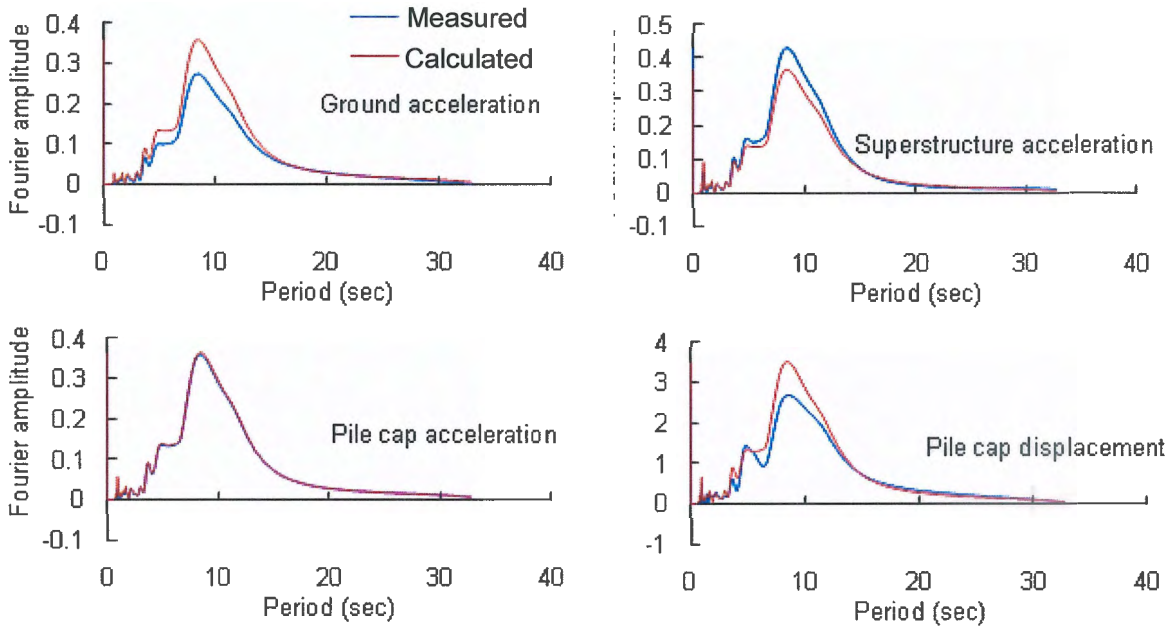

Fig. 7.16 Comparison of recorded and calculated Fourier spectra for ground, pile cap, and superstructure responses: with superstructure, 0.1 Hz

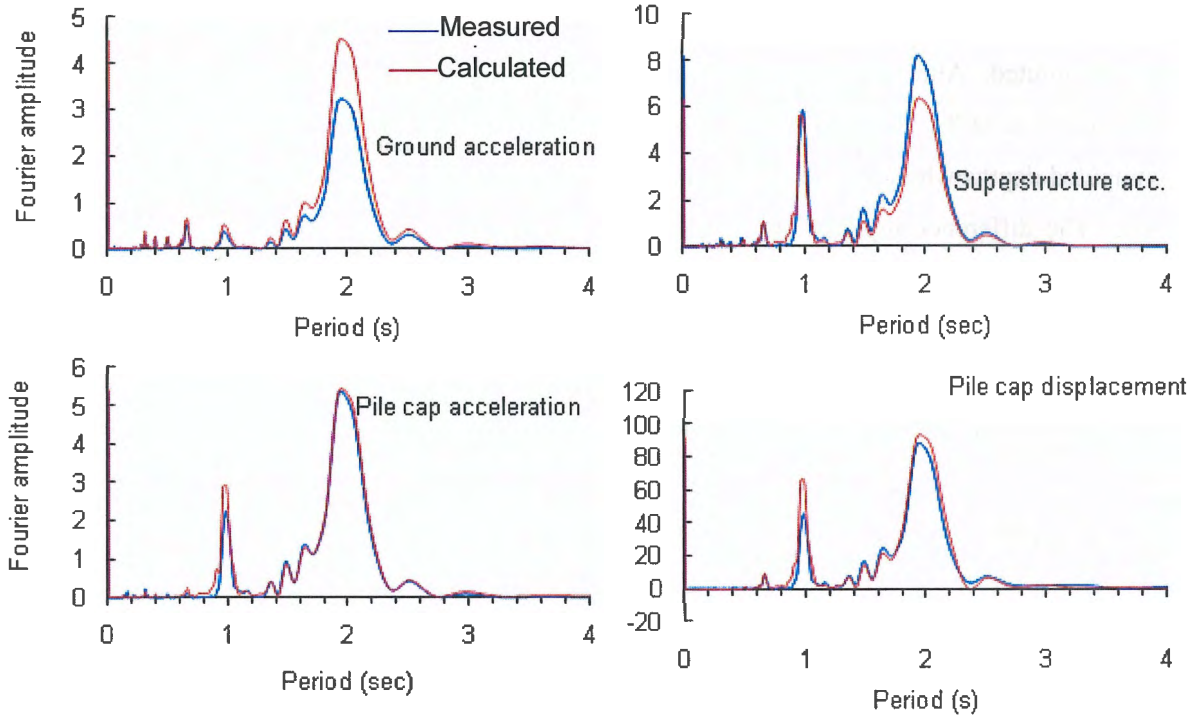

Fig. 7.17 Comparison of recorded and calculated Fourier spectra for ground, pile cap, and superstructure responses: with superstructure, 0.5 Hz

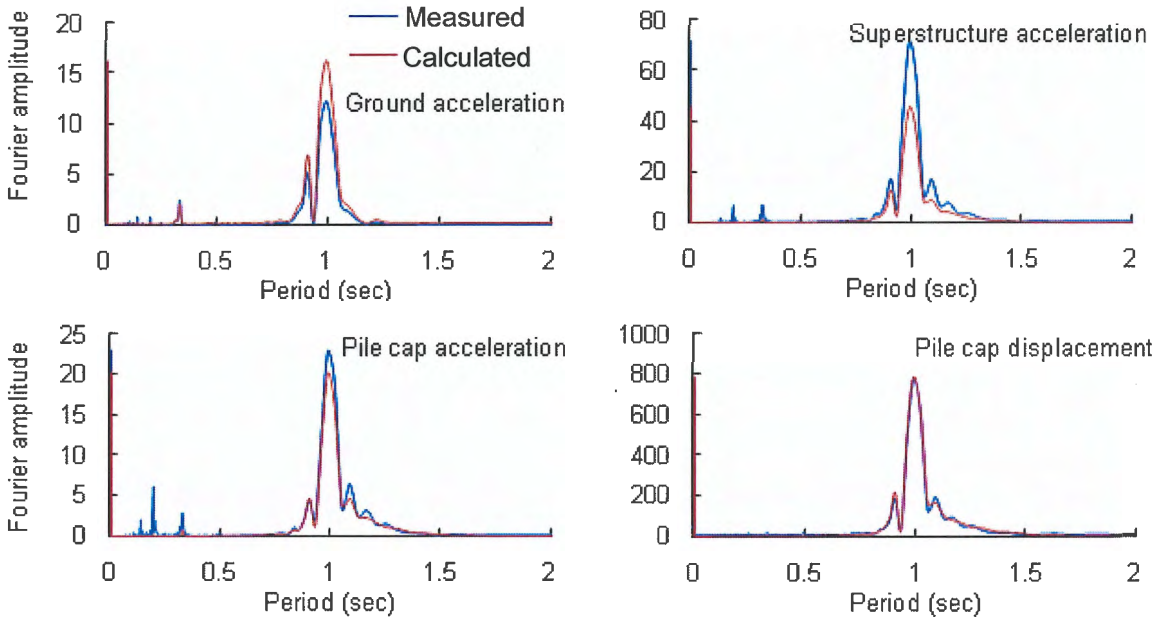

Fig. 7.18 Comparison of recorded and calculated Fourier spectra for ground, pile cap, and superstructure responses: with superstructure, 1.0 Hz

Figures 7.19 and 7.20 compare the depths where the maximum moments were measured and computed. Although, the depth of computed maximum moment agreed well with the measured one at 0.1 Hz, there is a difference at 1.0 Hz and this difference was about 1.5 m. The computed depths where the bending moment returned to zero were consistent with the measured ones. The difference between the measured and computed depths was within 1.0 m.. For the system without the superstructure mass, the computed bending moment profile agreed well with the measured one at 0.1 and 1.0 Hz. The FE is also successful at predicting the increase of peak bending moment profile after adding the superstructure mass but the computed increase of bending moment differed from the recorded one and this may be due to the empirical procedure for the setting of soil-pile interaction springs. Some calibration in the numerical modeling may be required to have more consistent results on the bending moments

7.5 Conclusions

This chapter presents a comparison between nonlinear seismic analyses using the 2D FE and the results of shaking table centrifuge model tests of pile-supported structures in a dense sand

profile. The FE analyses were reasonably able to approximate the recorded responses during shaking in centrifuge tests for the range of conditions covered in the experiments. The challenge was to approximate the recorded responses for a total of six cases using a common set of modeling parameters. As illustrated by the reprehensive time series , Fourier spectra , and bending moment profiles, the overall comparisons indicated that these FE models could now be used to parametrically evaluate the influence of other key factors, such as varying structural periods, pile slenderness, soil-pile relative stiffness, and input motions.

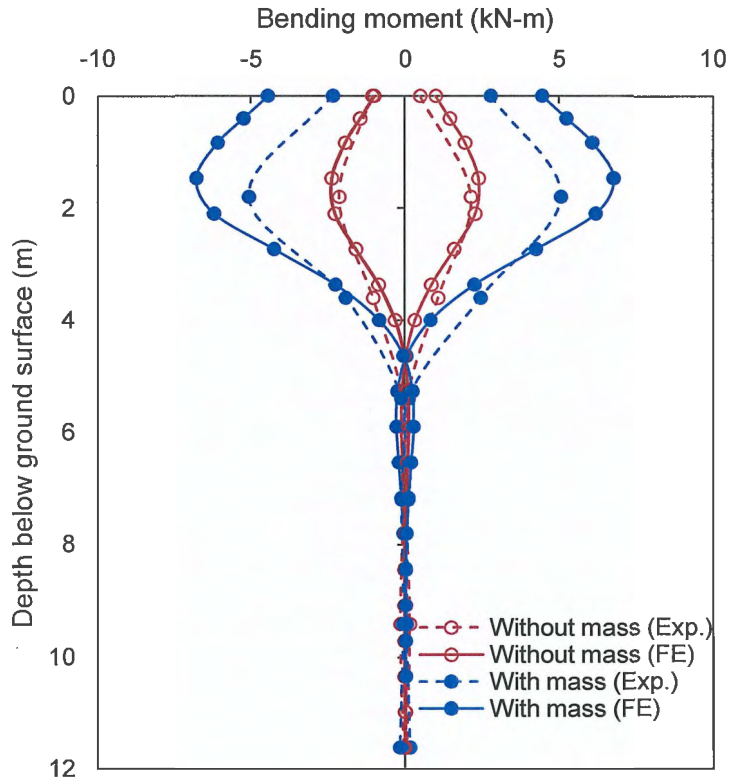

Fig. 7.19 Comparison of recorded and calculated peak bending moment profile, 0.1 Hz

References

1. Iai, S., Matsunaga, Y., and Kameoka, T. 1992. Strain space plasticity model for cyclic mobility. *Soils and Foundations*, 32(2): 1–15.
2. Ozutsumi, O. 2003. Numerical studies on soil-structure systems on liquefiable deposit during earthquakes, Doctors Dissertation, Kyoto University.

3. Schofield, A.N. 1980. Cambridge geotechnical centrifuge operations, 20th Rankine Lecture, Geotechnique, 30(3), pp.227-268.
4. Tan, T.-S. and Scott, R.F. 1985. Centrifuge scaling considerations for fluid-particle systems. *Geotechnique*, 35(4): 461-470.

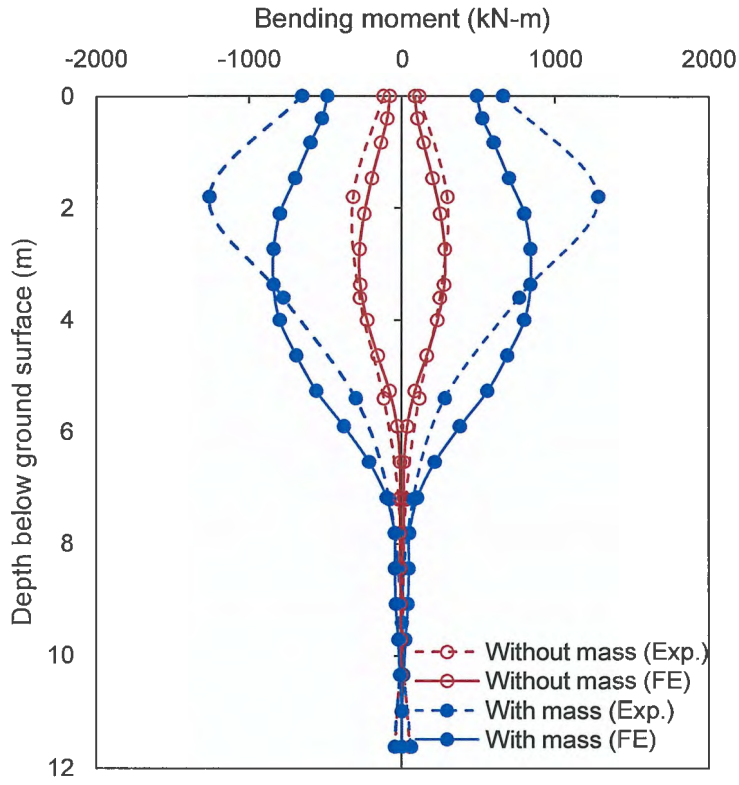

Fig. 7.20 Comparison of recorded and calculated peak bending moment profile, 1.0 Hz

CHAPTER 8

Effect of Soil-Pile-Structure Interaction on Performance of Pile Group: Centrifuge Model Tests

Contents

8.1 Introduction

A geotechnical centrifuge modeling has been established as a powerful technique over the past two decades in obtaining physical data of pile behavior under earthquake events. The advantage of this modeling lies in the ability of the centrifuge to reproduce prototype stress-strain conditions in a reduced scale model as well as the ability to provide a relatively rapid method for performing parametric studies. In this chapter, a series of systematic centrifuge tests is conducted in order to study the seismic response of end bearing single and 3×3 group piles embedded in dry sand layer and supporting SDOF and DDOF structures. The obtained results will provide a clear insight about the seismic coupled soil-pile-structure interaction as well as the seismic pile-soil-pile interaction. All the tests are conducted with the centrifugal acceleration of 40 g. A schematic view of the end bearing single and 3×3 group piles supporting DDOF structures are shown in Figs. 8.1(a) and (b), respectively. The scope of this study is fourfold: (a) to examine the kinematic soil-pile interaction, (b) to investigate the combined effect of kinematic and inertial interaction on the motion of the pile-head, by identifying the fundamental frequencies that dominate the response for both SDOF and DDOF structures, (c) to study the role of the frequency content of the input motion on the development of pile bending, and (d) to study group pile effects on the above mentioned items (from a-c).

Full description of principles of centrifuge modeling as well as centrifuge facilities at DPRI, Kyoto University was given in Chapter 7. In the next sections, centrifuge test procedure, test results, and analysis will be discussed in detail.

8.2 Material Properties

8.2.1 Sand

The model ground in this study was made of Silica sand No. 7 having the physical and mechanical properties given in Chapter 7. All tests were carried out in the centrifugal acceleration field of 40 g using a rigid soil container with nominal inner dimensions of 0.45 m (L) × 0.15 m (W) × 0.29 m (H). Air pluviation method was used to place the dry sand in the soil container as discussed in Chapter 7 and Appendix B5.

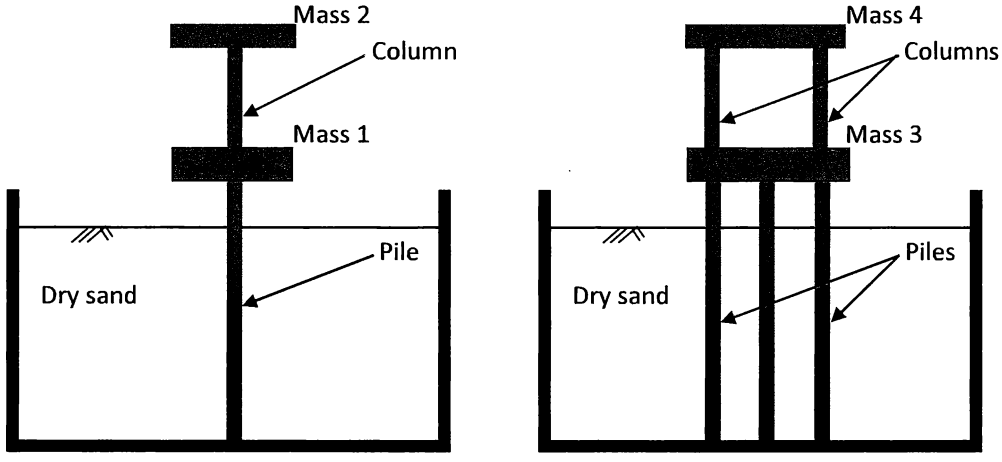

Fig. 8.1 A schematic view of end bearing single and 3×3 group piles supporting DDOF structures: (a) single; and (b) group piles

8.2.2 Piles

Model piles used in this study were made of steel tubes with the properties shown in Table 8.1.

8.2.3 Columns

Model columns used in this study were made of steel tubes with the properties shown in Table 8.2.

Table 8.1 Properties of piles modeling

	Steel tube		
	Model scale	Prototype scale	Units
Length	0.29	11.6	m
Outer diameter	10	400	mm
Wall thickness	0.75	30	mm
Young's modulus	206	206	GPa
2nd moment of inertia	2.35×10^{2}	6.00×10^{8}	mm^4
Bending stiffness	48.41	1.24×10^{8}	$MN\text{-}mm^2$

Table 8.2 Properties of columns modeling

	Steel tube		
	Model scale	Prototype scale	Units
Length	0.075	3.0	m
Outer diameter	10	400	mm
Wall thickness	0.75	30	mm
Young's modulus	206	206	GPa
2nd moment of inertia	2.35×10^{2}	6.00×10^{8}	mm^4
Bending stiffness	48.41	1.24×10^{8}	$MN\text{-}mm^2$

8.2.4 Structural mass 1 (single pile case)

A steel mass (Mass 1) with the properties shown in Table 8.3 fixed to the single pile (see Fig. 8.1(a)) is used in this study.

8.2.5 Structural mass 2 (single pile case)

A steel mass (Mass 2) with the properties shown in Table 8.4 fixed to the top of the column (see Fig. 8.1(a)) is used in this study.

8.2.6 Structural mass 3 (group pile case)

A steel mass (Mass 3) with Properties shown in Table 8.5 fixed to the group piles (see Fig. 8.1(b)) is used in this study.

8.2.7 Structural mass 4 (group pile case)

A steel mass (Mass 4) with Properties shown in Table 8.6 fixed to the top of the columns (see Fig. 8.1(b)) is used in this study.

8.3 Test Program

A total of 7 tests were performed and these tests are listed in Table 8.7. Typical cross sections of free-field, single and group pile model tests are shown in Figs. 8.2, 8.3, 8.4, and 8.5,

respectively. Assembly drawing of single and group pile supporting SDOF and DDOF structures are given in Appendix B1. Figure 8.6 shows a plane view of group pile arrangement. Group pile was lined up 3 by 3 with a spacing of 4 times a pile diameter. The pile tips were set in rotation fixed at the bottom of container using steel plate of 10 mm thickness.

Table 8.3 Properties of Mass 1 modeling

	Steel plate		
	Model scale	Prototype scale	Units
Side length	40	1600	mm
Thickness	30	1200	mm
Mass	0.3792	24269	Kg
2nd moment of inertia	9.0×10^{4}	2.30×10^{11}	mm^4
Bending stiffness	1.85×10^{4}	4.75×10^{10}	$MN\text{-}mm^2$

Table 8.4 Properties of Mass 2 modeling

	Steel plate		
	Model scale	Prototype scale	Units
Side length	50	2000	mm
Thickness	15	600	mm
Mass	0.297	19008	Kg
2nd moment of inertia	1.41×10^{4}	3.61×10^{10}	mm^4
Bending stiffness	2.90×10^{3}	7.42×10^{9}	$MN\text{-}mm^2$

8.4 Instrumentation

In a series of model tests in the present study, electronic instruments were used to measure bending moments of piles, accelerations of ground, piles heads, and superstructure masses. The general locations of instruments are shown in Figs. 8.2, 8.3, 8.4 and 8.5. The specification for accelerometers and strain gauges can be found in Appendix B2 and B4.

Table 8.5 Properties of Mass 3 modeling

	Steel plate		
	Model scale	Prototype plate	Units
Side length	120	4800	mm
Thickness	30	120	mm
Mass	3.4128	218419	Kg
2nd moment of inertia	2.7×10^{5}	6.91×10^{11}	mm^4
Bending stiffness	5.56×10^{4}	1.42×10^{11}	$MN\text{-}mm^2$

Table 8.6 Properties of Mass 4 modeling

	Steel plate		
	Model scale	Prototype scale	Units
Side length	105	4200	mm
Thickness	13.5	540	mm
Mass	1.176	75252	Kg
2nd moment of inertia	2.15×10^{4}	5.50×10^{10}	mm^4
Bending stiffness	4.434×10^{4}	2.65×10^{9}	$MN\text{-}mm^2$

Table 8.7 Tested cases

Test No	Test setup	Soil deposit	Relative density (%)	
			Before the test	After the test
1	Free field	Dry sand	77	81
2	Single pile		78	80
3	Single pile + SDOF structure		80	82
4	Single pile + DDOF structure		80	82
5	Group pile		78	82
6	Group pile + SDOF structure		82	83
7	Group pile + DDOF structure		82	84

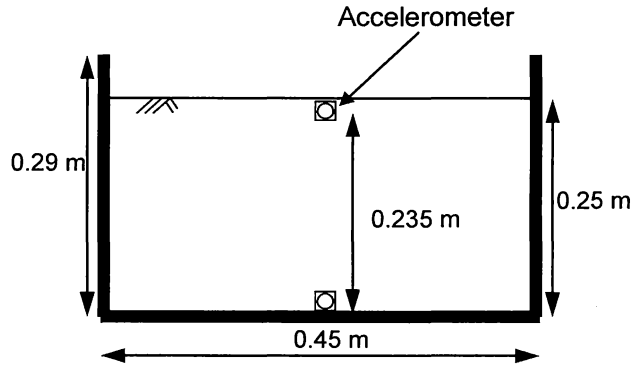

Test 1

Fig. 8.2 Illustration of free-field test setup (test 1)

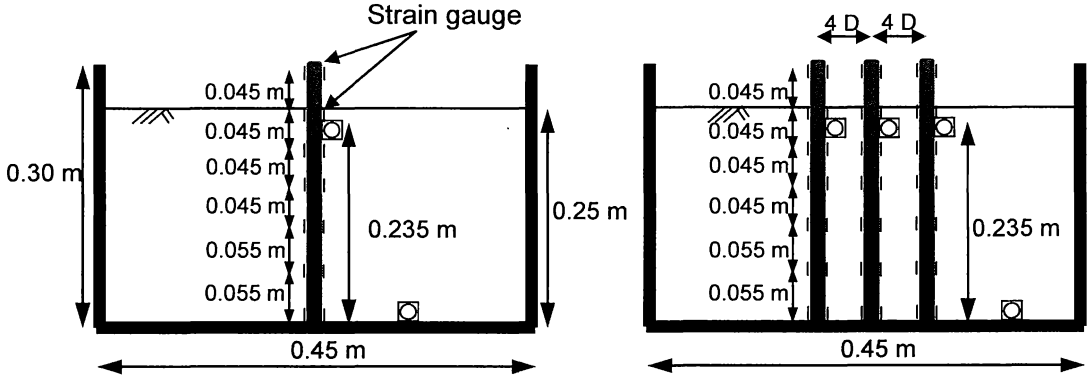

Test 2 Test 5

Fig. 8.3 Illustration of piles tests setup: single pile (test 2); and group pile (test 5)

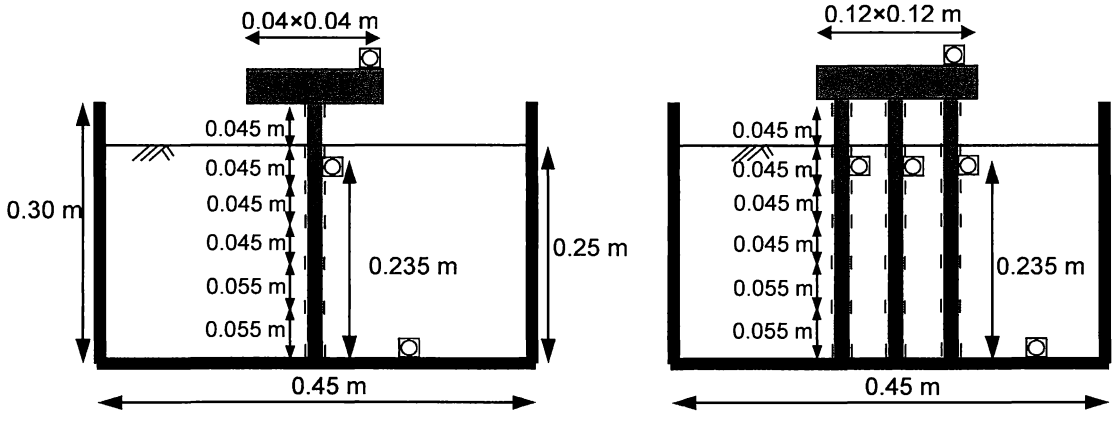

Test 3 Test 6

Fig. 8.4 Illustration of piles supporting single degree of freedom tests setup: single pile (test 3); and group pile (test 6)

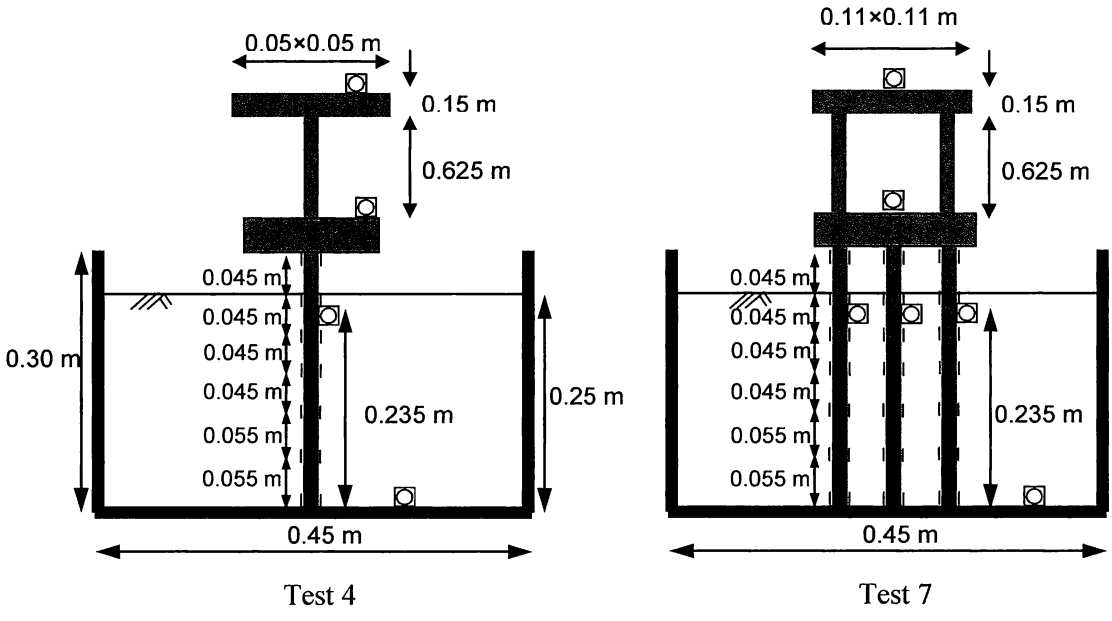

Fig. 8.5 Illustration of piles supporting double degree of freedom tests setup: single pile (test 4); and group pile (test 7)

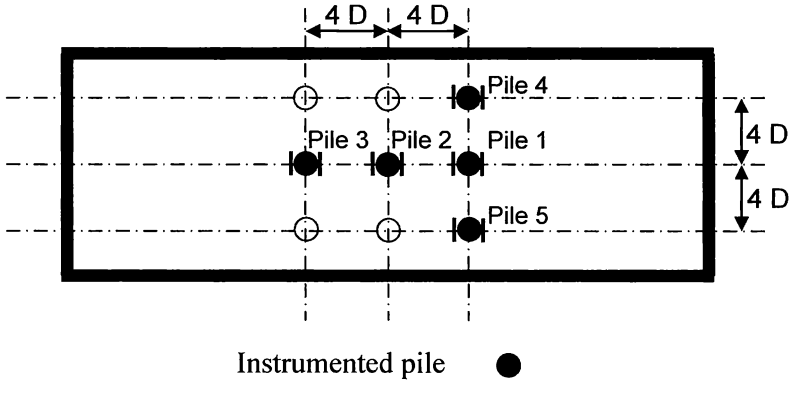

Fig. 8.6 Plan view of the pile group arrangement

8.5 Model Construction

The centrifuge model is normally prepared outside the centrifuge pit, and then transferred to the swinging platform. Each model was constructed very carefully so that all ground models were as identical to each other as possible:

1) For all tests except test 1, the single pile (Tests 2, 3, and 4) or the group piles (Tests 5, 6, and 7) were placed in the model before the dry sand was placed, attempting to simulate a pile installed with minimal disturbance to the surrounding soil, as may be the case when a pile inserted into a pre-augered hole. The piles in the group are kept vertical in their positions using a guided plate as shown in Fig 8.7.
2) After cleaning the box with Ethanol, dry sand was placed in the soil container using the air pluviation method described in Chapter 7.
3) Gaffer tape was used to supplementary fix the sensors in position as well as to fix the cables of the sensors to the back wall of the box to prevent unwanted influences on the sand deposit and movement of sensors.
4) Single (Tests 3 and 6) or double (Tests 4 and 7) DOF structure was placed and fixed at the head of single or group piles.
5) The completed model was weighed and fixed on the swinging platform of the centrifuge arm and the counterweight on the opposite arm was adjusted.

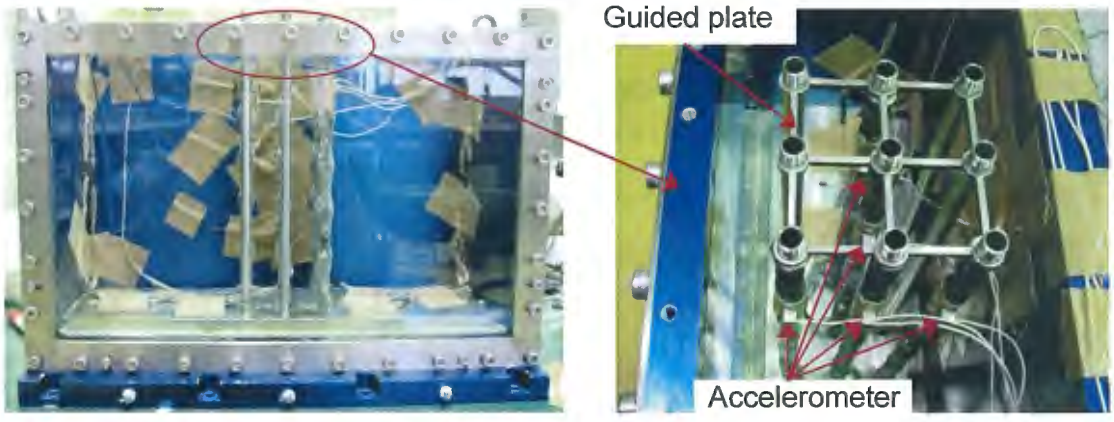

Fig. 8.7 Model setup of group pile test (test 5)

8.6 Test Procedures

After confirming that all equipments and sensors are well functioning without any abnormality, centrifugal acceleration was increased gradually up to 40 g. The sand deposit was then consolidated in 40 g centrifugal acceleration field for 5 min. By measuring the heights of the ground surface after the consolidation by a ruler, the actual relative density before shaking was

obtained. The centrifugal acceleration is again increased up to 40 g to apply the dynamic motion to the model. Each model was subjected to 12 sinusoidal waves as input base accelerations. These waves have constant amplitude of about 1.5 m/s^2 and frequencies ranging from 1 to 12 Hz. After shaking the ground surface settlement was measured again to determine the actual relative density after shaking. The actual relative densities of each tested case before and after shaking are given in Table 8.7.

8.7 Centrifuge Test Results

The comparative results presented in this section are given in terms of different spectral ratio moduli, corresponding to the ratio between displacements at different points in frequency domain. In determining a time history of displacement, measured acceleration was numerically integrated twice. Displacement values shown in this study were all calculated in the same way. Twelve key control points were defined in this study:

(1) A point located at the base of soil container, input motion, (**o**, in all tests).

(2) A point on the free-field (i.e. soil ground surface response without soil-structure interaction) (**ff**, in Test 1).

(3) A point located at the single pile head (at the same elevation with the free-field point) (**sp**, in Tests 2, 3, and 4).

(4) A point located at pile 1 in the group (at the same elevation with the free-field point) (**p1**, in Tests 5, 6, and 7).

(5) A point located at pile 2 in the group (at the same elevation with the free-field point) (**p2**, in Tests 5, 6, and 7).

(6) A point located at pile 3 in the group (at the same elevation with the free-field point) (**p3**, in Tests 5, 6, and 7).

(7) A point located at pile 4 in the group (at the same elevation with the free-field point) (**p4**, in Tests 5, 6, and 7).

(8) A point located at pile 5 in the group (at the same elevation with the free-field point) (**p5**, in Tests 5, 6, and 7).

(9) A point located at the top of M1 (**m1**, in Tests 3 and 4).

(10) A point located at the top of M2 (**m2**, in Test 4).

(11) A point located at the top of M3 (**m3**, in Tests 6 and 7).

(12) A point located at the top of M4 (**m4**, in Test 7).

The accelerations and then displacements of these control points were measured using accelerometers as shown in Figs. 8.2, 8.3, 8.4, 8.5, and 8.6.

8.7.1 Free-field response

The first step in any soil-structure seismic analysis is the evaluation of the free-field response of the site, that is, the spatial and temporal variation of motion before excavating or rigging the soil and superimposing the structure. Test 1 was used as a benchmark test and performed to monitor the free-field dynamic response of the dry sand deposit to be as a reference in the subsequent discussions of both kinematic and inertial effect on pile behavior. It is now a well-established fact of geotechnical earthquake engineering that soil deposits can amplify the seismic rock motion through the soil column toward the surface. In this study, time histories of the free-field displacements were obtained at different frequencies of excitations (1-12 Hz). From these time histories, the amplitude of steady-state displacement (U_{ff}) is noted and normalized with respect to the amplitude of the base displacement (U_o). Thus amplification of free-field response is derived at different frequencies and plotted as shown in Fig. 8.8. As shown in Fig. 8.9, the fundamental period of the ground (T_g is the period corresponds to the local maxima of the free-field response) equals to 0.14 sec and the corresponding fundamental frequency of the ground ($f_g \approx 7.0$ Hz).

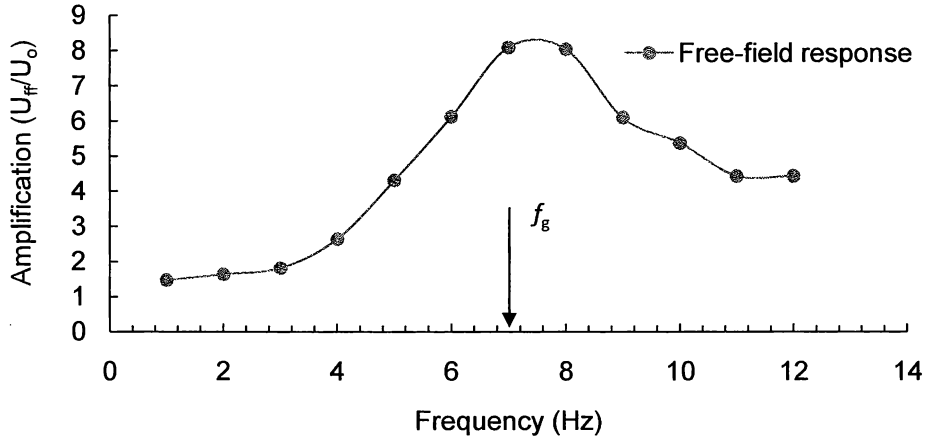

Fig. 8.8 Free-field amplification versus frequency

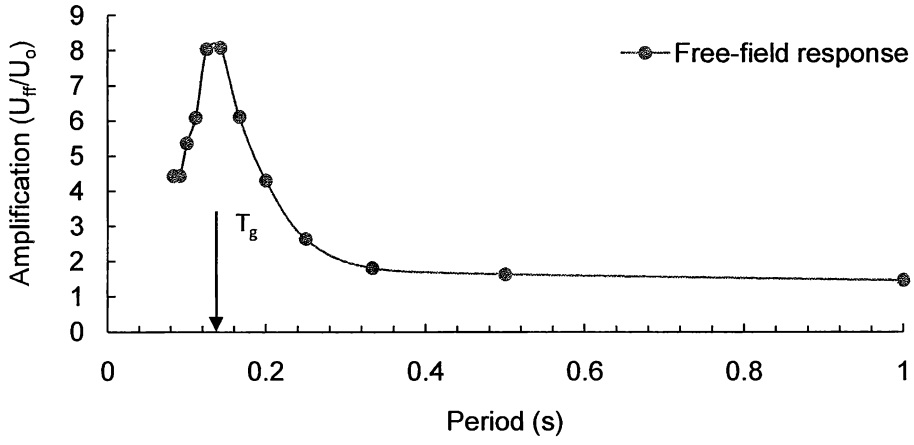

Fig. 8.9 Free-field amplification versus period

8.7.2 Single pile response: kinematic interaction

In the absence of the superstructure, the motion of the pile-head may be different from the free-field motion. This difference is due to the kinematic interaction mechanism. Kinematic effects are described by frequency dependent transfer functions. The transfer function (kinematic interaction factor, I_u) is defined by the ratio of the pile-head displacement (U_{sp}) to the free-field displacement (U_{ff}) in the absence of a structure. In order to study kinematic soil-pile interaction, test 2 was performed. Time histories of pile-head displacements were obtained at different frequencies of excitations (1-12 Hz). From these time histories, the amplitude of steady-state pile-head displacement is noted and normalized with respect to the amplitude of the free-field displacement. Normalized pile-head displacements (kinematic interaction factor) versus base excitation frequencies are shown in Fig. 8.10. It is worth to note from Fig. 8.10 that

- As expected and at a low-frequency region ($f \leq 4$ Hz), the pile-head displacement may be same as or very close to the dynamic response at the free-field surface.
- At a relatively high-frequency region ($f \geq 4$ Hz), the pile produces strong filtering effects of the base excitation. This difference between pile and free-field response in high frequency region is the result of the difference in pile and soil stiffness ($E_{pile}/E_{soil} \approx 1300$).

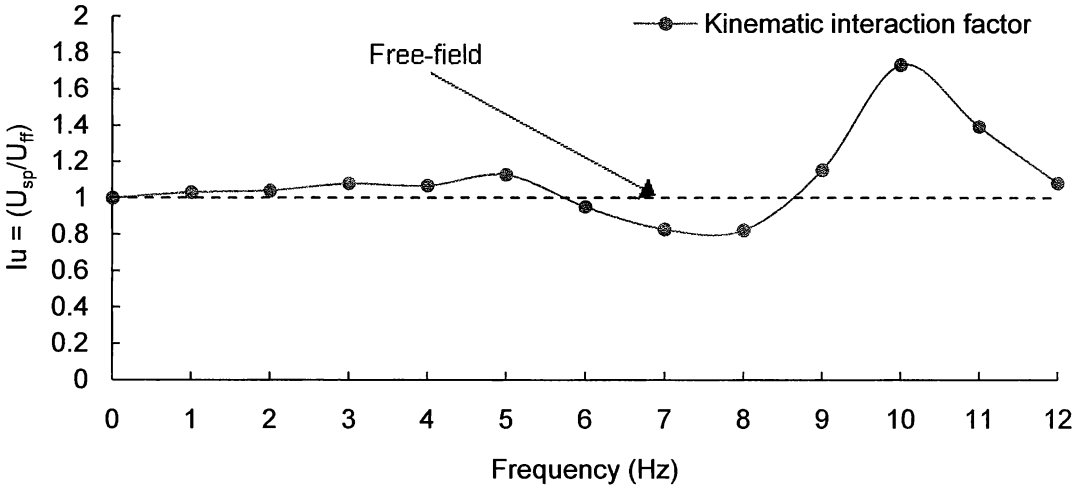

Fig. 8.10 Kinematic interaction factor versus base excitation frequencies

8.7.3 Coupled soil-pile-structure: combined kinematic and inertial action

Tests 3 and 4 were performed to investigate the coupled soil-pile-structure interaction by fixing a SDOF and DDOF structures on the single pile-head, respectively. Figure 8.11 and 8.12 shows the calculated amplification of the single (U_{m1}) and double (U_{m1} and U_{m2}) DOF structures displacement with respect to the base displacement (U_o), respectively. Figures 8.11 and 8.12 were obtained using the results of 2D FE analyses FLIP (Iai et al. 1992). In these analyses, structures were considered as fixed base structure. From Fig. 8.11, it is easy to realize that the fundamental frequency of the SDOF structure (f_{s0}) equals to 5.0 Hz, and from Fig. 8.12, it can be realize that the first and second fundamental frequencies of the DDOF structures (f_{s1} and f_{s2}) are 2.0 and 11.5 Hz, respectively.

The ratios of the pile-head to free-field horizontal displacements (U_{sp}/U_{ff}) are examined in Fig. 8.13. These ratio incorporates the combined effect of inertial and kinematic interaction-as opposed to the kinematic interaction factor ($I_u = U_{sp}/U_{ff}$) which expresses solely kinematic effects. As discussed in Chapter 6, the frequency variation of the ratio (U_{sp}/U_{ff}) is dominated by two discrete frequencies: a lower frequency (the effective natural frequency (f_{SSI})) where the pile-head motion is amplified and a higher one (the pseudo-natural frequency (f_{pSSI}) of the system) where the response is suddenly de-amplified with respect to the free-field motion. The centrifuge results shown in Fig. 8.13 depict this distinctive behavior of pile supporting structures.

It is worth noting that this variation pattern was found to exist in transient response analyses using real earthquake motions of a pile-supported structure (Ohata et al. 1980) as well as analytical studies of soil-pile-structure systems based on the principle of superposition (Mylonakis et al. 1997).

The frequency at which the ratio of structural mass to free-field horizontal displacement is maximized was computed for each examined case, to determine f_{SSI} of the soil-structure system. f_{SSI} of the system was then compared to the natural frequency of the structure under fixed-base conditions, thus quantifying SSI in terms of fundamental dynamics considerations.

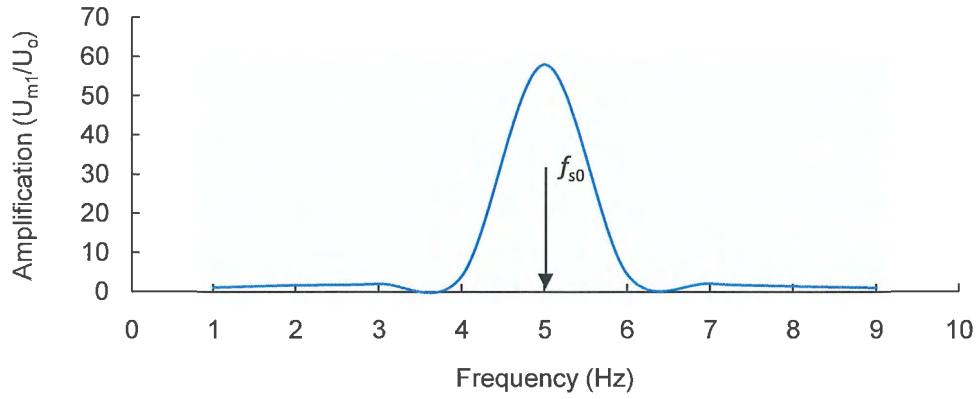

Fig. 8.11 Fixed base structure amplification versus frequency (test 3): Single degree of freedom

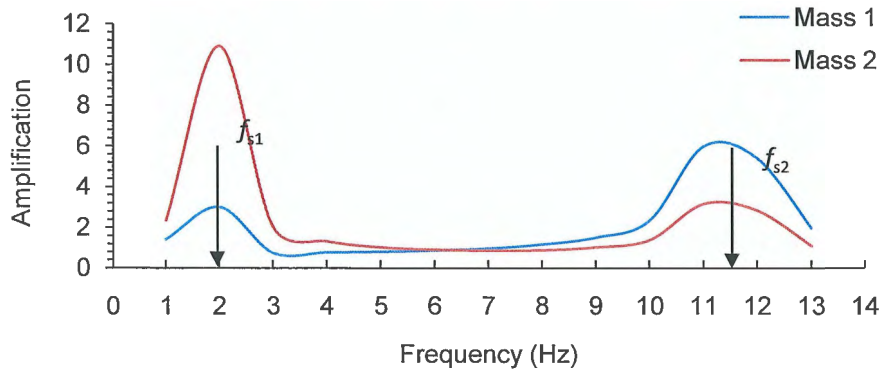

Fig. 8.12 Fixed base structure amplification versus frequency (test 4): Double degree of freedom

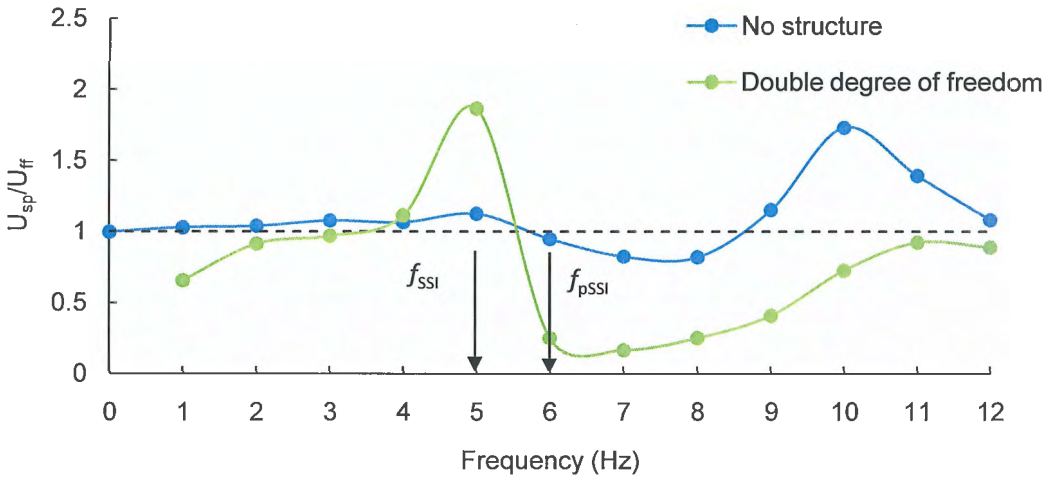

Fig. 8.13 Pile-head to free-field displacement ratio versus frequency

Figure 8.14 shows amplification ratios obtained from Test 3 that corresponds to single pile supporting a SDOF structure. In this test the fundamental period of the structure, $T_{s0} = 0.2$, is greater than the fundamental period of the ground, $T_g = 0.14$. Figure 8.14 shows that f_{SSI}, the frequency where both structural mass and pile-head motions are maximized relative to the free-field soil surface motion, coincides with f_{pSSI} of the system, the frequency where the pile-head motion is minimized relative to the free-field soil surface motion. In this case, f_{SSI} and f_{PSSI} are found to be equal to 2 Hz as shown in Fig 8.14. As a result of SSI, a significant reduction of the f_{SSI} with respect to the natural frequency of the structure under fixed-base conditions (f_s) is observed.

Figure 8.15 shows amplification ratios obtained from Test 4 that corresponds to a single pile supporting a DDOF structure. In this test, the relation between the first and second fundamental periods of the structure (T_{s1} and T_{s2}) and that of the ground (T_g) can be given as the following inequality:

$$T_{s2} < T_g < T_{s1} \tag{8.1}$$

or in term of frequency as:

$$f_{s1} < f_g < f_{s2} \tag{8.2}$$

Evidently, the response of the system is amplified at f_{SSI} of 5.0 Hz while the significant de-amplification of the pile-head motion with respect to the free-field motion takes place at the f_{pSSI} of 6.0 Hz. This means that there is a clear evident of the existence of effective and pseudo-natural frequencies not only in the SDOF structures but for DDOF structures also.

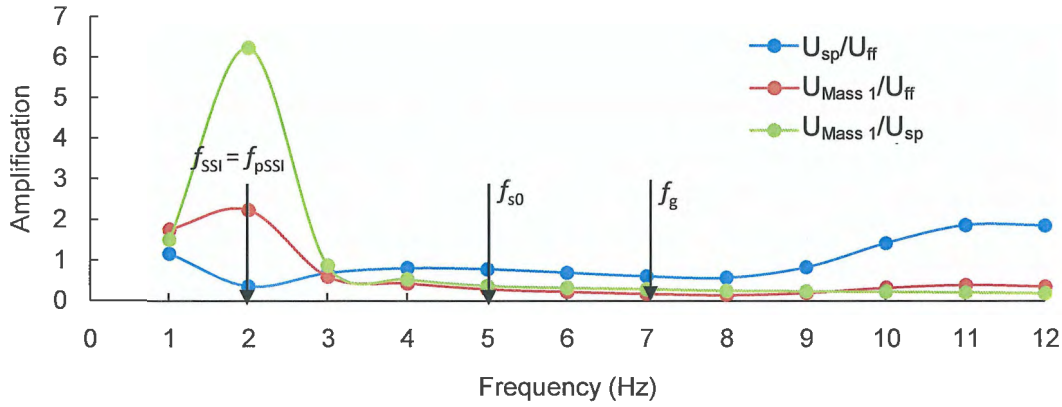

Fig. 8.14 Amplification ratios: single pile supporting a single degree of freedom structure

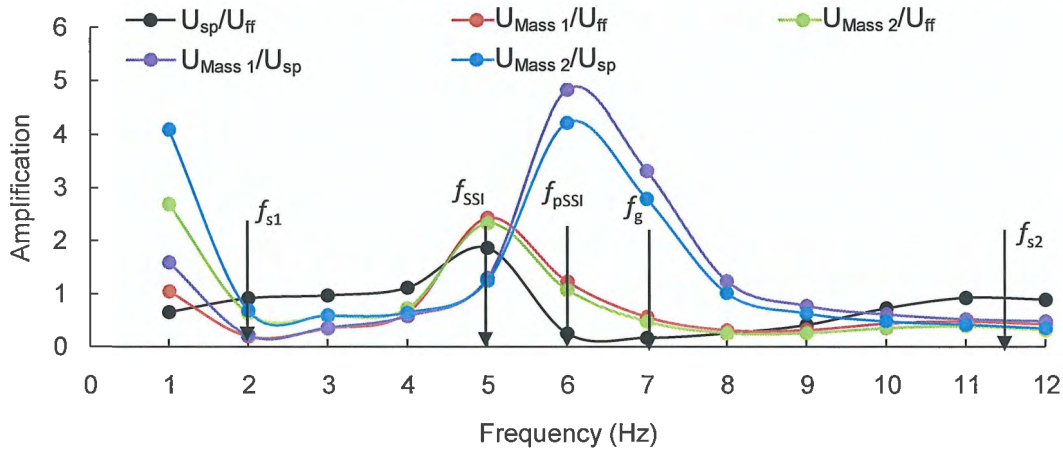

Fig. 8.15 Amplification ratios: double degree of freedom structure

8.7.4 Single pile: dynamic pile bending

The response of the coupled soil-pile-structure system is furthered examined in terms of pile bending as a function of frequency content of base excitation. The pile bending moments were

normalized to the amplitude of bedrock acceleration following Kavvadas and Gazetas (1993) and Rovithis et al. (2009):

$$M_{nor} = \frac{M}{\rho_p D_p^4 \ddot{U}_g} \tag{8.3}$$

where $\ddot{U}_g = w^2 U_g$ is the amplitude of the harmonic input motion introduced at the base of the soil profile.

To investigate the role of the frequency content of the input motion as well as the relative contributions of kinematic and inertial interactions on dynamic pile bending, pile bending moments profiles calculated at frequencies content of input motions closed to the natural frequency of the soil stratum and effective natural frequencies of coupled soil-pile-structure systems (for both SDOF and DDOF structures) are plotted and compared to the corresponding kinematic moments for free-head pile as shown in Fig. 8.16. Figure 8.16 (a), (b), (c), and (d) presents dynamic pile bending obtained at 1.5 m/s^2 input acceleration and 2, 5, 6, and 7.0 Hz, respectively.

When the frequency content of the base excitation is closed to 2 Hz as shown in Fig. 8.16 (a), the maximum pile bending moment occurs near the ground surface (pile-head) and it corresponds to the case of pile supporting SDOF structure. In this case, SSI has a major effect on the dynamic characteristics of the structure, resulting in an effective natural frequency f_{SSI} of 2 Hz significantly lower than the fixed base frequency of the SDOF structure (5 Hz). This case reveals the dominant role of inertial interaction in the development of bending moments on or near the pile head when the superstructure is close to resonance.

When the frequency content of the base excitation is closed to 5 Hz as shown in Fig. 8.16 (b), the maximum pile bending moment occurs near the ground surface (pile head) and it corresponds to the case of pile supporting DDOF structure. In this case, SSI has also a major effect on the dynamic characteristics of the structure, resulting in f_{SSI} of 5 Hz significantly lower than the second fixed base frequency of the DDOF structure (11.4 Hz). This case reveals also the dominant role of inertial interaction in the development of bending moments on or near the pile head when the superstructure is close to resonance.

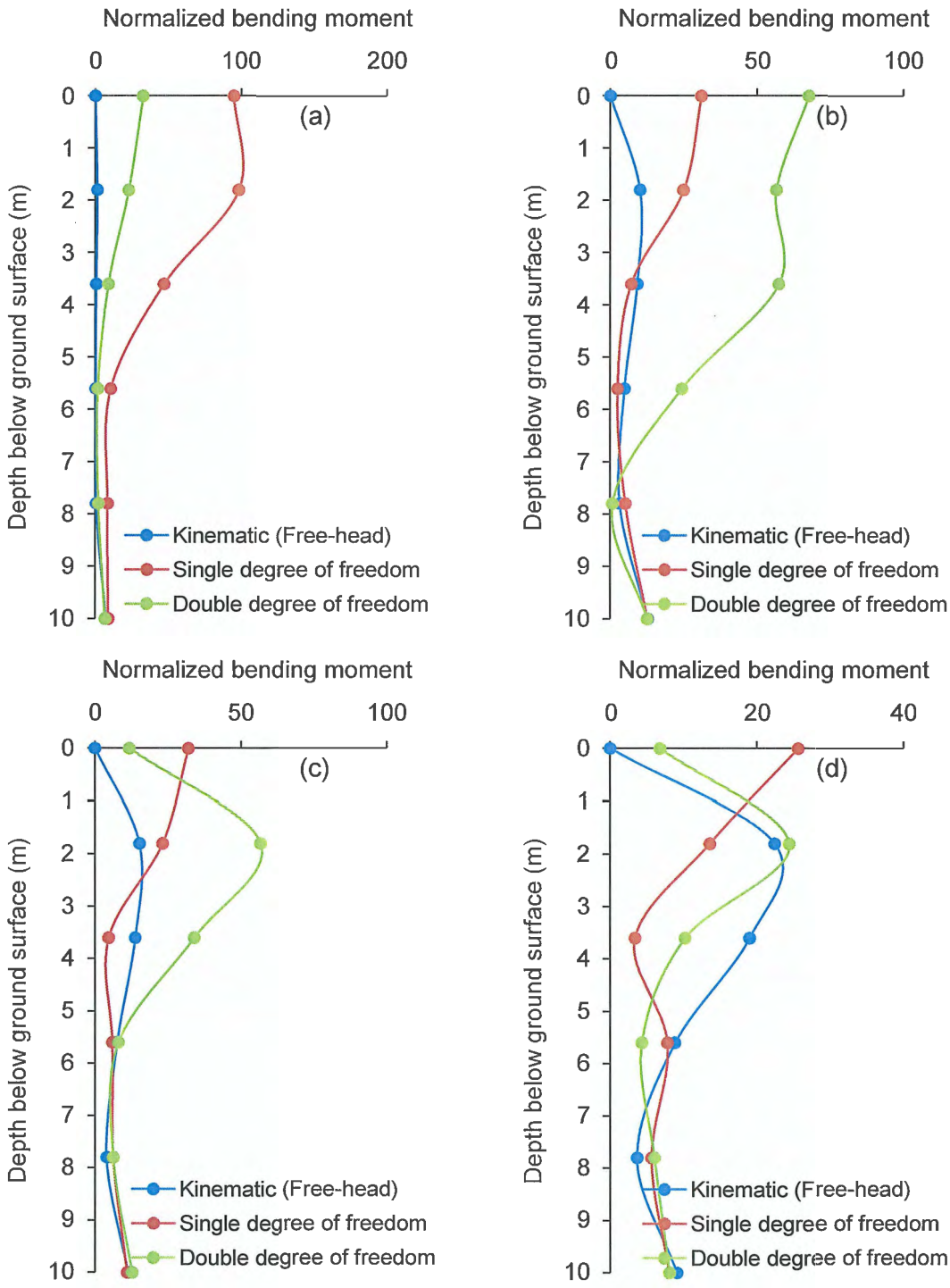

Fig. 8.16 Distributions of amplitudes of normalized steady state bending moments at: (a) 2.0 Hz, (b) 5.0 Hz, (c) 6.0 Hz, and (d) 7.0 Hz

For the DDOF structure, Fig. 8.16 (c) shows a substantial reduction in pile bending under the combined action of kinematic and inertial interaction when the frequency content of the input motion is closed to f_{pSSI} = 6.0 Hz. This reduction in pile bending may be important in pile design. It is worth to note that, although this significant reduction, the maximum pile bending still corresponds to the single pile supporting DDOF structure but it occurs at a depth of 2 m below ground surface.

When the frequency content of the base excitation is closed to 7.0 Hz as shown in Fig. 8.16 (d), the pile bending moment corresponding to the free-head pile case significantly increases indicating a clear kinematic effect.

8.7.5 Group pile response: kinematic interaction

In order to study kinematic soil-pile interaction in free-head group piles, Test 5 was performed. Time histories of pile-heads displacements were obtained at different frequencies of excitations (1-12 Hz). Due to symmetry, only the results of piles 1, 2, and 4 are presented here. From these time histories, the amplitudes of steady-state pile-heads displacements were noted and normalized with respect to the amplitude of the free-field displacement. Normalized pile-head displacements (kinematic interaction factor) for piles 1, 2, and 4 versus base excitation frequencies are shown in Fig. 8.17. Kinematic interaction factor for the single pile is plotted in Fig. 8.17 as a reference. Similar to the behavior of statically loaded pile group discussed in Chapters 4 and 5, Fig. 8.17 indicates that the displacements of the piles in the group are not the same, but a function of the pile position and this is the result of pile-soil-pile interaction.

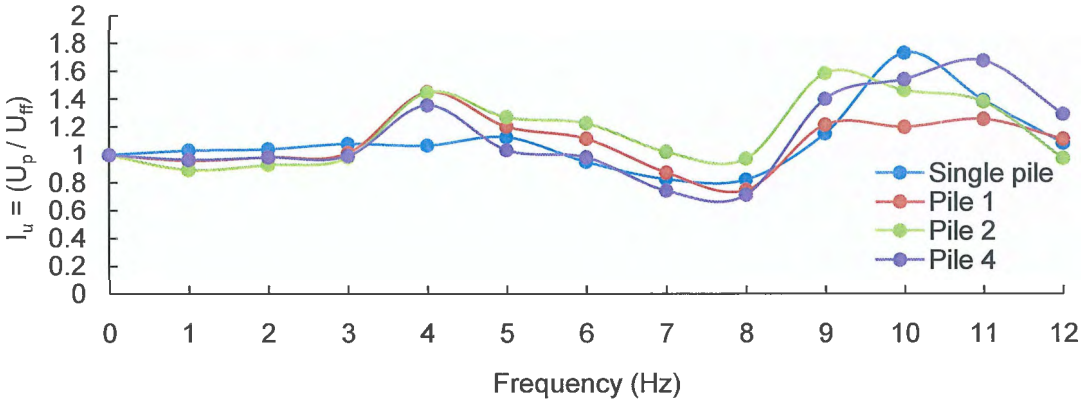

Fig. 8.17 Kinematic interaction factors of piles versus base excitation frequencies

To clearly address this difference in piles behavior, the amplitudes of piles displacements are normalized with respect to the corresponding amplitude of the single pile and plotted versus the frequency of the base excitation as shown in Fig. 8.18. It is obvious from Fig. 8.18 that the displacement of a pile in the group is neither similar to other piles nor the single pile. It is also clear from the figure that the behavior is frequency dependent. For relatively low frequency of the base excitation, displacements of piles in the group are lower than the corresponding displacement of the single pile. For a relatively close pile group embedded in a dense sand soil layer, and at low frequency of the base excitation, the pile group and the sand enclosed between the piles may serve as a block or a rigid pier that may resist rather than follow the seismic motion of the outside ground. With the increase of the frequency of the base excitation, the piles and the enclosed sand no longer serve as a rigid pier and pile-soil-pile interaction take place. When the frequency content of base excitation is close to the fundamental frequency of the ground, the effect of pile-soil-pile interaction is more pronounced as shown in Fig. 8.18.

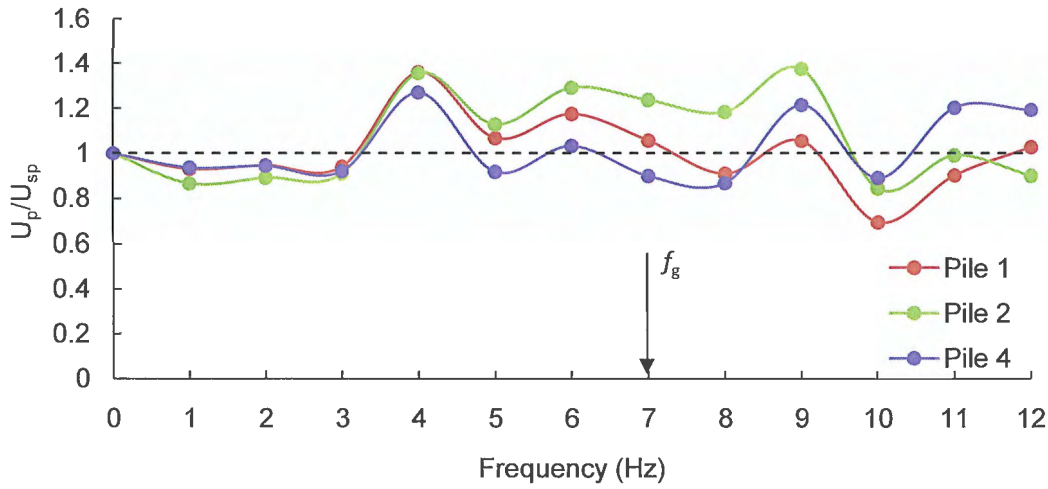

Fig. 8.18 Displacements of piles in a group normalized by single pile displacement versus base excitation frequencies

8.7.6 Coupled soil-pile-structure: combined kinematic and inertial action

Tests 6 and 7 were performed to investigate the coupled soil-pile-structure interaction by fixing a SDOF and DDOF structures on the piles heads in the group, respectively. Figures 8.19 and 8.20 show the calculated amplification of the single (U_{m3}) and double (U_{m3} and U_{m3}) DOF

displacement with respect to the base displacement (U_o), respectively. Figures 8.19 and 8.20 were obtained using the results of 2D FE program FLIP (Iai et al. 1992). In these analyses, structures were considered as fixed base. From Fig. 8.19, the fundamental frequency of the SDOF structure (f_{gp0}) equals to 9.0 Hz, and from Fig. 8.20, the first and second fundamental frequencies of the DDOF structures (f_{gp1} and f_{gp2}) are 6.0 and 11.0 Hz, respectively.

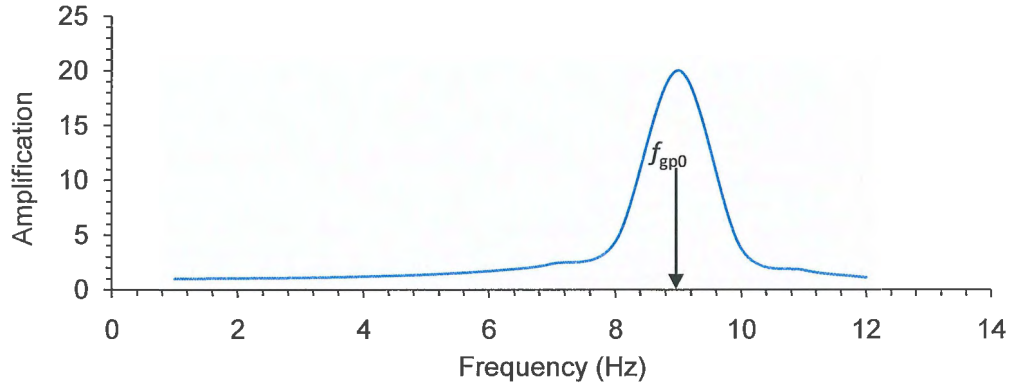

Fig. 8.19 Fixed base structure amplification versus frequency (test 6): single degree of freedom

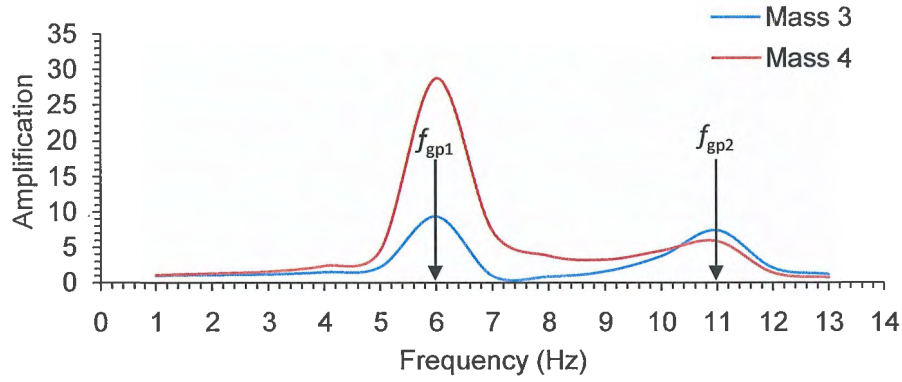

Fig. 8.20 Fixed base structure amplification versus frequency (test 7): double degree of freedom

Figures 8.21-8.23 shows amplification ratios obtained from Test 6 that corresponds to group pile supporting a SDOF structure. Figures 8.21-8.23 correspond to amplification ratios of pile 1, 2, and 4, respectively. Figures 8.21-8.23 indicate that f_{SSI} and f_{pSSI} are found to be existing in the analysis of seismic behavior of group pile supporting a DDOF structures, and the difference in the values of these frequencies among the piles is not significant. As a result of SSI,

a significant reduction of the effective natural frequency f_{SSI} with respect to the natural frequency of the structure under fixed-base conditions (f_{gp0}) is observed as shown in Figs, 8.21-8.23. In this test the fundamental frequency of the structure, f_{gp0} = 9.0 Hz, is larger than the fundamental frequency of the ground, f_g = 7.0 Hz. The following inequality is also observed form the test results:

$$f_{SSI} < f_{pSSI} < f_{gp0} \tag{8.4}$$

Figures 8.24-8.26 shows amplification ratios obtained from test 7 that corresponds to group pile supporting a DDOF structure. Figures 8.24-8.26 correspond to amplification ratios of pile 1, 2, and 4, respectively. These figures indicate that f_{SSI} and f_{pSSI} are found to be exist in the analysis of seismic behavior of group pile supporting a DDOF structures, and the difference in the values of these frequencies among the piles is not significant. As a result of SSI, a significant reduction of the effective natural frequency f_{SSI} with respect to the first natural frequency of the structure under fixed-base conditions (f_{gp1}) is observed as shown in Figs, 8.24-8.26. In this test, the relation between the first and second fundamental frequencies of the structure (f_{gp1} and f_{gp2}) and that of the ground (f_g) can be given as the following inequality:

$$f_{gp1} < f_g < f_{gp2} \tag{8.5}$$

or in term of fundamental periods as:

$$T_{gp2} < T_g < T_{gp1} \tag{8.6}$$

The following inequality is also observed form the test results:

$$f_{SSI} < f_{pSSI} < f_{gp1} \tag{8.7}$$

8.7.7 Group pile: dynamic pile bending

As the single pile case, the response of the coupled soil-pile-structure system is furthered examined in terms of normalized pile bending as a function of frequency content of base excitation.

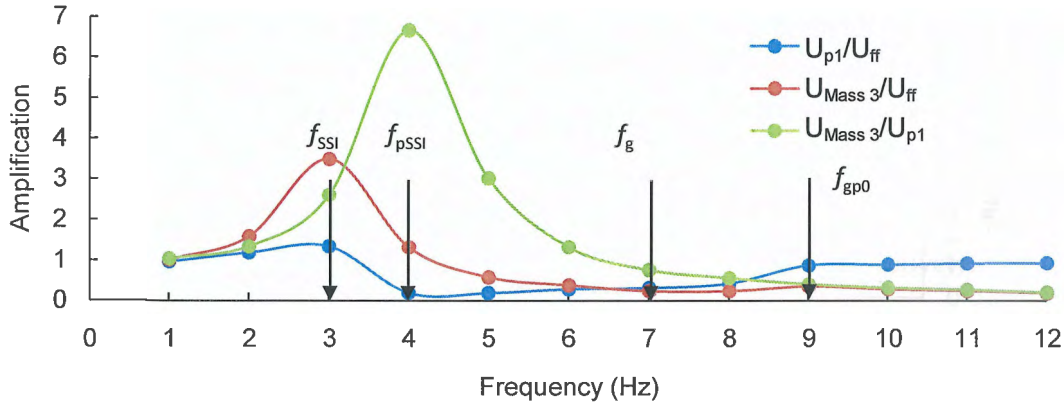

Fig. 8.21 Amplification ratios: pile 1 in a group supporting a single degree of freedom structure

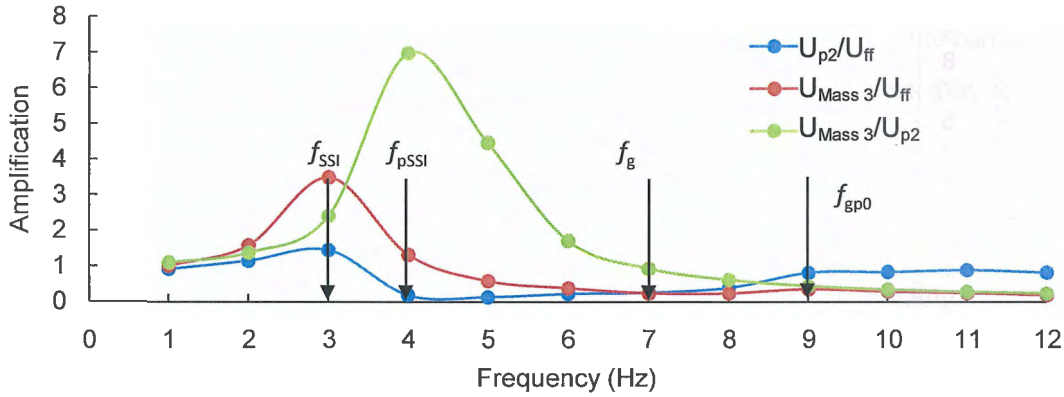

Fig. 8.22 Amplification ratios: pile 2 in a group supporting a single degree of freedom structure

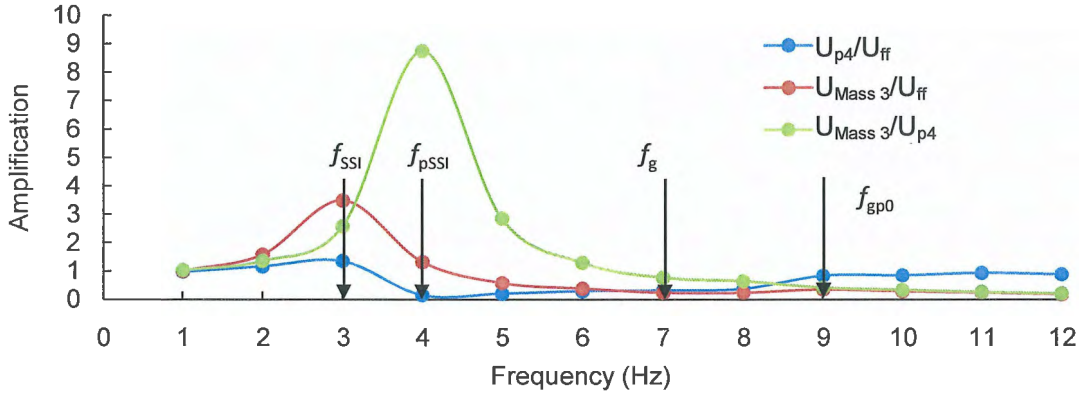

Fig. 8.23 Amplification ratios: pile 4 in a group supporting a single degree of freedom structure

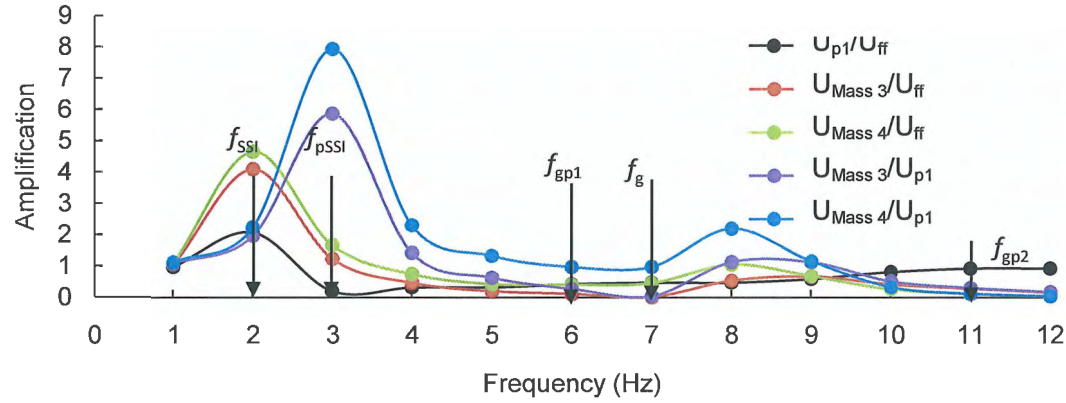

Fig. 8.24 Amplification ratios: pile 1 in a group supporting a double degree of freedom structure

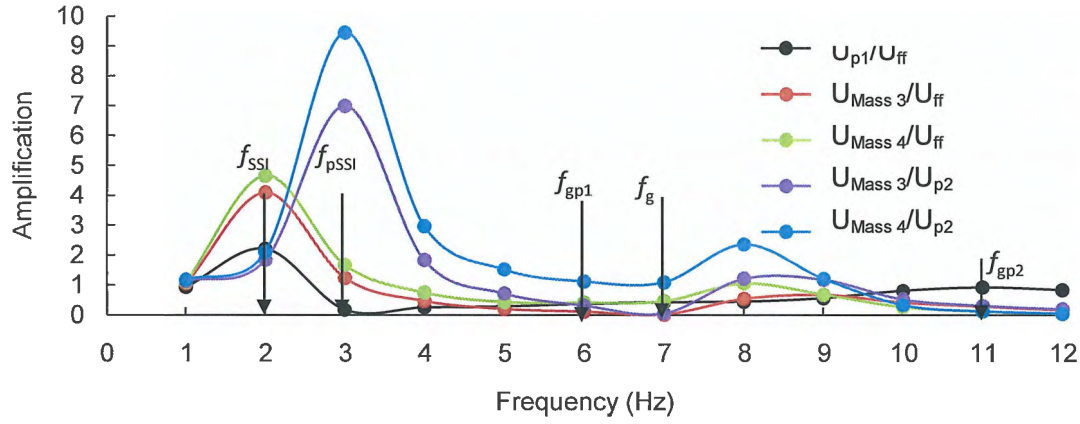

Fig. 8.25 Amplification ratios: pile 2 in a group supporting a double degree of freedom structure

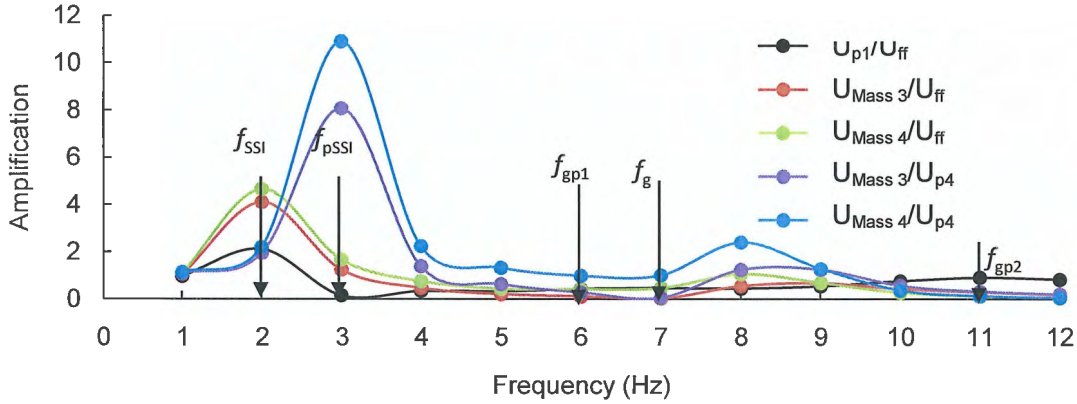

Fig. 8.26 Amplification ratios: pile 4 in a group supporting a double degree of freedom structure

To investigate the role of pile-soil-pile interaction as a function of the input motion of the frequency content of the base excitation on kinematic bending of piles, pile bending moments profiles corresponding to piles 1, 2, and 4 obtained from Test 5 are calculated at selected frequencies content of input motions including frequency closed to the natural frequency of the soil stratum and plotted as shown in Figs. 8.27. Figure 8.27 (a), (b), (c), and (d) presents dynamic pile bending obtained at 1.5 m/s^2 input acceleration and 2, 3, 4, and 7.0 Hz, respectively.

For relatively low frequencies of the base excitation (2 and 3 Hz) as shown in Figs 8.27 (a) and (b), the effect of pile-soil-pile interaction is not significant and the measured bending moments in all piles are the same. When the frequency content of base excitation is increase and become close to the fundamental frequency of the ground, bending moments of all piles increase as expected and the difference between piles bending moments also increases with the center pile (pile 2) having the maximum value followed by the side pile (pile 1) followed by the corner pile (pile 4). It is also worth to note that, the depth of maximum moments is not affected by the pile position or the frequency content of the base excitation.

To investigate the role of pile-soil-pile interaction as a function of the input motion of the frequency content of the base excitation on kinematic and inertial pile bending of piles supporting SDOF and DDOF structures, pile bending moments profiles corresponding to piles 1, 2, and 4 obtained from Tests 6 and 7 are calculated at selected frequencies content of input motions closed to f_{SSI} of the system as well as natural frequency of the soil stratum. Figures 8.28 and 8.29 present dynamic pile bending corresponding to Tests 6 (SDOF) and 7 (DDOF), respectively, and obtained at 1.5 m/s^2 input acceleration and 2, 3, 4, and 7.0 Hz.

When the frequency content is closed to the effective natural frequency of the coupled soil-pile-structure system, the dynamic bending moments of all piles in the group as well as the difference of piles bending increase indicating strong effect of pile-soil-pile interaction as depicted in Figs. 8.28 (b) and 8.29 (a). In particular Fig. 8.28 (b) corresponds to bending of piles at frequency content of excitation equal to f_{SSI} of the SDOF case, while Fig. 8.29 (a) corresponds to bending of piles at frequency content of excitation equal to f_{SSI} of the DDOF case. Unlike the kinematic bending moment's case, the center pile (pile 2) has the minimum value of bending moment followed by the side pile (pile 1) followed by the corner pile (pile 4). Similar to the kinematic bending moment's case, the depth of maximum moments is also not affected by the pile position or the frequency content of the base excitation.

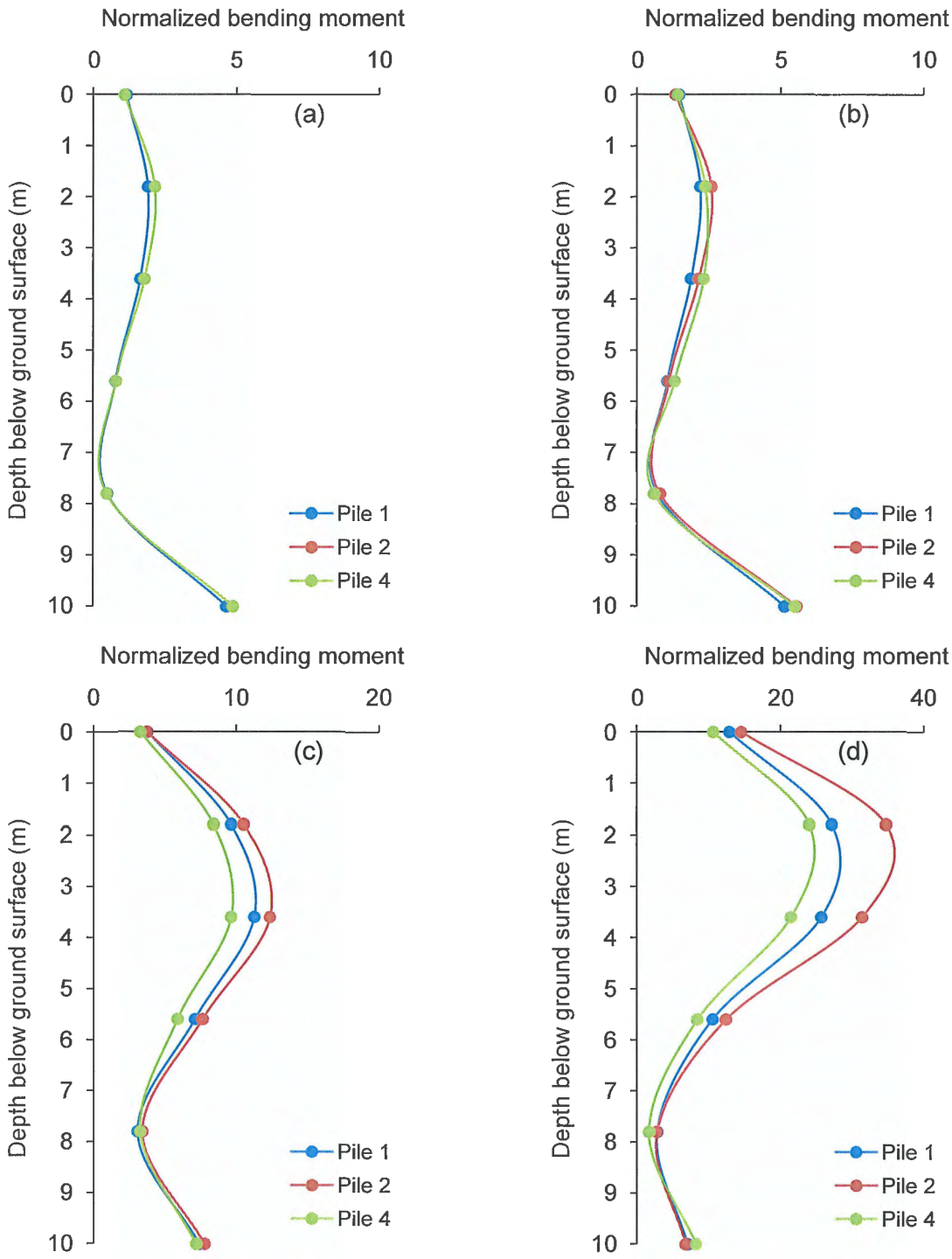

Fig. 8.27 Distributions of amplitudes of normalized steady state bending moments of piles in a group: (a) 2.0 Hz, (b) 3.0 Hz, (c) 4.0 Hz, and (d) 7.0 Hz

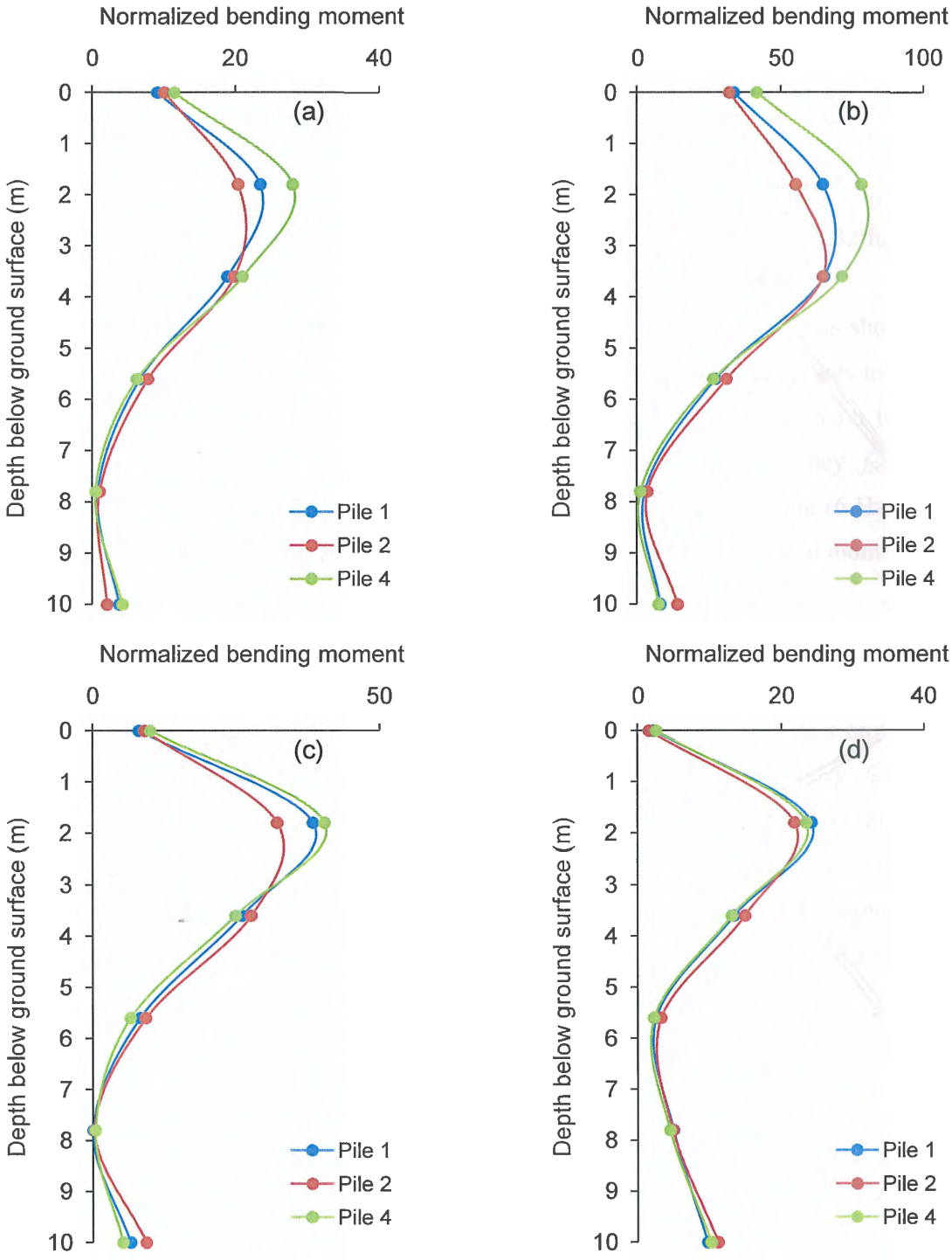

Fig. 8.28 Distributions of amplitudes of normalized bending moments of piles in a group supporting single degree of freedom structure: (a) 2.0 Hz, (b) 3.0 Hz, (c) 4.0 Hz, and (d) 7.0 Hz

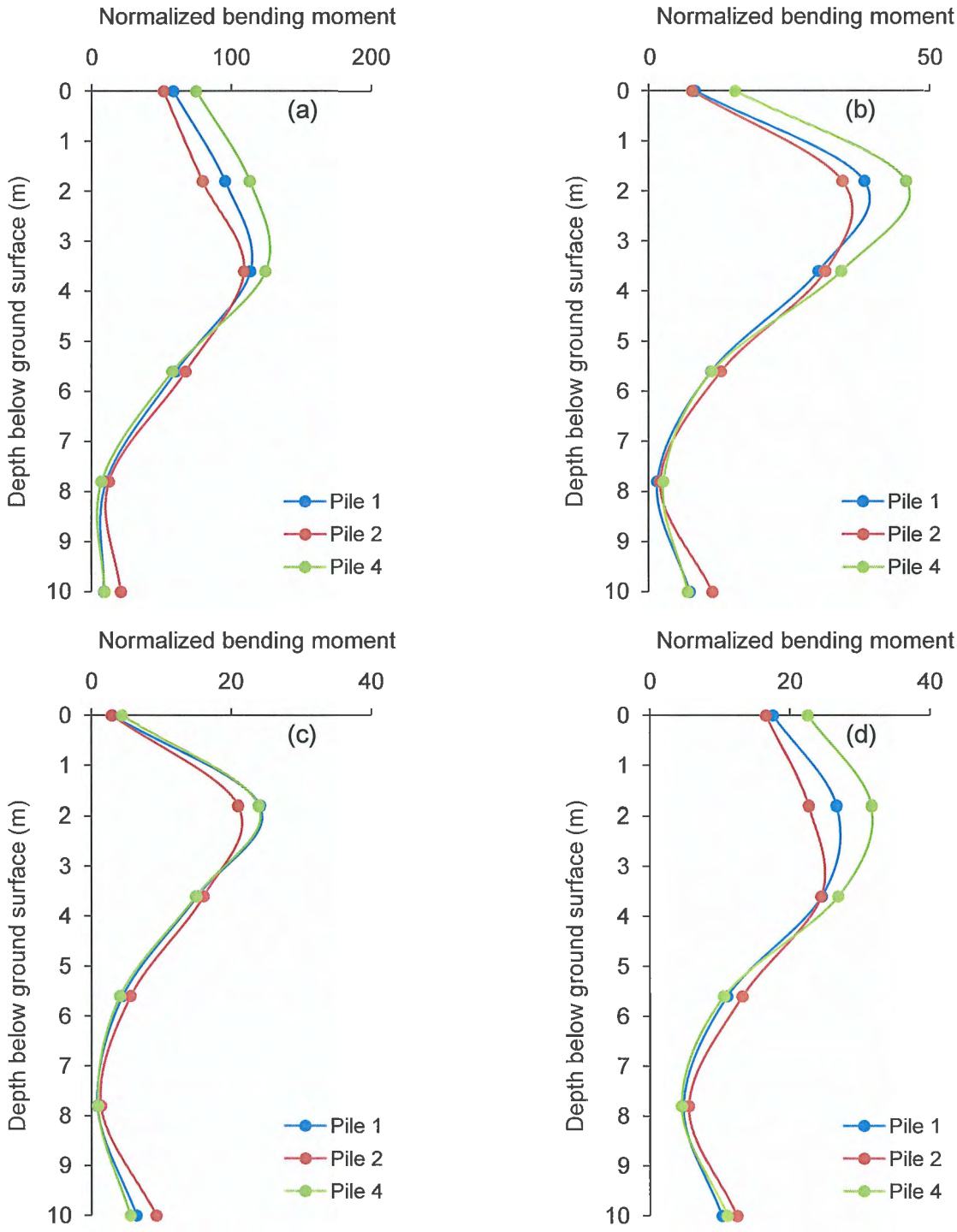

Fig. 8.29 Distributions of amplitudes of normalized bending moments of piles in a group supporting double degree of freedom structure: (a) 2.0 Hz, (b) 3.0 Hz, (c) 4.0 Hz, and (d) 7.0 Hz

To investigate the role of the frequency content of the input motion as well as the relative contributions of kinematic and inertial interactions on dynamic bending of piles, pile bending moments profiles calculated at frequencies content of input motions closed to the effective and pseudo-natural frequencies of the coupled soil-pile-structure systems (for both SDOF and DDOF structures) as well as natural frequency of the soil stratum are plotted and compared to the corresponding kinematic moments for free-head piles as shown in Figs. 8.30-8.32 for piles 1, 2, and 4, respectively.

When the frequency content of the base excitation is closed to 2 Hz as shown in Figs. 8.30 (a), 8.31 (a), and 8.32 (a), the maximum pile bending moment corresponds to the case of group pile supporting DDOF structure. In this case, SSI has a major effect on the dynamic characteristics of the structure, resulting in an effective natural frequency f_{SSI} of 2 Hz significantly lower than the first fixed base frequency of the DDOF structure (6 Hz). This case reveals the dominant role of inertial interaction in the development of bending moments of piles when the superstructure is close to resonance.

When the frequency content of the base excitation is closed to 3 Hz as shown in Figs. 8.30 (b), 8.31 (b), and 8.32 (b), the maximum pile bending moment it corresponds to the case of group pile supporting SDOF structure. In this case, SSI has also a major effect on the dynamic characteristics of the structure, resulting in an effective natural frequency f_{SSI} of 2 Hz significantly lower than the fixed base frequency of the SDOF structure (9.0 Hz). The increase of the bending of piles in a group supporting SDOF structure is associated with a significant decrease in piles bending of a group supporting DDOF structure as a result of frequency shifting from the effective natural frequency of the system (2.0 Hz) to the pseudo-natural frequency (3.0 Hz). This reduction in pile bending may be important in pile design.

For the SDOF structure, Figs. 8.30 (c), 8.31 (c), and 8.32 (c) show a substantial reduction in pile bending under the combined action of kinematic and inertial interaction when the frequency content of the input motion is closed to f_{pSSI} = 6.0 Hz. It is worth to note that, although this significant reduction, the maximum pile bending still corresponds to the group pile supporting SDOF structure.

When the frequency content of the base excitation is closed to 7.0 Hz as shown in Figs. 8.30 (d), 8.31 (d), and 8.32 (d), the pile bending moment corresponding to the free-head pile case significantly increases indicating a pronounced kinematic effect.

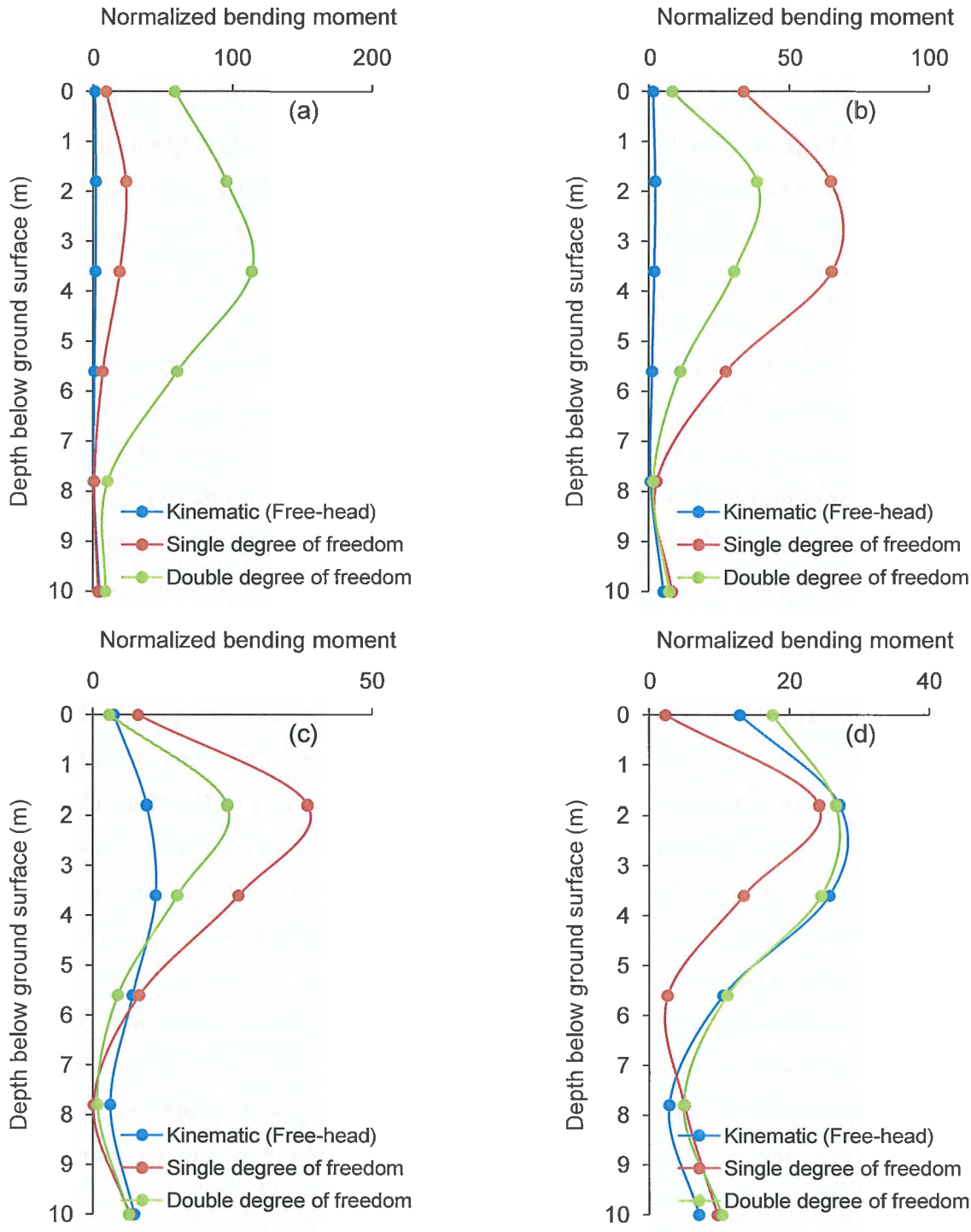

Fig. 8.30 Distributions of amplitudes of normalized bending moments of pile 1 in a group: (a) 2.0 Hz, (b) 3.0 Hz, (c) 4.0 Hz, and (d) 7.0 Hz

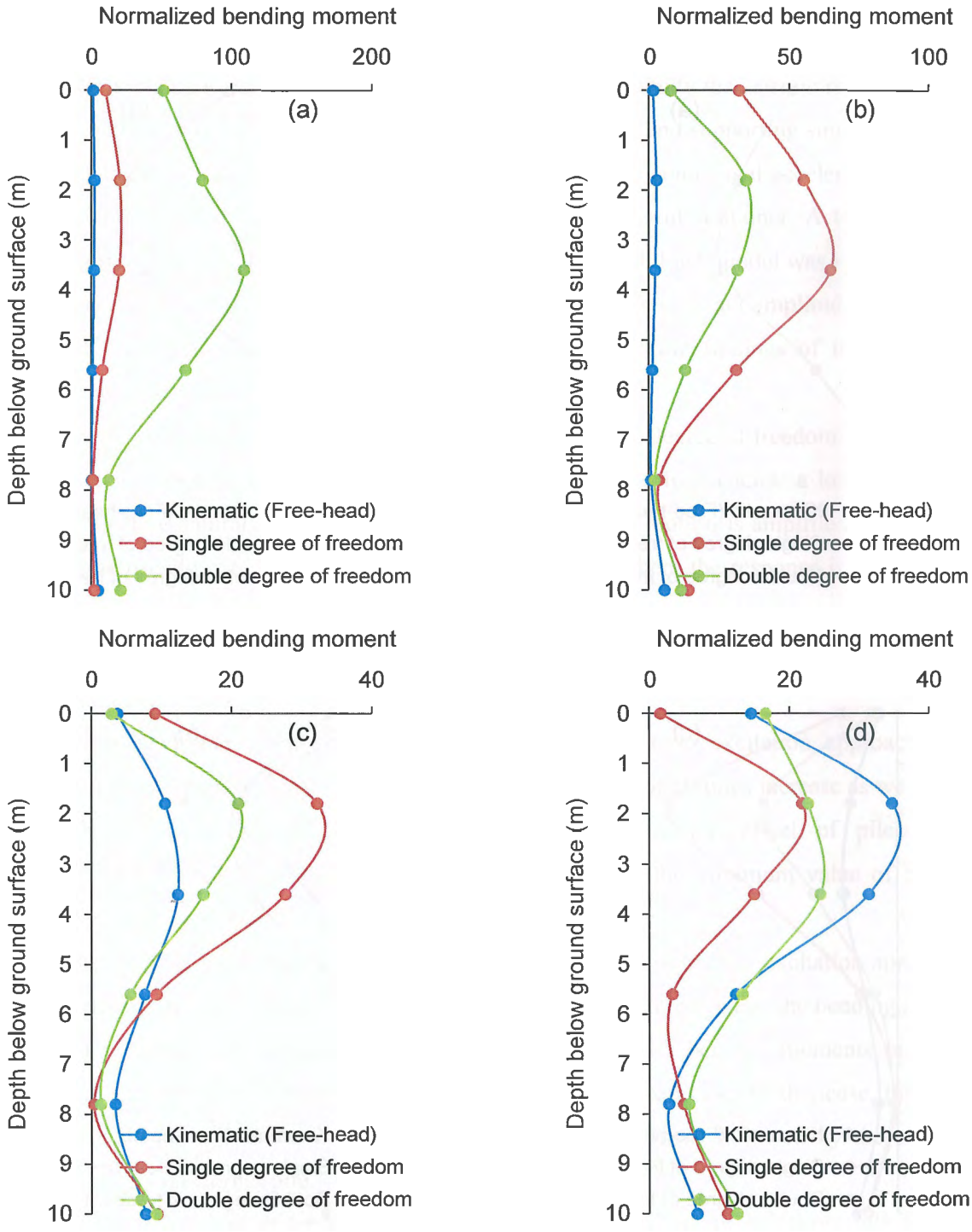

Fig. 8.31 Distributions of amplitudes of normalized bending moments of pile 2 in a group: (a) 2.0 Hz, (b) 3.0 Hz, (c) 4.0 Hz, and (d) 7.0 Hz

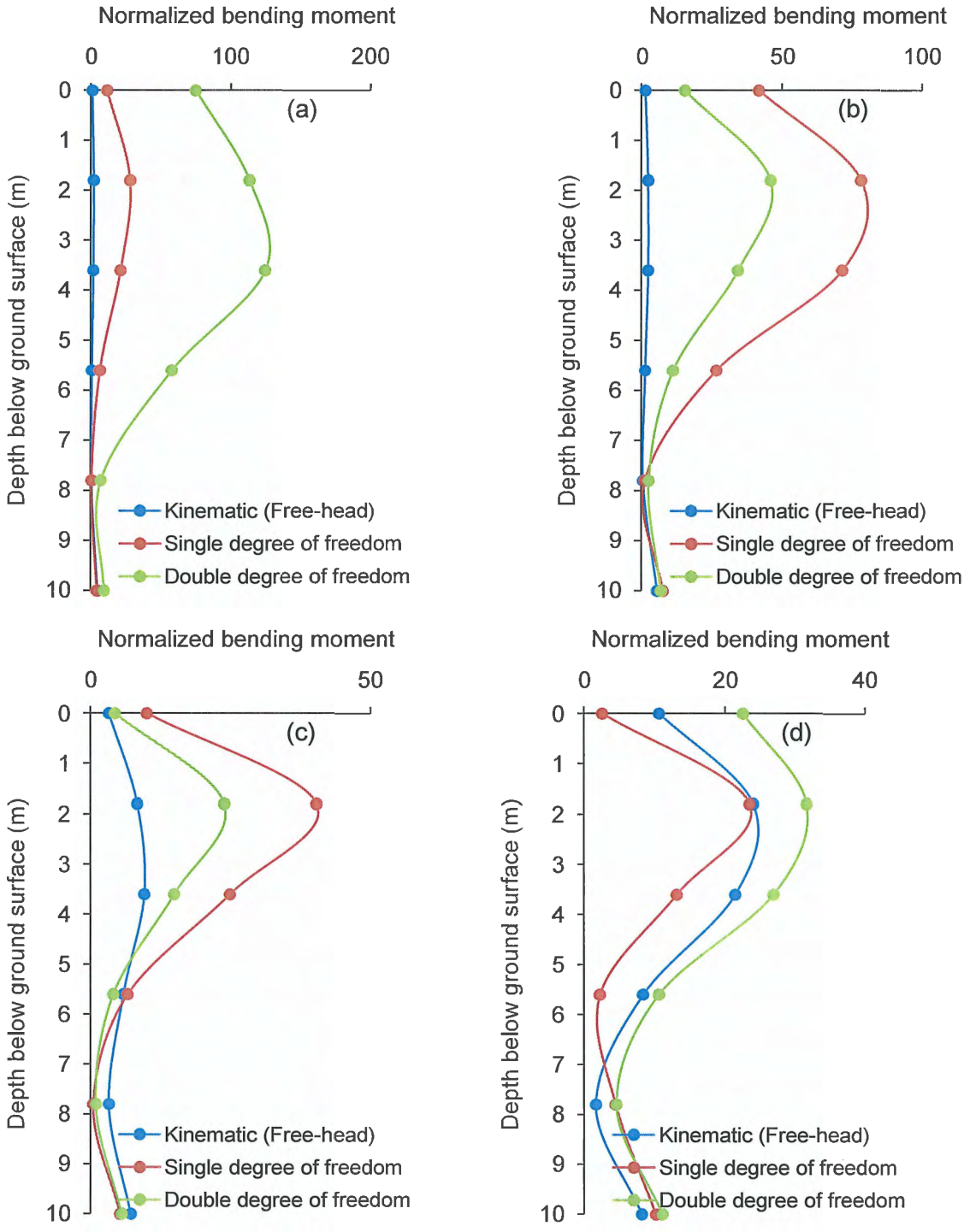

Fig. 8.32 Distributions of amplitudes of normalized bending moments of pile 4 in a group: (a) 2.0 Hz, (b) 3.0 Hz, (c) 4.0 Hz, and (d) 7.0 Hz

8.8 Conclusions

A series of systematic centrifuge tests is conducted in order to study the seismic response of end bearing single and 3×3 group piles embedded in dry sand layer and supporting single and double degree of freedom structures. All tests are conducted with the centrifugal acceleration of 40 g. Air pluviation method was used to place the dry sand in the soil container. A total of 7 tests including free-field, single and group pile cases were performed. Each model was subjected to 12 sinusoidal waves as input base accelerations. These waves have constant amplitude of about 1.5 m/s^2 and varying frequencies ranging from 1 to 12 Hz. Of the findings of this study, the following conclusions can be drawn:

1. For both single and group pile supporting a single or double degree of freedom structures, the pile-head motion is found to be dominated by two discrete frequencies: a lower frequency (the effective natural frequency (f_{SSI})) where the pile-head motion is amplified and a higher one (the pseudo-natural frequency (f_{pSSI}) of the system) where the response is suddenly de-amplified with respect to the free-field motion. These results confirm the numerical results found in the literature and generalize the finding to include group pile and higher degree of freedom structures.
2. For free-head pile group, as the frequency content of base excitation approaches the fundamental frequency of the ground, the bending moment of all piles increase as well as the difference between piles bending moments indicating strong effect of pile-soil-pile interaction. In this case, the center pile in the group has the minimum value of bending moment followed by the side pile followed by the corner pile.
3. For group piles supporting structure, as the frequency content of base excitation approaches the effective natural frequency of the coupled soil-pile-structure system, the bending moment of all piles increase as well as the difference between piles bending moments indicating strong effect of pile-soil-pile interaction. Unlike the free-head case, In this case, the center pile in the group has the maximum value of bending moment followed by the side pile followed by the corner pile.
4. For both single and group piles, Structural vibrations tend to impose large pile bending moments, when the frequency of excitation is close to the effective natural frequency of the system. On the contrary, when the input motion is close to the fundamental frequency of the ground, strong kinematic effects are mobilized and generate significant pile bending.

References

1. Iai, S., Matsunaga, Y., and Kameoka, T. 1992. Strain space plasticity model for cyclic mobility. *Soils and Foundations*, 32(2): 1–15.
2. Kavvadas, M., Gazetas, G. 1993, Kinematic seismic response and bending of free-head piles in layered soil. *Geotechnique*, 43(2), 207-22.
3. Mylonakis, G., Nikolaou, A. and Gazetas, G. 1997, Soil-pile-bridge seismic interaction: kinematic and inertial effects. PartI : Soft soil. *Earthquake Engineering and Structural Dynamics*; 26: 337 – 59.
4. Ohata, T., Uchiyama, S., Niwa, M. and Ueno, K. 1980, Earthquake response characteristics of structure with pile foundation on soft subsoil layer and its simulation analysis. *In: Proceedings of the 7th world conference on earthquake engineering.* Vol. 3. Istanbul, Turkey.
5. Rovithis, E.N., Pitilakis, K.D., Mylonakis, G.E. 2009, "Seismic analysis of coupled soil-pile-structure systems leading to the definition of a pseudo-natural SSI frequency," *Soil Dynamics and Earthquake Engineering*, 29(6), 1005-1015.

CHAPTER 9

Seismic Performance of Coupled Soil-Pile-Structure System: Parametric Study

Contents

9.1 Introduction

Chapter 8 has shown clearly using centrifuge test results that a structure founded on a deformable soil could respond differently compared to a fixed base situation. Indeed, in flexible supported case, mutual interaction between structure and adjacent soil takes place inducing modifications in the dynamic response. The design of a superstructure-foundation system for earthquake loads must take into account the effects of the foundation on the earthquake ground motion, the effect of foundation compliance on the loads experienced by the structure (*kinematic effect*), and the effects of the inertial loads imposed by the structure on the foundation (*Inertial effect*). In the past, free-field accelerations or velocities or displacements were considered as input motion for the seismic design of structures without considering the effects of kinematic interaction. However, depending on the soil profile, pile properties and dimension, and the excitation frequency, pile response may be greater than or less than the free-field response. Up to date, no tool or chart is available to calculate the vibrational characteristics of structures supported by piles embedded in deformable soil taking into account pile properties and dimensions and soil profile, and soil nonlinearity as well as the relative soil-pile stiffness or the relative stiffness of the soil and the structure.

In this chapter, linear and nonlinear seismic response of a SDOF structure supported on a single pile embedded in dry sand is parametrically studied, emphasizing on the vibrational characteristics of the soil-structure system and the dynamic bending of the pile. These series of parameter study are the base to develop simple charts for predicting linear and nonlinear seismic response of a SDOF structure supported on piles. For this reason, a fully 2D FE model of the coupled soil-pile-structure system is analyzed in the frequency domain under harmonic excitation introduced at the base of the soil profile. This chapter cover particular issues that can be summarized as follows: (a) to examine soil-pile-structure interaction in terms of the modified dynamic properties of the coupled system, (b) to investigate the combined effect of kinematic and inertial interaction on the motion of the pile-head, by identifying the fundamental frequencies that dominate the response, and (c) to develop design charts of linear and nonlinear seismic soil-pile-structure systems.

9.2 Definition of the Examined Parameters

The system under investigation as shown in Fig. 9.1 comprises of a single pile supporting a SDOF structure founded on a homogeneous dry sand layer over rigid rock.

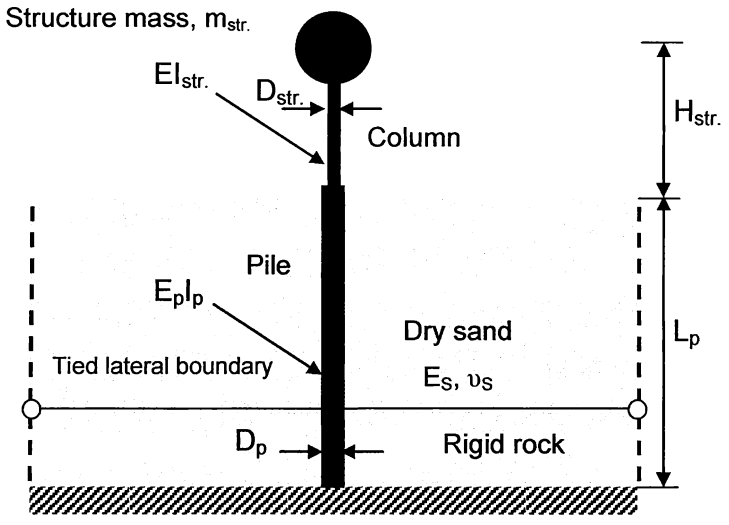

Fig. 9.1 A schematic view of the system under investigation

Due to the large number of parameters involved, the parametric analyses focus on a limited set of factors, namely the fixed-base fundamental frequency $f_{str.fixed}$, the pile slenderness ratio (L_p/D_p) and the relative initial soil-pile stiffness (E_p/E_s). The effect of these characteristics was thoroughly investigated, implementing dimensionless parameters towards a generalized description of the coupled system.

To this end, the wave parameter ($1/w.p$) (Veletsos et al. 1974):

$$\frac{1}{w.p} = \frac{f_{st.fixed}.H_{st}}{V_s} \tag{9.1}$$

which may be looked upon as a measure of the relative stiffness of the soil and the structure or, equivalently, as a normalized fundamental frequency of the structure. Obviously, higher values of parameter $1/w.p$ correspond to stiff structures on soft soil and vice versa.

For the pile, the dimensionless parameter S_H (Dobry et al. 1982):

$$S_H = (L_P / D_P)(E_P / E_S)^{-0.25} \tag{9.2}$$

was adopted as a measure of foundation flexibility. Thus, low values of S_H ($S_H < 5$) correspond to short (small L_p/D_p) and/or stiff (large E_p/E_s) piles, while long and flexible piles are characterized by higher S_H values.

9.3 Parametric Study

A total of 16 cases of coupled soil-pile-structure systems as shown in Table 9.1 were analyzed assuming linear behavior of the system. Seismic signals are imposed at very low amplitude (0.0001 m/s^2) to ensure linear-elastic soil behavior. To study the nonlinear response of the coupled system, the analyses then repeated with higher amplitudes of seismic waves. All input motion are specified at bedrock level in the form of a harmonic horizontal displacement U_g (t) $=U_g.\exp(i2\pi ft)$, where U_g = amplitude of the input bedrock displacement; f = frequency of excitation; $i^2 = -1$.

Table 9.1 Cases of coupled soil-pile-structure systems considered

Case		Soil	Pile				Structure			
		Vs (m/s)	D_p (m)	L_p/D_p	E_p/E_s	S_H	EI_{str}/EI_p	$f_{stfixed}$ (Hz)	$T_{stfixed}$ (s)	$1/w.p$
A	1	225	3	10	1000	1.78	0.1010	8.00	0.125	0.36
	2						0.0394	5.00	0.200	0.22
	3						0.0049	1.75	0.571	0.08
	4						0.0009	0.75	1.333	0.03
B	1	225	1.5	20	1000	3.56	1.620	8.00	0.125	0.36
	2						0.630	5.00	0.200	0.22
	3						0.078	1.75	0.571	0.08
	4						0.014	0.75	1.333	0.03
C	1	225	1.5	20	500	4.23	3.240	8.00	0.125	0.36
	2						1.261	5.00	0.200	0.22
	3						0.312	1.75	0.571	0.08
	4						0.056	0.75	1.333	0.03
D	1	225	1.5	20	100	6.32	16.20	8.00	0.125	0.36
	2						6.300	5.00	0.200	0.22
	3						1.560	1.75	0.571	0.08
	4						0.285	0.75	1.333	0.03

9.4 Finite Elements and Parameters Identification

The 2D effective stress FE analysis, FLIP (Iai et al. 1992), has been used to analyze the seismic soil-pile-structure interaction (SSPSI) problem. A 30 (m) thick soil stratum was meshed with quad plane elements. The length of each element was adequately defined according to the anticipated wavelength propagating in the soil. The maximum element size, E_{max}, was less than one-fifth to one-eighth the shortest wavelength (λ) to ensure accuracy (Kramer 1996).

The FE analyses were performed in two stages. In the first stage (self-weight analysis), the *in-situ* stresses were initialized in the soil due to the own weight of the soil. Properties of pile and soil-pile interaction spring were set to be zero during this stage of analysis. During the second stage of analysis (seismic response analysis), the actual properties of soil, pile, and soil-pile interaction spring were assigned. The total mesh size was extended to a horizontal distance from the pile of 30-pile diameter to prevent spurious wave reflections at the boundaries. Moreover, tied lateral boundary approach (a simpler alternative to the boundary approach suggested by Zienkiewicz et al. (1988) that illustrated in Fig. 9.1. is used in the analysis. In this approach, the values of displacements, stresses, etc. are identical on both side boundaries. This condition is explicitly imposed in FLIP by an equivalent node concept (MPC).

9.4.1 Soil model

The soil model used in this study consists of a multiple shear mechanism (Iai et al. 1992). Details of this model are given in Chapter 3. Parameters for dry sand used in the current FE analysis are shown in Table 9.2. The bulk modulus of the soil skeleton K was determined assuming a Poisson's ratio υ of 0.33. The initial shear wave velocity (Vs) is calculated using:

Table 9.2 Model parameters for soil elements

Density, ρ_t (t/m^3)	G_{ma} (kPa)	υ	σ'_{ma} (kPa)	ϕ_f	H_{max}
1.55	84,500	0.33	98	39.67	0.24

$$V_s = (G_{ma} / \rho_s)^{0.5} \tag{9.3}$$

and found to be = 225 m/s. The parameter m_G that controls the shear modulus distribution with the depth is kept equal to 0.5 for both linear and non-linear analyses.

9.4.2 Pile column system

Bilinear beam elements with three degrees of freedom per node are used for modeling pile and column. Normal force, shear force, and bending moment of each element are obtained directly. It is assumed that both the pile and the column have a circular cross-section of diameter depend on the case under consideration as shown in Table 9.1. The Pile length is assumed to be equal to the thickness of the soil stratum (L_p = 30 m). The elastic properties of both pile and column are related to that of the soil as shown in Table 9.1. The mass density and Poisson's ratio for pile and column were considered 2.5 kg/m^3 and 0.3, respectively.

To minimize the number of parameters, structural mass ($m_{str.}$) and height ($H_{str.}$) were kept equal to 100 Mg and 10 m, respectively.

9.5 Numerical Results: Linear analyses

9.5.1 Free-field response

The first step in any SSI seismic analysis is the evaluation of the free-field response of the soil layer. Elastic response time histories for free-field were derived at different frequencies of excitations. From these time histories, the amplitude of steady-state response is noted and normalized with respect to the amplitude of input bedrock motion. Thus amplification of soil stratum is plotted in Fig. 9.2. From this figure, the first and the second fundamental frequencies of the soil layer are 2.25 and 6.0 Hz, respectively.

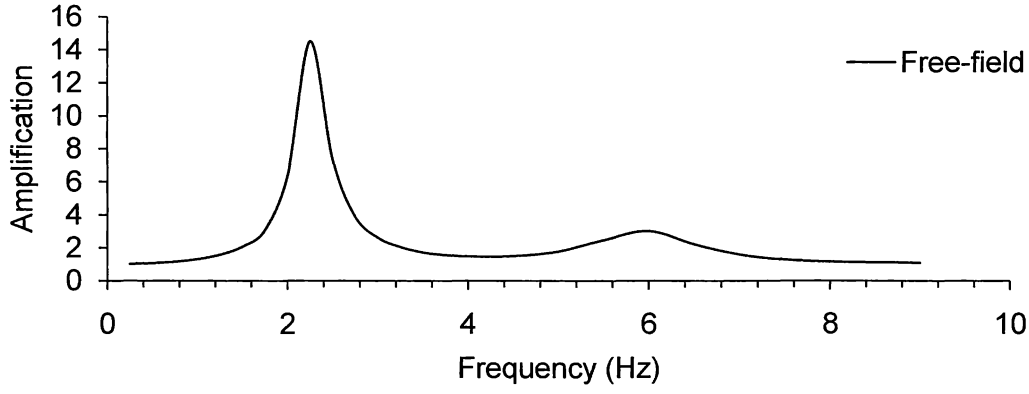

Fig. 9.2 Free-field response

9.5.2 Kinematic soil-pile interaction analysis

As it well known, a cylindrical pile diffracts the incident and reflected 1D vertical S-waves, thereby modifying the "free" wave field forming what we call kinematic interaction. This effect can be assesses using translation and rotational kinematic interaction factors I_u and I_ϕ, respectively. These interaction factors depend on many factors such as relative stiffness between the pile and soil (S_H value) and pile-head fixation condition. The influence of foundation flexibility on kinematic interaction factors for both fixed and free-head conditions is portrayed in Fig. 9.3. Figure 9.3 declares that, in the normalized frequency range studied (a_o = 0 - 0.42), the filtering by a pile of the high frequency components of the base excitation may be substantially greater with lower values of S_H for both free and fixed-head conditions. At high frequency components of the base excitation, the rotational components of motion decrease with lower value of S_H.

9.5.3 Coupled soil-pile-structure analysis

A concentrated mass attached to the structural column was introduced to the model, and the dynamic response of the coupled soil-pile-structure system was parametrically studied. The ensuing parametric investigations aim at evaluating the pile-head to free-field horizontal displacement (U_p/U_{ff}), the effective and the pseudo-effective natural frequencies of the system, and the relative contribution of kinematic and inertial interaction to the pile bending.

9.5.3.1 Pile head response under the combined action of kinematic and inertial interactions

Similar to Fig. 9.3, the influence of foundation flexibility (S_H) on pile-head to free-field horizontal displacement (U_p/U_{ff}) is portrayed in Figs. 9.4 (a) - (d) for different values of ($1/w.p$) of 0.36, 0.22, 0.08, and 0.03. For ($1/w.p$ = 0.25) as shown in Fig. 9.4 (b), the maximum amplification increases as S_H decreases (i.e. pile become stiffer). For ($1/w.p$ = 0.36) as shown in Fig. 9.4 (a), and for the case of (S_H = 1.78), a reduction in amplification is observed. This case corresponds to stiff structure founded on a stiff or short pile. For lower values of ($1/w.p$ = 0.03), the effect of S_H on the pile-head motion is not significant. The inertial interaction is most pronounced at higher values of $1/w.p$.

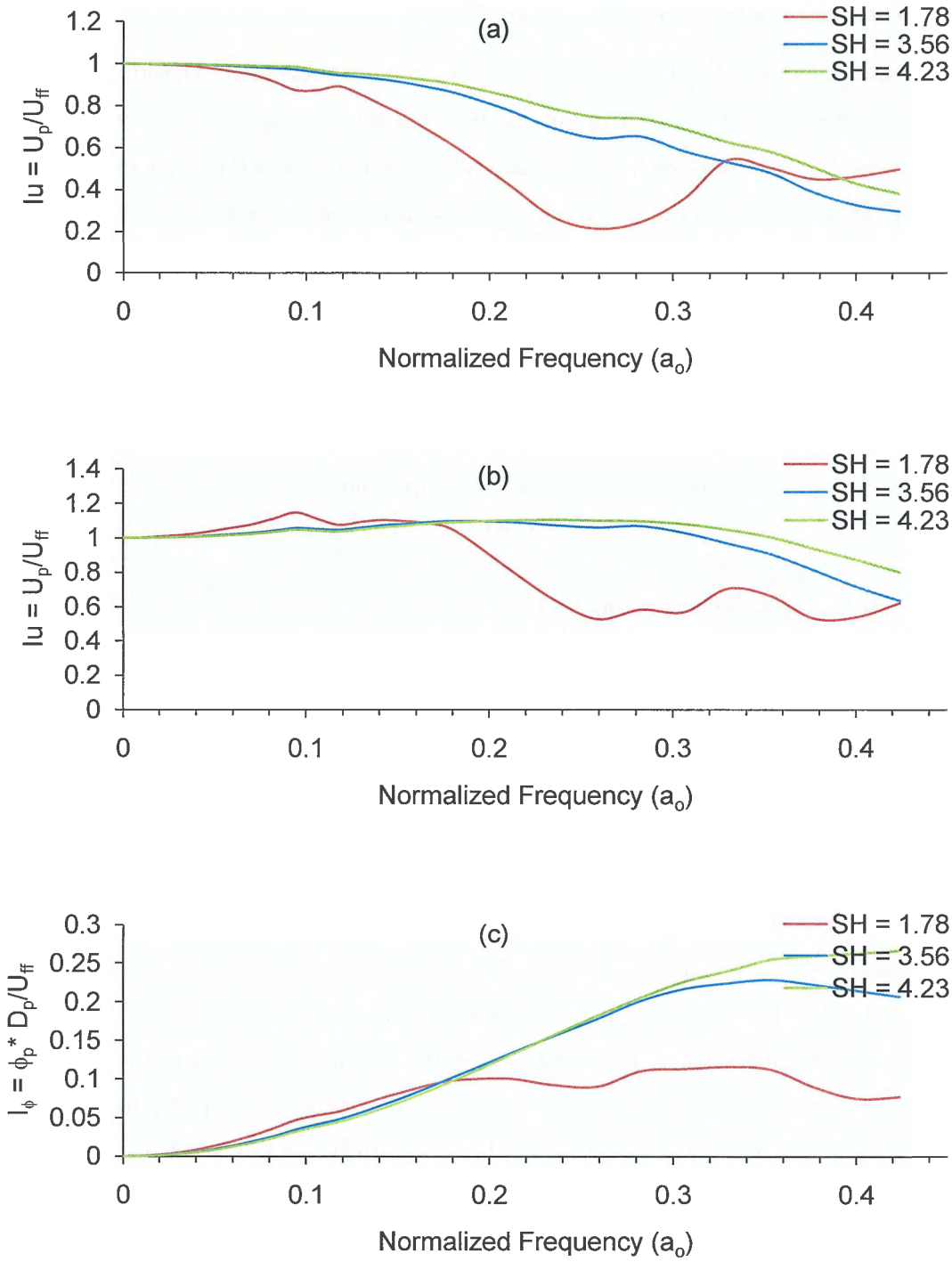

Fig. 9.3 Effect on the foundation flexibility: (a) I_u (Fixed-head); (b) I_u (free-head); and (c) I_ϕ (free head)

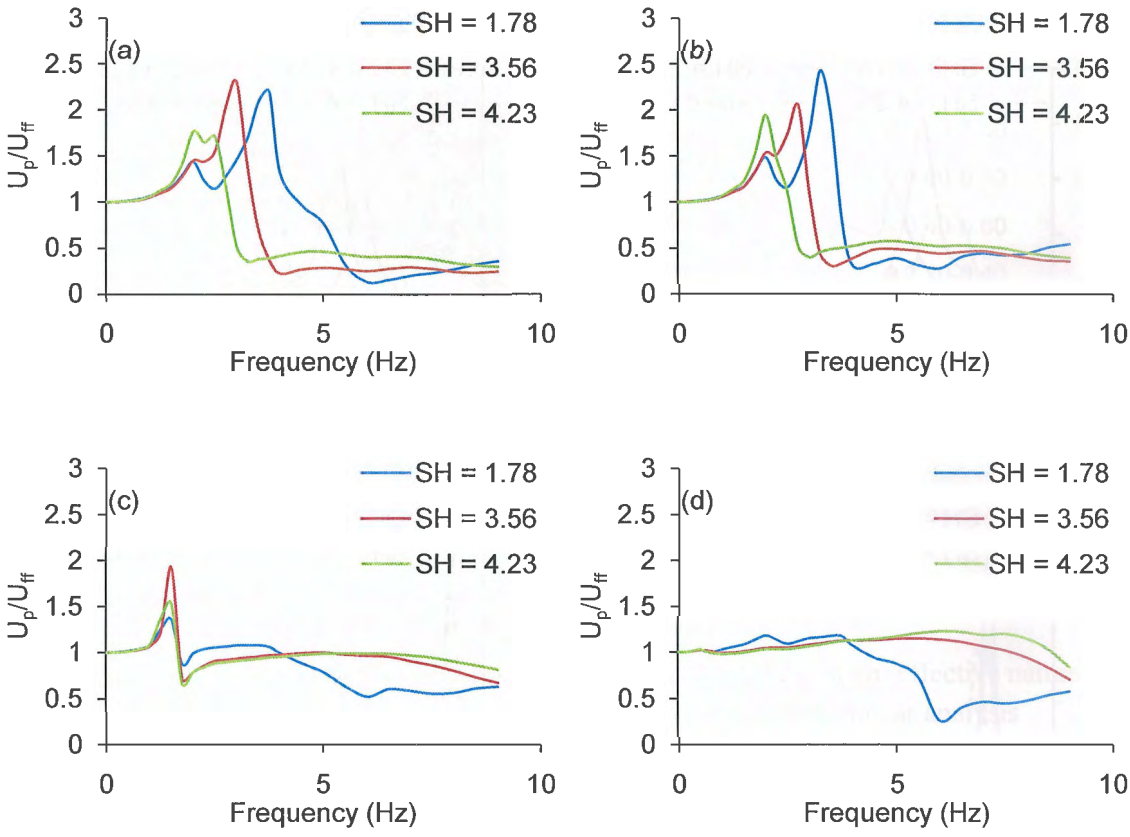

Fig. 9.4 Pile-head to free-field displacement response of the coupled system for: (a) $1/w.p$ = 0.36, (b) $1/w.p$ = 0.22, (c) $1/w.p$ = 0.08, and (d) $1/w.p$ = 0.03

9.5.3.2 Effective natural frequency of the coupled system

As we see in the Chapters 6 and 8, the effective natural frequency of the coupled soil-pile-structure system can be defined as the frequency at which the structure displacement is maximized relative to the free-field displacement. The effect of (S_H) on structure to free-field horizontal displacement (U_s/U_{ff}) is shown in Figs. 9.5 (a) - (d) for different values of ($1/w.p$) of 0.36, 0.22, 0.08, and 0.03. For ($1/w.p$ = 0.36 and 0.25) as shown in Figs. 9.5 (a) and (b), a significant reduction of the natural frequency of the structure is observed. The percentage of reduction in the natural frequency of the structure increases with the increase of S_H. For lower values of $1/w.p$ as shown in Figs. 9.5 (c) and (d), the reduction of the natural frequency is not significant.

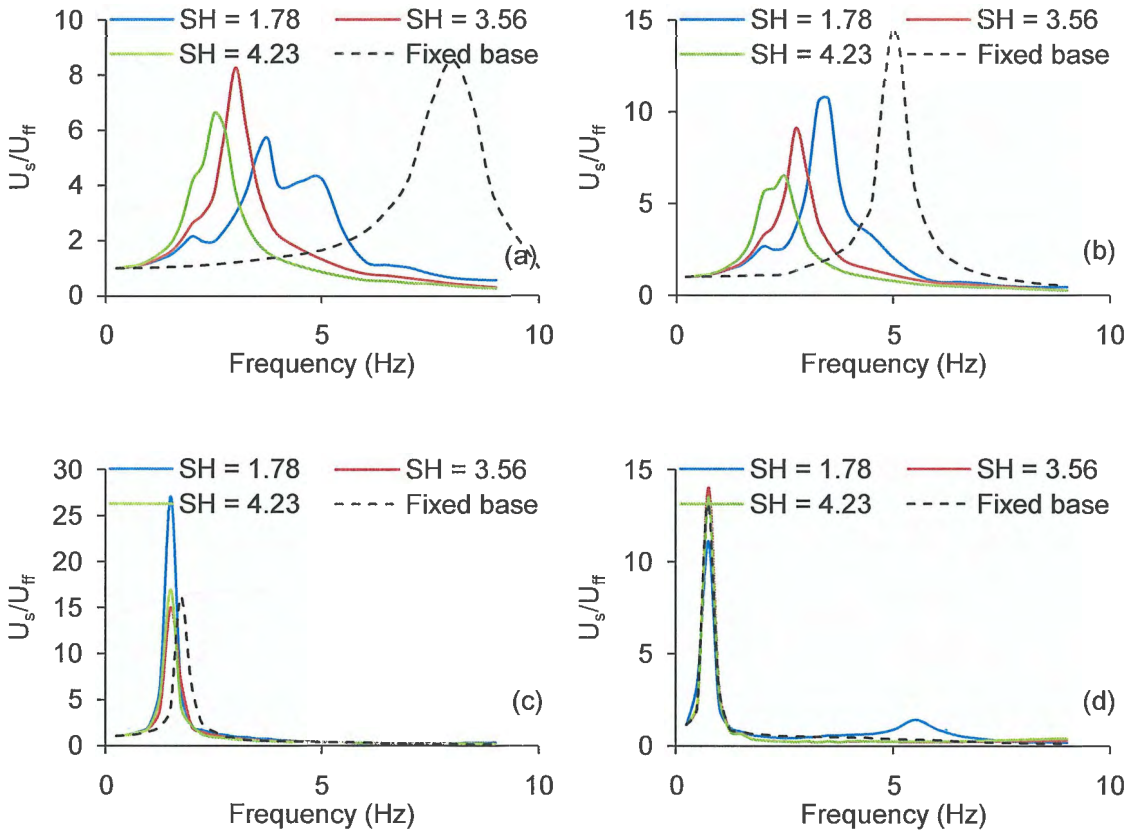

Fig. 9.5 Structure to free-field displacement response of the coupled system for: (a) $1/w.p$ = 0.36, (b) $1/w.p$ = 0.22, (c) $1/w.p$ = 0.08, and (d) $1/w.p$ = 0.03

The ratio of the effective natural frequency of the coupled system to the fixed base frequency of the structure ($f_{SSI}/f_{str.fixed}$) is plotted against both ($1/w.p$) and (S_H) in Fig. 9.6. Soil-structure interaction effects are stronger for higher levels of relative soil-structure stiffness (i.e., higher values of $1/w.p$), resulting in a significant reduction of the effective natural frequency f_{SSI} with respect to the natural frequency of the structure under fixed-base conditions ($f_{str.fixed}$). For these cases, SSI effects are controlled primarily by the structural properties of the pile (parameter S_H). More specifically, it is observed that increasing the flexibility or slenderness of the pile results in lower values of the effective frequency f_{SSI} of the system, which implies a stronger soil-structure interaction effect. On the contrary, for low values of parameter $1/\sigma$ (0.08–0.03), soil-structure interaction has a minor effect on the vibrational characteristics of the structure, regardless of the adopted SH parameter.

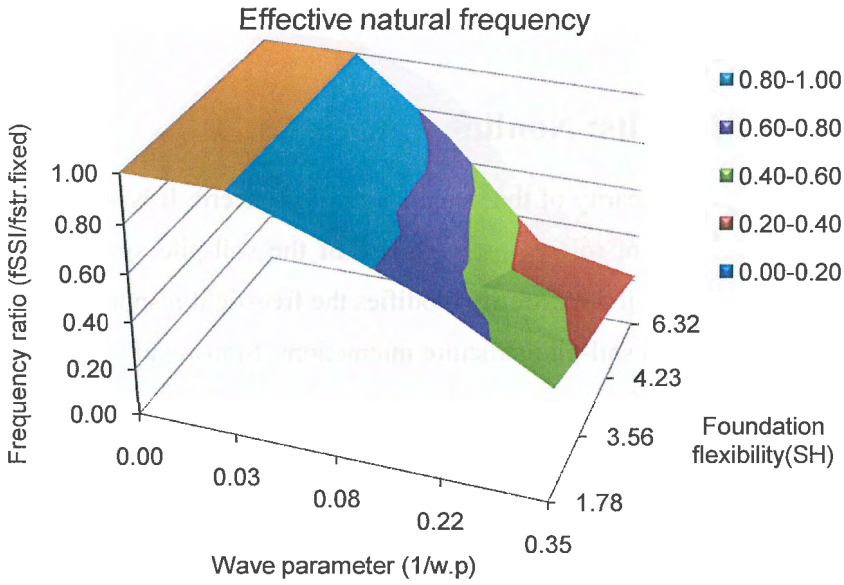

Fig. 9.6 Effect of SSI on the vibrational characteristics of the system: effective natural frequency against the fixed base frequency of the structure; linear analysis

9.5.3.3 Pseudo-effective frequency of the coupled system

As we see in the Chapters 6 and 8, the pseudo-effective natural frequency of the coupled soil-pile-structure system can be defined as the frequency at which the structure displacement is minimized relative to the pile-head displacement. The effect of (S_H) on structure to pile-head horizontal displacement (U_s/U_p) is shown in Figs. 9.7 (a) - (d) for different values of ($1/w.p$) of 0.36, 0.22, 0.08, and 0.03. For ($1/w.p$ = 0.36 and 0.25) as shown in Figs. 9.7 (a) and (b), the pseudo-effective frequency (f_{pSSI}) increases with the decrease of S_H. For lower values of $1/w.p$ as shown in Figs. 9.7 (c) and (d), f_{pSSI} is closed to the fixed base fundamental frequency of the structure.

The ratio of the pseudo-effective frequency of the coupled system to the fixed base frequency of the structure ($f_{pSSI}/f_{str.fixed}$) is plotted against both ($1/w.p$) and (S_H) in Fig. 9.8. For higher values of $1/w.p$ and S_H, a significant reduction of the effective natural frequency f_{pSSI} with respect to the natural frequency of the structure under fixed-base conditions ($f_{str.fixed}$) is observed. More specifically, it is observed that increasing the flexibility or slenderness of the pile results in lower values of the pseudo-effective frequency f_{pSSI} of the system; on the contrary, for low

values of parameter $1/\sigma$ (0.08–0.03), f_{pSSI} approaches the fixed base fundamental frequency of the structure, regardless of the adopted S_H parameter.

9.6 Numerical Results: Nonlinear analyses

The effects of material nonlinearity of the soil are a major concern. It is anticipated that the soil nonlinearity plays a significant role in the response of the soil-pile system. In the following sections, it is observed how soil nonlinearity modifies the free-field response, kinematic soil-pile interaction, as well as coupled soil-pile-structure interactions. Sinusoidal waves of unit amplitude (1.0 m/s^2) and varying frequency are used in these cases.

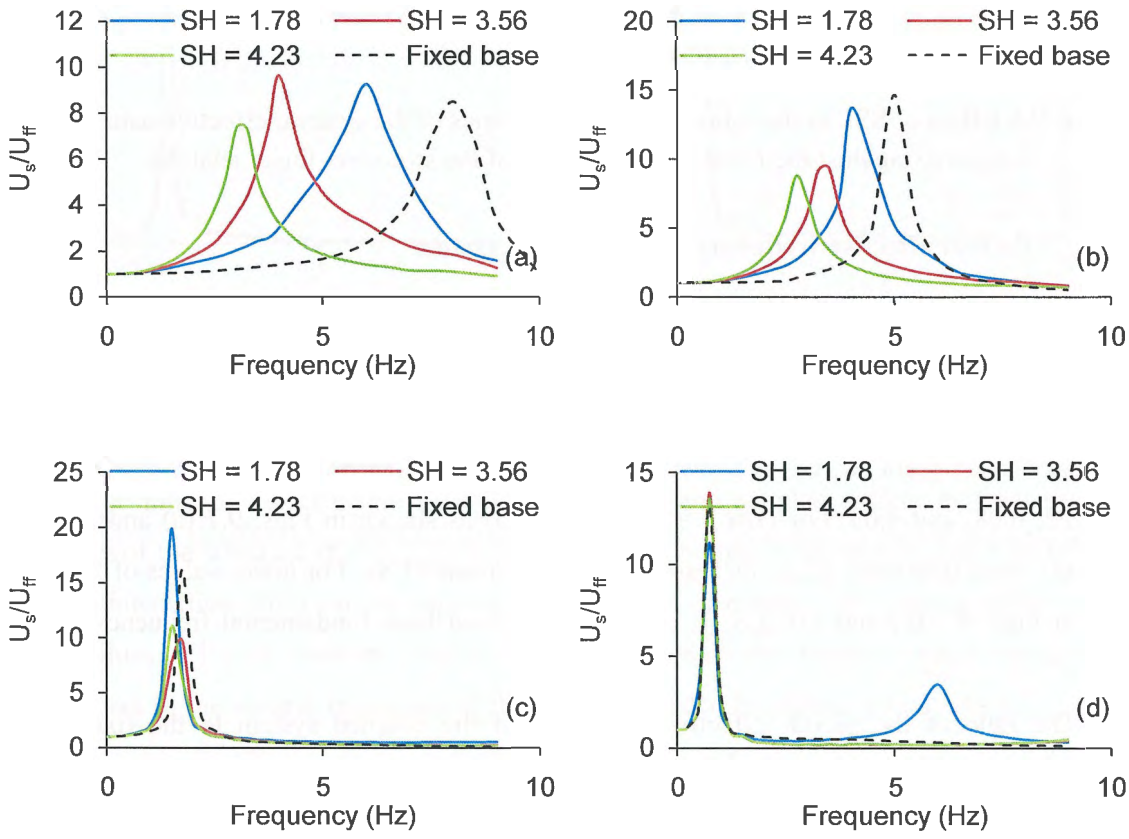

Fig. 9.7 Structure to pile-head displacement response of the coupled system for: (a) $1/w.p$ = 0.36, (b) $1/w.p$ = 0.22, (c) $1/w.p$ = 0.08, and (d) $1/w.p$ = 0.03

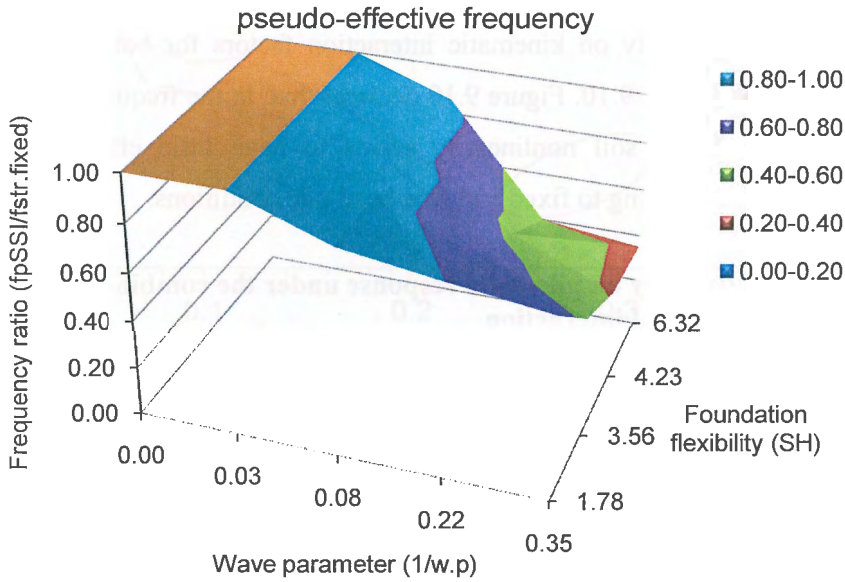

Fig. 9.8 Effect of SSI on the vibrational characteristics of the system: pseudo-effective frequency against the fixed base frequency of the structure; linear analysis

9.6.1 Effects of nonlinearity on free-field response

Figure 9.9 shows the effect of soil nonlinearity on the free-field response. Figure 9.9 shows the fundamental periods lengthening due to soil nonlinearity as well as the substantial reduction in the peak amplification accompanied with the period lengthening.

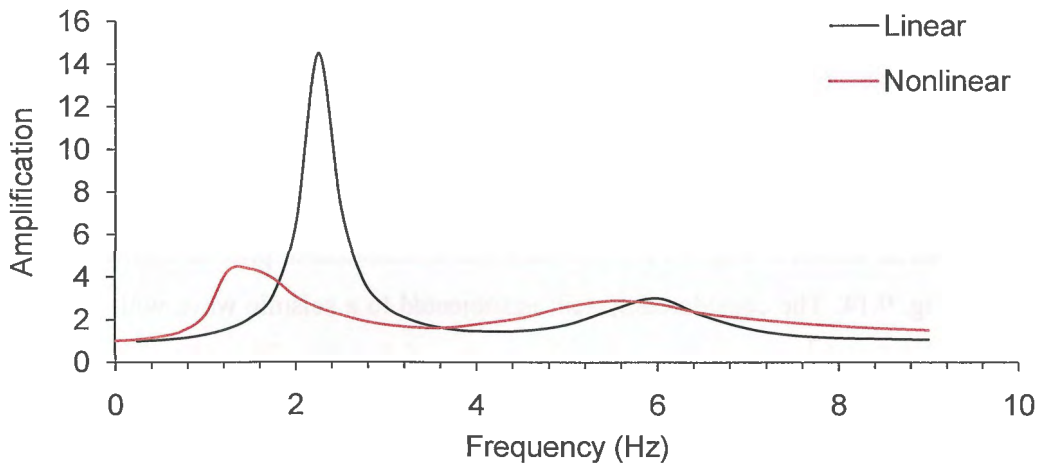

Fig. 9.9 Effect of nonlinearity on the free-field response at different frequency

9.6.2 Effects of nonlinearity on kinematic soil-pile interaction analysis

The effect of soil nonlinearity on kinematic interaction factors for both fixed and free-head conditions is portrayed in Fig. 9.10. Figure 9.10 declares that, in the frequency range studied (f = 0.25-9.0 Hz), the effect of soil nonlinearity seems to have little effect on the kinematic interaction factors corresponding to fixed and free-head pile conditions.

9.6.3 Effects of nonlinearity on pile-head response under the combined action of kinematic and inertial interaction

The influence of S_H on pile-head to free-field horizontal displacement (U_p/U_{ff}) in nonlinear case is portrayed in Figs. 9.11 (a) - (d) for different values of ($1/w.p$) of 0.36, 0.22, 0.08, and 0.03. Similar to the linear case, the effect of S_H is significant at higher $1/w.p$ values as shown in Fig 9.11 (a) and (b). A significant reduction in the amplification ratio is observed due to soil nonlinearity.

9.6.4 Effects of nonlinearity on effective and pseudo-effective frequencies of the coupled system

The ratios of the effective and pseudo-effective frequencies of the coupled system to the fixed base frequency of the structure ($f_{SSI}/f_{str.fixed}$ and $f_{pSSI}/f_{str.fixed}$) are plotted against both ($1/w.p$) and (S_H) as shown in Figs. 9.12 and 9.13. These figures indicate that the frequency ratios ($f_{SSI}/f_{str.fixed}$ and $f_{pSSI}/f_{str.fixed}$) become smaller for larger wave parameter and larger foundation flexibility. Compared to Figs 9.6 and 9.8, Figs. 9.12 and 9.13 indicate that the nonlinearity of the ground induces larger reduction in frequency ratio.

9.7 An example problem

To show how charts presented in this chapter can be used in a practical way, a numerical example is given as shown in Fig. 9.14. Properties and dimensions of pile, structure, and soil are given in also Fig. 9.14. The considered system is subjected to a seismic wave with peak ground acceleration of 1.0 m/s^2 and predominant frequency of 2.0 Hz. The effective and pseudo effective natural frequencies as well as pile head displacement can be estimated based on charts given in this chapter as follows:

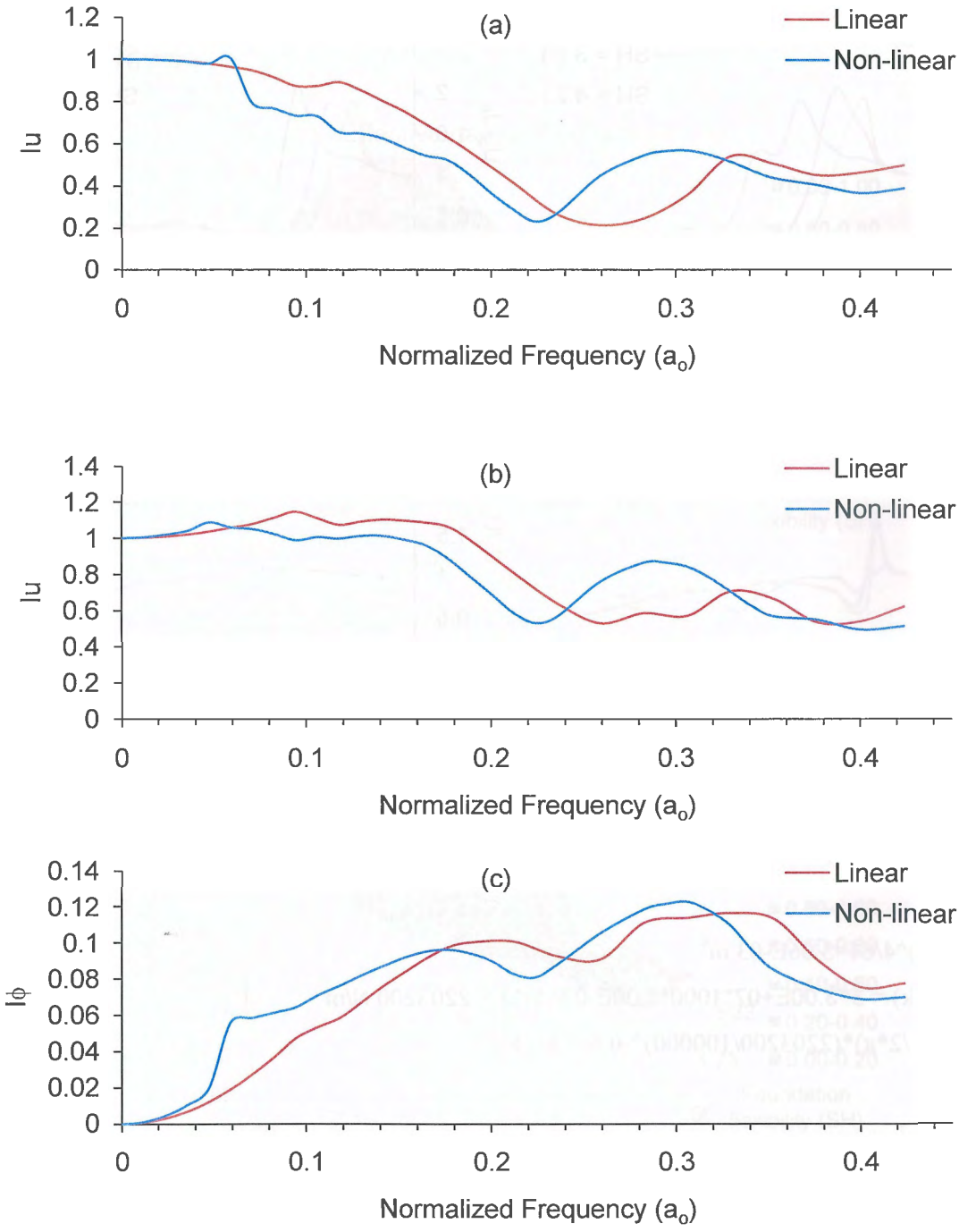

Fig. 9.9 Effect of nonlinearity on kinematic interaction factors: (a) I_u (Fixed-head); (b) I_u (free-head); and (c) I_ϕ (free head)

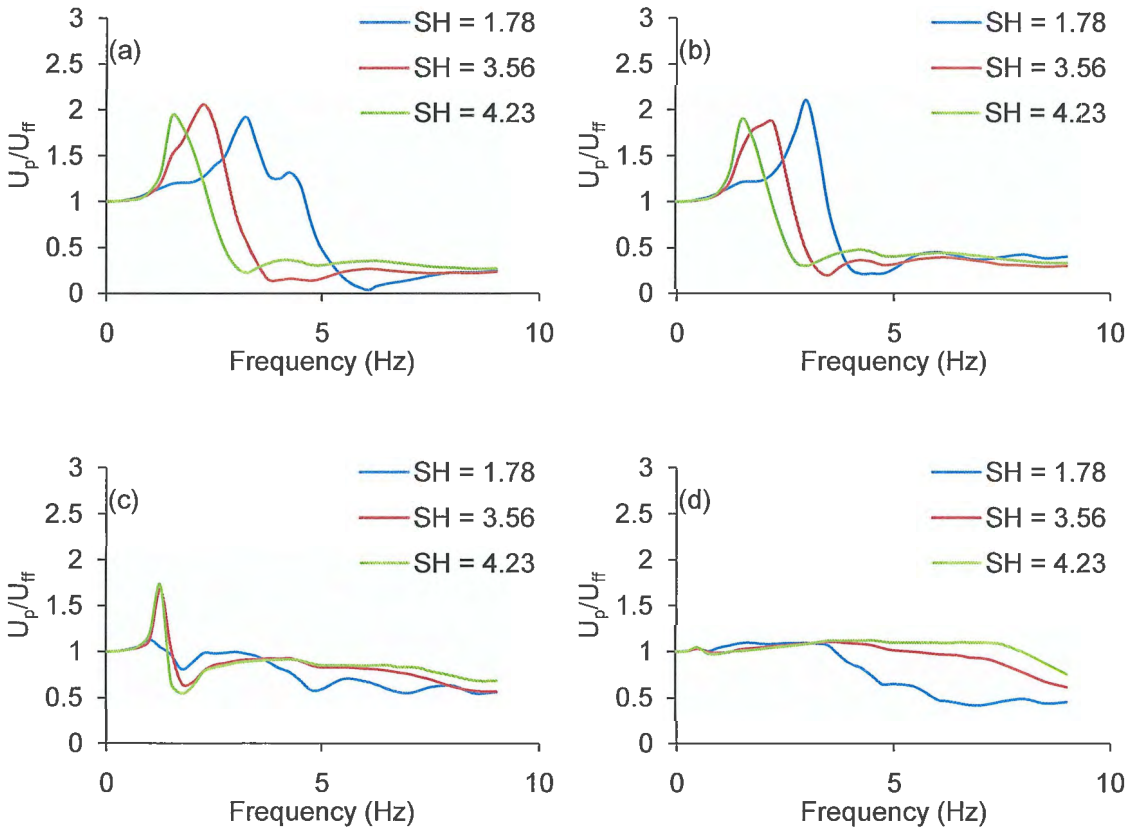

Fig. 9.11Pile-head to free-field displacement non-linear response of the coupled system for: (a) $1/w.p = 0.36$, (b) $1/w.p = 0.22$, (c) $1/w.p = 0.08$, and (d) $1/w.p = 0.03$

Structure:

I = π*(0.5)^4/64=3.06E-03 m^4

Stiffness (k) = 3*3.00E+07*1000*3.06E-03/(5)^3 = 2203200 N/m

$f_{st.\ fixed}$ = (1/2*π)*(2203200/100000)^-0.5 = 3.5 Hz

Dimensionless parameters:

Wave parameter (*1/w.p*) = (3.5*5.0/200) = 0.08

SH parameter = (12.5/1)*(3.00E+07/2.00E+05) ^-0.25 = 3.57

Using these values and from charts given in Figs. 9.12 and 9.13, the effective and pseudo effective natural frequencies could be estimated as follows:

$f_{SSI} = 3.5 * 0.8 = 2.8$ Hz

$f_{pSSI} = 3.5 * 0.9 = 3.15$ Hz

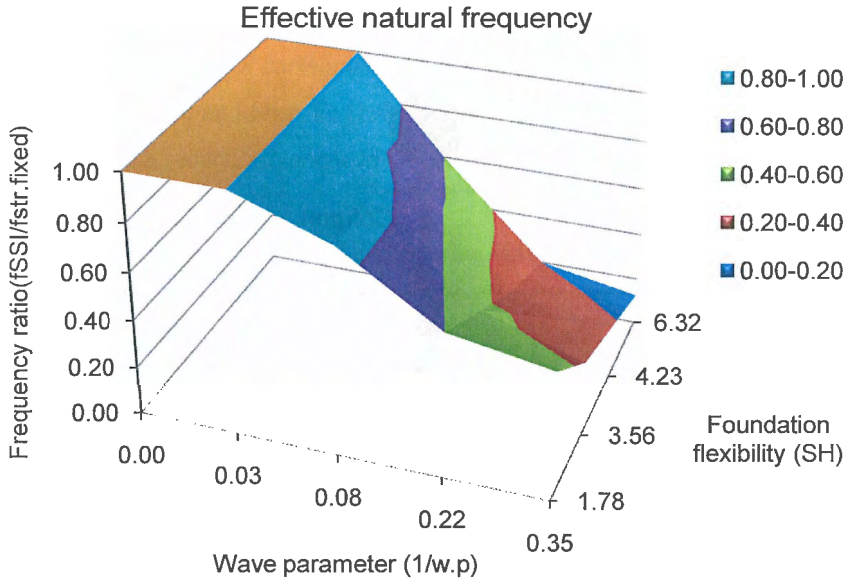

Fig. 9.12 Effect of SSI on the vibrational characteristics of the system: effective natural frequency against the fixed base frequency of the structure, nonlinear analysis

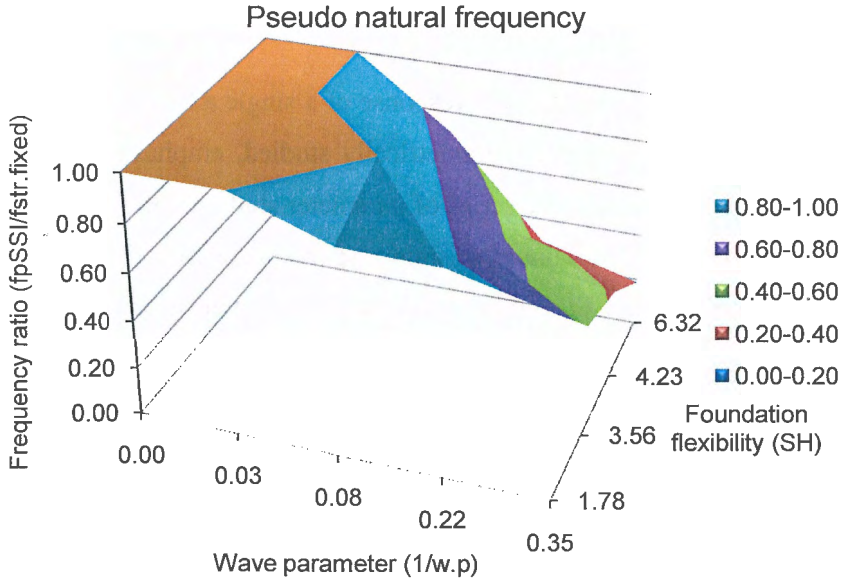

Fig. 9.13 Effect of SSI on the vibrational characteristics of the nonlinear system: pseudo-effective frequency against the fixed base frequency of the structure, nonlinear analysis

Based on the values of (1/w.p = 0.08) and SH = 3.57, Fig. 9.11(c) will be used to determine pile-head displacement relative to free-field displacement. At predominant frequency of input motion of 2.0 Hz, U_p/U_{ff} will be 0.68.

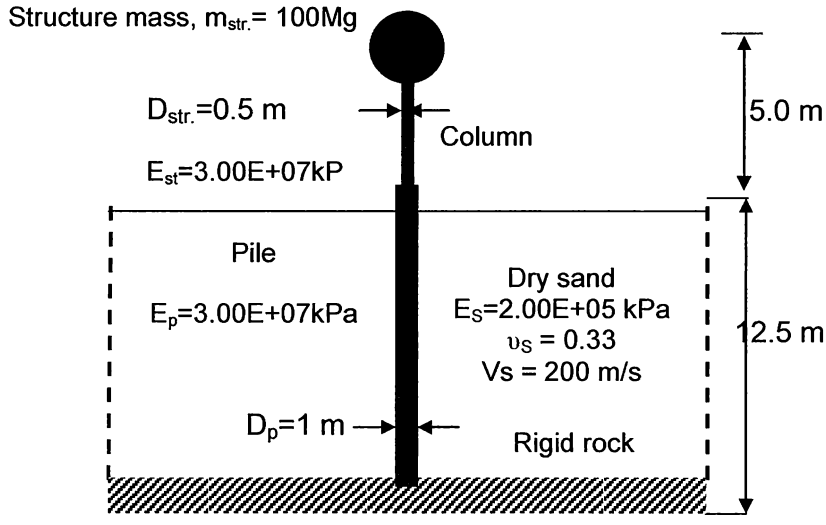

Fig. 9.14 An example problem

9.8 Conclusions

In this chapter linear and non-linear seismic response of a single a SDOF structure supported on a single pile embedded in dry sand is parametrically studied, emphasizing on the vibrational characteristics of the SSI system. These series of parameter study are the base to develop simple charts for predicting linear and nonlinear seismic response of a SDOF structure supported on piles. For this reason, a fully 2D FE model of the coupled system is analyzed in the frequency domain under harmonic excitation introduced at the base of the soil profile. The following conclusions can be drawn:

1. Strong soil-structure interaction effects were observed for coupled systems that comprise of stiff superstructures founded on flexible and/or long piles, leading to significant reductions in effective natural frequency of the system.
2. The nonlinearity of the ground induces larger reduction in frequency ratio.

References

1. Iai, S., Matsunaga, Y., and Kameoka, T. 1992. Strain space plasticity model for cyclic mobility. *Soils and Foundations*, 32(2): 1–15.
2. Dobry, R., Vicente, E., O'Rourke, M. J., and Roesset, J. M., 1982, Horizontal stiffness and damping of single piles, *Journal of the Geotechnical Engineering Division*, ASCE, 108 (3): 439–459.
3. Kramer, S.L.,(1996) *Geotechnical earthquake engineering*. Prentice Hall inc. Englewood Cliffs, N.J.
4. Zienkiewicz, O., Bicanic, N. and Shen, F., (1988) Earthquake input definition and the transmitting boundary conditions. In Doltsinis, I. S., editor, *Advances in Computational Nonlinear Mechanics*, Springer-Verlag, 109–138.
5. Gazetas, G. (1984), "Seismic response of end bearing single piles," Soil Dynamics and Earthquake Engineering, 3(2), 82–93.

CHAPTER 10

Conclusions

Contents

10.1 Summary

In the preceding chapters we have investigated various aspects SSI and their effects of the lateral behavior of piles. Even if this problem has been the subject of numerous investigations, the previous studies currently face the following three problems: (1) Level of loadings assumed for the previous study and existing design practice is often for the condition of moderate strain level induced in the ground. Lateral behavior of piles at extensive non-linearity induced in the ground, such as for liquefaction or soil-pile gap formation, as encountered in recent strong earthquakes, is not fully studied, (2) In the conventional study, the lateral behavior of piles has been studied independently from the vertical resistance of piles. Interaction between the lateral and vertical loads is not fully studied, (3) in the seismic loading condition, soil-pile-structure interaction becomes the primary mechanism for lateral behavior of piles. The previous studies on the soil-pile interaction are limited for evaluating the effects of resonant frequencies of soil, structure, and pile. The effect of input frequency on soil-pile-structure interaction is not fully studied.

The major goal of this thesis was to advance the knowledge and understanding on the above mentioned three issues. This study presents the most recent results for lateral behavior of piles through numerical analyses and centrifuge model tests. The study is systematically performed from the most fundamental single pile to group piles, and from the most fundamental loading condition for applying the static and dynamic load at pile heads to dynamic response of soil-pile-structure system.

10.2 Overall Conclusions

In Chapter 3, recent developments on the soil-pile interaction in horizontal plane are presented. The primary conclusions from this chapter may be summarized as follows:

1. Local displacement field of soil in the vicinity of a pile associated with global displacement of soil around pile foundation shows vortexes at the pile side. Displacement at the pile side shows strain localization at the soil-pile interface, indicating a mechanism similar to a sliding. This fact implies that the finite element mesh size should be sufficiently small in the vicinity of the pile in order to represent these essential features of the local displacement field.

2. Computed local displacement field of soil through a multiple shear mechanism model in a horizontal plane are basically consistent with those measured. The computed load-displacement curves indicates that, for dry sand, the curves have similar shapes to those currently used in design practice in terms of *p-y* curve.
3. Although the mechanisms involved in the load displacement curve are the results of complicated soil-pile interaction as exemplified by the local displacement field described above, the load-displacement curves have practically the same shapes as those of the shear stress-shear strain of a single soil element under static and cyclic simple shear. Based on this finding, the soil-pile interaction in horizontal plane is idealized as a soil-pile interaction spring element using a fictitious single soil element.
4. In addition to the soil-pile interaction spring, a joint element is used to idealize the soil-pile interface effect, including soil-pile separation and sliding effects.

In Chapter 4, the effect of soil-pile separation on the performance of a laterally loaded pile group is studied based on a comprehensive set of full-scale tests, consisting of a single and 3x5 group pile under static and dynamic loads and thereby reduces the limitations that were often caused by arbitrary parameter adjustment or back-fitting to the measured data. Two dimensional finite element analyses performed in this study lead to the following conclusions:

1. For a statically loaded single pile, at the same load level, the analysis without soil-pile separation underestimates both deflection and maximum bending moment. The percentage of underestimation increases with the progress of loading and reaches, at the maximum applied load, 50% for deflection and 22% for maximum moment. At a target deflection of 90 mm, ignoring soil-pile separation leads to 43% overestimation of the ultimate lateral load-carrying capacity of the pile.
2. For a statically loaded pile group, the effect of soil-pile separation is most distinctive at the trailing pile. The effect of soil-pile separation is not significant for other piles in the group including the leading pile. The potential soil-pile gap for these piles appeared to be closed by the soil deformation pushed forward by the next column of pile trailing behind. In the analysis without soil-pile separation, the soil behind the trailing pile pulls back the pile opposite to the loading direction and resulting in the excessive increases in the overall soil resistance during pile deformation. At any load level, the analysis without soil-pile separation

underestimates the deflection of the trailing pile. The percentage of underestimation increases with the progress of loading and reaches to 70% at the maximum applied load. At a maximum target deflection of 83.4 mm, ignoring soil-pile separation leads to 73% overestimation of the ultimate lateral load-carrying capacity of the trailing pile.

3. For dynamically loaded pile group, the effect of soil-pile separation is significant not only in the loading phase but also in the unloading phase. At maximum applied load, the deflection obtained without separation is smaller than that obtained from field data. The percentages of reduction were 8.6, 16.0, 17.3, 21.8, and 23.3% for target deflections of 13, 25, 38, 64, and 89 mm, respectively. Ignoring the effect of soil-pile separation significantly underestimates both deflection and bending moment values, leading to unconservative design of group piles.

In Chapter 5, the effect of vertical loads on the lateral response of a free head and capped pile group (3×5) embedded in sandy soil has been studied in this chapter through a series of two-dimensional finite element analyses. Of the findings of this study, the following conclusions can be drawn:

1. The influence of vertical loads on the lateral response of piles is to increase the confining pressure in the sand deposit surrounding the pile, leading to an increase in the lateral pile resistance. A vertical load applied to a single pile with a vertical displacement of 0.1-pile diameter (D = 324 mm) increases the lateral pile resistance, at a 60 mm lateral deflection, by 8 %.
2. The same vertical load applied to a pile group spaced at 3.92-pile diameters increases the overall lateral resistance of the group by 9 %.
3. The effect on individual piles depends on the pile position. The vertical load leads to a 10 % decrease in the lateral resistance of the leading pile (pile 1) and 9, 14, 17, and 35 % increases in the lateral resistances of piles 2, 3, 4, and 5, respectively.
4. The vertical load applied on the pile group increases the confining pressures in the sand deposit confined by the piles but the rate of increase in those outside the group is relatively small, resulting in the difference in a balance of lateral soil pressures acting at the back of and in front of the individual pile.
5. The middle pile (pile 3) behaves approximately the same as the single pile as a result of no net lateral stress induced by the vertical load. For the leading pile (pile 1), the net horizontal

stress due to the vertical load acts in the same direction with the prospective lateral load, leading to a decrease in the pile resistance to the subsequent lateral load. For the trailing (pile 5), the net horizontal stress acts against the prospective lateral load, leading to an increase of the pile resistance to the subsequent lateral load.

6. In addition to soil-pile interaction, soil-pile cap interaction play an important role in the increase of the confining pressure surrounding a capped single pile leading to an amplification of the effect of the vertical load on the lateral response of the pile.
7. The effect of vertical loads on the lateral load carrying capacity of individual pile in a capped pile group is similar to the free head case but with higher percentages of decrease or increase.

In Chapter 6, applicability of the simplified FE model, proposed by Ozutsumi et al. (2003), to the analysis of SSPSI in the frequency domain is examined. The verification process has been executed assuming elasto-dynamic behavior of the soil and comparing the results obtained using the simplified FE model with those found using other established results from the literature. Based on the comparative results in the paper, it is established that It has been shown that this procedure can be used successfully for a provision of the response of a single pile to inertial loading caused by the lateral forces imposed on the over structure and kinematic loading caused by the soil developed during an earthquake. In addition, the effects of soil profile and material nonlinearity of the soil on the kinematic and inertial interaction as affected by the frequency content of input motion are parametrically investigated and the following conclusions can be drawn from this study:

1. Kinematic soil-pile interaction: the filtering of pile to the high frequency components of the base excitation is substantially greater with inhomogeneous than with homogeneous soil deposits. On the other hand the effect of nonlinear soil behavior seems to be not significant.
2. Combiend kinematic and inertial interaction: a significant reduction in f_{SSI} due to soil inhomogeneity as well as soil nonlineartiy.
3. In contrast to the clear effect of soil nonlinearity on f_{SSI}, f_{pSSI} seems to be not affected by it.

In Chapter 7, a comparison between nonlinear seismic analyses using the 2-D finite element (FE) and the results of shaking table centrifuge model tests of pile-supported structures in a dense sand profile is preseneted. The FE analyses were reasonably able to approximate the recorded responses during shaking in centrifuge tests for the range of conditions covered in the

experiments. The challenge was to approximate the recorded responses for a total of six cases using a common set of modeling parameters. As illustrated by the representive time series , Fourier spectra , and bending moment profiles, the overall comparisions indicated that these FE models could now be used to parametrically evaluate the influnce of other key factors, such as varying structural periods, pile slenderness, soil-pile relative stiffness, and input motions.

In Chapter 8, a series of systematic centrifuge tests is conducted in order to study the seismic response of end bearing single and 3×3 group piles embedded in dry sand layer and supporting single and double degree of freedom structures. All the tests are conducted with the centrifugal acceleration of 40 g. Air pluviation method was used to place the dry sand in the soil container. A total of 7 tests including free-field, single and group pile cases were performed. Each model was subjected to 12 sinusoidal waves as input base accelerations. These waves have constant amplitude of about 1.5 m/s^2 and varying frequencies ranging from 1 to 12 Hz. Of the findings of this study, the following conclusions can be drawn:

1. For both single and group pile supporting a single or double degree of freedom structures, the pile-head motion is found to be dominated by two discrete frequencies: a lower frequency (the effective natural frequency (f_{SSI})) where the pile-head motion is amplified and a higher one (the pseudo-natural frequency (f_{pSSI}) of the system) where the response is suddenly de-amplified with respect to the free-field motion. These results confirm the numerical results found in the literature and generalize the finding to include group pile and higher degree of freedom structures.
2. For free-head pile group, as the frequency content of base excitation approaches the fundamental frequency of the ground, the bending moment of all piles increase as well as the difference between piles bending moments indicating strong effect of pile-soil-pile interaction. In this case, the center pile in the group has the minimum value of bending moment followed by the side pile followed by the corner pile.
3. For group piles supporting structure, as the frequency content of base excitation approaches the effective natural frequency of the coupled soil-pile-structure system, the bending moment of all piles increase as well as the difference between piles bending moments indicating strong effect of pile-soil-pile interaction. Unlike the free-head case, In this case, the center

pile in the group has the maximum value of bending moment followed by the side pile followed by the corner pile.

4. For both single and group piles, Structural vibrations tend to impose large pile bending moments, when the frequency of excitation is close to the effective natural frequency of the system. On the contrary, when the input motion is close to the fundamental frequency of the ground, strong kinematic effects are mobilized and generate significant pile bending.

In chapter 9, linear and non-linear seismic response of a single degree of freedom (SDOF) structure supported on a single pile embedded in dry sand is parametrically studied, emphasizing on the vibrational characteristics of the soil-structure system. These series of parameter study are the base to develop simple charts for predicting linear and nonlinear seismic response of a single degree of freedom (SDOF) structure supported on piles. For this reason, a fully two dimensional (2D) finite element (FE) model of the coupled system is analyzed in the frequency domain under harmonic excitation introduced at the base of the soil profile. The following conclusions can be drawn:

1. Strong soil-structure interaction effects were observed for coupled systems that comprise of stiff superstructures founded on flexible and/or long piles, leading to significant reductions in effective natural frequency of the system.
2. The nonlinearity of the ground induces larger reduction in frequency ratio.

APPENDIX A1

Calculation of the ultimate vertical capacity of single pile

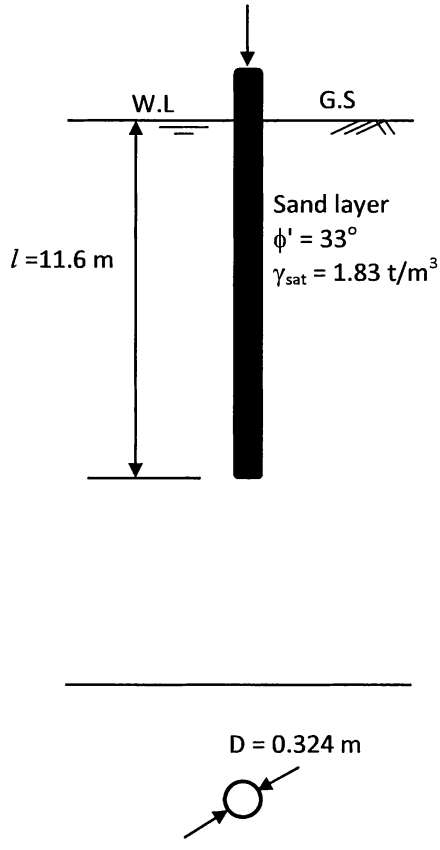

Fig. A11 Closed end steel single pile embedded in sandy soil

The ultimate vertical capacity of a closed end steel single pile embedded in sandy soil with the properties shown in Fig. A11can be calculated as follows:

(1) Based on conventional method

$$P_u = P_s + P_b \tag{A11}$$

with

P_u: ultimate loading capacity

P_s: ultimate skin friction

P_b: ultimate base resistance

$$P_s = pK tan\delta \int_0^l \sigma_v' \, dz \quad \text{(A12)}$$

$$p = 0.324\pi = 1.0178\, m$$

$$K = 1.2\, K_o = 1.2(1 - sin33) = 0.546$$

$$\delta = 0.67\, \phi' = 22^{\circ}$$

$$\int_0^l \sigma_v' \, dz = 0.5(11.6 * 11.6 * 0.83) = 55.84\, t/m^2$$

$$P_s = 1.0178 * 0.546 * tan22 * 55.84 * 9.81 = 122.99\, kN$$

$$P_b = A_p N_q \sigma_v' \quad \text{(A13)}$$

$$A_p = 0.0825\, m^2$$

$$N_q = 47$$

$$\sigma_v' = 0.83 * 11.6 = 9.628\, t/m^2$$

$$P_b = 0.0825 * 47 * 9.628 * 9.81 = 366.23\, kN$$

$$P_u = 366.23 + 122.99 = 489.22\, kN$$

(1) Based on FE analysis

Figure A12 shows vertical load versus vertical displacement curve obtained using FE analysis of a closed end steel single pile embedded in sandy soil with the properties shown in Fig. A11 and given in details in Chapter 5.

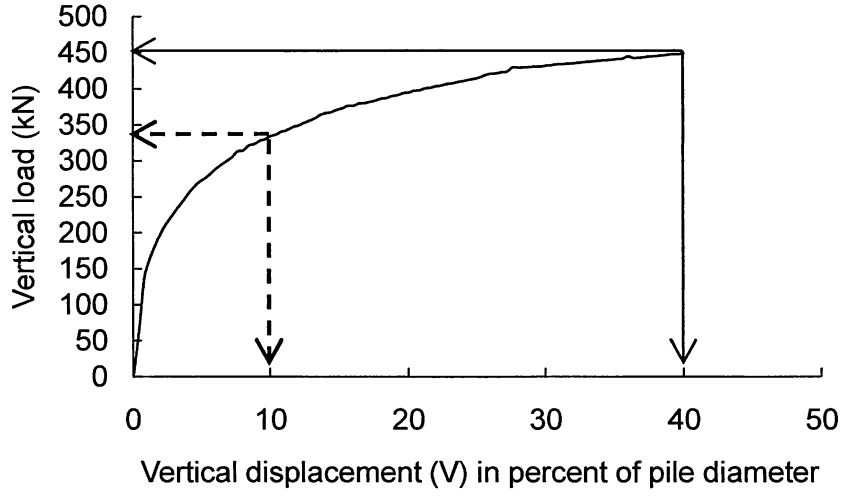

Fig. A12 Vertical load versus vertical displacement of the single pile embedded in sandy

From Fig. A12, the ultimate vertical capacity of the pile equals 450 kN and corresponds to vertical displacement equals to 40% D. The vertical load used in the analyses in Chapter 5 equals to 336 kN and corresponds to 10% D (i.e. vertical load = 75 % of the ultimate vertical capacity of the pile (P_u)).

APPENDIX A2

Calculation of the normal stiffness and shear stiffness of the interface elements

The normal and shear stiffness of joints are selected based on sensitivity FE analyses of the single pile embedded in sandy soil and having the properties given in Fig. A11. In these analyses, the pile is loaded either vertically or laterally. Figure A21 shows the vertical load-vertical displacement curves calculated with different normal and shear stiffness of joint elements (in this analysis, the normal and shear stiffness is assumed to be equal). The figure indicates that the change in the load-deflection curve is become insignificant as the joint stiffness becomes high (i.e. K=10^5, 10^6 kN/m^3). It is worth to note that if K exceeds 10^6 kN/m^3, the analysis is stopped due to divergence.

Figure A22 shows the vertical load and soil shear stress variations with depth. This figure shows that except for stiffness value of 100 kN/m^3, the vertical load and soil shear stress variations with depth are independent on the joint stiffness values.

Figure A23 Confining stress and soil strain variations with depth. This figure shows that except for stiffness value of 100 kN/m^3, confining stress and soil strain variations with depth are independent on the joint stiffness values.

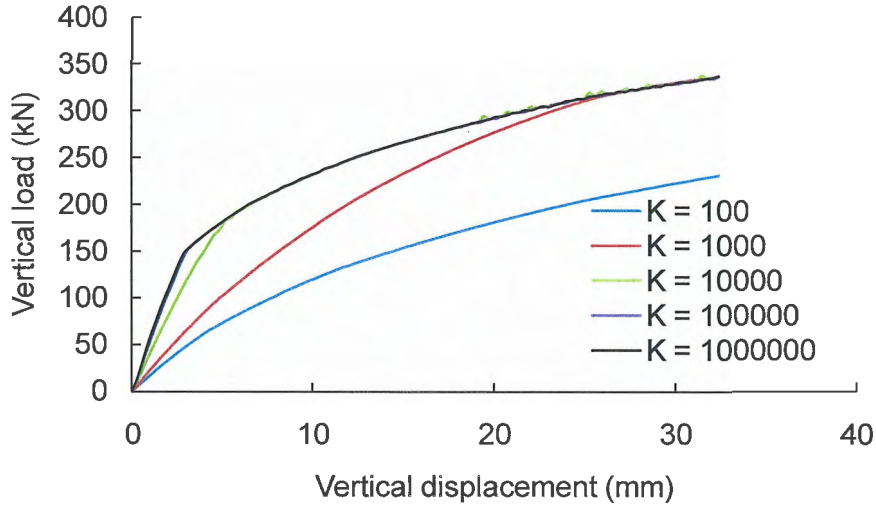

Fig. A21 vertical load-vertical displacements curves at different joint element stiffness

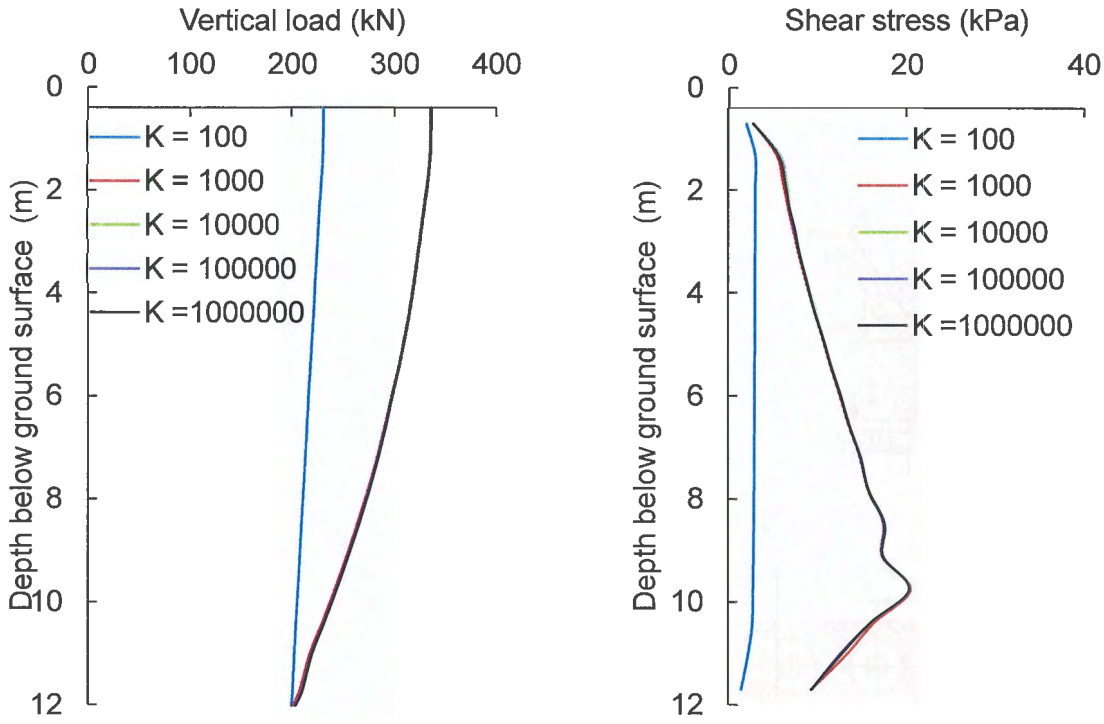

Fig. A22 Vertical load and soil shear stress variation with depth; (a) vertical load and (b) soil shear stress

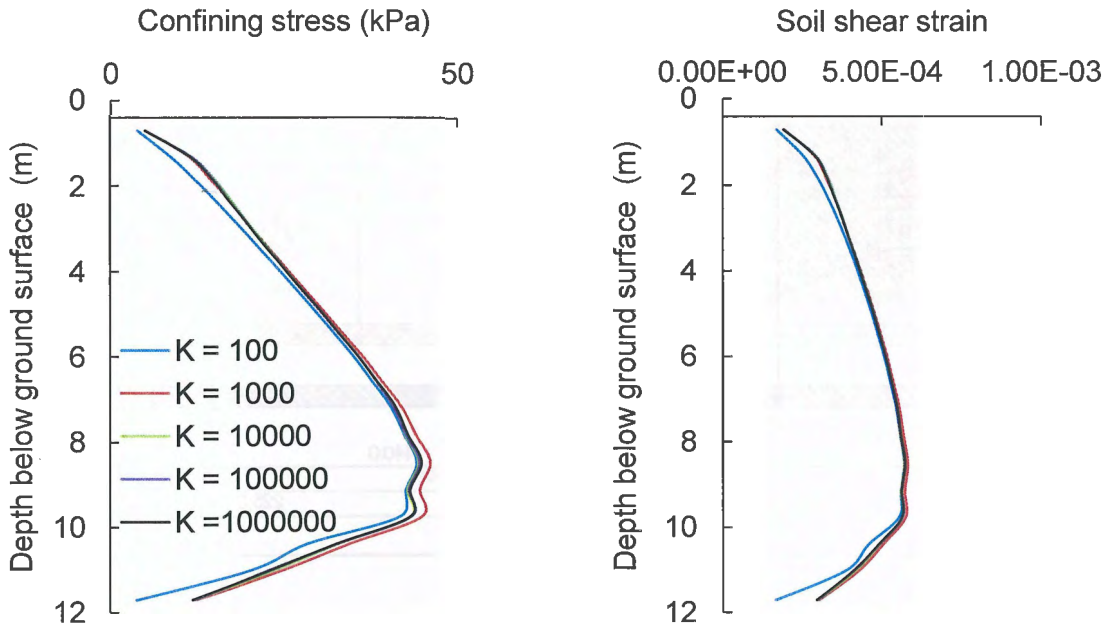

Fig. A23 Confining stress and soil strain variation with depth; (a) confining stress and (b) soil strain

APPENDIX B1

Assembly Drawing of Single Pile Support Double Degree of Freedom Structure

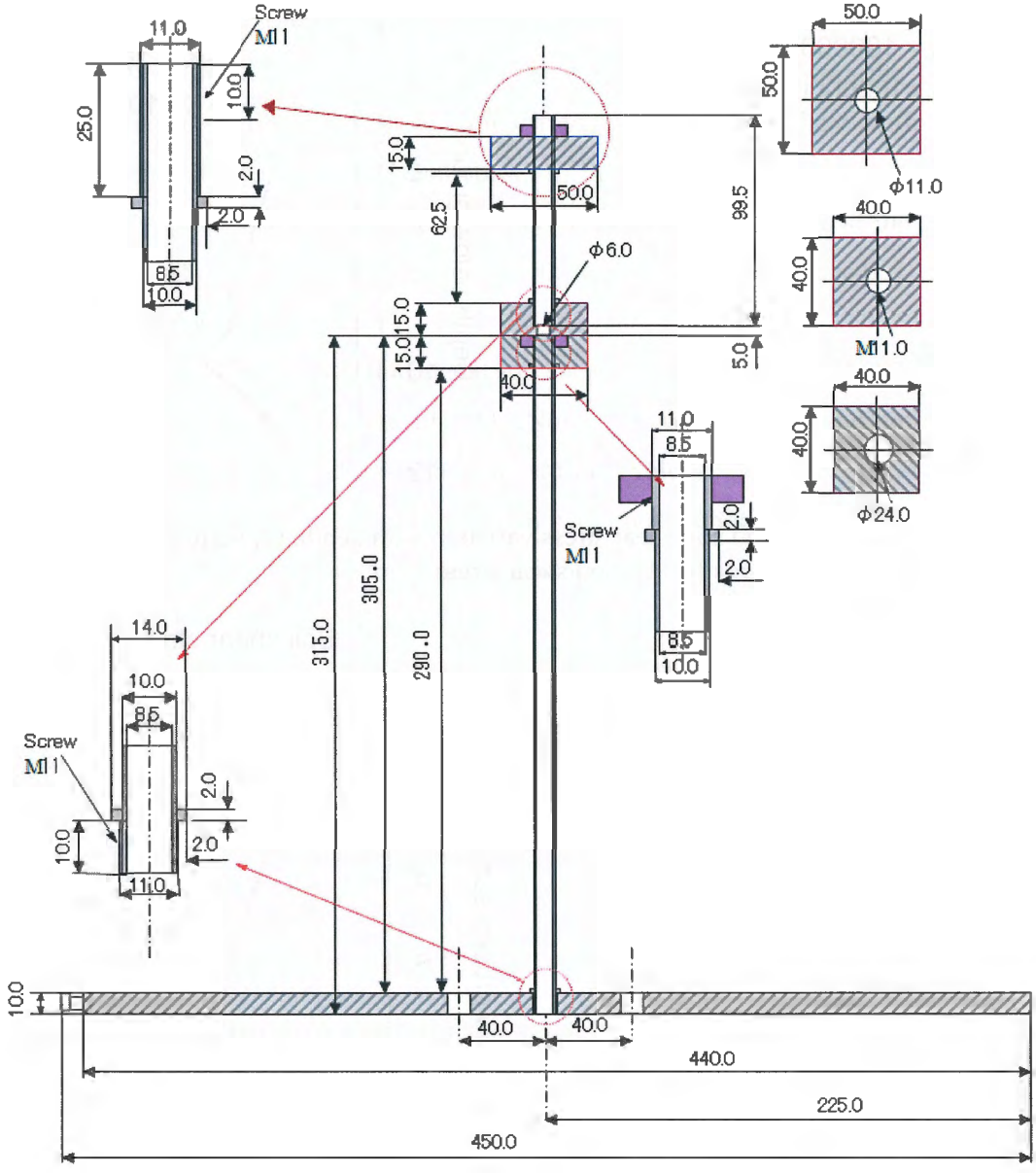

Assembly Drawing of 3×3 Group Pile Support Double Degree of Freedom Structure

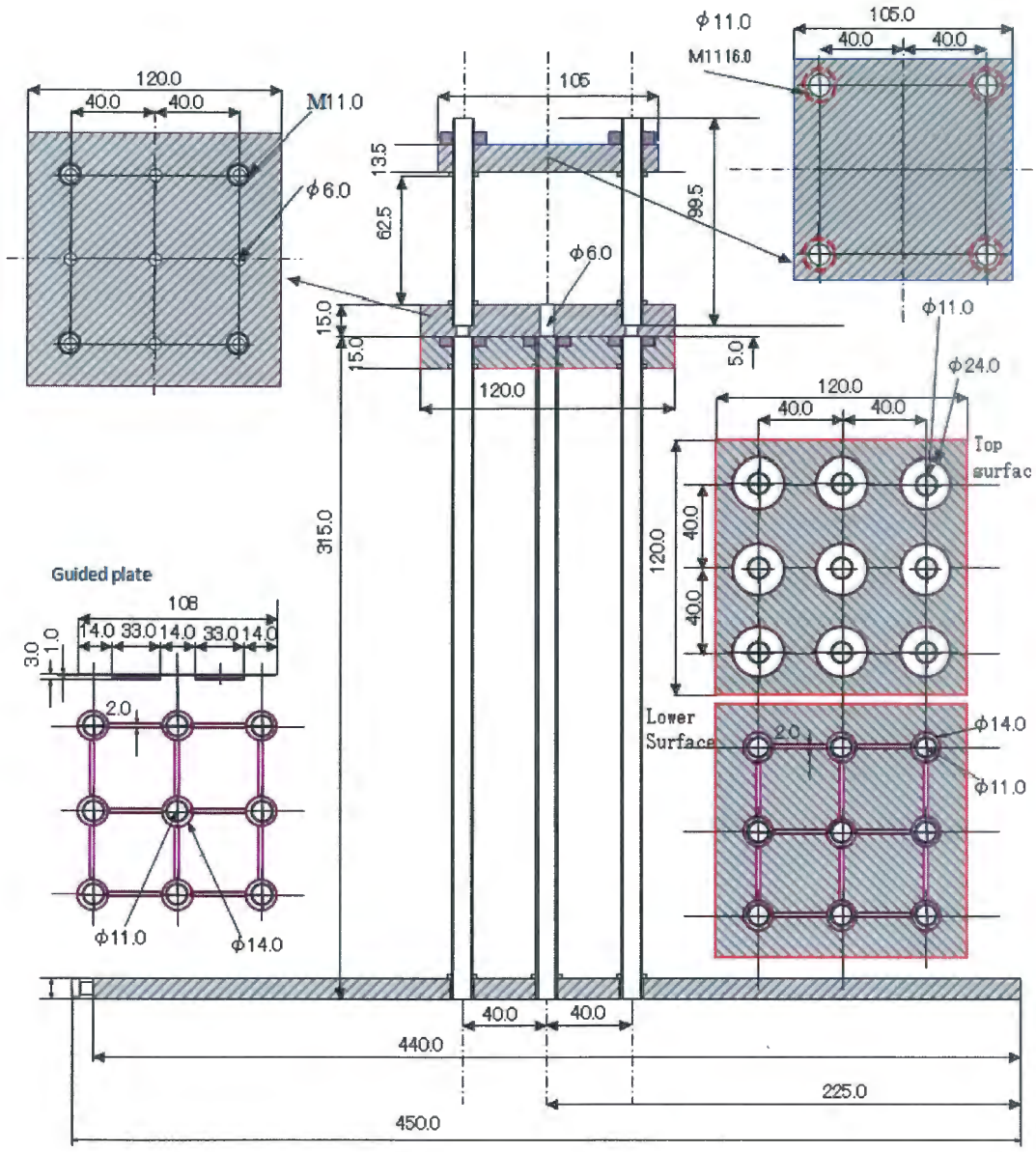

APPENDIX B2

Specifications of Sensors

SSK **Micro (for high G) Accelerometers**
A-H Series (Model A6H & Model A10H)

A6H A10H

Features:
- Micro type
- High output(high sensitivity)
- High resolution
- From DC to high frequency
- Very small phase shift

Overview: The A-H series accelerometers are high G type accelerometers designed by integrated SSK transducer technology and used mainly for centrifugal loading test and also suitable for impact test in the engineering works and construction fields.

Specifications:

	±50G	±100G	±200G	±500G	±1000G	±2000G	±5000G
Model A6H	A6H-50	A6H-100	A6H-200	A6H-500	A6H-1000	A6H-2000	A6H-5000
Model A10H	A10H-50	A10H-100	A10H-200	A10H-500	A10H-1000	A10H-2000	A10H-5000
Natural oscillation Frequency	1KHz	1.4KHz	2KHz	3.2KHz	4.4KHz	6.2KHz	10KHz

Output voltage	100mVRO	option: An output for strain gauge of 5000μor 10,000μRO
Overlord	200%RO	is available
Non-linearity (& hysteresis)	1%RO	
Reproducibility	0.2%RO	
Temperature characteristic	0.05%RO/℃(0 to 40℃)	option:0.02%RO/℃ is available
Operating temperature range	-15℃ to +75℃	
Input/output resistance	500Ω	
Bridge voltage	6VDC(8VDC MAX)	
Cord length	3m with exposed ends	option: A type with a cord extension connector is available

Measuring Blocks:

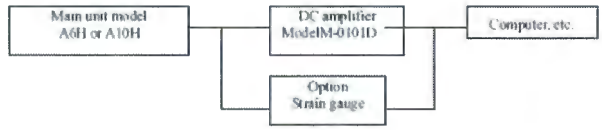

External View:

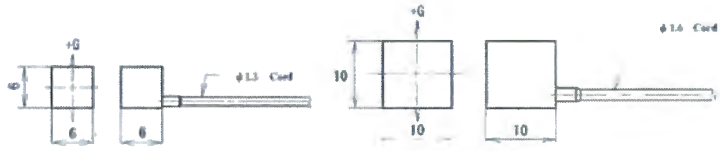

Model A6H Model A10H

SSK Co., Ltd.
Head Office and Sales Office
3-3-29, Minami Ohizumi, Nerima-ku, Tokyo 178-0064
TEL 03-3921-2191 FAX 03-3921-2291
info@ssk-co.jp www.ssk-co.jp

APPENDIX B3

Specifications of Sensors

センサヘッド
LB-080

仕様

種類		ロングレンジタイプ
型式	センサヘッド	LB-080
	アンプユニット	LB-1100
基準距離		80mm
測定範囲		±15mm
光源	種類	赤色半導体レーザ
	波長	670nm（可視光） JISクラス1M
	出力	最大2.5mW
スポット径（基準距離にて）		1×2mm
直線性（白紙にて）		0.25% of F.S.
分解能（白紙で基準距離にて）		8μm（LO時）
アナログ出力	電圧出力	±5V (3mm/V)
	インピーダンス	100Ω
	電流出力	4-20mA（適用負荷350ΩMAX）
アラーム出力		NPNオープンコレクタ最大100mA（40V以下） 残留電圧1V以下（N.C）
応答性		915Hz（HIGH時）/36Hz（MID時）/9Hz（LO時） 各−3dBにて
副機能		オートゼロ/応答性切換/オートレスポンスコントロール/ 互干渉防止回路（30Hz）内蔵
定格	電源電圧	AC100～240V±10% 50/60Hz
	消費電力	約15VA
温度特性	センサヘッド	0.02% of F.S./℃
	アンプユニット	0.02% of F.S./℃
耐環境性	使用周囲照度	白熱ランプ・蛍光灯：2500lx以下
	使用周囲温度	アンプユニット0～＋50℃ センサヘッド0～＋45℃
	使用周囲湿度	35～85%RH（結露しないこと）
	耐振動	10～55Hz 複振幅1.5mm X、Y、Z各方向2時間

材質		センサヘッド：アルミダイキャスト アンプユニット：ポリカーボネート
質量（コード含む）	センサヘッド	約170g
	アンプユニット	約530g

※（ 本機はアンプユニット、センサヘッドのセットで調整されていますので、
注） 必ず同一ナンバーの組み合わせでご使用ください。

※（ 米国へ輸出される時は、FDA規格品を用意しておりますのでお問い合わせください。
注）

外形寸法図

単位：mm

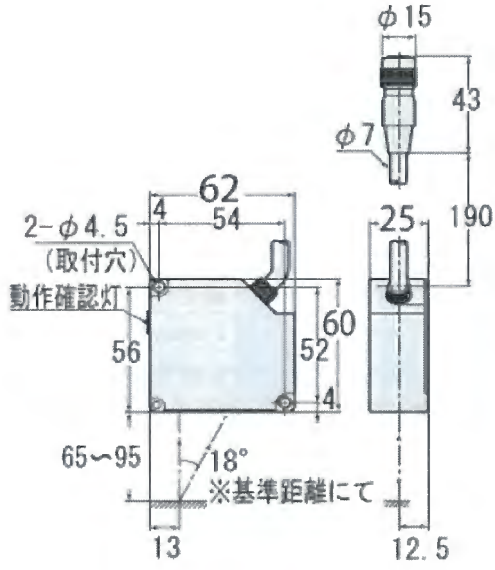

APPENDIX B4

Specifications of Sensors

FOIL STRAIN GAUGE series "F"

Compatible adhesive & Operational temperature
CN : −20~+80℃
P-2 : −20~+80℃ EB-2 : −20~+60℃

GENERAL USE

Gauge pattern		Type	Gauge size L	Gauge size W	Backing L	Backing W	Resistance Ω
			L : length		W : width (Unit : mm)		
		FLA-6-1000-11 -17 -23	6	4.6	13.5	7.0	1000
FLA-10	Single-element	FLA-10-11 -17 -23	10	2.5	16.7	5.0	120
FLA-30		FLA-30-11 -17 -23	30	2.0	36.1	5.1	120
FLK-1	FLK-type with narrow gauge width	FLK-1-11 -17 -23	1	0.7	4.5	1.4	120
FLK-2		FLK-2-11 -17 -23	2	0.9	5.5	1.5	120
FLK-6		FLK-6-11 -17 -23	6	1.0	11.2	2.2	120
FLK-10		FLK-10-11 -17 -23	10	1.6	16.2	3.8	120

FLA-1 -11 Materials for S-T-C
Gauge length
-11 Mild steel
-17 Stainless steel
-23 Aluminium

Each package contains 10 gauges.

APPENDIX B5

Air Pluviation Method

Figure B5.1 shows the equipments used in the air pluviation process of sand. The falling head (H) of sand is determined based on the target relative density (% Dr).

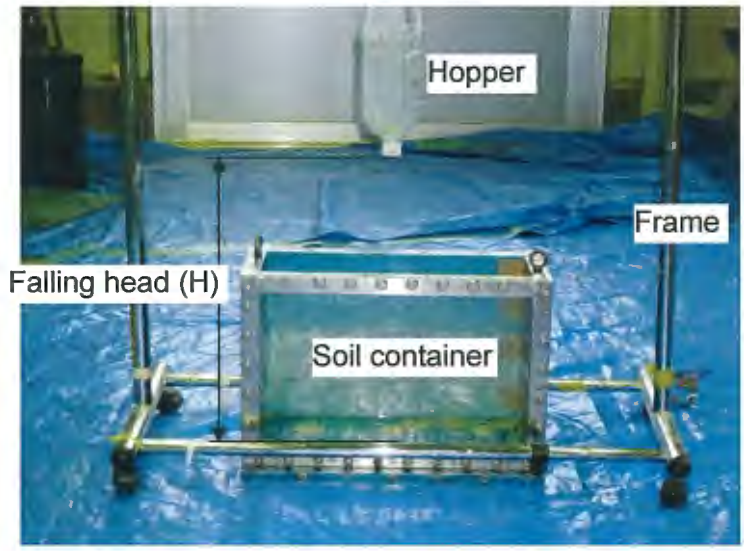

Fig. B5.1 Equipments setup used in air pluviation

The relation between the falling head (H) and the relative density (% Dr) is calibrated using steel cylindrical container. The volume of the container or sand is calculated as follows:

The container volume (volume of sand) = $(\pi*D^2/4)*d = (\pi*6.0^2/4)*3.2=90.478\ cm^3$

Sand falls from different heights into the cylindrical container and the corresponding weights of sand are measured, then the relative density is calculated using the following:

$$\%D_r = \left[\frac{\gamma_{d\max}}{\gamma_d}\right]\left[\frac{\gamma_d - \gamma_{d\min}}{\gamma_{d\max} - \gamma_{d\min}}\right]$$

where $\gamma_{dmin} = 1.21\ g/cm^3$ and $\gamma_{dmax} = 1.56\ g/cm^3$

Table B5.1 Relation between falling height and relative density

Falling Height (cm)	Weight (g)	γ_d (g/cm^3)	%Dr
43.5	128.61	1.42	65.96
46.5	131	1.45	73.82
49.5	32.14	1.46	76.37
52.5	132.74	1.47	78.88
55.5	132.44	1.46	76.37
58.5	133.95	1.48	81.36
61.5	133.56	1.48	81.36
64.5	135.34	1.5	86.23

Used in the tests

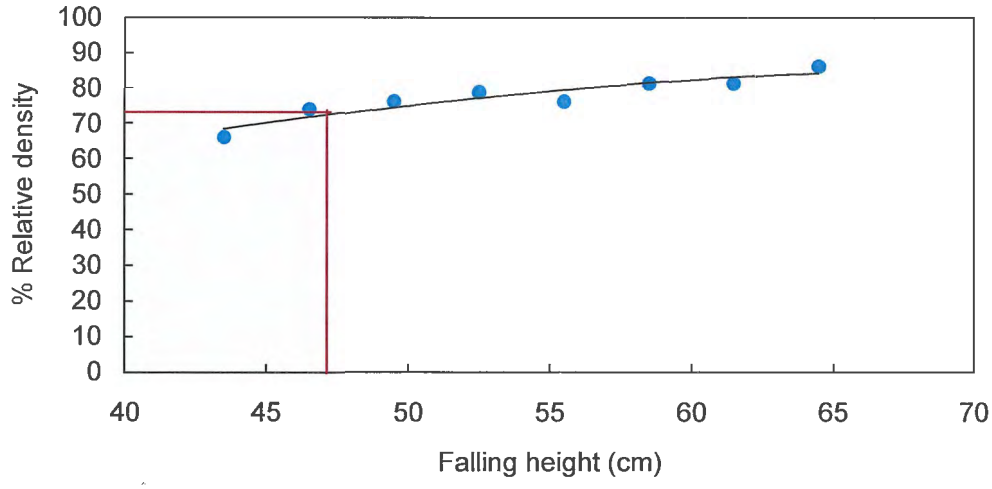

Fig. B5.1 Relation between falling height and relative density